Structural and Electronic Properties of PTCDA Single Molecules and Molecular Layers on Metal and Semiconductor Surfaces

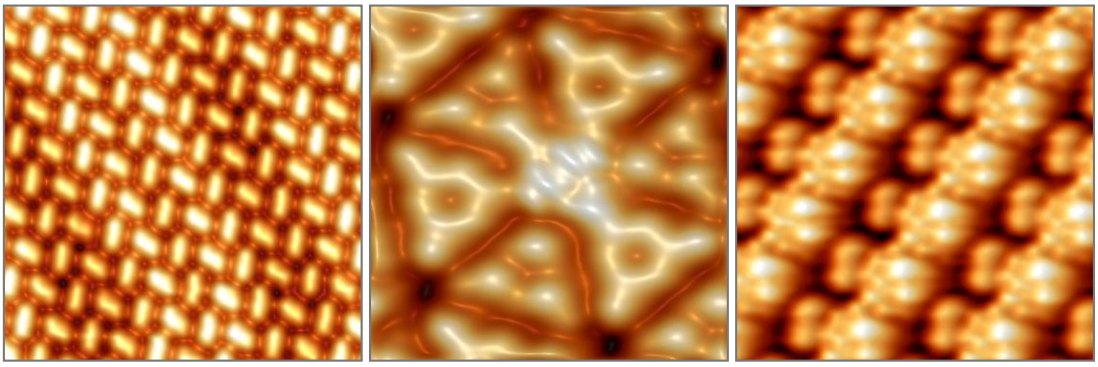

DOCTORAL THESIS

Submitted to the Department of Condensed Matter Physics

Universidad Autónoma de Madrid

Nicoleta Nicoara

September 2007

Advisors: Dr. Javier Méndez and Dr. José María Gómez Rodríguez

Contents

Resumen

En esta tesis se presenta un detallado estudio experimental de la adsorción, crecimiento y propiedades de una molécula orgánica prototipo - PTCDA (3, 4, 9, 10 perileno-tetracarboxílico dianhídrido)- sobre diversas superficies metálicas, semiconductoras o de materiales semiconductores pasivados. La motivación primordial del trabajo se basa en el hecho de que los materiales híbridos orgánico-inorgánicos constituyen una nueva clase de sistemas cuyo desarrollo, caracterización y explotación representan en la actualidad un campo de investigación muy activo y en plena expansión dentro del área de la electrónica molecular. Las atractivas propiedades de los semiconductores orgánicos (tales como su fácil procesabilidad de bajo coste, su flexibilidad mecánica, la posibilidad de prediseñar sus propiedades ópticas y electrónicas, además de su eficiente electroluminiscencia y sus razonables movilidades de portadores de carga) combinadas con las propiedades de los materiales inorgánicos (tales como el amplio abanico de propiedades electrónicas que permiten el diseño de aislantes, semiconductores y metales, su alta dureza mecánica y su gran estabilidad térmica) han llevado a expectativas de crear una nueva electrónica con aplicaciones que abarcan desde diodos orgánicos de emisión de luz (OLEDs) [Tang 1987, Baldo 1998, Friend 1999, Baldo 2000], transistores de láminas delgadas orgánicas [Ostrick 1997, Xue 2001, Xu 2007], paneles solares orgánicos [Tang 1986, Meissner 2001] y fotodetectores [Peumans 2003].

Más allá de las aplicaciones, se encuentra la investigación de carácter fundamental que puede proporcionar un importante conocimiento en la física de semiconductores orgánicos. El avance en la tecnología de ultra-alto vacío (UHV), el desarrollo de técnicas controladas de crecimiento de láminas delgadas (tales como la deposición de materiales orgánicos por haces moleculares-OMBD [Forrest 1997]-o a partir de la fase vapor [Baldo 1997, Shtein 2001]) junto con el de técnicas espectroscópicas con sensibilidad superficial ha llevado a la posibilidad de crecer láminas delgadas orgánicas de alta calidad y de explorar sus propiedades estructurales y electrónicas. El estudio de estas propiedades permite, así, profundizar en el conocimiento de los mecanismos involucrados en la formación y ordenamiento de las capas orgánicas y en los procesos de transporte de carga.

El propósito del presente trabajo de investigación es conocer el comportamiento de diferentes sistemas orgánico/inorgánicos formados por moléculas orgánicas de PTCDA crecidas sobre muy distintos substratos (tanto metálicos como semiconductores, pasivados estos últimos o no) que poseen propiedades estructurales y electrónicas muy diversas. Un especial interés se ha prestado a la formación de la intercara substrato-PTCDA, la cual está directamente influida por las propiedades del substrato, y que juega un papel fundamental en el ordenamiento molecular y en las propiedades electrónicas de las láminas orgánicas. De esta forma, se abordan aspectos fundamentales para el comportamiento de las intercaras, tales como el sitio de adsorción y orientación de las moléculas (los cuales determinan el orden, el modo de crecimiento y la morfología de las láminas orgánicas), las interacciones químicas y electrónicas entre moléculas y substrato (esto es, la formación de enlaces químicos por solapamiento de las funciones de onda de las moléculas y del substrato), los niveles de energía electrónicos de las moléculas y su posición con respecto de los del substrato, así como potenciales modificaciones de las propiedades del substrato. Este trabajo de investigación experimental se ha llevado a cabo utilizando principalmente como técnica la microscopía y espectroscopía de efecto túnel (STM/STS) en ultra-alto vacío (UHV). Adicionalmente, se utilizaron como técnicas complementarias la espectroscopía de fotoemisión en el ultra-violeta (UPS) y de rayos X (XPS) en el caso de la intercara metal/moléculas orgánicas.

La tesis está organizada de la siguiente forma:

El **capítulo 1** describe algunos conceptos básicos relacionados con semiconductores moleculares orgánicos y presenta una introducción de la molécula de PTCDA utilizada en el presente trabajo. Asimismo, se presenta un breve resumen del sistema experimental utilizado.

El **capítulo 2** presenta un estudio combinado mediante STM/STS y UPS/XPS de las propiedades electrónicas del sistema formado por el substrato metálico Au(111) y las moléculas orgánicas de PTCDA. En estas superficies inertes, el crecimiento molecular viene determinado esencialmente por las interacciones intermoleculares más que por la interacción molécula substrato, favoreciéndose así el auto-ensamblado de las moléculas en la superficie. Esta débil interacción molécula-substrato (fisisorción) se pone de manifiesto en la posibilidad de detectar estados moleculares (HOMO y LUMO) muy

similares a los de la molécula libre, con diferencias de energía entre ellos similares a las que presenta el cristal molecular de volumen. Además, la presencia de un estado electrónico en la intercara, próximo en energía al nivel de Fermi, y directamente derivado del estado de superficie de tipo Shockley del Au(111), indica una muy pequeña influencia mutua entre substrato y adsorbato y apoya la existencia de un proceso de fisisorción en la intercara.

El **capítulo 3** presenta el estudio de la adsorción de moléculas de PTCDA individuales en una superficie altamente reactiva: Si(111)-(7×7). La combinación de experimentos de STM con cálculos de primeros principios basados en la teoría del funcional de la densidad (DFT) ha permitido descubrir los complejos desplazamientos y desdoblamientos en energías a partir de los orbitales moleculares (OM) del PTCDA como resultado del proceso de quimisorción en la superficie de silicio. Como se muestra en este capítulo, la resolución intramolecular observada en los experimentos de STM realizados en este sistema no puede entenderse de forma sencilla a partir de un desplazamiento "rígido" de los OM de la molécula libre. Por el contrario, los cálculos DFT del sistema molécula-superficie así como la correspondiente simulación de imágenes de STM con puntas realistas muestran la existencia de grandes desdoblamientos de los OM originales cuando se adsorbe el PTCDA en la superficie de silicio, los cuales contribuyen de forma compleja a la corriente de túnel. Estos desdoblamientos se pueden entender utilizando argumentos de simetría y de transferencia de carga y caracterizan un fuerte enlace covalente parcialmente iónico que involucra los grupos carbonilo de la molécula y los enlaces colgantes de los átomos de silicio de la superficie.

El **capítulo 4** presenta un estudio sistemático mediante STM de la formación de las intercaras y el crecimiento de láminas delgadas de PTCDA en varias superficies de semiconductores "pasivadas": Pb/Si(111), Sn/Si(111) y S/GaAs(100). En estas superficies relativamente inertes, resultado de la saturación de los sitios químicamente activos, es esperable que la interacción adsorbato-substrato sea significativamente menor que en el caso de superficies de semiconductores no pasivadas como las superficies de silicio estudiadas en el capítulo 3. En particular, en el presente capítulo se muestra, en primer lugar, métodos alternativos de pasivación de superficies de silicio utilizando átomos de Pb o de Sn. De esta forma, se ha investigado la formación y

evolución de capas ordenadas de PTCDA en substratos cuya reactividad superficial se varía de forma sistemática cambiando el recubrimiento de los átomos utilizados en el proceso de pasivación. Por último, en el caso de las superficies de GaAs(100) se han utilizado dos métodos diferentes de pasivación con átomos de azufre. El primero se basa en un método de ataque químico reactivo *ex situ*, mientras que el segundo consiste en la pasivación *in situ* (en UHV) de superficies de GaAs(100) crecidas por epitaxia por haces moleculares (MBE). Así, se ha comparado el crecimiento de PTCDA y la morfología de las muestras crecidas en los dos tipos de superficies S/GaAs(100). Asimismo, se han estudiado las propiedades electrónicas de las láminas orgánicas crecidas en las muestras preparadas por MBE, las cuales presentan un mayor grado de orden molecular.

Summary

This thesis presents an experimental investigation focused on the adsorption, growth and thin film formation of an archetypal organic molecule PTCDA (3, 4, 9, 10 perylene-tetracarboxylic dianhydride) on metallic, semiconductor and passivated semiconductor surfaces. The primary motivation of this work arises from the fact that organic-inorganic hybrid materials constitute a new class of systems whose development, characterization and exploitation represent nowadays an active and rapidly expanding research field within the organic electronics area. The attractive properties of organic semiconductors (easy and low costs processability, mechanical flexibility, tailorability of their electronic and optical properties, efficient electroluminescence, and reasonable charge carrier mobilities) in combination with inorganic materials properties (wide range of electronic properties enabling the design of insulators, semiconductors and metals, substantial mechanical hardness and thermal stability) have led to expectations of new electronics with applications ranging from organic light emitting devices (OLEDs) [Tang 1987, Baldo 1998, Friend 1999, Baldo 2000], organic thin films transistors (OTFTs) [Ostrick 1997, Xue 2001, Xu 2007], organic solar cells [Tang 1986, Meissner 2001] and photodetectors [Peumans 2003].

Beyond applications, however, lies the fundamental research which provides valuable knowledge related to the physics of organic semiconductors. The progress in the ultra-high vacuum (UHV) technology, the controlled thin film growth techniques (organic molecular beam deposition, OMBD [Forrest 1997] or organic vapor phase deposition [Baldo 1997, Shtein 2001] along with the development of surface sensitive spectroscopic techniques have led to the production of high quality organic thin films and allowed the exploration of their structural and electronic properties. Studies of the structural and electronic properties of organic films deposited on metallic or semiconducting substrates give a challenging opportunity to get insight into the mechanisms governing the formation of organic layers, ordering and charge transport.

In this sense, the aim of the present work was to gain knowledge on the behavior of different organic/inorganic systems formed by the organic PTCDA molecules and different substrates (metal, semiconductor and passivated semiconductors) with evident different structural and electronic properties. Particular emphasis is given to the

interface formation which is directly influenced by the substrate properties and which plays a crucial role in the molecular ordering and the electronic properties of the organic films. Thus, issues relevant to the behavior of the interfaces such as: the adsorption site and molecular orientation (which strongly determine the ordering, growth and morphology of the organic films), the chemical and electronic interactions between the molecule and the substrate (e.g. chemical bonding overlap of substrate and molecular wavefunctions), the electronic energy levels of the molecule and their relative positions with respect to the substrate and potential modifications of the substrate properties are mainly addressed in this study.

This investigation was carried out mainly by scanning tunneling microscopy (STM) and spectroscopy (STS) in ultra-high vacuum (UHV) and complementary techniques as ultraviolet photoemission spectroscopy (UPS) and X-ray photoelectron spectroscopy (XPS) were also used in the case of the organic/metal interface.

The thesis is organized as follows:
Chapter 1 describes some basic concepts related to organic molecular semiconductors and provides an introduction to the PTCDA molecule used in the present work. A brief summary of the experimental set-up is given.

Chapter 2 presents a combined STM/STS and UPS/XPS study of the electronic properties of a system formed by the metallic substrate Au(111) and the organic PTCDA molecules. On these inert surfaces, the molecular growth is mainly determined by the intermolecular interactions rather than by the molecule-substrate interaction, favoring the molecular self-assembly at the interface. This weak molecule-substrate interaction (physisorption) is reflected by the possibility of detecting derived molecular states (HOMO and LUMO) very similar to those of the free PTCDA, with a band gap relatively close to values of the bulk PTCDA band gap. Furthermore, an interface state, localized close to the Fermi level, and directly derived from the Shockley-type surface states of the Au(111) substrate, indicates a rather small mutual molecule-substrate influence and support a physisorption process at the interface.

Chapter 3 presents a study of the adsorption of single PTCDA molecules on a highly reactive surface: Si(111)-(7×7). The combination of scanning tunneling microscopy

(STM) experiments and density functional (DFT) first-principles calculations have allowed us to elucidate the complex shifts and splitting of the original molecular orbitals (MO) of the PTCDA molecule upon adsorption. The intramolecular resolution observed in the experimental STM images can not be understood as the result of a simple rigid shift of the MO of the free molecule. On the contrary, our DFT calculations of the molecule-surface system and the corresponding simulation of STM images with realistic tips show large splittings of the original MO when PTCDA is adsorbed on the silicon surface, that contribute in a complex way to the tunnel current. These splittings can be understood under symmetry and charge transfer arguments that characterize a strong partially-ionic covalent bonding involving the carbonyl groups of the molecule and the silicon dangling bonds of the surface.

Chapter 4 presents a systematic STM study of the interface formation and PTCDA thin film growth on different "passivated" semiconductor surfaces such as Pb/Si(111), Sn/Si(111) and S/GaAs(100). On these relatively inert surfaces, resulting from the saturation of the chemically active sites, it is expected that the adsorbate-substrate interaction will be significantly lower than in the case of unpassivated silicon surfaces. By exploiting an alternative passivation method for the silicon surface employing Pb or Sn, the evolution of PTCDA film formation is investigated, for substrates whose reactivity is systematically varied.

For GaAs(100) surfaces two different approaches were employed for the substrate passivation. The first one is based on an *ex situ* wet chemical etching method and the second one consists in an *in situ* passivation of MBE prepared GaAs(100) surfaces. The molecular growth and sample morphology are compared for the PTCDA deposition on the two different passivated S-GaAs(100) surfaces. The electronic properties of the organic thin films on MBE prepared sample, which present an improved ordering, are probed.

CHAPTER 1

Introduction

1 Introduction

1.1 Organic molecular solids

The organic semiconductors are formed by individual molecular units which consist mainly of carbon, oxygen, nitrogen and hydrogen atoms. Planar aromatic molecules, such as perylene derivatives contain several benzene rings which are characterized by sp^2 hybridized carbons. The interactions between atomic orbitals of the bonding atoms in the molecule will exhibit two types of bond symmetry. The orbitals in the plane of the benzene ring form localized σ-orbitals that bind either C-C atoms or C-H atoms. P_z atomic orbitals of carbon atoms, positioned perpendicular to the benzene ring but parallel to each other overlap giving rise to delocalized π-orbitals with highest densities above and below the plane of the benzene ring. In most of the cases the highest π states give rise to the highest occupied molecular orbital (HOMO) while the lowest π^* states give rise to the lowest unoccupied molecular orbital (LUMO).

In contrast to the covalent bonding in covalent inorganic solids, the forces within organic solids are relatively weak. While the molecular structure is determined by covalent bonding, the structure of a molecular crystal depends on several interactions including the van der Waals interaction, the electrostatic interaction and in some cases the hydrogen bonds.

Due to the weakly interacting van der Waals forces, the organic materials are widely regarded as poor electronic conductors as they intrinsically contain very few carriers and exhibit weak overlap between orbitals of neighboring molecules. Electrons and holes are more localized in organic solids than in covalently bound inorganic solids resulting in narrow energy bands. The conduction process occurs mainly via tunneling and hopping between molecular sites, explaining the modest mobilities.

The electronic properties of molecular semiconductors are determined by the atomic structure of the molecule and the molecule-molecule interaction [Ishii 1997]. The formation of electronic levels in a single molecule and in a molecular crystal is shown in figure 1.1. For a single molecule, as shown in figure 1.1(a), the molecular orbitals are formed by combining the atomic orbitals of all the atoms contained in the molecule. The potential well formed by the atomic nuclei and the electrons is shown schematically. The potential wells of the nuclei are merged in the upper part and form a broad well. The deep atomic orbitals (core levels) are still localized in atomic wells. The upper

atomic orbitals interact and form the localized σ and delocalized π molecular orbitals. The topmost part of the well represents the vacuum level (VL). The difference between the HOMO and VL corresponds to the ionization energy (IE). The energy separation between the LUMO and VL represents the electron affinity (EA).

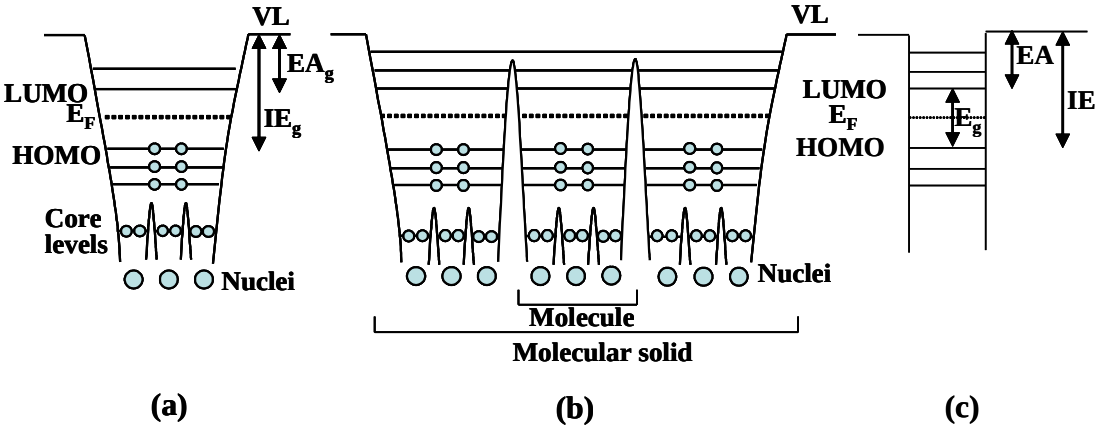

Figure 1.1 *Electronic structures represented with potential wells for a polyatomic molecule in (a) and an organic solid in (b), respectively. Simplified model in (c). IE_g, gas phase ionization energy; EA_g gas phase electron affinity; IE, solid state ionization energy; EA solid state electron affinity; VL, vacuum level; Eg, HOMO-LUMO band gap. Adapted from [Ishii 1997].*

Figure 1.1(b) presents the case of a molecular solid where molecules interact by weak van der Waals forces. The top part of occupied valence states and the lower unoccupied states are usually localized in each molecule, and have narrow intermolecular bandwidths. Thus, the electronic structure of an organic solid often preserves that of a molecule. Nevertheless, experiments have proven that the energy levels are relatively different in molecules and in the organic solid. It has been found that these differences in the electronic structure are mainly due to localization and polarization phenomena [Hill 2000, Tsiper 2001, Tsiper 2002].

Several effects may contribute to polarization and reorganization of molecular levels upon addition or removal of a charged particle: the electronic polarization of the surrounding molecules, which accounts for most of the screening of the central charge, molecular relaxation, which accounts for conformational changes of the molecular ion due to the charge, and lattice relaxation, which accounts for response of the structure of the molecular film due to the presence of the charge. These effects, usually not considered in inorganic semiconductors, play an important role in the electronic properties of organic solids. The transport gap, E_t, or the single particle gap, represents the energy required to create a separated electron-hole pair and has a considerable

polarization energy contribution. (1-2eV) [Hill 2000] exceeding so the optical gap E_{opt} by ~1 eV.

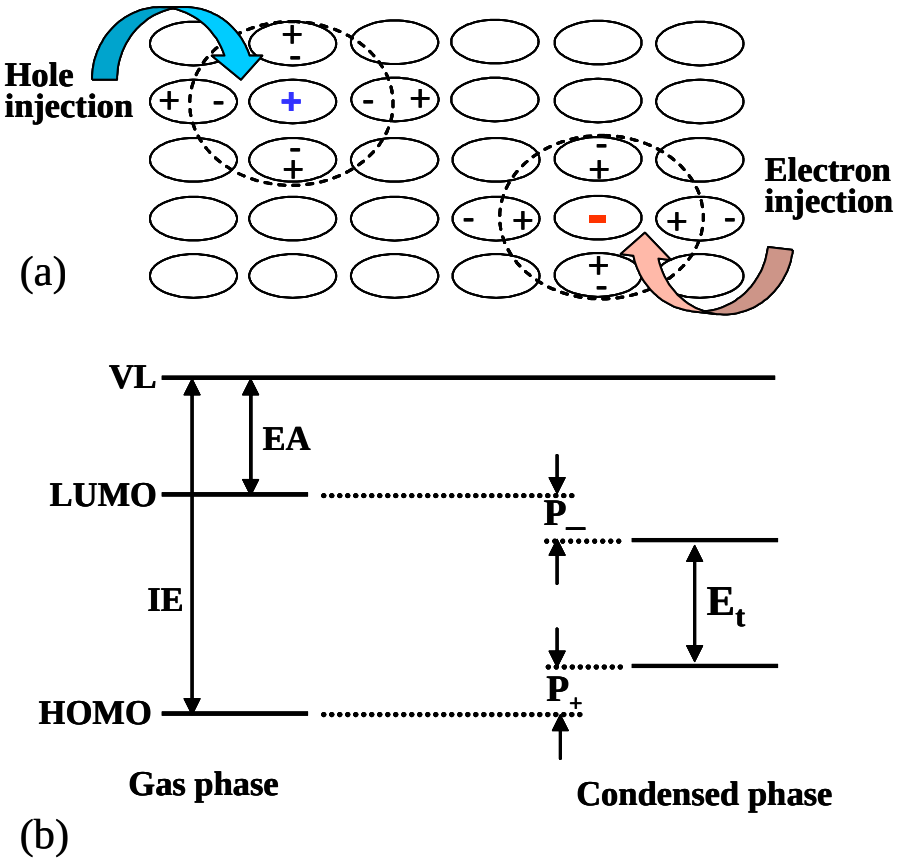

Figure 1.2 *(a) Schematic representation of a charge generation-process in crystalline molecular films. (b) Energy diagram showing the ionization energy (IE) and electron affinity (EA) of the gas phase molecule (on the left) and the relaxed electronic structure including polarization P_+ and P_- of the molecule in the condensed phase. Adapted from references [Tsiper 2002] and [Hill 2000], respectively.*

As shown in figure 1.2, E_t is equal to the difference between the ionization energy (IE) and electron affinity (EA) of the gas phase molecules reduced by the sum P of the energies of the electronic polarization. When a charge carrier is brought into a molecular solid, its field polarizes the surrounding molecules. A secondary polarization field, created by polarized molecules, contributes to the self-consistent polarization clouds that surround each charged particle. Formation of these polarization clouds is associated with the stabilization energy P_+ for cations (the holes) and P_- for anions (the electrons). The relation between the transport gap and polarization energy is given by:

$$E_t=IE-EA-(P_++P_-)$$

Since Coulomb interactions are long-ranged, polarization clouds can extend over many lattice constants and P, and hence E_t can be significantly different at the free surface,

near a metal-organic interface, in thin organic layers and in the bulk [Tsiper 2001]. The optical gap (E_{opt}) corresponds to the onset of optical absorption and the formation of a bound electron-hole pair or exciton. Because of the strong localization of carriers in molecular solids the exciton is generally an on-molecule (Frenkel) exciton. The difference between E_t and E_{opt} yields the binding energy of the exciton [Hill 2000].

Organic material	$E^{UPS/IPES}$ ±0.2 (eV)	E_t (surface) ±0.2 (eV)	E_t ±0.4(eV)	E_{opt}*(eV)	$E_t - E_{opt}$ ±0.4 (eV)
PTCDA	4.0	3.8	3.2	2.6	0.6

Table 1.1 *Parameters of transport gap, optical gap and exciton binding energy for thin films (50-100Å) of PTCDA on polycrystalline Au according to reference [Hill 2000].*

Table 1.1 summarizes some values related to the PTCDA thin films (50-100Å) grown on polycrystalline gold as obtained from a combined UPS and IPES experiment [Hill 2000]. The $E^{UPS/IPES}$ value represents the measured HOMO-LUMO peak-to-peak gap. The "surface" transport gap E_t(surface) is obtained from the $E^{UPS/IPES}$ value subtracting the vibrational contribution. The bulk transport gap E_t is obtained by subtracting the difference between the bulk and surface polarization energy (P_++P_-). The optical gap E_{opt} is obtained from the onset of the absorption experiments. The charge separation energy E_t-E_{opt} represents the exciton binding energy.

Considering these reported values, concepts such as polarization, molecular relaxation, electron-electron correlation must be taken into account when dealing with organic semiconductors, in particular when organic/inorganic are investigated to determine the charge injection barriers.

1.2 The PTCDA molecule

The aromatic compound 3, 4, 9, 10-perylene tetracarboxylic dianhydride, abbreviated PTCDA, is an electrically neutral pigment, commercially available in its form of a red powder (Sigma-Aldrich). Crystalline molecular materials such as PTCDA have been usually used as organic dyes, but the technological potential of their semiconducting and optical properties for device applications has been recognized several years ago [Forrest 1997].

The first organic-on-inorganic semiconductor heterojunction (OI-HJ) was demonstrated at Bell laboratories [Forrest 1982], although the objective of these early investigations was not the demonstration of an organic device. Rather, they were directed at understanding the properties of the organic semiconductor PTCDA. The test structure that was investigated consisted of a metal contact and a 100-500nm thick layer of PTCDA deposited onto the surface of a p-type Si substrate. It was anticipated that the PTCDA in the untreated state was an insulator, and that the structure would result in a simple metal-insulator-semiconductor (MIS) capacitor from which the dielectric constant and breakdown voltage of the organic film could be inferred. Surprisingly, rather than MIS capacitor characteristics, it was found that PTCDA formed a rectifying contact on Si, resulting in the first organic-inorganic semiconductor diode with nearly ideal characteristics.

After the demonstration of this first organic-inorganic (O-I) device, new lines of investigations of such O-I structures resulted in an increased number of publications and patents. It was found that the charge transport across the PTCDA film was primarily by injected hole conduction. Nevertheless, the question whether PTCDA is preferably a hole or an electron conductor is still opened currently. This is due to the fact that while the dianhydride groups of PTCDA are electron withdrawing, suggesting that it should behave as an n-type semiconductor; this is not the most important factor determining the conductive properties of the material.

In crystalline solids the relative mobilities of electrons and holes are determined by the crystal structure itself. For PTCDA thin films, grown under ultra-high vacuum conditions, hole-mobilities between μ_p=0.01 and 1cm^2 V^{-1}s^{-1}, were consistently found. As expected, higher mobilities are achieved under growth conditions that lead to a higher degree of stacking order [Forrest 1984].

In addition, large anisotropies in conductivity have been found as a result of intrinsic properties of PTCDA crystals. The hole mobility (μ_p) was found larger than that of electrons (μ_n) along the stacking direction, whereas the opposite situation was found parallel to the stacks.

The potential application of PTCDA as an optical material arises from large dielectric anisotropies ($\varepsilon_{\|}$=1.9±0.1 and $\varepsilon_{\perp}$=4.5±0.2) and high birefringence resulted, also, from the films structural anisotropy. Indices of refraction parallel to the plane of $n_{\|}$=2.0 and out of plane of $n_{\perp}$=1.36 were reported [Zang 1991b]. The ability of PTCDA to self-organize even on amorphous substrates and the above mentioned properties have been exploited in a waveguide-coupled detector [Zang 1991a].

PTCDA has been also exploited in the development of high frequency Schottky diodes for telecommunication purposes. In a recent application it was shown that the use of PTCDA in hybrid Ag/PTCDA/InP [Kowalski 1998] and Ag/PTCDA/GaAs [Park 2002] junctions results in a lowering of operating voltages. An estimate of 42 GHz is given for the high frequency limit for an optimized InP device, which is about one third of the frequencies obtained in the currently commercially available GaAs Schottky diodes.

1.2.1 Structural properties

PTCDA belongs to the class of perylene derivatives. It consists of 24 carbon atoms, 8 hydrogen atoms and 6 oxygen atoms ($C_{24}O_6H_8$), having a molecular mass of 392 amu. A schematic picture of the molecular structure is shown in figure 1.3. PTCDA has a planar rectangular geometry, consisting of a perylene core with two anhydride endgroups (O=C-O-C=O). The endgroups give rise to a quadrupole moment with the positive charge localized around the aromatic core and the negative charge localized around the anhydride groups.

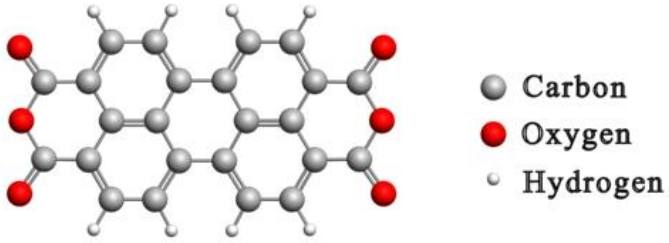

Figure 1.3 *Chemical structure of PTCDA (3, 4, 9, 10-perylene tetracarboxylic dianhydride).*

The PTCDA molecules crystallize in a monoclinic structure with the space group $P2_1/c$ and with two molecules per unit cell. Two polymorphic phases of very similar lattice constants but of different inclination of the axes (stacking axis) were observed. PTCDA

form crystals with layered molecular stacks. These layers are approximately parallel to the (102) planes. Within the layers the molecules are arranged in a herringbone like structure. All molecules are nearly coplanar within the layer.

The two polymorphs reported for thin films are: the α-PTCDA [Lovinger 1984] and the β-PTCDA [Mobus 1992, Ogawa 1999]. The crystal parameters are summarized in Table 1.2 and the two polymorphs are schematically shown in figure 1.4(a) and (b).

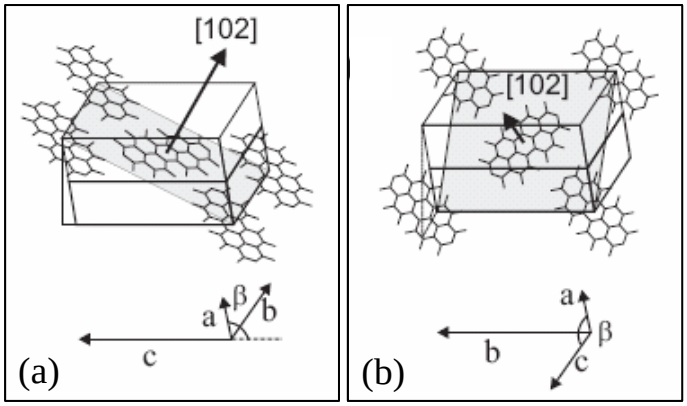

Figure 1.4 *Unit cells of α- and β-polymorph. After [Krause 2002].*

Bulk	**α-PTCDA**	**β-PTCDA**
Point group	C_{2h}	C_{2h}
a (Å)	3.74	3.78
b (Å)	11.96	19.30
c (Å)	17.34	10.77
β (º)	98.8	83.5
d_{102} (Å)	3.21	3.25
b_1 (Å)	19.91	19.30
b_2 (Å)	11.96	12.45
Volume (Å^3)	766.5	780.8
Unit cell area (Å^2)	238.1	240.3

Table 1.2 *Parameters of the monoclinic unit cell of PTCDA. a ,b, c and β are the parameters of the three-dimensional bulk unit cell; $\mathbf{b_1}$ and $\mathbf{b_2}$ are the parameters of the two-dimensional unit cell of PTCDA (102) plane; d_{102} is the distance between adjacent planes.*

The molecules are almost coplanar: an 11° tilt angle of the molecular plane with respect to the (102) lattice plane was reported for both crystal structures.

The distance (d_{102}) between adjacent molecular layers in the direction normal to the (102) lattice plane is 3.21Å for the α-polymorph and 3.25Å for the β-polymorph, respectively.

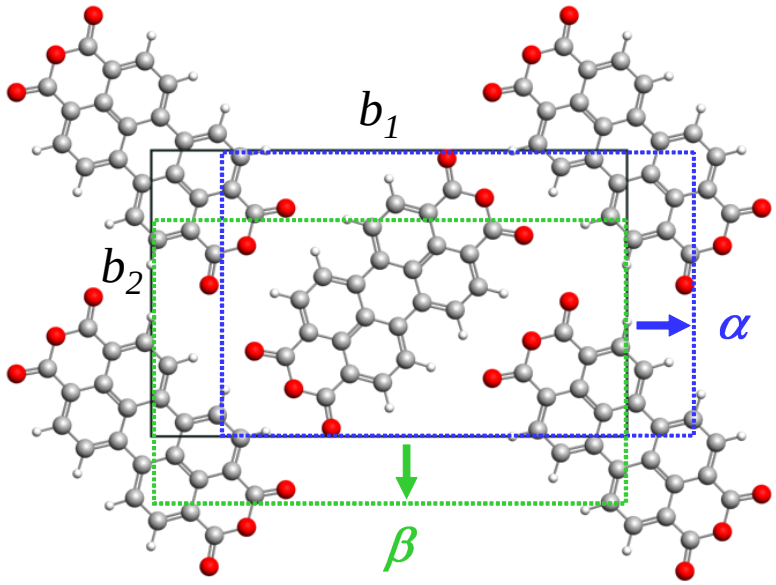

Figure 1.5 *Herringbone packing of PTCDA in the (102) plane. The solid line corresponds to the rectangular unit cell with the lattice vectors* $\boldsymbol{b_1}$ *and* $\boldsymbol{b_2}$*. Dashed lines blue/green represent the in plane projected unit cells of a consecutive molecular layer, translated in the direction characteristic to* α*- and* β*-polymorphs.*

The main difference between both polymorphs is the vertical stacking direction of adjacent molecular layers. This is schematically shown in figure 1.5. The translation of the unit cell of a consecutive layer along the $\boldsymbol{b_1}$ lattice vector corresponds to the α-phase, whereas the translation along the $\boldsymbol{b_2}$ lattice vector corresponds to the β-phase.

1.2.2 Electronic structure

This section presents the electronic structure of the free PTCDA molecule according to DFT (density functional theory) first-principles calculations performed by O. Paz and J. M. Soler at Departamento de Física de Materia Condensada at Universidad Autónoma de Madrid. The electronic structure was calculated using the SIESTA method [Soler 2002] in the local density approximation (LDA) [Perdew 1981]. Figure 1.6 shows the energy level diagram of the PTCDA molecular orbitals relative to the Fermi level. The molecular orbitals are labeled according to their symmetry. The

PTCDA molecule has three C_2 axis of symmetry which can transform the molecule into itself upon rotation of 180º, three planes with reflection symmetry *σ(xy)*, *σ(xz)*, *σ(yz)* and an inversion (*I*) center. As a result, the symmetry of all molecular orbitals can be described by the D_{2h} point group (see Table 1.3).

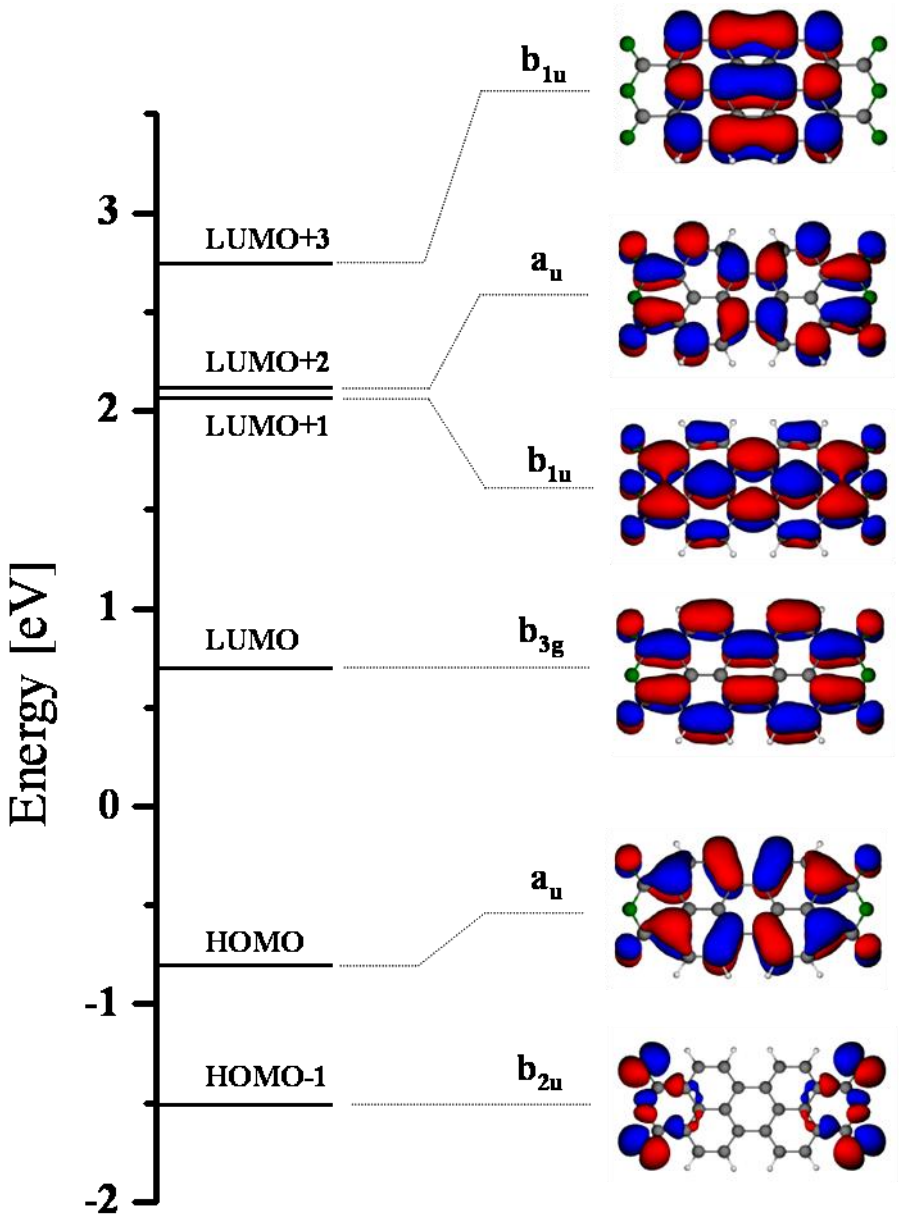

Figure 1.6 *Energy level diagram of PTCDA molecular orbitals with respect to the Fermi level calculated for the free PTCDA molecule using DFT-LDA. The molecular orbitals are labeled according to their symmetry operation corresponding to the D_{2h} point group. The molecular orbitals are represented slightly rolled, relative to their longitudinal axis for a better visualization of the sign of the molecular orbital wave function, represented by red/blue colors (from O. Paz).*

D_{2h}	E	$C_2(z)$	$C_2(y)$	$C_2(x)$	i	$\sigma(xy)$	$\sigma(xz)$	$\sigma(yz)$
a_g	1	1	1	1	1	1	1	1
b_{1g}	1	1	-1	-1	1	1	-1	-1
b_{2g}	1	-1	1	-1	1	-1	1	-1
b_{3g}	1	-1	-1	1	1	-1	-1	1
a_u	1	1	1	1	-1	-1	-1	-1
b_{1u}	1	1	-1	-1	-1	-1	1	1
b_{2u}	1	-1	1	-1	-1	1	-1	1
b_{3u}	1	-1	-1	1	-1	1	1	-1

Table 1.3 *Character table corresponding to the D_{2h} point group. First column represents the symmetry labels, first line corresponds to symmetry elements and the numbers represent the effect of the symmetry operations on the molecule properties.*

Table 1.4 summarizes the energy position of the molecular orbitals, according to the DFT-LDA calculations, relative to the Fermi level, along with the energy separation between consecutive orbitals. It can be observed that the highest occupied molecular orbital (HOMO) is well separated from the lowest unoccupied molecular orbital (LUMO). Nevertheless, the PTCDA gap represented by the HOMO-LUMO energy difference has a smaller value (~1.5eV) in comparison to values reported experimentally for the PTCDA gas phase. DFT is known to underestimate the gap.

Molecular orbitals	$E-E_F$(eV)	Energy difference (eV)
LUMO+3	2.75	0.63
LUMO+2	2.12	0.05
LUMO+1	2.07	1.37
LUMO	0.70	1.51
HOMO	-0.81	0.70
HOMO-1	-1.51	

Table 1.4 *Energy positions of the molecular orbitals relative to the E_F and the corresponding energy separation between consecutive molecular orbitals.*

The calculated electronic structure of the free PTCDA molecule will be used as a reference in the following chapters, since a direct comparison of the original molecular orbitals to those resolved in STM images will help in the understanding of the adsorption process and the interaction strength at different molecule-substrate interfaces. The degree of molecule-substrate interaction at different interfaces can be inferred from the modification of the spatial distribution of the molecular orbitals and their relative energy positions.

1.3 Experimental details

Most of the experiments presented in this thesis, in particular the STM experiments performed at room temperature, were carried out in an ultra-high vacuum (UHV) system designed by J. I. Pascual at the Laboratorio de Nuevas Microscopias (LNM) at Universidad Autónoma de Madrid [Pascual 1998] (figure 1.7(a)). The UHV system is divided in two parts: the preparation chamber and the STM chamber. The chambers separated by a valve, are individually pumped by two ion pumps, reaching a base pressure below 1×10^{-10} Torr. The pumping capacity may be increased by two titanium sublimation pumps existing in each of the chambers. The forevacuum stage consists of a turbomolecular pump which is coupled in series with an oil-free primary pump. A load-lock entry allows a rapid exchange of samples and tips without breaking the vacuum.

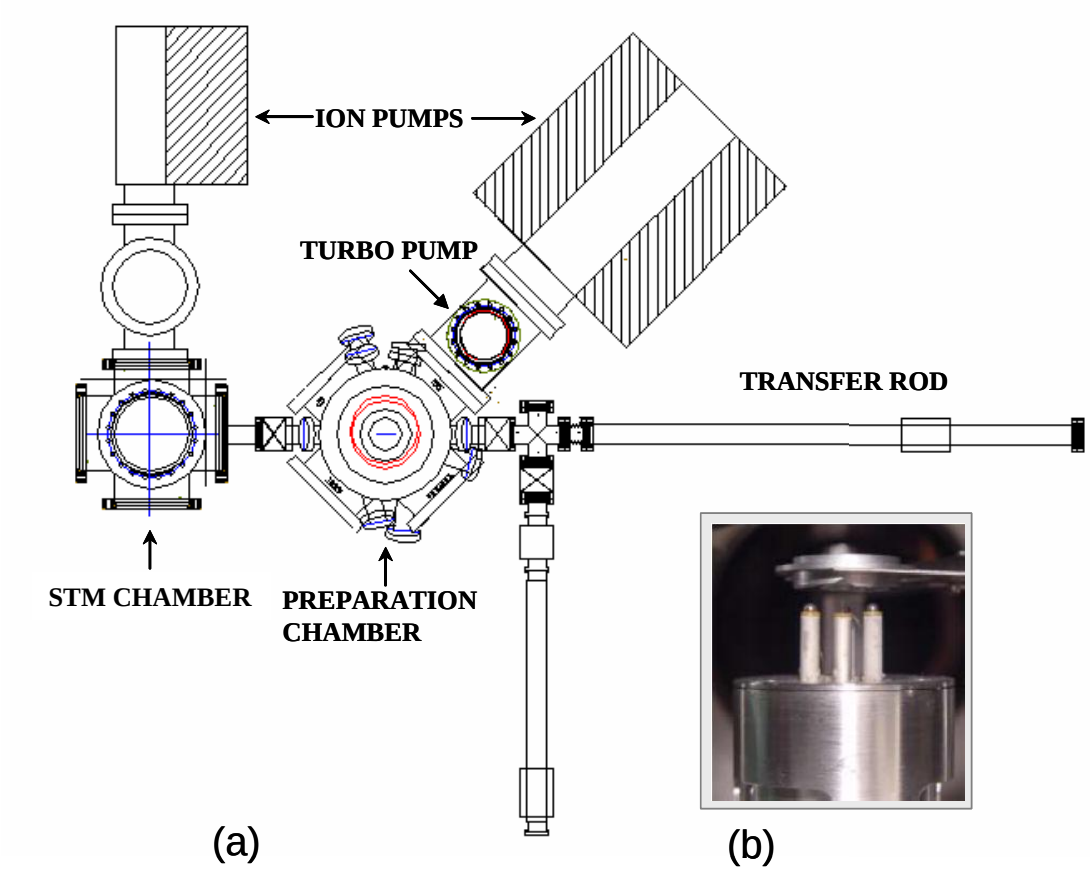

Figure 1.7 *Schematic top view of the UHV system shows the different components. [Pascual 1998]. (b) Beetle type microscope [Custance 2002].*

The preparation chamber includes several facilities for sample preparation and characterization. The cleaning of the samples is carried out by means of heaters by electron bombardment and/or ion sputtering with an ion gun. Several home-made

evaporators with tantalum crucibles are available for the evaporation/sublimation of different materials. The evaporation rate and the purity of evaporated materials (PTCDA, Pb, or Sn) are monitored by a quartz crystal microbalance and a quadrupole mass spectrometer (QMS), respectively. The surface structure and the sample cleanness are check by using low energy electron diffraction (LEED) and Auger electron spectroscopy (AES). STM tips (W, 0.3mm diameter) are prepared by electrochemical etching followed by *in situ* preparation by means of field emission treatment [Mendez 1996, Mendez 1998].

The scanning tunneling microscope (figure 1.7(b)) housed in the other chamber is a home-built Beetle type microscope, operated at room temperature, designed and mounted by O. Custance at the LNM. Details of the microscope properties are found in reference [Custance 2002]. Some STM data were measured at low temperature (40K) by means of a home-made UHV variable temperature STM microscope (VT-STM) also completely designed and built by O. Custance at the LNM [Custance 2002].

The main part of this work, which represents the STM data acquisition and processing, was possible thanks to the versatile and user-friendly WS×M software, which controls a hardware system, based on a DSP (digital signal processor) board incorporated in the main computer. Features of the software and hardware may be found in a recent review [Horcas 2007].

Photoemission experiments (angle-resolved ultraviolet photoemission spectroscopy, ARUPS, and X-ray photoelectron spectroscopy, XPS), have been performed in a separate UHV chamber located in ICMM and equipped with a HeI (21.2eV) radiation source, an X-ray Mg K_α source and a hemispherical energy analyzer Phoibos 100 (Specs GmbH). The UHV chamber has similar facilities for sample preparation and molecular deposition.

References

[Baldo 1997] M. A. Baldo, V. G. Kozlov, P. E. Burrows, S. R. Forrest, V. S. Ban, B. Koene and M. E. Thompson, *Low Pressure Organic Vapor Phase Deposition of Small Molecular Weight Organic Light Emitting Device Structures*, Applied Physics Letters **71**, 3033 (1997).

[Baldo 1998] M. A. Baldo, D. F. O'Brien, Y. You, A. Shoustikov, S. Sibley, M. E. Thompson and S. R. Forrest, *Highly Efficient Phosphorescent Emission from Organic Electroluminescent Devices,* Nature **395**, 151 (1998).

[Baldo 2000] M. A. Baldo, M. E. Thompson and S. R. Forrest, *High-Efficiency Fluorescent Organic Light-Emitting Devices Using a Phosphorescent Sensitizer*, Nature **403**, 750 (2000).

[Custance 2002] O. Custance, *PhD Thesis*, Universidad Autónoma Madrid (2002).

[Forrest 1982] S. R. Forrest, M. L. Kaplan, P. H. Schmidt, W. L. Feldmann and E. Yanowski, *Organic-on-Inorganic Semiconductor Contact Barrier Devices*, Applied Physics Letters **41**, 90 (1982).

[Forrest 1984] S. R. Forrest, *Organic-on-Organic Semiconductor Contact Barrier Diodes. Dependence on Organic Film and Metal Contact Properties*, J. Appl. Phys. **56**, 543 (1984).

[Forrest 1997] S. R. Forrest, *Ultrathin Organic Films Grown by Organic Molecular Beam Deposition and Related Techniques*, Chemical Reviews **97**, 1793 (1997).

[Friend 1999] R. H. Friend, R. W. Gymer, A. B. Holmes, J. H. Burroughes, R. N. Marks, C. Taliani, D. D. C. Bradley, D. A. D. Santos, J. L. Bredas, M. Logdlund and W. R. Salaneck, *Electroluminescence in Conjugated Polymers*, Nature **397**, 121 (1999).

[Hill 2000] I. G. Hill, A. Kahn, Z. G. Soos and R. A. Pascal, *Charge-Separation Energy in Films of Pi-Conjugated Organic Molecules*, Chemical Physics Letters **327**, 181 (2000).

[Horcas 2007] I. Horcas, R. Fernandez, J. M. Gomez-Rodriguez, J. Colchero, J. Gomez-Herrero and A. M. Baro, *WSxM: A Software for Scanning Probe Microscopy and a Tool for Nanotechnology*, Review of Scientific Instruments **78**, 013705 (2007).

[Ishii 1997] H. Ishii and K. Seki, *Energy Level Alignment at Organic/Metal Interfaces Studied by UV Photoemission: Breakdown of Traditional Assumption of a Common Vacuum Level at the Interface*, IEEE Transactions on Electron Devices **44**, 1295 (1997).

[Kowalski 1998] W. Kowalsky, DFG-Abschlussbericht Ko 1040/7-1, TU Braunschweig, Institut für Hochfrequenztechnik (1998).

[Krause 2002] B. Krause, *PhD Thesis*, Stuttgart University (2002).

[Lovinger 1984] A. J. Lovinger, S. R. Forrest, M. L. Kaplan, P. H. Schmidt and T. Venkatesan, *Structural and Morphological Investigation of the Development of Electrical Conductivity in Ion-Irradiated Thin Films of an Organic Material*, Journal of Applied Physics **55**, 476 (1984).

[Meissner 2001] D. Meissner and J. Rostalski, *Photovoltaics of Interconnected Networks*, Synthetic Metals **121**, 1551 (2001).

[**Mendez 1996]** J. Méndez, *PhD Thesis*, Universidad Autónoma Madrid (1996).

[**Mendez 1998]** J. Méndez, J. Gómez-Herrero, J. I. Pascual, A. M. Baró, *Formation of new terraces via diffusion induced by the field gradient in scanning tunneling microscopy*, Applied Physics A **66**, S767(1998).

[Mobus 1992] M. Mobus, N. Karl and T. Kobayashi, *Structure of Perylene-Tetracarboxylic-Dianhydride Thin Films on Alkali Halide Crystal Substrates*, Journal of Crystal Growth **116**, 495 (1992).

[Ogawa 1999] T. Ogawa, K. Kuwamoto, S. Isoda, T. Kobayashi and N. Karl, *3,4,9,10-Perylenetetracarboxylic Dianhydride (PTCDA) by Electron Crystallography*, Acta Crystallographica B-Structural Science **55**, 123 (1999).

[Ostrick 1997] J. R. Ostrick, A. Dodabalapur, L. Torsi, A. J. Lovinger, E. W. Kwock, T. M. Miller, M. Galvin, M. Berggren and H. E. Katz, *Conductivity-Type Anisotropy in Molecular Solids*, Journal of Applied Physics **81**, 6804 (1997).

[Park 2002] S. Park, *PhD Thesis*, Chemnitz University (2002).

[Pascual 1998] J. I. Pascual, *PhD Thesis*, Universidad Autónoma Madrid (1998).

[Perdew 1981] J. P. Perdew and A. Zunger, *Self-Interaction Correction to Density-Functional Approximations for Many-Electron Systems*, Physical Review B **23**, 5048 (1981).

[Peumans 2003] P. Peumans, A. Yakimov and S. R. Forrest, *Small Molecular Weight Organic Thin-Film Photodetectors and Solar Cells*, Journal of Applied Physics **93**, 3693 (2003).

[Shtein 2001] M. Shtein, H. F. Gossenberger, J. B. Benziger and S. R. Forrest, *Material Transport Regimes and Mechanisms for Growth of Molecular Organic Thin Films Using Low-Pressure Organic Vapor Phase Deposition*, Journal of Applied Physics **89**, 1470 (2001).

[Soler 2002] J. M. Soler, E. Artacho, J. D. Gale, A. Garcia, J. Junquera, P. Ordejon and D. Sanchez-Portal, *The Siesta Method for Ab Initio Order-N Materials Simulation*, Journal of Physics-Condensed Matter **14**, 2745 (2002).

[Tang 1986] C. W. Tang, *Two-Layer Organic Photovoltaic Cell*, Applied Physics Letters **48**, 183 (1986).

[Tang 1987] C. W. Tang and S. A. VanSlyke, *Organic Electroluminescent Diodes*, Applied Physics Letters **51**, 913 (1987).

[Tsiper 2001] E. V. Tsiper and Z. G. Soos, *Charge Redistribution and Polarization Energy of Organic Molecular Crystals*, Physical Review B **64**, 195124 (2001).

[Tsiper 2002] E. V. Tsiper, Z. G. Soos, W. Gao and A. Kahn, *Electronic Polarization at Surfaces and Thin Films of Organic Molecular Crystals: PTCDA*, Chemical Physics Letters **360**, 47 (2002).

[Xu 2007] M. Xu, M. Sakai, K. Kudo, *High-Performance Bottom-Contact Organic Thin-Film Transistors with Controlled Molecule-Crystal/Electrode Interface*, Advanced Materials **19**, 371 (2007).

[Xue 2001] J. Xue and S. R. Forrest, *Organic Thin-Film Transistors Based on Bis(1,2,5-Thiadiazolo)-P-Quinobis (1,3-Dithiole)*, Applied Physics Letters **79**, 3714 (2001).

[Zang 1991a] D. Y. Zang, Y. Q. Shi, F. F. So, S. R. Forrest and W. H. Steier, *Optical Waveguides in Crystalline Organic Semiconductor Thin Films*, Applied Physics Letters **58**, 562 (1991).

[Zang 1991b] D. Y. Zang, F. F. So and S. R. Forrest, *Giant Anisotropies in the Dielectric Properties of Quasi-Epitaxial Crystalline Organic Semiconductor Thin Films*, Applied Physics Letters **59**, 823 (1991).

CHAPTER 2

The Weakly Interacting System PTCDA/Au(111)

2 The Weakly Interacting System PTCDA/Au(111)

2.1 Introduction

PTCDA and its derivatives have been considered as model systems and have been extensively studied on a wide range of substrates. Due to the vast literature covering this topic, we will briefly mention only the adsorption of PTCDA molecules on close-packed noble metal surfaces, highlighting the structural and electronic properties at the organic/metal interface which are relevant for the discussion of the results obtained in this work.

Most of previous studies have been focused on structural properties and the growth mode of PTCDA on several metal substrates such as silver [Seidel 1997, Krause 2002, Chkoda 2003, Kilian 2004, Braun 2005, Temirov 2006], copper [Stohr 2002, Wagner 2004, Gerlach 2007] and gold [Fenter 1995, Fenter 1996, Fenter 1997, Schmitz-Hübsch 1997, Chizhov 2000, Mannsfeld 2001, Kilian 2006, Méndez 2006, Henze 2007]. On clean noble metal surfaces, the deposition of PTCDA molecules generally results in the formation of highly ordered layers. In the sub-monolayer regime PTCDA forms large domains consisting of well-ordered molecules, with PTCDA adsorbed with the molecular plane nearly parallel to the substrate. On most of the substrates, PTCDA molecules assemble in a herringbone structure, with a rectangular unit cell consisting of two almost coplanar molecules. Besides the typical herringbone arrangement, a square phase has been reported upon PTCDA deposition on gold surfaces [Chizhov 2000]. For higher coverage, a layer-by-layer growth has been generally reported for the first several layers [Fenter 1995], followed by island formation for multilayer coverage [Chizhov 2000]. Nevertheless, preparation conditions, e.g. evaporation rate or substrate temperature, can significantly influence the structure, morphology and the growth mode.

It is generally accepted that the structure and the morphology of the molecular layers are strongly related to the processes that take place at the organic/metal interface. Therefore, a better understanding of molecule-substrate coupling and the resulting local electronic structure has motivated recent research. In earlier studies of these organic/metal interfaces, it has been assumed that PTCDA molecules, which are adsorbed in a flat lying geometry on metal surfaces, interact with the substrate mainly via π states, delocalized over the perylene core. This interaction would explain the high molecular mobility on these surfaces, favoring the self assembly [Stahl 1998], but could

not account for site selectivity. As well, it was expected that due to the relative large size of the PTCDA molecule with respect to the substrate periodicity, the molecules could not anchor in preferred adsorption sites.

More recently, it has been found that the structural relation between molecular overlayer and substrate is highly influenced by the interaction strength [Hooks 2001]. A weak adsorbate-substrate interaction usually leads to incommensurate structures, whereas site specific bonding promotes the formation of commensurate structures, as in the case of PTCDA/Ag(111) [Umbach 1998]. Additionally, it has been observed an intermediate type of epitaxy, the so-called point-on-line coincidence [Hoshino 1994], which has been found for organic/metal systems where weak or negligible chemical reaction take place at the interface, e.g. PTCDA/Au(111) [Schmitz-Hübsch 1997].

The most extensive research, related to molecule-substrate coupling has been dedicated to the PTCDA/Ag(111) interface, which has been considered as a model system, due to the commensurate structure which PTCDA forms on this surface.

A first evidence of a covalent π-bonding at the PTCDA/Ag(111) interface has been observed in near-edge X-ray absorption fine structure (NEXAFS) measurements [Taborski 1995]. These results have been supported later by scanning tunneling microscopy data. Submolecularly resolved STM images obtained for the adsorbed PTCDA monolayer, as displayed in figure 2.1(a), have indicated that the LUMO is the dominant contribution to the bonding [Glockler 1998, Shklover 2000].

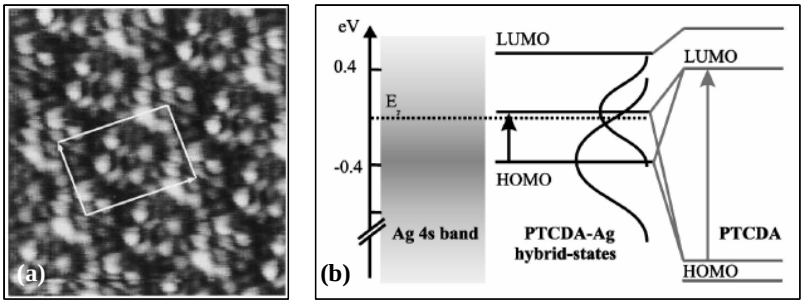

Figure 2.1 *(a) STM image of the PTCDA monolayer on the Ag(111) surface. Tunneling parameters V=+0.2V; I=1.3nA; scan area: 45Å×45Å. The partial occupancy of the original LUMO can be concluded from the fact that it can be imaged under positive and negative voltage. (adapted from reference [Glockler 1998]). (b) Semi-quantitative energy level scheme for PTCDA/Ag(111) interface indicating the hybridization of PTCDA molecular orbitals with the Ag 4s band (adapted from reference [Tautz 2002]).*

A partial occupancy of the original LUMO has been proved by the fact that this orbital can be imaged under positive and negative bias conditions for energies close to the Fermi level, resulting in the metallic character at the interface.

A chemisorption process has been confirmed afterwards, from high-resolution electron energy-loss spectroscopy (HREELS) and ultraviolet photoemission spectroscopy (UPS) measurements. Experimental results have shown that both HOMO and LUMO PTCDA molecular levels are broadened significantly due to the hybridization with the silver 4s band. The results have been explained by a charge transfer due to a chemical bond formation. An energy level scheme has been proposed for the PTCDA/Ag(111) interface [Tautz 2002], as shown in figure 2.1(b).

Recent findings [Eremtchenko 2003, Eremtchenko 2004], have indicated the existence of two different adsorption sites on Ag(111). Moreover, it has been proposed that the PTCDA central aromatic ring is the main contribution to the bonding with the Ag surface. Hauschild *et al*. have found by normal incidence X-ray standing wave measurements (NIXSW) that the carboxylic O atoms could also be involved in the bonding, as density functional theory (DFT) calculations have shown that at the interface, the molecule is adsorbed in a distorted configuration with the carboxylic O atoms slightly closer to the Ag surface than the central aromatic core [Hauschild 2005].

The electronic properties of a similar system, formed by PTCDA molecules and another noble metal surface have been recently investigated [Ugeda M.M]. The adsorption of 1ML PTCDA on Cu(111), has been studied by STM and STS and the results obtained are qualitatively comparable with those reported for PTCDA/Ag interface. Scanning tunneling spectroscopy results, obtained on the PTCDA monolayer adsorbed on Cu(111) have shown a broadened band crossing the Fermi level, indicating metallic character at the interface.

It has been proposed that as a result of chemisorption, a charge transfer from Cu(111) metal surface into the lowest unoccupied molecular orbital (LUMO), leads to a shift of the LUMO molecular band close to the Fermi level, hence explaining the metallic character of the interface. This assumption is confirmed by high resolution STM images, acquired for energies close to the Fermi level, as shown in figure 2.2(a) and 2.2(b). It can be observed that the spatial distribution observed for individual molecules in both images acquired at low positive and negative bias voltage is closely related to the calculated LUMO of the free molecule, displayed in figure 2.2(d).

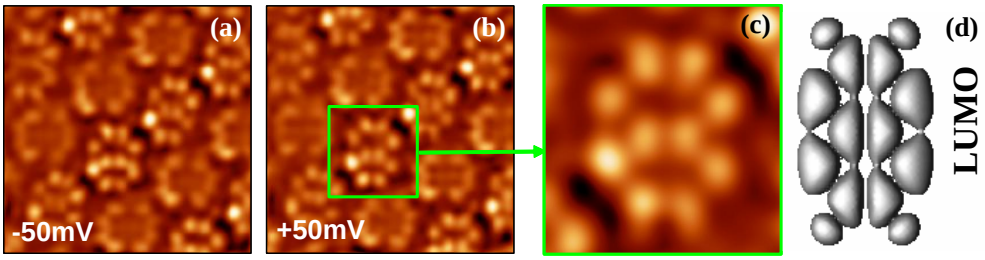

Figure 2.2 *Electronic structure at the PTCDA/Cu(111) interface. Intramolecular resolution is observed in simultaneously acquired STM constant height images where the PTCDA LUMO is resolved under negative (a) and positive (b) bias voltage for energies close to the* E_F*. A qualitative agreement is observed from the comparison of the spatial distribution of an individual molecule obtained in STM images (c) and the calculated LUMO of the free PTCDA molecule (d). From [Ugeda M. M.].*

Although details related to the adsorption configuration, bonding site or interaction strength are most likely distinct for these two PTCDA/Ag and PTCDA/Cu interfaces, an essential feature of the molecular adsorption can be remarked from the above mentioned results. The molecule-substrate coupling at these organic/metal interfaces has been proven to rely on a charge transfer process, as a consequence of a chemical bond formation.

The PTCDA adsorption on Au(111) noble metal surfaces has also received considerable attention. While most of the studies have investigated the structural and morphological aspects for the growth of PTCDA on Au surfaces, detailed knowledge about metal-molecule bonding are currently undefined, in particular due to the lack of information concerning the adsorption sites or precise adsorption configuration on this substrate. Reports on the electronic properties at PTCDA/Au(111) interface [Tsiper 2002, Vazquez 2004, Vazquez 2007] suggest a much weaker interaction as compared with the other PTCDA/metal interfaces, in spite of the similarity among noble metal surfaces.

The aim of the study presented in this chapter was to gain further knowledge concerning the electronic properties of the PTCDA/Au(111) interface, in order to contribute to a more complete picture of this system and to compare it with the results obtained for other similar PTCDA/noble metal interfaces. In particular, in the detailed analysis of this organic/metal interface, it has not been investigated so far the influence of an organic adsorbate layer on Shockley-type surface states existing on Au(111) surface, issue which is addressed in the present work. In this chapter we have investigated the electronic properties of the PTCDA/Au(111) interface using a combination of several surface characterization techniques.

The STM has demonstrated its ability for the investigation of ordered organic films grown on different substrates, providing structural and morphological properties. Besides the topographical imaging, information about the surface density of states from the voltage dependence of the current can be obtained from scanning tunneling spectroscopy (STS). The advantage of STS, compared to other spectroscopic techniques, is to locally probe the electronic properties. Nevertheless its interpretation is not straightforward due to the convolution with the tip states. In this sense the combination of STS and ultraviolet photoemission spectroscopy (UPS) has proved to be a powerful tool to determine electronic properties at the interface.

Interfacial electronic coupling (mixing of the molecular orbitals with the metal bands together with electrostatic effects as interface dipole formation) is known to determine the energetic alignment of the molecular levels with the metal Fermi level. Experimentally, this interfacial coupling may be determined by surface electronic spectroscopies, such as ultraviolet photoemission spectroscopy (UPS) or line shape analysis in core level photoemission spectroscopy (XPS), as will be shown in this chapter for the PTCDA/Au(111) system.

2.2 Sample preparation and experimental set-ups

STM and STS experiments were carried out with a home-built ultra-high vacuum (UHV) STM [Pascual 1998, Custance 2002] system described in section 1.3. Photoelectron spectroscopy measurements (ARUPS and XPS) were performed in a separate UHV chamber equipped with a HeI (21.2eV) radiation source, an X-ray Mg Kα source and a hemispherical energy analyzer, Phoibos 100 (Specs GmbH).

The Au(111) single crystal (hat shape Ø=9mm, 1.2mm thickness) was purchased from MaTeck GmbH, (99.999% purity, surface roughness<0.03μm, orientation accuracy <0.1°). The Au(111) surface was prepared by several standard sputter-annealing cycles (sputtering at energies of ~1kV, with an Ar pressure of ~1×10^{-6}, sample current 3-4μA, and annealing for 10-15 minutes at ~800 K).

PTCDA was sublimated from a home-made Ta crucible. Previous degassing of the PTCDA source was performed for several hours. In all experiments, the Au(111) substrate was kept at room temperature during the deposition. A deposition rate of about 0.5ML per minute was calibrated via scanning tunneling microscopy and previously by a quartz crystal microbalance. In this study 1ML corresponds to a PTCDA close-packed structure with ~2.4 PTCDA molecules/substrate unit cell area (i.e. 316.2Å^2, corresponding to the $22\times\sqrt{3}$ reconstructed Au(111) surface). Prior to the photoemission experiments, a careful estimation of the PTCDA coverage was performed from XPS measurements.

2.3 Au(111) substrate

2.3.1 Structural properties

In contrast to all other (111) faces of noble metals, the Au(111) surface exhibits a particular reconstruction, which was extensively studied by different techniques, such as low energy electron diffraction (LEED) [Perdereau 1974, Van Hove 1981], transmission electron microscopy (TEM) [Heyraud 1980, Tanishiro 1981] and scanning tunneling microscopy (STM) [Wöll 1989, Barth 1990].

In STM images, as shown in figure 2.3, the reconstructed Au(111) surface shows a periodic zig-zag pattern, consisting of pairs of parallel lines, which are observed with an enhanced contrast in the images.

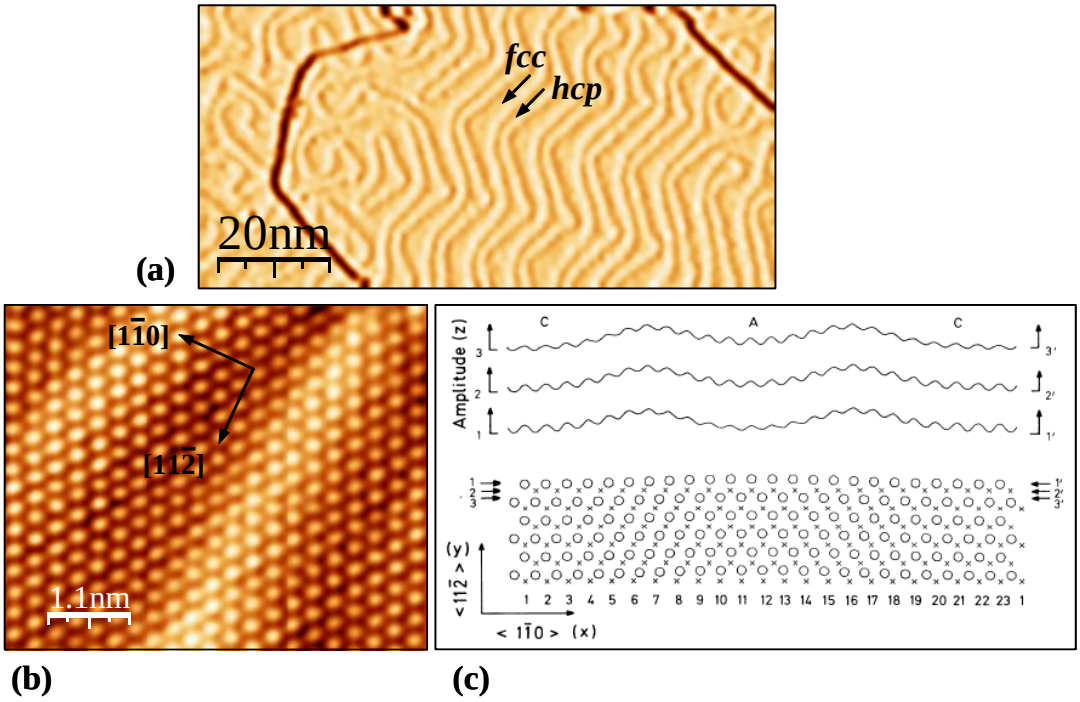

Figure 2.3 *(a) Topographic STM image showing the herringbone reconstructed Au(111) surface, where alternating fcc and hcp stacking domains are visible (98nm×47nm, V=-0.6V, I=0.3nA). (b) Atomically resolved STM image (5.5nm×4.5nm, V=+0.5V, I=2.3nA). (c) Schematic of the Au(111)-22×$\sqrt{3}$ reconstruction, after [Harten 1985].*

It has been found that the surface rearrangement is based on a compression of the outermost atomic layer. While the atoms of the unreconstructed surface reside on fcc positions, the reconstructed surface presents a contraction of the topmost layer along the [1$\bar{1}$0] direction. This contraction gives rise to alternate regions, with the atoms residing on fcc and hcp positions, respectively. The narrow and wide regions between parallel

lines, observed in the images, correspond to these hcp and fcc stacking regions, respectively. This anisotropic contraction along $[1\bar{1}0]$direction is due to the fact that 23 gold atoms of the surface layer are arranged over 22 bulk lattice sites, leading to a (22×√3) overlayer structure and the creation of alternating domains of hcp and fcc stacking. The fcc and hcp areas are separated by ~0.2Å height domain walls, which are formed by surface atoms located near bridge sites. The direction of the boundaries along the $[11\bar{2}]$ direction is periodically rotated by 120°, forming the characteristic herringbone pattern.

2.3.2 Electronic properties

The broken periodicity at single crystal Au(111) surfaces modifies the electronic structure at the surface compared to that of the bulk and gives rise to surface localized states. Electrons in the surface states are confined to the surface region by a projected bulk band-gap on one side, and by the vacuum barrier on the other side. The wave function of surface states electrons has the maximum amplitude near the surface, and it decays exponentially both into the vacuum side and the bulk side. Electrons occupying such states are therefore confined in the direction perpendicular to the surface. In the directions parallel to the surface, they have a free electron like behavior, and correspondingly the wave function associated to surface states can be described as a plane wave, $\psi_{k_\parallel}(r) \propto e^{(ik_\parallel r)}$, where $k_\parallel$ is a wave vector parallel to the surface.

Since the first observation of the Shockley-type surface states [Shockley 1939, Gartland 1975] on (111) surfaces of noble metals (Cu, Ag, Au), there has been a continuous interest in the study of their dispersion relation, temperature dependence, life time or their interaction with adsorbates.

Au(111) exhibits a surface state, laying in the projected "neck" (L-gap) of bulk states as shown in figure 2.4(a). The behavior of this surface state has been investigated in numerous studies [Kevan 1987, Paniago 1995, LaShell 1996, Reinert 2001, Reinert 2003, Forster 2006]. It has been reported a parabolic dispersion, centered at the $\bar{\Gamma}$ -point of the surface Brillouin zone. This parabolic dispersion can be described according to the 2D free electron gas model expressed by: $E(k_\parallel) = E_0 + \hbar^2 k_\parallel^2 / 2m^*$, where E_0 is the band bottom and m^* is the effective mass. For Au(111) surface, recent high resolution and low temperature photoemission experiments determined: E_0=-487±1meV,

k_F=0.167/0.192Å^{-1} and m^*/m_0=0.255, where m_0 is the free electron mass and k_F is the Fermi wavevector [Reinert 2001].

A particular characteristic of the Au(111) is a splitting of the surface states, as reported first by [LaShell 1996]. This particular splitting, not observed for other noble metal surfaces, is currently explained as due to a spin-orbit coupling that breaks the spin degeneracy in the system. This splitting results in a two dimensional Fermi surface contour consisting of two concentric rings and a split dispersion giving two parabolas shifted in opposite $k_{\|}$ direction from the high symmetry $\overline{\Gamma}$ -point, as shown in figure 2.4.

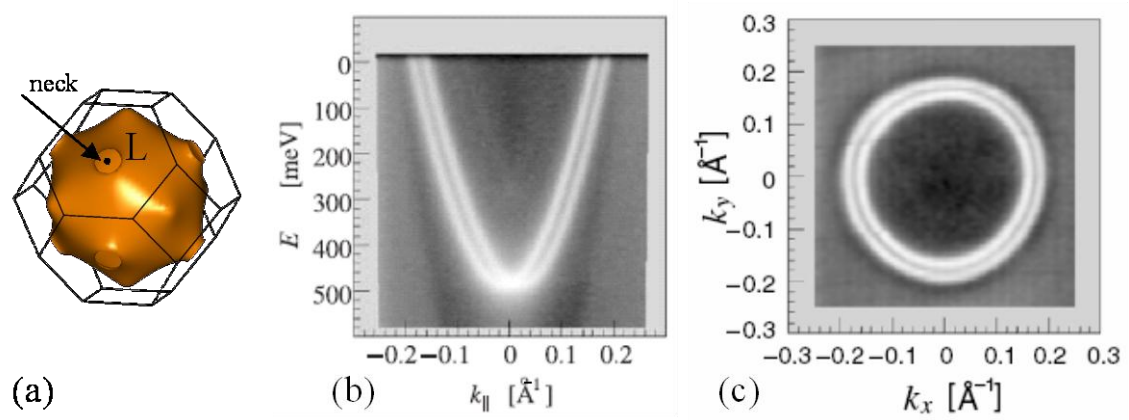

Figure 2.4 *(a) Bulk Fermi surface of Au(111). (b) Photoemission intensity of the Shockley-type surface states on Au(111) as a function of energy and momentum. (c) The two dimensional Fermi surface map displays two concentric rings representing the spin-orbit split of the surfaces states embedded in the projected L-gap of the bulk states. (b) and (c) from reference [Reinert 2004].*

Although photoemission spectroscopy experiments were usually employed for the investigation of the surface states, recently, results obtained by means of STM/STS have demonstrated that properties of surfaces states, such as lifetime width of Shockley states at the band minimum can be determined, in excellent agreement with results from photoemission experiments. Furthermore, a detailed analysis of the energy dependent spatial distribution of the tunneling current can give information about the surface state dispersion, both below and above the Fermi level, and the topology of the Fermi surface. Direct imaging in real space of surface states on (111) noble metals by STM was first reported by Crommie *et al*. [Crommie 1993] and by Hasegawa and Avouris [Hasegawa 1993].

As indicated by their parabolic dispersion around $k_{\|}$=0, the Shockley-type surface states can be considered as a 2D free electron gas. Interference of incident and scattered 2D electron waves with substrate imperfections, caused by steps, defects or adsorbates,

results in the periodic oscillations in the local density of states (LDOS). The visualization of these oscillations in the local density of states can be successfully done by acquiring STM images at low voltage and at low temperature. By using such a low tunneling bias voltage, constant current STM images can be interpreted as a map of LDOS at the Fermi level. These oscillations have a characteristic wavelength λ, which is related to the $k_{\|}$ vector by the relation $k_{\|}=2\pi/\lambda$. Since the LDOS is proportional to the square of the wave function, the relation will be $k_{\|}=\pi/\lambda$.

When an electron wave is incident on a step, the reflected part of the wave can then interfere with the incident part, resulting in an oscillatory local density of states (LDOS), in the vicinity of a step. A qualitative interpretation for the observed oscillations, close to the step edge, can be obtained if the surface states in the presence of a step edge are modeled as a 2D free electron gas, in the presence of a single hard wall barrier. The step is taken to lie perpendicular to the x-direction and infinitely extended along the y-direction. If we consider the plane-wave character of the wave function:

$$\psi_{k_x,k_y}(x,y) \propto (e^{-ik_x x} - e^{ik_x x}) e^{ik_y y} \tag{2.1}$$

And the expression of LDOS with the form:

$$\rho(E,x,y) = \sum_k |\Psi_k(x,y)|^2 \delta(E - E_k) \tag{2.2}$$

Close to the step edge, the LDOS can be expressed as:

$$\rho(E,x,y) = \frac{2L_0}{\pi} \int_0^{k_0} \frac{1-\cos(2k_x x)}{\sqrt{k_0^2 - k_x^2}} dk_x \tag{2.3}$$

Where $L_0 = \frac{m^*}{\pi\hbar^2}$ is the LDOS of a 2D electron gas in absence of any scattering and

$$k_0 = \sqrt{\frac{2m^*}{\hbar^2}(E - E_0)} \tag{2.4}$$

The integral in equation (2.3) can be solved analytically and yields:

$$\rho(E,x,y) = L_0(1 - J_0(2k_0 x) \tag{2.5}$$

where J_0 is the zero-order Bessel function.

For $x > \pi/2k_0$, the LDOS can be approximated as:

$$\rho(E,x,y) \approx L_0\left(1 - \sqrt{\frac{1}{\pi k_0 x}}\cos\left(2k_0 x - \frac{\pi}{4}\right)\right), \quad x > \frac{\pi}{2k_0} \tag{2.6}$$

The value of *k*-wave vector can be directly determined from the STM images, measured at low bias voltage and low temperature. Figure 2.5(a) shows a constant current STM image (40K) of the Au(111) surface acquired at V=-1.0mV. At this low bias the STM image roughly corresponds to the surface local density of states (LDOS) at the Fermi level.

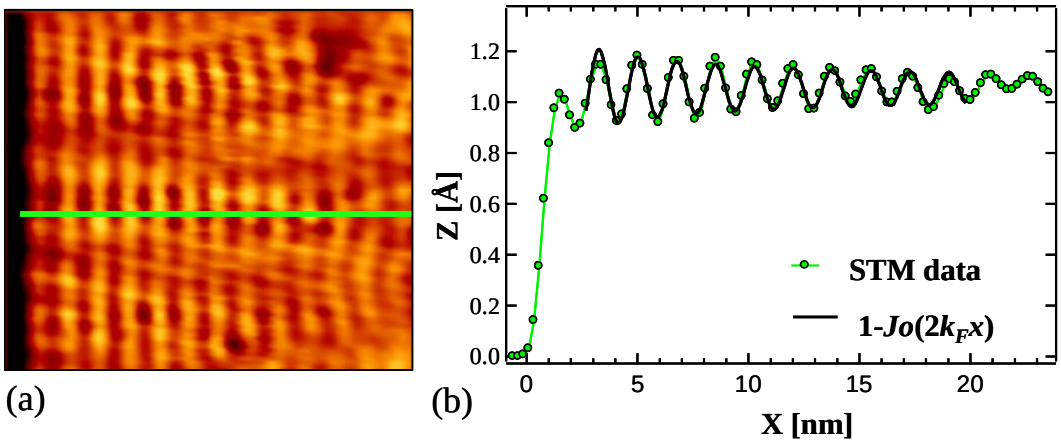

Figure 2.5 *Constant current STM image of Au(111) surface at 40K (24nm×21nm, V=-1.0mV, I=0.1nA). The step edge on the left acts as a scattering center giving rise to interference effects. (b) The experimental line scan (green circles) and the plot of equation 2.5 show a good agreement of the oscillatory behavior of the measured LDOS.*

An experimental line scan, across the step edge (green circles in figure 2.5(b)), shows the periodic oscillations of the surface LDOS. A good agreement is observed by comparison of the experimental line scan and the expression (2.5) plotted in figure 2.5(b) (solid black line). For the plotted expression, a free constant was added, representing the contribution of bulk states to the tunneling current.

The equation (2.5) gives a good fit to the decaying, oscillatory behavior of the measured LDOS. The estimated Fermi wavevector, k_F=0.174±0.1Å^{-1} is in good agreement with previous reported values [Reinert 2001].

Photoemission experiments have shown a parabolic and isotropic dispersion of the surface states. This isotropic behavior can be observed also in STM images, if the 2D Fourier transform is applied to the real-space STM image, where point defects in the surface act as scattering centers for surface states electrons. In this case, a point defect is screened from all directions, thus 2D Fourier transform of a standing wave STM image produces a map of all *k*-vectors contributing to the wave pattern.

Figure 2.6(a) shows an STM image obtained at low bias voltage where standing waves around several point defects can be seen.

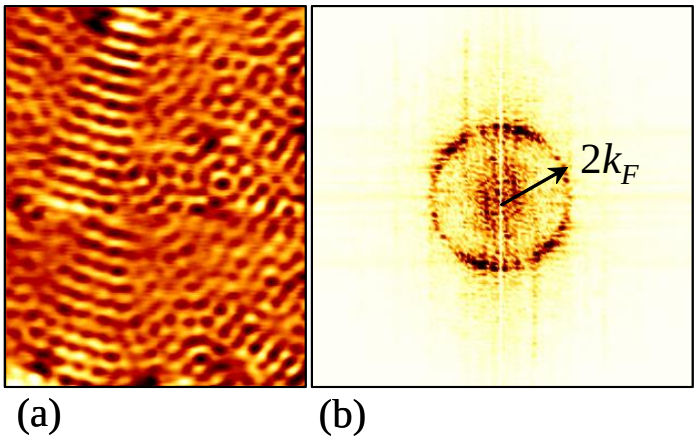

Figure 2.6 *Constant current STM image of Au(111) at 40K (33nm×41nm, V=-9.0mV, I=0.02nA) showing the standing wave pattern as a result of interference effects. (b) 2D Fourier transform of STM image showing the circular Fermi surface contour.*

The 2D Fourier transform (figure 2.6(b)) of the image shows a circular shape of the Fermi surface contour, which confirms the isotropic behavior of surface states electrons. Because STM images are sensitive to the square of the wave function, the Fourier transform will display the Fermi contour scaled by a factor of two.

From the average radius of the circle, the Fermi wave vector for the surface state on Au(111) is determined to be (0.17± 0.05) $Å^{-1}$.

Apart from the estimation of k_F, the energetic position of the minimum of the surface state band (E_0) can be determined by measuring current-voltage characteristics in STS experiments. Figure 2.7 shows a differential conductance plot obtained on bare Au(111) substrate. The sharp rise in the dI/dV *vs* V plot, near to ~-0.4V, reflects the onset of tunneling from the surface state band.

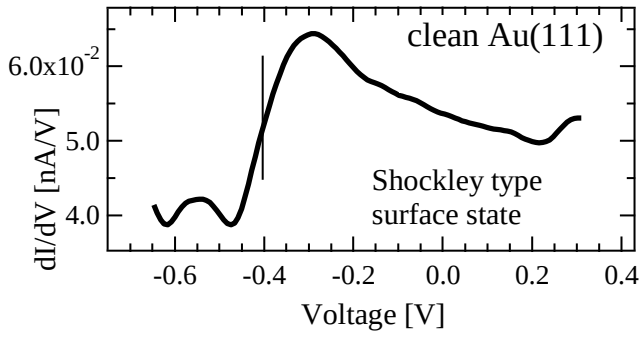

Figure 2.7 *Differential conductance plot obtained for the Au(111) surface at room temperature (the stabilization voltage was V=–1.0V and the set-point tunneling current was I =0.12nA).*

These results demonstrate that the surface states dispersion properties (k_F and E_0), can be estimated from the combination of STM and STS results. This approach will be used in the study of the PTCDA adsorbed layer influence on the Shockley-type surface states on Au(111), as it will be described in section 2.10.

2.4 Structural and morphological properties: STM analysis

2.4.1 Morphology of PTCDA/Au(111) interface

As we have mentioned in the previous section, the motivation of the present work was to study the electronic properties of the PTCDA/Au(111) interface. When starting the experiments, preliminary work had to be dedicated to the preparation and characterization of ordered PTCDA layers. In the following, several aspects, concerning the structural properties and morphology of the sample are remarked, as they are relevant for subsequent discussion of the spectroscopic results.

Figure 2.8(a) shows a representative STM image, obtained after PTCDA deposition on the Au(111) substrate.

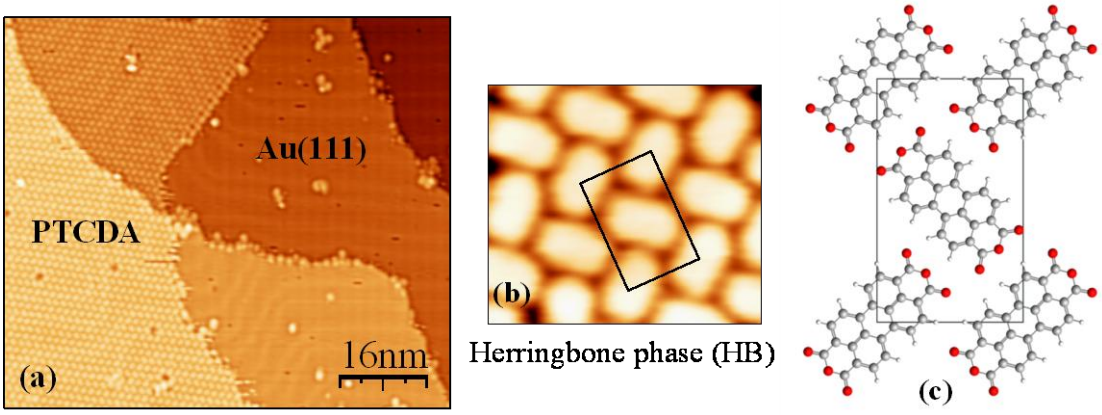

Figure 2.8 *(a) Representative STM image (80nm×70nm, V=–1.3V, I=0.5nA) corresponding to 0.5ML PTCDA deposited on Au(111) surface at room temperature. (b) Detail of the PTCDA herringbone reconstruction, with the PTCDA rectangular unit cell marked in the image (4.8nm×4.1nm, V=–2.0V, I=1.0nA). (c) Structural model of the herringbone structure.*

The STM image corresponding to ~0.5ML PTCDA shows on the left side the Au substrate partially covered by a PTCDA single layer, whereas the right side shows a clean gold area. It can be observed that PTCDA molecules spontaneously assemble on this surface. This indicates a high mobility of the adsorbate during the film growth, which can be expected in the case of a metal surface due to a rather weak substrate-molecule interaction. With exception of few isolated molecules adsorbed at the step edges, PTCDA grows in an ordered manner, leading to the formation of a structured layer on top of the substrate terraces.

With increasing coverage, long range PTCDA ordered domains are found to expand on the gold terraces. For a coverage of 1ML, the Au(111) surface is entirely covered by a well ordered PTCDA layer. The molecular structure found for the first adsorbed monolayer is the herringbone (HB) like structure characteristic of PTCDA bulk structure. In this arrangement as displayed in figure 2.8(b) and (c) PTCDA molecules are alternatively ordered in a zig-zag form. The rectangular unit cell marked in the image consists of two PTCDA molecules. The dimensions of the unit cell measured from STM images obtained in this work are (13±0.5)Å×(20±0.5)Å, parameters which are in agreement with those previously reported in the literature [Fenter 1997, Schmitz-Hübsch 1997]. The obtained lattice parameters for the first adsorbed layer are very close to the two-dimensional unit cell parameters of PTCDA (102) plane 19.91Å×11.96Å, as reported for the bulk structure [Mobus 1992].

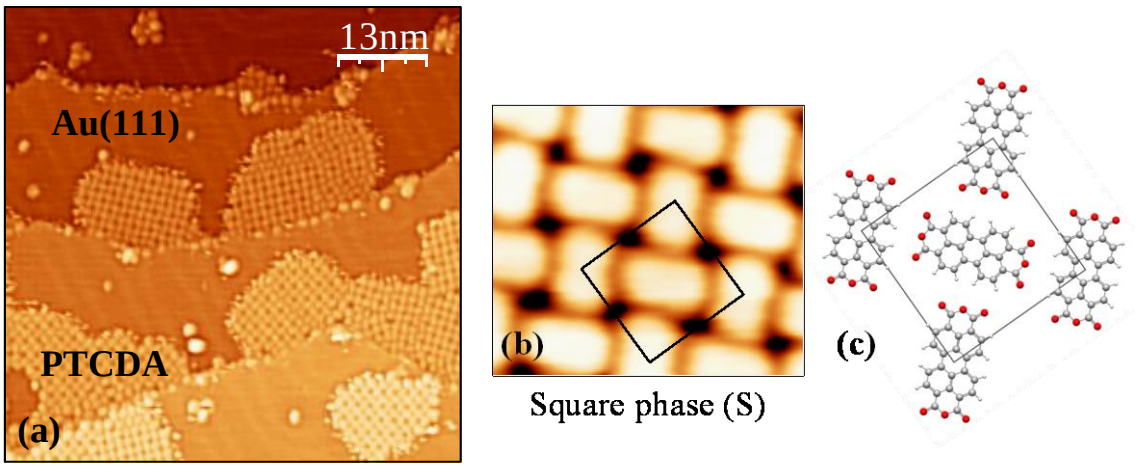

Figure 2.9 *(a) STM results obtained for submonolayer PTCDA coverage. The molecular structure with a square pattern is observed on the small PTCDA islands formed on the Au(111) substrate (63nm×63nm, V=–1.8V, I=0.2nA). (b) High resolution STM image (4.8nm×4.1nm, V=–2.0V, I=1.0nA) indicating the square unit cell marked in the image. (c) Structural model of the square structure according to STM results.*

In addition to this specific geometric arrangement, which PTCDA adopt on most of the substrates, a different structure with a square shape can be obtained (see figure 2.9(a)). The molecules, oriented in a T-like form are slightly less compact in the square phase as is shown in the STM image in figure 2.9(b). The unit cell parameters of the square structure determined from STM results are (17±0.5)Å×(17±0.5)Å.

A detailed structural dependence with substrate temperature has been reported previously [Chizhov 2000]. It was concluded that the equilibrium growth condition (high temperature and low evaporation rate) leads to mostly herringbone phase, while non-

equilibrium condition (low temperature and high evaporation rate) favors the formation of the square phase.

In general STM images showed that, at room temperature, the molecules are free to move on the surface. The small islands, formed on samples with low PTCDA coverage, are not very stable as indicated by the blurred appearance of their borders. Moreover, it has been frequently observed that under the tip influence it is possible to separate isolated molecules from the borders of PTCDA islands. These isolated molecules are mobile on the surface, giving sometimes a noisy appearance of the images in the uncovered areas of the Au(111) substrate.

The apparent average height of the molecules, relative to the clean Au(111) surface, measured in STM images is approximately 1.8±0.1Å. This height value, although not accurate (depends on the tunneling conditions) suggests that the molecules adsorb in a flat lying geometry, with the molecular plane parallel to the surface. A precise height of the PTCDA molecule with respect to the substrate can not be determined from STM experiments as it can exist a strong influence of the electronic properties of the molecular layer with respect to the metallic surface (and in particular the different densities of states) in the measured height difference values. Very recently, normal incidence X-ray standing wave (NIXSW) experiments reported a 3.27±0.02Å vertical bonding distance of the PTCDA perylene core relative to the Au(111) substrate [Henze 2007].

In agreement with earlier findings, the present STM data showed that the substrate reconstruction is not modified by the PTCDA adsorption. The underlying Au(111)-(22×√3) reconstruction is preserved under the PTCDA layer and this is clearly observed in all STM images where the reconstruction lines remain visible as a modulation of the image contrast (see figure 2.8(a) and 2.9(a)).

Present STM results obtained at the PTCDA/Au(111) interface have shown several aspects which are indicative of a weak interaction at the interface. Spontaneously assembling of molecules and high diffusion on the surface, together with the fact that the reconstructed substrate is not modified at the interface and moreover the arrangement of molecules in a structure characteristic to the PTCDA molecular crystal suggest that a weak molecule-substrate coupling exists at the PTCDA/Au(111) interface.

2.4.2 Multilayer regime

With increasing PTCDA coverage beyond 1ML, it is observed that a second ordered layer grows on top of the first one. An STM image corresponding to approximately 1.5ML PTCDA coverage is presented in figure 2.10(a). A region presenting 1ML PTCDA coverage is still seen in the center of the image, while the surrounding areas exhibit a second layer. We have observed that islands of the second layer start to form only when the first layer is complete. This indicates that at least the first two layers follow a layer-by-layer growth mode. As the image illustrates, the (22×√3) gold reconstruction is still seen through the first layer but is not visible anymore with the additional layer.

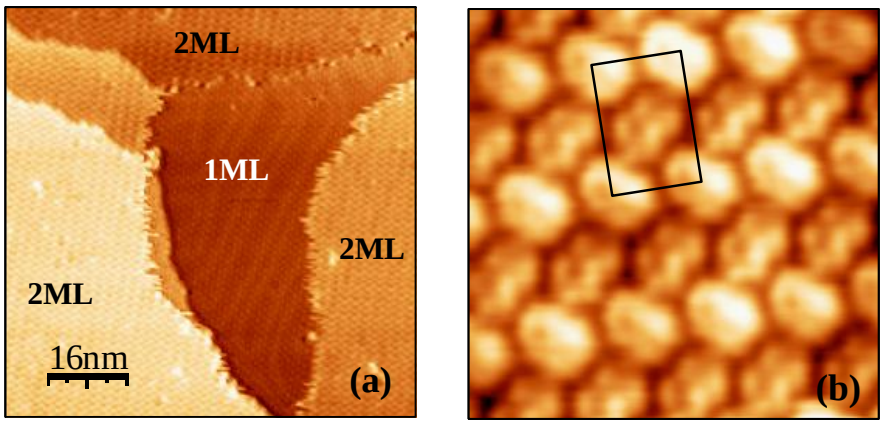

Figure 2.10 *(a) Representative STM image (78nm×78nm, V=+1.8V, I=0.25nA) obtained for the deposition of 1.5ML PTCDA on Au(111). Coexisting areas of both 1ML and 2ML are observed in the center of the image and the surrounding areas, respectively. (b) A close-up view shows the herringbone molecular structure in the second layer.*

The PTCDA herringbone structure is maintained in the second layer as shown in figure 2.10(b). For the bulk PTCDA a misalignment in the lateral direction for successive molecular stacks, leads to the existence of two different phases, the so-called α- and β-phases. In the α phase the consecutive layers of the PTCDA (102) planes are shifted along the long unit cell vector; while in the β-phase the consecutive layers are shifted along the short unit cell vector.

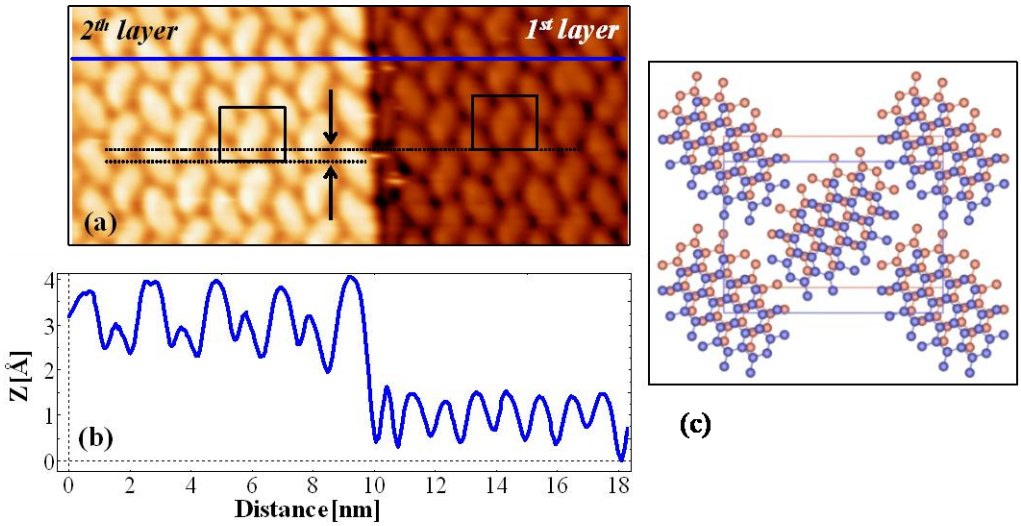

Figure 2.11 *(a) STM image (17.4nmx7.0nm, V=–2.0V, I=0.2nA) obtained for 1.5ML PTCDA on Au(111). The unit cells marked in the image indicate the difference between the first and second layer. The second PTCDA layer is laterally displaced with respect to the first one, along the short unit cell vector, as indicated by the dashed line. (b) Profile along the x scan direction showing the discontinuity in the layer periodicity. (c) Schematic model corresponding to the β-phase of bulk PTCDA structure.*

The alignment of the second PTCDA layer with respect to the first one can be obtained from STM images acquired on samples where both areas of 1ML and 2ML coexist, as shown in figure 2.11(a). A profile along the x scan direction marked in the image and displayed in figure 2.11(b) shows a discontinuity in the layer periodicity at the separation between the first and the second layer. The long vector of the PTCDA unit cell in the 2ML area is not aligned to the one of the unit cell corresponding to the 1ML area. This indicates that molecules in successive layers are not aligned one on top of each other. Instead, a lateral displacement along the short unit cell vector can be measured by comparing the position of the two unit cells marked in the image.

Within the accuracy of the STM calibration we have determined a lateral shift of the second layer with respect to the first one of approximately 3.0Å. As we have mentioned before, a lateral shift along the short unit cell vector corresponds to the β-phase. The lateral shift determined from the STM images indicate that already in the second layer the molecules tend to adopt the molecular structure specific to the bulk PTCDA. The growth of PTCDA above 2ML coverage results in high quality crystalline films. A large scale STM image as displayed in figure 2.12(a) shows the formation of large and smooth PTCDA islands.

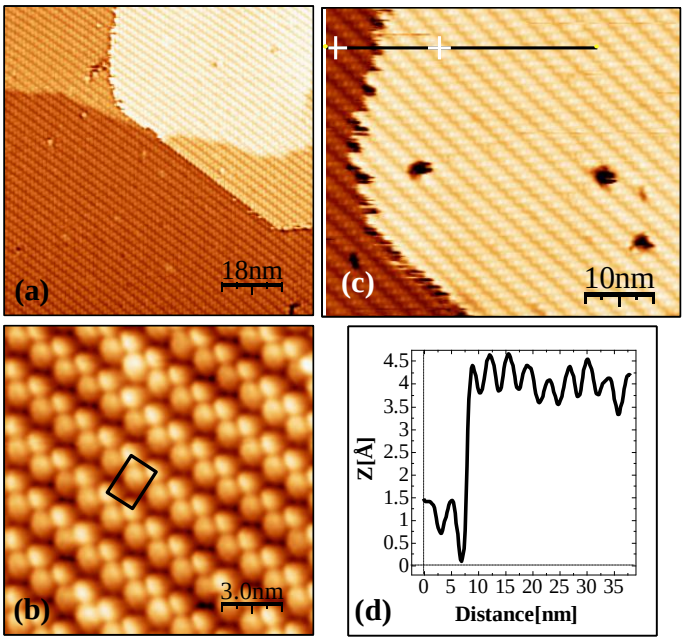

Figure 2.12 *(a) Large scale STM image obtained on approximately 8ML PTCDA evaporated on the Au(111) substrate. (88nm×88nm, V=–2.7V, I=0.1nA) (b) High resolution STM image (15nm×15nm, V=–2.7V, I=0.1nA) showing the herringbone structure which is maintained for thick PTCDA films. (c) STM image (50nm×43nm, V=-3.0V, I=0.16nA) and the corresponding profile (d) showing a ~3.0Å height between consecutive PTCDA layers.*

Molecular resolution obtained on these islands indicates the herringbone arrangement, with parameters of the unit cell similar to the bulk structure. The tilted orientation of molecules out of the plane of the substrate is visible in high resolution images (see figure 2.12(b)), and gives the impression of row formation in the large scale images. The apparent height between adjacent layers as determined from STM results (see figure 2.12(c) and (d)) is ~3.0Å which is in agreement with the reported interplanar distance between layers in the (102) plane of bulk PTCDA [Forrest 1997].

In summary, the STM results obtained for multilayer PTCDA coverage show a layer-by-layer growth at least for the first 7-8 layers, with well ordered molecular films. It was observed that already in the second PTCDA layer the molecules tend to adopt the PTCDA bulk structure. By measuring a lateral shift in consecutive layers we have been able to identify the PTCDA bulk β-phase characteristics.

2.5 Intramolecular resolution in STM images: molecular orbitals

Further information regarding the molecule-substrate interaction can be inferred from bias voltage dependent STM images, presenting intramolecular resolution of individual PTCDA molecules in the monolayer film. Figures 2.13(a) and (d) show topographic STM images, acquired simultaneously, at different polarities on a region covered by 1ML PTCDA.

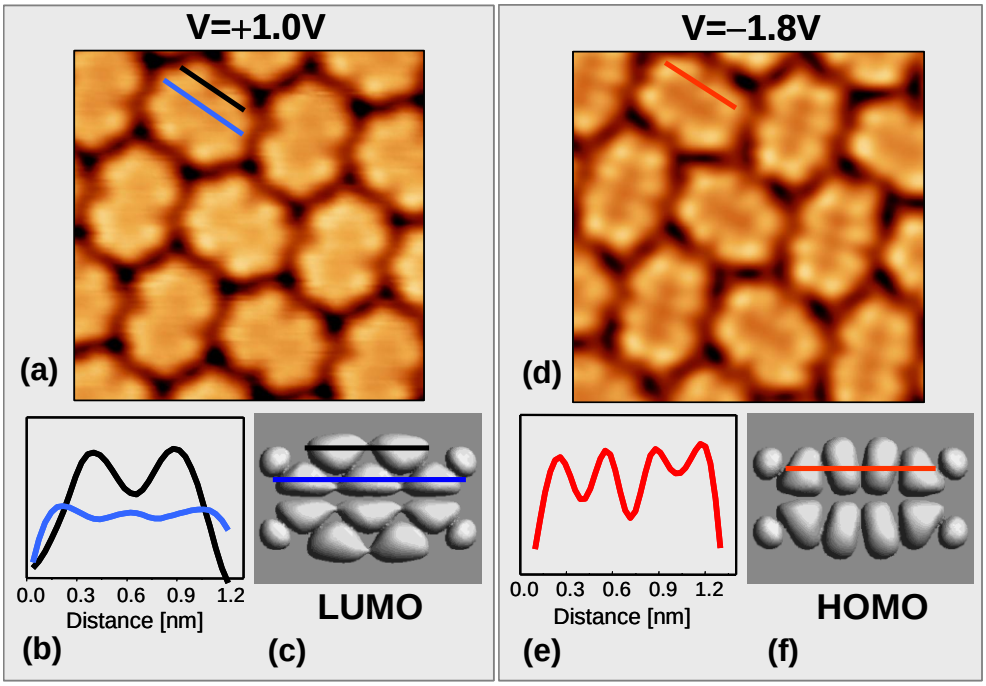

Figure 2.13 *(a), (d) Simultaneous STM images of 1ML PTCDA on Au(111) at RT, obtained at V=+1.0V (unoccupied states) and V=–1.8V (occupied states), respectively. Images size: 4.2nm×4.2nm, I=0.6nA. Intramolecular contrast is observed for each individual molecule. (b), (e) Profile lines extracted from experimental STM images are shown for a better comparison of intramolecular features with the spatial distribution of molecular orbitals calculated for the free PTCDA molecule. (c), (f) LUMO and HOMO calculated by DFT for the free PTCDA molecule.*

The images reveal distinct internal features for unoccupied molecular states (V=+1.0V) and for occupied molecular states (V=–1.8V). For positive sample bias, ten maxima for each molecule can be observed in the STM image shown in figure 2.13(a).

In the case of negative bias, the image reveals eight maxima for each molecule (Fig. 2.13(d)), and all the molecules present a deeper area parallel to the long axis, which splits the molecules in two parts.

These internal structures of molecules obtained at positive/negative bias can be obtained not only for the particular bias values corresponding to the figures 2.13(a) and (d). These features can be resolved in a small range of bias voltages close to those shown. In particular the HOMO related features were observed between -1.8V and -2.0V, whereas LUMO derived features were observed for an energy interval comprised between +0.9Vand +1.2V.

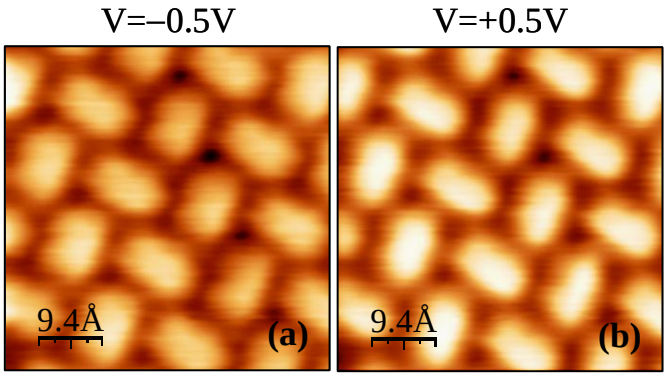

Figure 2.14 *(a) and (b) Simultaneously acquired topographic STM images for low bias sample. Images size: 4.7nm×4.7nm, I=1.0nA. Featureless molecules with almost no dependence on bias polarity are observed.*

STM topographic images acquired for bias voltages close to the Fermi energy do not display any internal structure of PTCDA molecules. STM images acquired simultaneously at -0.5V/+0.5V show featureless molecules and almost no dependence on bias polarity, as shown in figure 2.14.

In order to gain insight into the meaning of the intramolecular features obtained for large bias voltage, we have performed first principles calculations for the PTCDA free molecule. These calculations were done within density functional theory (DFT) in the local density approximation (LDA) [Perdew 1981], using the SIESTA method [Ordejon 1996, Soler 2002]. Core electrons were replaced by norm-conserving pseudopotentials [Troullier 1991] whereas valence electrons were described using a double-ζ plus polarization (DZP) basis set. A real-space grid with a cutoff of 50 Ry was used. Only the Γ point was used in reciprocal space. The geometries were relaxed until the maximum residual force was below 0.04eV/Å.

Figures 2.13(c) and (f) represent charge density isosurfaces obtained from DFT calculations corresponding to the lowest-unoccupied molecular orbital (LUMO) and to the highest-occupied molecular orbital (HOMO) of the free molecule. According to DFT calculations, the energy difference between HOMO and LUMO is ~1.5eV. This value, much lower than the experimental one (DFT methods are known to

underestimate gap values), is consistent with previous DFT calculations [Oszwaldowski 2003]. The experimental STM image shown in Fig. 2.13(a) measured at V=+1.0V clearly resembles the calculated LUMO of the isolated molecule, while the STM image measured at V=−1.8V can be directly related to the calculated HOMO. Profile lines extracted from experimental STM images are shown in figures 2.13(b) and (e) for a better comparison of intramolecular features with the spatial distribution obtained for molecular orbitals calculated for the free PTCDA molecule

Previous studies focused on the electronic properties of organic molecules/metal interfaces have shown that a strong coupling between adsorbate and substrate states generally results in a modification of the adsorbate electronic structure. Several main effects such as broadening of the molecular orbitals, admixture of metal-molecular states and charge transfer have been observed as a consequence of a chemisorption process.

Common features or general trends related to a chemisorptive bond have been observed for both of the noble metals Ag(111) and Cu(111) upon PTCDA adsorption.

At the PTCDA/Ag(111) interface a strong coupling between LUMO, HOMO and HOMO-1 molecular states and Ag 5s- and 4d-states results in the formation of interface states, which point out to a covalent interaction [Zou 2006]. In particular, STM images obtained at low bias have shown LUMO derived states close to the Fermi level, indicating the partial filling of this orbital as a consequence of charge transfer [Glockler 1998].

Comparable results have been obtained for a similar system PTCDA/Cu(111). Although this interface has not been so intensively studied, preliminary STM/STS results indicate a chemisorption process in which at least the LUMO is involved. High resolution STM images with intramolecular features resembling the LUMO are observed for energies close to the Fermi level [Ugeda M. M.]. Similar behavior is observed for PTCDA adsorption on highly oriented pyrolytic graphite (HOPG) which is considered one of the less reactive metal surfaces [Hoshino 1994]. STM results have shown that the LUMO can be imaged for values close to the Fermi level, which implies that a relatively strong interaction takes place also at this interface.

The comparison of the PTCDA/Au(111) interface, studied in this work, with the previously mentioned ones, yields a qualitatively different picture. Except a molecular orbital broadening no other effects related to a chemisorption process are observed.

The observation of almost unperturbed molecular orbitals, closely resembling the native LUMO and HOMO indicates a rather weak interaction at the interface. Moreover the energy difference between LUMO and HOMO is closely related to the PTCDA bulk band gap, which indicates that the PTCDA electronic structure is barely modified upon adsorption. The interface states formation if present (LUMO or HOMO derived states) should be reflected in considerable changes of low bias STM images. Instead we observe featureless molecules at low bias, which indicate again weakly bonding at the interface.

Proofs that the lack of significant molecule-substrate interaction preserves the native molecular orbitals have been recently reported in an STM study of pentacene/NaCl/Cu(111) interface [Repp 2005]. In this case the molecular layer is electronically decoupled from the supporting Cu(111) substrate by an intermediate insulating NaCl thin film. Unperturbed pentacene LUMO and HOMO are observed in STS experiments and bias dependent images.

The above presented experimental findings for the PTCDA/Au(111) interface together with the aspects remarked for other PTCDA/noble metal interfaces indicate a physisorption process, rather than chemisorption. This conclusion is supported by additional results which are presented in the next sections.

2.6 Scanning tunneling spectroscopy

2.6.1 Monolayer coverage

Besides the topographical imaging, information about the local density of states (LDOS) as a function of energy can be obtained by means of scanning tunneling spectroscopy. The advantage of STS, compared to other spectroscopic techniques is to locally probe the electronic properties, providing simultaneously information about both occupied and unoccupied states of the sample. Thus by performing STS, the electronic structure of PTCDA/Au(111) interface can be obtained. Details about the energetic position of the LUMO and HOMO upon adsorption will give further information about the strength of molecule-substrate interaction at the interface.

Tunneling spectroscopy measurements have been performed at room temperature on samples with submonolayer coverage, where highly ordered PTCDA domains and areas of clean Au (111) substrate coexist [Nicoara 2006].

For the system investigated here, both tungsten (W) and Pt-Ir (80%-20%) tips have been used in the experiments, but the most reproducible spectroscopic data were obtained with mechanically cut Pt-Ir tips. Generally, the I-V spectra were recorded at relatively large tip-sample distances in order to avoid strong interaction between the tip and the organic layer. Stabilization bias voltages close to ±2.0V, and set-point currents as low as possible have been mainly used. Higher voltages damaged or lifted up the molecules from the surface. Each I-V plot is averaged over several successive curves acquired at the same lateral position. The I-V curves are numerically differentiated and displayed as the differential conductance curve (dI/dV *vs* V) which is related to the local density of states (LDOS) of the sample.

Before and after recording spectroscopic data on the PTCDA adsorbate layer, reference I-V curves were recorded on the clean Au areas. Only when the Au(111) spectrum with the characteristic Shockley type surface state is achieved, we follow recording current-voltage curves on the PTCDA molecules.

With this approach we assume a minimum contribution of the tip LDOS to the spectra and we ensure that the additional features which appear in the case of STS on molecules are indeed related to PTCDA molecular states.

Figure 2.15 presents scanning tunneling spectroscopy results obtained for the PTCDA/Au(111) interface. The I-V curves were measured successively on the uncovered gold substrate and on a PTCDA island, as shown in figure 2.15(a).

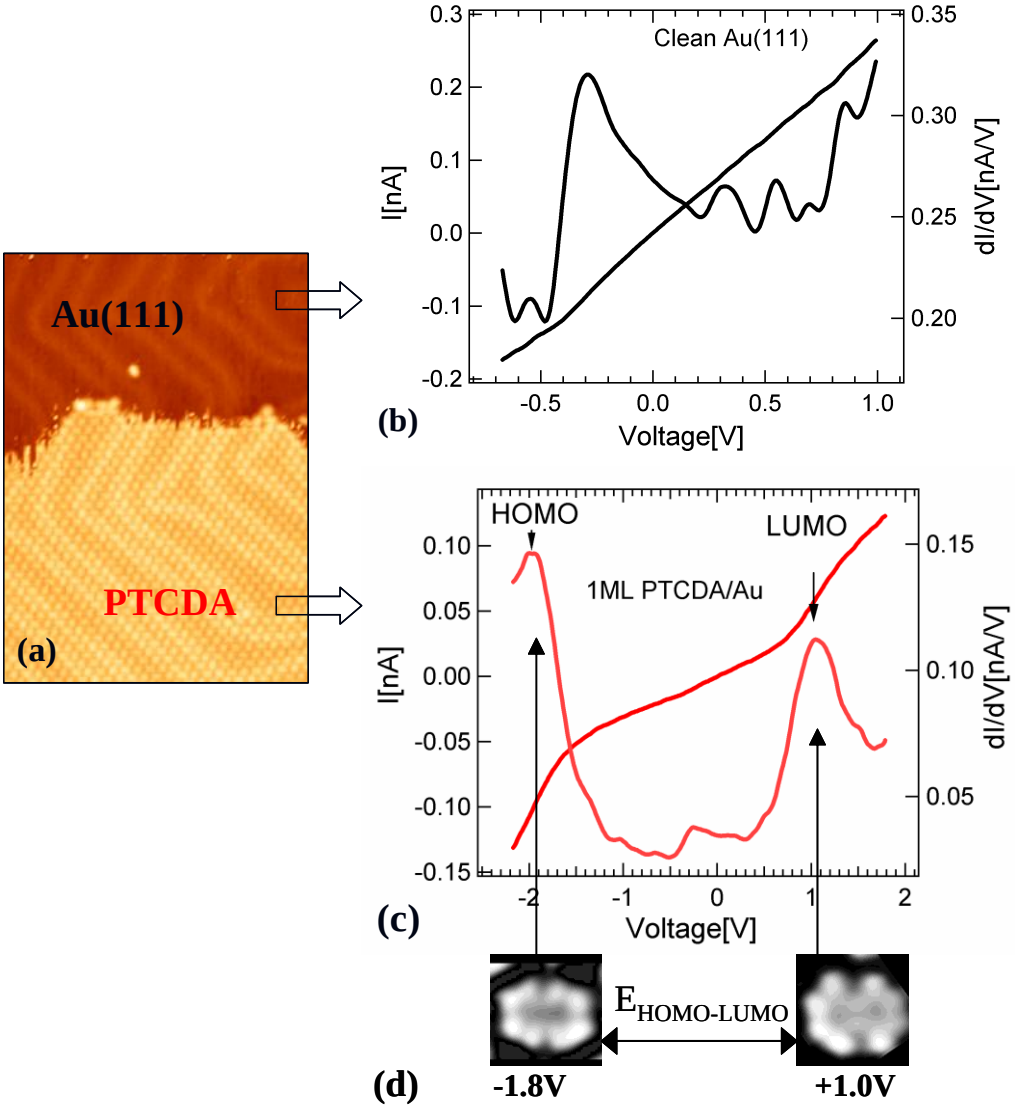

Figure 2.15 *Tunneling spectroscopy performed at RT on clean Au(111) and on PTCDA islands. (a) Topographic STM image (47nm×50nm, V=–2.0V, I=0.16nA) of a sample area, where STS has been performed. I-V plots and the corresponding differential conductance plots (dI/dV vs V) obtained on bare Au(111) substrate in (b) and on 1ML PTCDA/Au(111) in (c). Molecular related features found at relatively large bias values are attributed to HOMO and LUMO resolved in previous STM images (d). (Tunneling parameters: the stabilization voltage was V=–1.0V (b) and V=+1.8V(c); the set-point tunneling current was I =0.12nA for both (b) and (c).*

Figure 2.15(b) shows tunneling spectroscopy results obtained on the Au(111) substrate. As already described in section 2.3.2, the Au(111) presents a Shockley-type surface state whose band minimum is localized at several meV, below the Fermi level. The

differential conductance curve (dI/dV *vs.* V), displayed in figure 2.15(b) exhibits a pronounced peak below the Fermi level, corresponding to the onset of this surface state band. The obtained value of ~400meV represents the minimum of the surface state band and agrees well with previously reported STM and UPS experimental results [Kevan 1987, Reinert 2001].

Once the Au substrate is measured and the characteristic spectrum is reproducibly obtained, we follow recording I-V curves on the PTCDA molecules. The STS results are shown in figure 2.15(c).

The differential conductance plot displayed in figure 2.15(c) is characterized by three distinct features, which are reproducibly obtained in the STS experiments. Two pronounced peaks at relatively large bias voltage values are clearly observed in the spectrum. For negative bias voltage we observe a peak at approximately -1.9V below the Fermi energy, while for positive sample bias we observe a peak at approximately +1.0V. Small variations in the energy peak position are observed for different tips.

These peaks should be related to PTCDA molecular states as the gold spectra does not present any feature at these bias voltages. Moreover the direct correlation of these spectroscopic features to the bias dependent STM images obtained in the previous section shows that they can be unambiguously attributed to the HOMO and LUMO (see figure 2.15(d)). We remind that the intramolecular resolution obtained in STM images recorded at negative bias voltage (-1.8V) was closely related to the spatial distribution of the HOMO calculated for the free molecule. STM images, recorded at positive sample bias (+1.0V) show a molecular internal structure similar to the LUMO.

Further details of the interface electronic structure are provided by the direct comparison of STS data (see figure 2.16(a)) measured on clean and on the PTCDA covered Au(111) surface. The dI/dV *vs*. V plot obtained at the PTCDA/Au interface shows that besides the two features found at ~-1.9V and ~+1.0eV, related to PTCDA molecular states, an additional peak exists at negative bias, close to the Fermi energy.

The presence of the peak at ~–0.4eV, in the conductance plot is somehow unexpected, since it is known that the organic semiconductor PTCDA has no molecular states in this region, and LUMO and HOMO, as we determined, are located relatively far from the Fermi level.

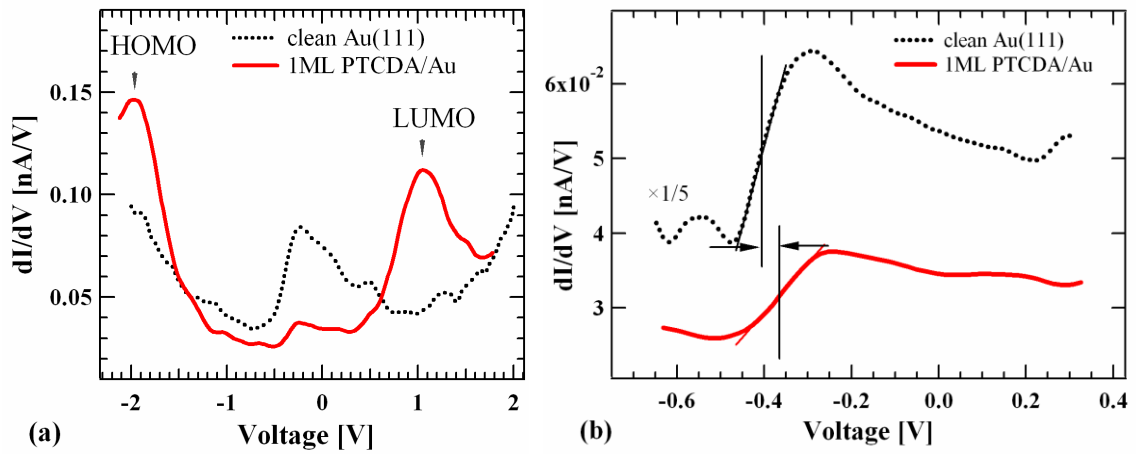

Figure 2.16 *(a) STS acquired on clean and PTCDA covered gold. (b) Zoom of the energy region where the gold surface states band is visible. A shift of ~40meV can be observed. Tunneling parameters: clean gold, V=–2.0V, I=0.23nA; PTCDA layer V=+1.8V, I =0.12nA.*

A detailed view, in the region close to the Fermi level, of conductance plots corresponding to bare Au and PTCDA/Au, is displayed in figure 2.16(b). It can be noticed a close similarity in the peak shape for both Au(111) and PTCDA/Au(111) STS spectra. The direct comparison of both peaks shows attenuation and a slight shift in energy of the peak arising at the interface, in comparison to the peak corresponding to the Shockley-states on Au surface.

In the limit of the RT-STS experimental resolution, we estimate a shift of ~40meV toward the Fermi level, which has been reproducibly obtained for the peak present at the PTCDA/Au interface. The thermal broadening of the STS data measured at room temperature can be estimated as ~4kT≈100meV. This value is compatible with the width of the Au(111) surface state band onset measured in figure 2.16(b).

In order to investigate the nature and origin of this peak, the electronic structure of higher PTCDA coverage has been investigated. The results are presented in the next section.

2.6.2 Multilayer coverage

The interpretation of STS results obtained for 2ML or multilayer coverage is complicated in the absence of uncovered gold areas. We remind that the formation of a second layer begins only when the first layer is complete. In this situation no reference spectra is available (i.e. Au(111) spectra), which would assure a "good" tip condition. Therefore, in the absence of uncovered gold areas, various experiments with different tips were performed until reproducible results were obtained.

Scanning tunneling spectroscopy results obtained for 2ML PTCDA/Au(111) indicate a semiconductor behavior, as observed in the differential conductance plot displayed in figure 2.17.

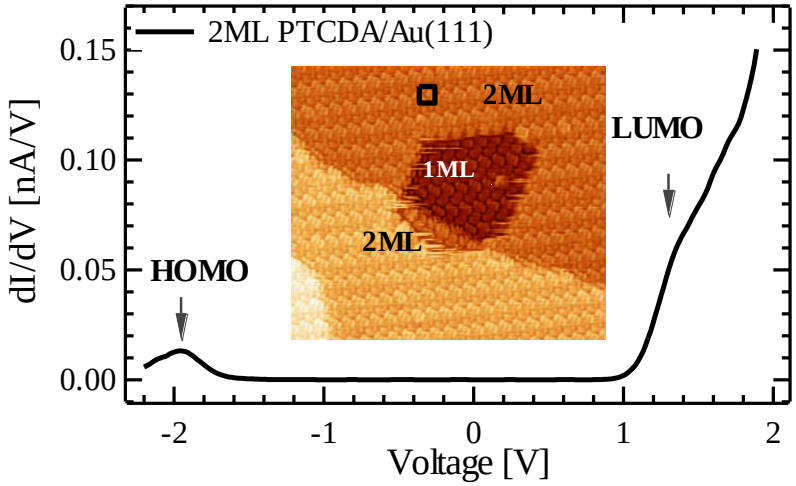

Figure 2.17 *Tunneling spectroscopy performed on 2ML PTCDA on Au(111) shows semiconductor behavior. The plot corresponds to the differential conductance that was derived from averaging several I-V curves and subsequent numerical differentiation. Inset: topographic image of a sample with approximately 2ML coverage where STS was performed. Tunneling parameters: V=–2.2V, I=1.0nA.*

Two pronounced features, which are reproducibly obtained, are observed for large bias voltages. At empty states we observe a peak at ~+1.3V, while at occupied states we observe a peak at ~-1.9V. According to the results obtained for the PTCDA monolayer, we can attribute these peaks to PTCDA molecular states: LUMO and HOMO, respectively. The energetic position of both features may slightly vary in STS experiments as a function of tip configuration or tunneling parameters. The energy difference between the centers of these peaks yields a HOMO-LUMO gap of 3.2±0.1eV, which is in agreement with values reported for PTCDA thin films.

It is worth mentioning that we have never observed a metallic behavior for the second PTCDA layer. None of STS spectra have shown any feature inside the PTCDA gap, in between the HOMO and LUMO, in contrast to the situation found for 1ML.

For higher PTCDA coverage (3-8ML), the results are similar to the 2ML case, with the only difference that the gap value slightly increases, approaching a value of 3.3eV. Other authors have reported even larger gap values [Hill 2000, Tsiper 2002] with a similar dependence on the coverage, which was interpreted in terms of polarization effects, as described in section 1.1.

2.7 Valence band photoelectron spectroscopy

In order to gain further insight on the electronic structure of the PTCDA/Au(111) system we have used several complementary photoelectron spectroscopic techniques. In particular, both valence band (UPS) as well as core level (XPS) experiments have been performed and will be described in this section.

The photoelectron spectroscopy experiments have been mainly focused on the interfacial electronic structure. The discussion of the results obtained at the PTCDA/Au(111) interface is as follows. First, we characterize the electronic structure for PTCDA thin films (~12ML), and then we focus on electronic properties at the interface, in particular we concentrate on the influence of PTCDA on the Shockley-type surface state of the Au(111) substrate.

2.7.1 Electronic structure of PTCDA thin films

Generally, the interface investigation is based on a comparison of the electronic structure of the adsorbate/substrate and the adsorbate itself. Therefore, initially we characterized the electronic properties of PTCDA thin films. Experimental results providing information on the density of occupied states in PTCDA have been obtained by means of ultraviolet photoemission spectroscopy (UPS).

The normal emission spectra of approximately 4nm thick PTCDA film on Au(111) surface is shown in figure 2.18. The spectrum is background corrected and plotted as a function of binding energy with respect to the Fermi level. The Fermi level (E_F) is indicated by the dotted line.

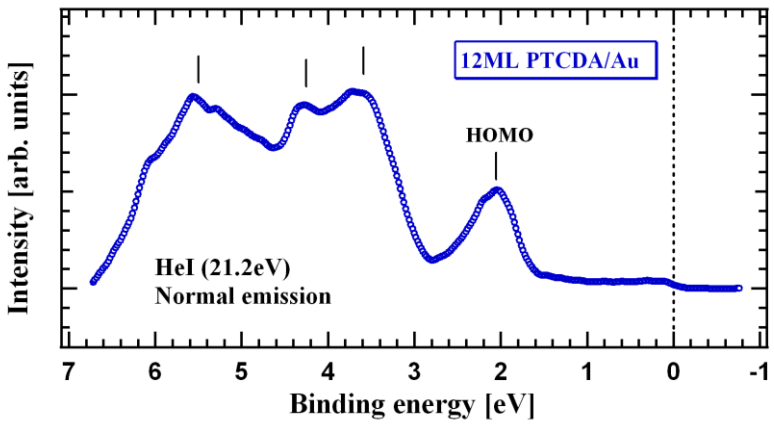

Figure 2.18 *HeI UPS spectra of PTCDA on Au(111). Extended valence band spectra of a ~4nm thick PTCDA film deposited on gold substrate.*

The valence band of PTCDA multilayer is characterized by several features identified at ~2.0eV, 3.6eV, 4.2eV and 5.6eV. These results are in agreement with theoretical and experimental results previously reported [Azuma 2000, Yamane 2003, Dori 2006]. The main features observed in the spectrum originate from π states. In particular, the band at the lowest binding energy (~2.0eV), which is clearly separated from the rest of the bands, represents the highest occupied molecular orbital, HOMO. This band has π character and is mainly distributed over the perylene core. The other features are associated to contribution with π character from the perylene core and to molecular orbitals derived from oxygen $2p_x$ and $2p_y$ atomic orbitals of C=O groups. The HOMO level identified at 2.0eV, below the Fermi level is in good agreement with the STS results presented in the previous section.

2.7.2 Electronic structure at the PTCDA/Au(111) interface

Once the reference spectra corresponding to PTCDA thin film electronic structure has been obtained, further experiments have been performed in order to observe the evolution of the valence band spectra as a function of PTCDA coverage, with emphasis on the electronic properties at the PTCDA/Au(111) interface. Figure 2.19 shows the extended valence band photoemission spectra recorded at normal emission as a function of PTCDA coverage on Au(111).

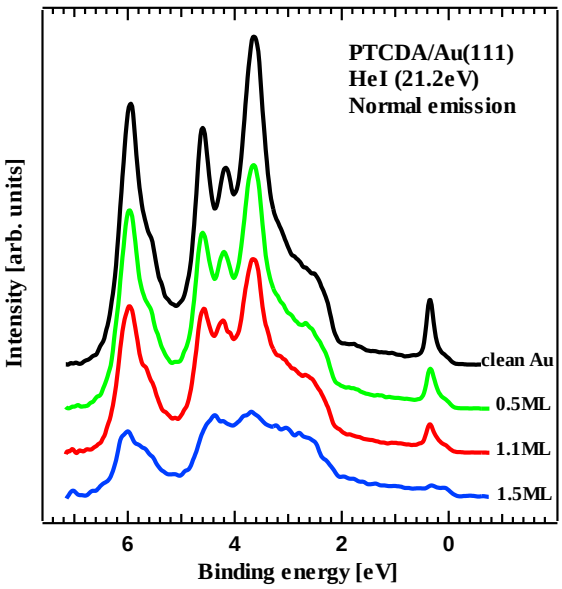

Figure 2.19 *Photoemission spectra (He I) showing the extended valence band of PTCDA/Au(111) for various thicknesses of the organic layer. The spectra are background corrected and vertically offset for a better visualization.*

The upper plot corresponds to the clean Au(111) substrate and is characterized by a pronounced peak, at 0.4eV below the Fermi level, which represents the contribution of

Au(111) surface states. The rest of the sequence spectra show the evolution of the valence band after each subsequent growth step. From the comparison of individual plots in figure 2.19 we observe that the overall intensity of the Au(111) valence band spectra decreases, as the PTCDA coverage is increased, with an homogenous attenuation of the substrate valence band. PTCDA related electronic features are not discernable up to few monolayers due to the huge contribution and the large mean free path of the valence band gold electrons. No extra states close to the Fermi level can be resolved, neither for the PTCDA/Au(111) interface, nor for coverage larger than 1ML.

Detail spectra of the region close to the Fermi level is shown in figure 2.20. The plot corresponding to the bare gold surface shows the known peak of Shockley-type surface states [Kevan 1987, Reinert 2001] at a binding energy of E_B=0.4eV, relative to the Fermi level.

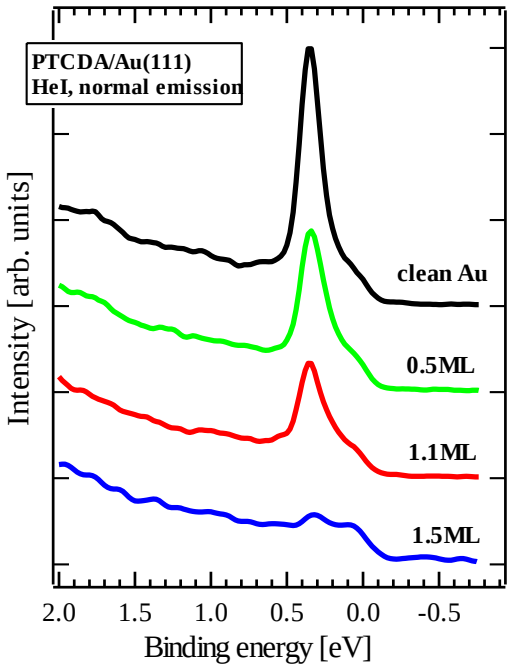

Figure 2.20 *Normal photoemission spectra obtained at room temperature for different PTCDA coverages of on Au(111). The clean gold spectrum shows the Shockley-type surface states at a binding energy of 0.4eV. For 1.1 ML the peak corresponding to the Au (111) surface state is attenuated, but still visible. Binding energies are referred to the Fermi level. The plots are vertically offset.*

In the subsequent spectra, for PTCDA coverage between 0.5 and 1.5ML, we observe a similar peak, though slightly attenuated in intensity, as PTCDA coverage is increased. The peak is clearly seen at 1.1ML PTCDA, and it is still noticeable at approximately 1.5ML. Within the experimental resolution (120meV), we do not have a clear evidence of a change in its energetic position as the coverage is increased. For more than 2ML PTCDA this peak is not observed anymore.

These findings are in very good agreement with the STS results reported in the previous section. By means of both techniques STS and UPS we determine a high density of states at the Fermi level for the PTCDA/Au(111) interface.

2.7.3 Surface states band dispersion

It remained to clarify the nature of this electronic state observed at the PTCDA/Au(111) interface. UPS results have shown a peak with almost the same shape and energetic position as compared to the characteristic one for the Au(111) substrate.

With the assumption that the original Shockley state of the underlying substrate is mainly contributing to this peak, we proceeded to further experiments. If indeed it is related to the Shockley states, ARUPS experiments which are commonly used to describe the behavior of surface states should confirm it.

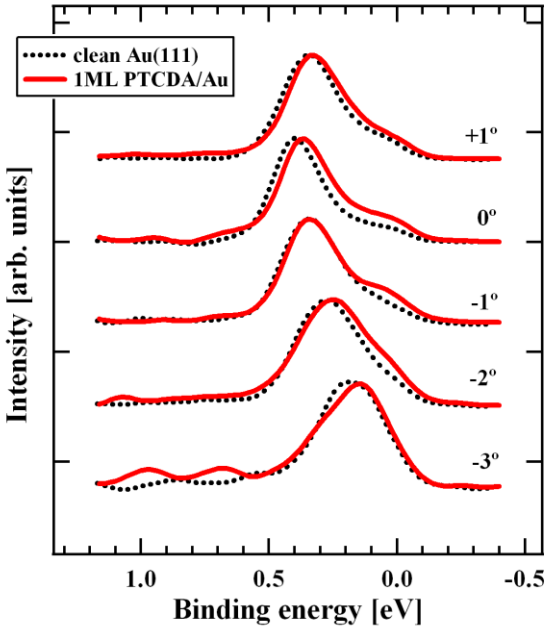

Figure 2.21 *Angular resolved photoemission spectra for the surface states of clean Au (111) (dotted line) and 1ML PTCDA covered Au (solid line). Both states display a similar angular dispersion.*

In figure 2.21 we present the comparison between the photoemission spectra for the clean gold substrate and for a 1ML PTCDA covered surface, as the emission angle is varied close to the surface normal. Both UPS spectra show an identical dispersion, corresponding to the well known nearly free-electron-like parabolic dispersion of the Shockley-type surface states [Reinert 2001].

It is important to remark that any electronic state related to a single well-ordered PTCDA overlayer should present a band dispersion induced by the lateral periodicity of

the layer, which is different from that of Au substrate. The lateral lattice constant for the PTCDA/Au system were found to be (13±0.5)Å and (20±0.5)Å. Hence the electronic features should repeat with the surface reciprocal space-lattice i.e., about $0.15Å^{-1}$ and this $k_{\|}$ periodicity should be measured in ARUPS spectra as a dispersive band.
Since the observed band dispersion is similar to that of the bare gold substrate we can conclude that the Shockley-type states are the dominant contribution to the states close to E_F at the PTCDA/Au interface.

These findings indicate a weak molecule-substrate interaction, sufficient to preserve the Au(111) surface states, upon PTCDA monolayer adsorption. Besides, the unambiguously determination of the nature of this peak and the absence of any other state in the HOMO-LUMO PTCDA gap evidence that the detected interface state in the PTCDA/Au(111) system is, essentially, the almost unperturbed Shockley-type surface state of Au(111).

2.8 Core level photoelectron spectroscopy

By means of X-ray photoelectron spectroscopy (XPS) we have investigated the initial stage of PTCDA deposition on Au(111) with the aim of monitoring any interfacial interaction. Experiments mentioned in the previous sections have indicated that PTCDA molecules are weakly adsorbed onto the gold surface and additionally ARUPS measurements allowed unambiguously to determine the nature of electronic states close to the Fermi level for the PTCDA/Au(111) interface.
Core-level photoemission spectroscopy is a powerful tool for chemical analysis, as the binding energy of a core level strongly depends on the local chemical environment of the atom to which the level belongs. Considerable changes in the core level binding energies at the interface, as compared to bare PTCDA could bring new evidences of processes which appears at the PTCDA/Au(111) interface. Thus a significant increase in electron density of the adsorbate, as a result of charge transfer upon adsorption would be reflected in XPS spectra in a lower binding energy of adsorbate core electrons.
Therefore complementary information regarding the strength of molecule-substrate interaction and hypothetical charge transfer can be found from changes in the core levels of PTCDA upon adsorption on Au substrate.

The XPS core levels were probed using a non-monochromatized Mg K_α (1253.6 eV) radiation source. Scan spectra were recorded with analyzer pass energy of 15eV which give a resolution of 100meV for Au4f core levels. All spectra are calibrated by using the Au4f core level emission spectra. XPS core levels peak positions were determined by nonlinear least squares fitting of Gaussians (due to the limited instrumental resolution) after appropriate background substraction. The background was assumed to be of Shirley form, which accounts for inelastic electron scattering.

The Au(111) substrate was prepared by standard procedure and the cleanness was check by XPS. The PTCDA film thickness of the samples was calibrated using the C1s intensity and an inelastic mean-free path (λ) of 15Å for PTCDA [Knoth 2002] characteristic for π-conjugated molecules.

One approach to interpret the XPS data is to monitor the changes in the substrate core levels after molecular adsorption. We have performed XPS measurements for the Au4f core levels and we found no modification either in the binding energy or in the peak shape upon PTCDA adsorption: only a gradual attenuation of peak intensity with increasing PTCDA coverage was observed. However, recent photoelectron spectroscopy studies have demonstrated that a better estimation of results is obtained when comparison between multilayer and monolayer spectra is performed [Zou 2006].

Therefore, we have initially characterized the PTCDA multilayer deposited on a clean Au(111) surface. Figure 2.22 shows the C1s and O1s core levels photoemission spectra of multilayer PTCDA deposited on Au(111) substrate.

For ~12 ML PTCDA the C1s core level spectra are characterized by two main peaks as shown in figure 2.22(a). The peak located at lower binding energy (284.8eV), labeled α, is attributed to the carbon atoms associated to the perylene core of the molecule, while the peak at higher binding energy (288.6eV) labeled β, is attributed to the carbon atoms of the anhydride end groups of the PTCDA molecule. A less pronounced peak is observed at 291.8eV and is attributed to a shake-up satellite associated with the carbonyl group.

The O1s core level spectra recorded for the same PTCDA thickness is shown in figure 2.22(b). The main features observed in the spectra originate from the two different oxygen species in the PTCDA molecule. The most intense peak, labeled δ, with maximum at 531.6eV binding energy is attributed to the oxygen atoms in the carbonyl group (C=O), while the other peak labeled ε, located at 533.4eV binding energy

corresponds to the O atom in the anhydride group (-O-). The component at ~536.5eV is a shape-up satellite of the (-O-) peak.

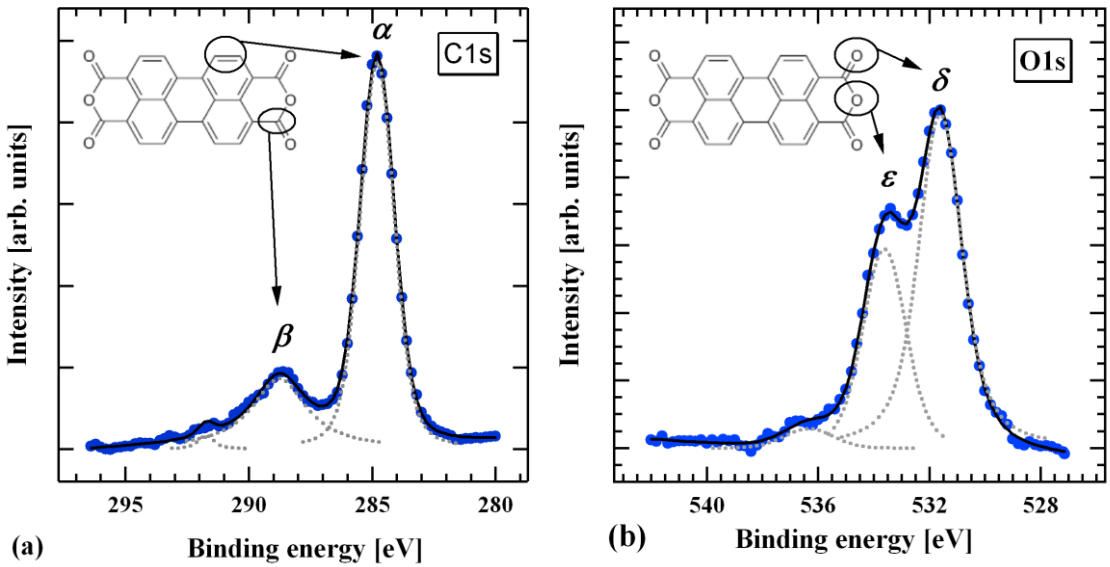

Figure 2.22 *XPS spectra of C1s (a) and O1s (b) core levels spectra of ~4nm PTCDA film deposited on Au(111) substrate. The main peaks refer to distinct C and O environments in the PTCDA molecules as marked in the inset.*

From the peak fit analysis of the C1s core level spectra we have observed that the stoichiometric ratio (5:1) of carbon atoms in the aromatic part (20 C atoms) to those in the functional groups (4 C atoms) is reproduced in the multilayer recorded spectra. For the two different oxygen species in the molecule the ratio is 2:1 and it is also reproduced if the relative peak area is analyzed in the O1s core level spectra.

As was previously reported [Zou 2006], a better estimation of the changes in the core levels at the interface is obtained when PTCDA multilayer core levels spectra are compared with interface (1ML PTCDA/Au) XPS spectral features. Hence, further XPS experiments have been performed, analyzing the evolution of C1s and O1s core levels spectra for various PTCDA thicknesses. Figure 2.23 displays the evolution of the C1s and O1s core levels with increasing PTCDA coverage.

The spectra were recorded after each PTCDA deposition step. First of all, we observed that the plots corresponding to three different PTCDA coverages are very similar, regarding the relative peak areas ratio and the line shapes. The C1s (α)/C1s (β) relative peak areas ratio (5:1) remains approximately constant, when multilayer to monolayer spectra are compared. The same observation is found for the relative peak areas of the O1s core levels for different PTCDA thicknesses.

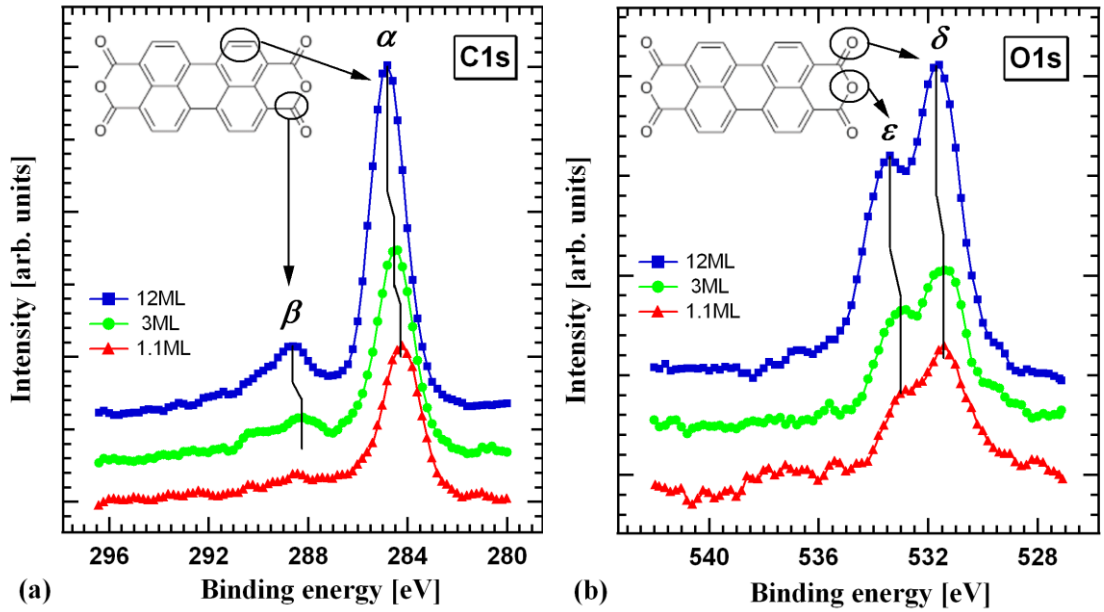

Figure 2.23 *XPS (Mg Kα) spectra of the evolution of C1s (a) and O1s (b) core levels with increasing PTCDA coverage. The plots are vertically offset for better visualization.*

Nevertheless, small differences are observed in the binding energy values for different features in the XPS plots. In the sequence spectra, displayed in figure 2.23(a) we observe a gradual shift toward lower binding energy for both components in the C1s core levels with decreasing PTCDA coverage. The α component in PTCDA multilayer plot (square markers) is found to be shifted 0.6eV toward lower binding energy in the 1.1ML spectra (triangle markers). A similar tendency is observed for the β component when multilayer and monolayer spectra are compared.

PTCDA Θ[ML]	C1s		O1s	
	α	β	δ	ε
~12	284.8	288.6	531.6	533.4
~3	284.4	288.2	531.4	533.0
~1.1	284.2	288.2	531.4	533.0
	s=0.6eV	s=0.4eV	s=0.2eV	s=0.4eV

Table 2.1 *Shift values as a function of PTCDA coverage, for different components in the C1s and O1s core level spectra.*

Comparable results are obtained when a similar analysis is performed for the δ and ε components in the O1s core levels spectra (Figure 2.23(b)). Both O1s features in the monolayer spectra are slightly shifted toward lower binding energy with respect to their

energetic position in the multilayer spectra. We have observed a shift of 0.2eV and 0.4eV binding energy, for the δ and ε spectral features, respectively.

It is worth noticing that the values of these shifts are not equivalent for the different components in the XPS spectra. At the PTCDA/Au(111) interface noticeable changes are observed mainly for the component associated to the C atoms in the aromatic part, whereas the other components suffer only subtle shifts in the energetic position. For example, the δ component associated to the oxygen atom of the carbonyl group (C=O) is almost unmodified at the interface as seen in fig 2.23(b). As well, the β component related to carbon atoms in the above mentioned carbonyl group undergoes only subtle changes.

The fact that the carboxylic parts of the PTCDA molecule are not considerably affected by the PTCDA adsorption on gold suggests the absence of a chemical bond involving the oxygen atom related to the C=O group. A chemical reaction at the PTCDA/Au interface would result in a weakening of the C=O bond as is expected for compounds which contain anhydride groups. Previous studies [Umbach 1990] have shown that PTCDA adsorption on noble metals as Ag(111) or Ag(110) can result in a strong interaction between the metallic surface and the carboxylic group of PTCDA. As a result the core levels attributed to these specific elements are drastically modified, reflecting a chemical bonding at the interface.

For other different metal/organic interfaces as it is the case of deposited Al, In, Sn and Ti metals onto PTCDA films [Hirose 1996], it was also reported a strong chemical reaction at the interface. In particular, the reaction occurs at the carboxylic end groups of the PTCDA molecule. For these reactive interfaces, core level spectra clearly show the metal oxidation and the reduction of the carbonyl carbon atoms. Besides the rapid attenuation of the core levels attributed to the C atoms in the carboxylic group, drastic changes are observed in the metal core levels, too. Large shifts of metal core levels of order of 1.7-3.2eV, towards higher binding energies are explained by positively charged metal atoms as a result of charge supplied to PTCDA molecules. Moreover, the strong metal/organic interaction induces the formation of large density of states in the PTCDA band gap, interface states which were detected in both XPS/UPS experiments. In contrast when Au or Ag metal atoms are evaporated onto a PTCDA thick film (a reversed interface as compared to the one presented in this work) the interface is

characterized as unreacted, as the metal atoms neither diffuse, nor react with PTCDA molecules [Hirose 1997].

Hence, the XPS results obtained in this work enable us to describe the PTCDA/Au system as a weak reactive interface. From the present XPS experiments we have no evidence of new states formation at the interface. The absence of significant changes in the binding energies or peak shape of C1s, O1s or Au4f corelevels at the interface indicates a weak PTCDA/Au(111) interaction. XPS spectra have shown that core levels components related to the carboxyl end groups in the PTCDA are almost unmodified upon adsorption. At the same time it has been observed that the perylene core retains its original structure as seen from the C1s core levels, except for a gradual shift towards lower binding energy. The small value of the C1s core level shift (0.6eV) towards lower binding energy can not account for a charge transfer, but is more likely a screening effect. A very recent study of the PTCDA/Au interface [Zou 2006] shows similar results to those obtained here. The authors interpreted the small shift towards lower binding energy as a "better screening of the core hole final state by the image charge or by charge transfer screening in the case of Au as compared to less effective delocalization or polarization of the PTCDA neighbors in the multilayer case".

All these observations support therefore the formation of an unreacted PTCDA/Au(111) interface, in good agreement with STS and UPS results shown in the previous sections. These XPS results are an additional proof that the interface states in the PTCDA band gap that appear for 1ML PTCDA coverage are due to the metallic gold substrate rather than being the result of a chemical reaction at the interface.

2.9 Interface energy level diagram

Further investigation was dedicated to the formation of the PTCDA/Au(111) interface in terms of energy level alignment between the metal and the organic semiconductor. This could provide further insight into the process of electron charge transfer at the interface. The mechanism of charge injection process from an electrode to an organic layer is important for the efficiency of the devices since the lowering of the operational voltage can decrease the eventual degradation of the devices. Prior to the results reported by Seki and co-workers [Ishii 1997] it was generally assumed that when an electrode and an organic layer are brought into contact, the vacuum levels of both materials would simply align. With this assumption the determination of the charge injection barrier is only a matter of calculating the difference between the metal work function (ϕ) and the electron affinity (EA) or ionization potential (IP) of the organic solid, as it was described in the introductory chapter.

Nevertheless, various experimental data have demonstrated that the vacuum level alignment or the so-called Schottky-Mott rule does not hold for any organic/inorganic interface. Besides, it has been found that neglecting the processes which occur at the interface may lead to incorrect estimation of the hole and electron injection barriers which are important parameters for an optimum device design.

Ultraviolet Photoemission Spectroscopy measurements have allowed us to establish the energy band diagram for PTCDA/Au interface. The energy level diagram can be estimated from the properties of both components (the clean substrate and the organic overlayer) that are experimentally accessible by UPS: the work function of the clean metal and the ionization potential of the organic molecules. The procedure to determine the energy level diagram consists in recording UPS spectra for a clean substrate and then compare it with the UPS spectra recorded after the overlayer adsorption. The UV photoemission spectra consist of photoelectrons which have suffered no energy loss in their way out of the solid and these provide information on the binding energy of the occupied states. Additionally, excited photoelectrons can suffer inelastic scattering processes. These secondary electrons contribute to the background signal, with an increased number of counts in the low kinetic energy side. To release an electron from the medium into the vacuum the kinetic energy of photoelectrons has to be higher than the vacuum level energy. As a result an abrupt cutoff in the UPS spectra occurs when the kinetic energy is equal to the vacuum level

energy. To improve this low energy cut-off, usually a negative voltage is applied between the sample and detector. From UPS spectra the position of the vacuum level is determined by adding the photon energy ($h\nu$) to the low kinetic energy cutoff. The Fermi edge energy is given by the high kinetic energy onset of the UPS spectra. Hence the work function of the metal is given by the difference between the vacuum level energy and the Fermi edge energy.

$$\Phi_{Au} = h\nu + E_{kin}^{min}(Au) - E_{kin}^{max}(Au) \qquad (2.7)$$

Similar to the work function of the metal, the ionization potential (IP) of the organic material is given by:

$$IP = h\nu + E_{kin}^{min}(PTCDA) - E_{kin}^{max}(PTCDA) \qquad (2.8)$$

In this case the high kinetic energy corresponds to the emission from the highest occupied molecular orbital (HOMO) of PTCDA.

To construct the energy band diagram for PTCDA on Au(111) we have initially characterized the clean gold substrate. Subsequently, PTCDA molecules have been deposited by incrementally amounts, while the UPS spectra were recorded after each deposition step. With this approach we have studied the changes in the electronic structure of the PTCDA/Au system as a function of the organic overlayer thickness.

Figure 2.24 shows the UPS spectrum for clean Au(111) surface and for multilayer (12 ML) PTCDA film. Both spectra were recorded with a potential difference of -4V between sample and analyzer, to improve the low energy kinetic cutoff. The typical valence band spectra of clean Au(111), recorded in normal emission, is shown in the lower spectrum. The characteristic features observed in the spectrum have been mentioned in the previous section. According to expression 2.7 we have determined the Au work function ϕ=4.95±0.05eV, which is comparable to values reported in the literature.

The multilayer PTCDA spectrum in figure 2.24(a) shows the characteristic valence band for thick PTCDA films. If the energy position of organic molecular levels is conventionally taken as the intersection between the tangent of the low binding energy side of the peak and the zero intensity background line we obtain a HOMO energy position of 1.7eV below the Fermi level. If the peak center is considered, the HOMO position would be at 2.0eV below to Fermi level.

Hence, according to expression 2.8 the obtained ionization energy (IP) for the PTCDA film is ~6.8eV, similar to surface ionization energy reported for thick PTCDA film [Hill 1998].

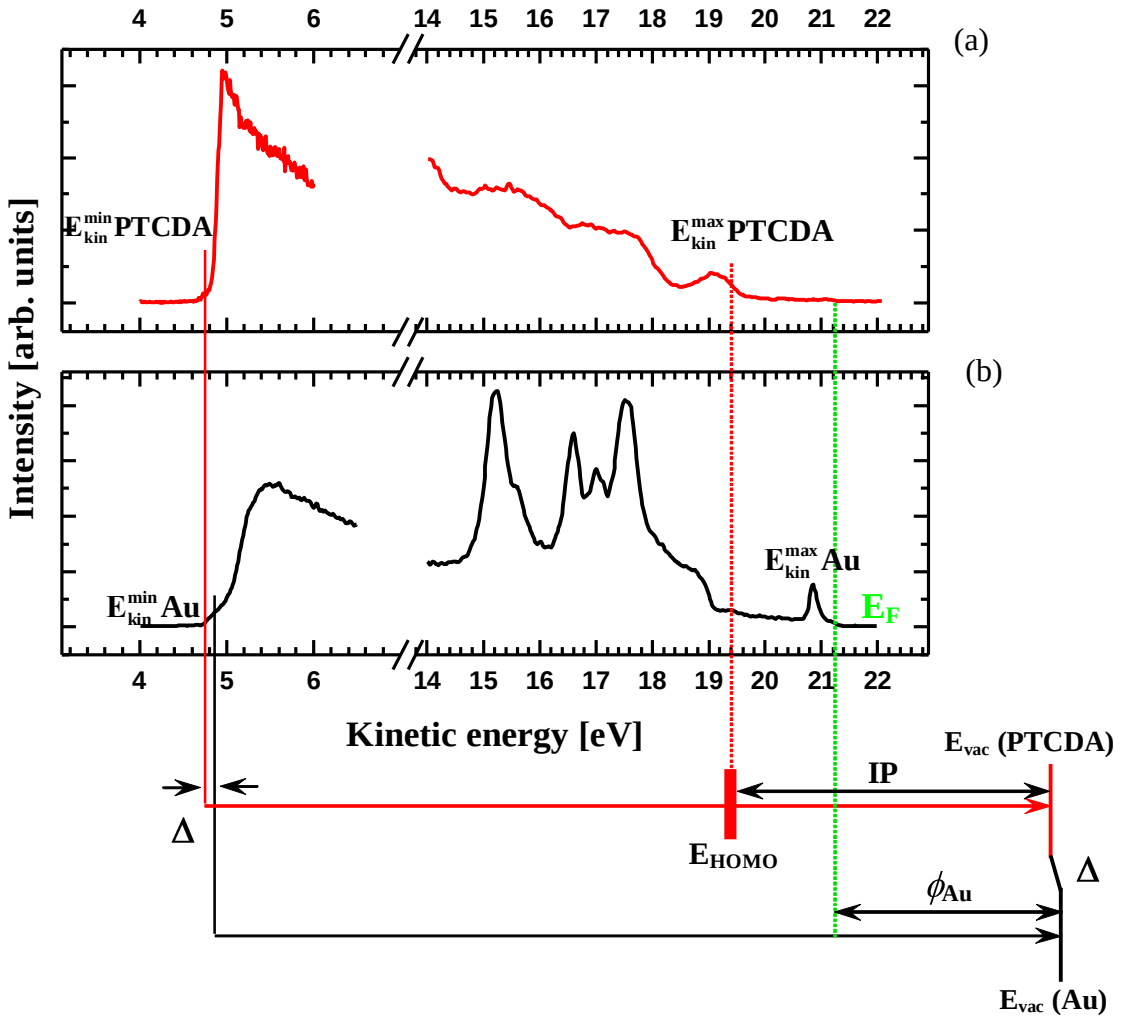

Figure 2.24 *Energy band diagram of PTCDA/Au(111) system determined by means of ultraviolet photoemission spectroscopy. (a) UPS spectra of 4nm PTCDA and (b) UPS spectra of clean Au(111). The lower panel shows a schematic of the energy band alignment inferred from photoemission measurements. The shift of the low kinetic energy cut-off (Δ) between the vacuum levels of the metal and PTCDA overlayers is marked on the left side by vertical lines.*

By comparing both UPS spectra in the low kinetic energy region we observe a misalignment of the vacuum levels of the gold metal and the organic overlayer. There is a small shift of Δ=0.15±0.05eV to lower kinetic energy for the PTCDA film, as compared to the cut-off of the bare gold spectra. An equivalent shift has been observed, as well for 1ML PTCDA, which indicates that change in the work function, occurs mainly at the interface and it remains constant with increasing PTCDA coverage.

Vacuum level discontinuity across an interface is commonly attributed to the formation of an electric dipole. A downward or an upward shift gives the sign and the quantity of shift gives the magnitude of the interface dipole. Accordingly to the nomenclature used in the current literature a downward shift of the organic layer vacuum level means a positive charge on the organic material side and a negative charge on the metal side and yields a negative interface dipole. In view of that, our UPS results show the formation of a negative dipole at the PTCDA/Au(111) interface. In the simplest way this can be interpreted as a charge transfer from molecule to metal. The obtained negative interface dipole, in good agreement with previous measurements [Hill 1998], could be naively considered unexpected for PTCDA molecules, which are rather electron acceptor type, than donor type. However, as already pointed out by Ishii *et al*. [Ishii 1999] the changes in the work function must arise (or must be compensated) from effects other than charge transfer from molecule to metal. The formation of an interface dipole may be the consequence of several contributions. These include direct charge transfer, change in the work function as a result of the perturbation of the metal surface electronic density tail due to adsorbed molecules or other more specific origins such permanent dipole of organic molecules [Ishii 1999], or metal induced gap states [Vazquez 2004, Vazquez 2007].

A direct charge transfer can not be inferred directly from the XPS measurements. As shown previously, small shifts of the core level can not account for a significant charge transfer, being more likely related to a screening effect. Besides, by using independent techniques (STS/UPS/XPS) we have found no evidence of chemisorption, indicating also the absence of new interface states in the PTCDA gap as a result of the interaction at the interface. Polar molecules having a permanent dipole could contribute to the net surface dipole only if the dipole moment would have a component perpendicular to the surface which is not the case of PTCDA.

Taking into account all these observations we consider that the main contribution to the interface dipole formation is related to a work function change, due to the perturbation of the electronic structure of the metal surface as a consequence of the Pauli repulsion. The repulsion between the molecule electrons and the metal surface leads to a compression of the electron tail leading to a lowering of the metal work function upon adsorption. This downward shift of the organic vacuum level at the interface is mainly responsible for the interface dipole formation.

Though a partial charge transfer can not be excluded at the interface, we have no direct evidence of it. The existence of the Au surface states close to the Fermi level would allow a partial charge transfer necessary to align the organic-metal Fermi levels.
Hence, the overall energy band diagram can be completed by including the LUMO energy position with respect to the Fermi level. Usually, in the reported literature the LUMO position of an organic material is inferred by the combination of UPS and optical absorption measurements (which yield the optical gap).

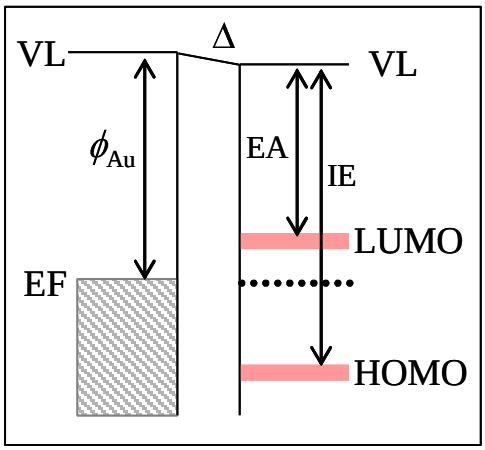

Figure 2.25 *Energy band diagram at the PTCDA /Au(111) interface determined from combination of independent technique (UPS/STS).*

In this work the LUMO position may be added, accordingly to the STS results mentioned in a previous section. Our scanning tunneling spectroscopy results yield a bang gap of ~3.0eV at the PTCDA/Au(111) interface. We have determined the LUMO at approximately 1.0±0.1V above the Fermi level and the HOMO 1.9±0.1V below the Fermi level. With this approach we were able to construct a complete energy band diagram which illustrates the alignment of molecular level at the interface, as shown in figure 2.25.

2.10 Low temperature STM experiments

2.10.1 Standing waves in the surface electron density

With the aim of a further investigation of the Au(111) Shockley-type surface states upon PTCDA adsorption we have also performed low temperature (40K) STM experiments, with a home-made variable temperature STM described elsewhere [Custance 2002, Custance 2003].

The fact that the surface states on the (111) surfaces of noble metals are localized in the first atomic layers from the surface, implies that they may contribute and also be influenced by various processes taking place at the surface e.g., surface reconstruction, adatoms or molecules adsorption. Being highly sensitive to surface modifications, the surface states can serve to monitor the strength of interaction at different interfaces.

It is well known that adsorption of foreign atoms or molecules modify the geometric structure, the work function and the surface electronic states of a clean surface. In many cases the adsorption removes the surface electronic states. It has been observed that chemisorbed atoms often completely quench the surface states [Lindgren 1978]. In the case of alkali metals and rare gases, however, their adsorption modifies the surface states so slightly that the surface states are persistent. The modification of surface states dispersion with adsorbates has been often studied with photoemission spectroscopy. Recently, the modification of Shockley states by adsorbed rare gases overlayers has been studied in detail by STS and/or photoemission spectroscopy [Forster 2003, Andreev 2004, Forster 2004]. The reported experiments have shown that surface states were shifted in energy a few meV, towards lower binding energy.

While most of the studies were concentrated on isolated scattering centers for electrons, or rare gases adsorption, until very recently [Bannani 2007] there were no studies concerning the influence of adsorbed organic layers.

This section presents experimental low temperature STM results obtained at the PTCDA/Au(111) interface. Figure 2.26(a) shows a representative STM image acquired at low temperature (T=40K) and relatively high bias voltage, for 1ML PTCDA on the Au(111) substrate. The image exhibits mostly the topographic nature of the sample. A gold monoatomic step observed on the left side of the image separates Au terraces which are almost completely covered by a PTCDA monolayer.

A close-up view (figure 2.26(b)) of a gold area completely covered by a PTCDA monolayer indicates that the Au(111)-(22×√3) reconstruction is still visible through the ordered PTCDA layer.

This is confirmed by the corresponding Fourier transform (FT) pattern which exhibits both PTCDA and Au periodicities. The features observed close to the centre of the FT pattern in figure 2.26(c) have a periodicity of (2π/L) with L≅63Å, distance which corresponds to neighboring pairs of Au reconstruction lines. Simultaneously resolved is the PTCDA characteristic periodicity which can be recognized in the FT pattern.

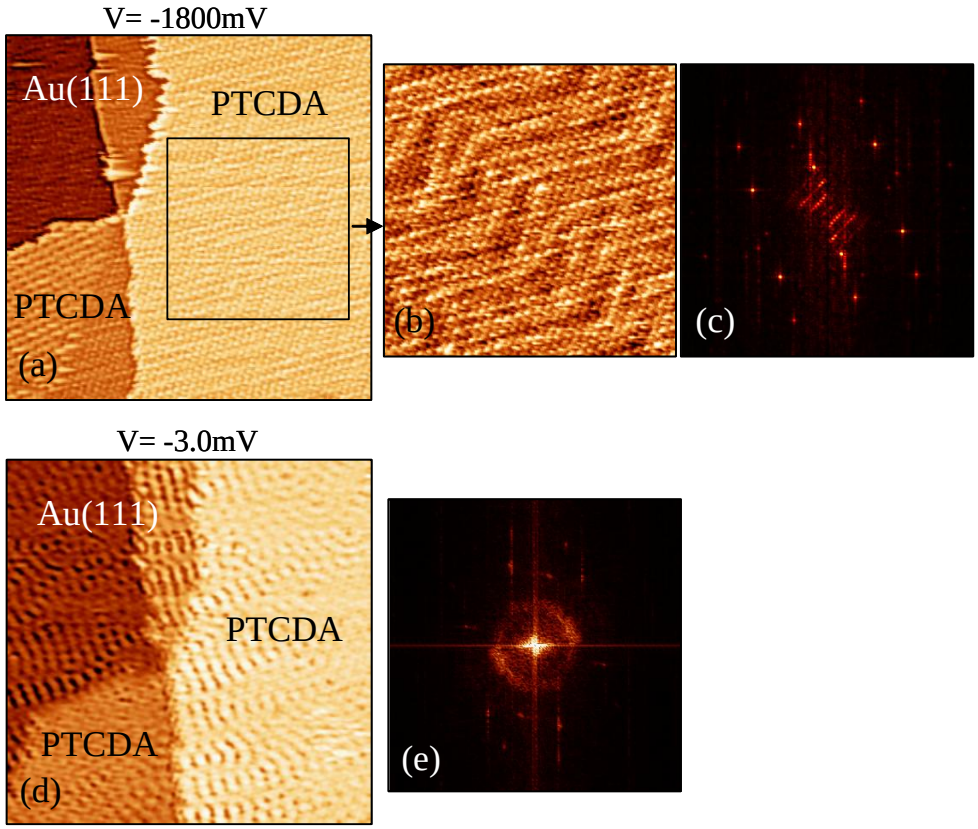

Figure 2.26 *(a) Constant current STM image of 1ML PTCDA on Au(111) at 40K. (72nm×72nm, V=-1800mV, I=0.02nA). (b) Close-up view of scan area marked in (a), where the Au reconstruction is still visible through the PTCDA monolayer covering the substrate. (c) The Fourier transform pattern of image (b) shows both PTCDA and Au reconstruction periodicities. (d) Constant current STM image acquired at low bias voltage (72nm×72nm, V=-3.0mV, I=0.02nA). Standing waves are seen on both clean and PTCDA covered Au areas. (e) Fourier transform of image (d) shows a circular shape with a broaden edge of the surface Fermi contour.*

An STM image, acquired this time at low bias voltage (-3.0mV), in the same sample area as before, shows significant changes as can be observed in figure 2.26(d). Long range spatial oscillations can be seen in the LDOS as a result of standing waves formation due to the step edge and point defects in the surface. Standing waves are

observed on both areas: on the clean Au areas in the upper left part of the image and on the PTCDA covered gold substrate.

The Fourier transform of the image shows a circular shape of the Fermi contour which indicates an isotropic behavior of surface states existing on the surface, as seen in figure 2.26(e). Nevertheless, it can be noticed that the surface Fermi contour presents a broaden edge, which suggests the existence of two possible concentric rings. Two Fermi contours, with a different radius, could be explained by the contribution to the FT pattern of two Fermi wave vectors with a slightly different value.

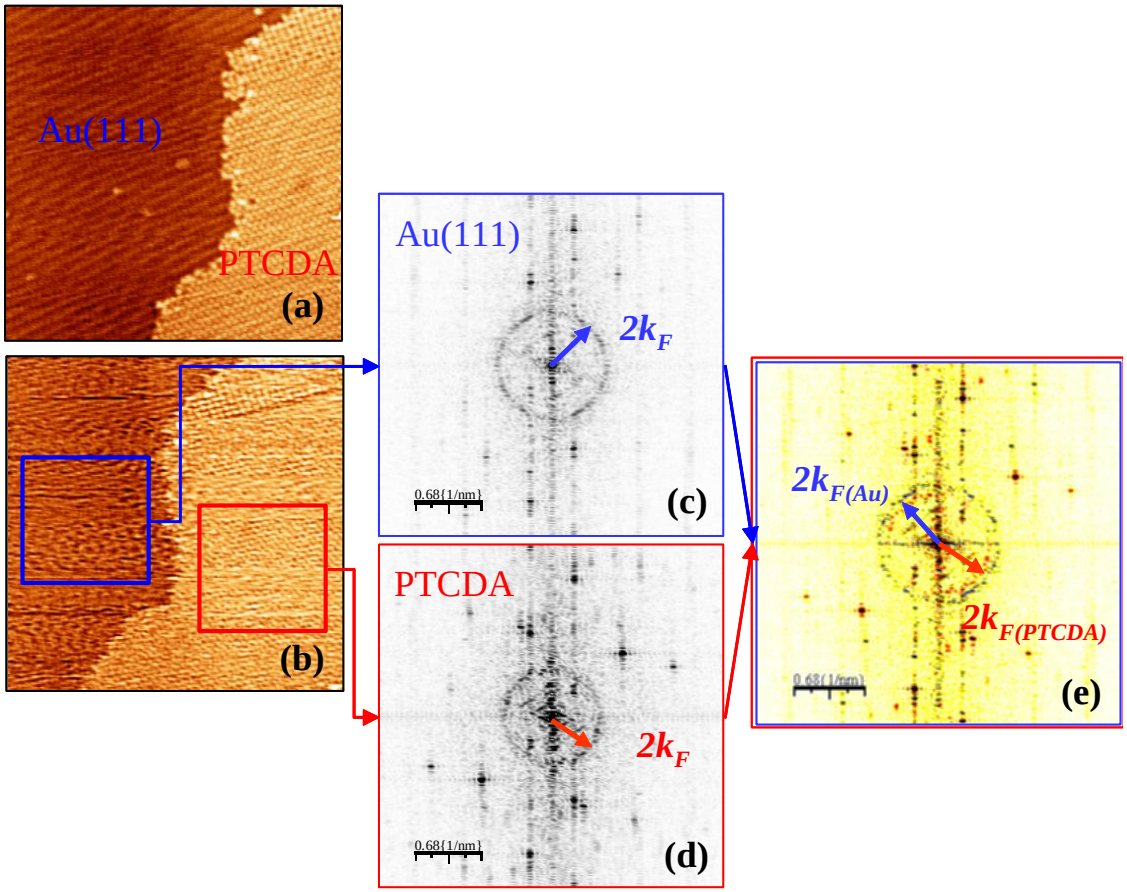

Figure 2.27 *(a) Constant current STM image acquired at 40 K of 1ML PTCDA partially covering the Au(111) substrate (70nm×70nm, V=-1800mV, I=0.02nA). (b) STM image (70nm×70nm, V=+4.0mV, I=0.02nA) acquired at low bias and 40K. Standing waves are observed on both areas. While the left side corresponds to clean Au substrate the right side corresponds to a PTCDA covered Au area. (c) and (d) are FT patterns corresponding to the scan area marked in image (b). (e) Superposition of the two FT transforms corresponding to clean and PTCDA covered Au(111) substrate.*

In order to clarify if indeed the broaden edge of the Fermi contour comes from the superposition of two different wavelength contributions, a new example is shown. A sample area where both clean and PTCDA covered substrate coexist is scanned first

at relative high bias voltage as shown in figure 2.27(a). We mention that due to the tip condition, it is not always possible to resolve the molecular structure at low bias voltage; therefore a check scan is always acquired first at high bias voltages.

When the bias voltage is reduced down to values close to the Fermi energy, we observe again standing waves patterns on both clean gold areas, in the left part of the image (figure 2.27(b)) and on PTCDA monolayer, on the right side of the image.

By applying 2D Fourier transform to each area marked in the STM image of figure 2.27(b), the *k*-space image can be extracted for both clean Au and PTCDA covered areas, respectively.

The circular shape seen in FT pattern of figure 2.27(c) corresponds to the Fermi contour of the Au(111) surface. As the STM image was taken at low bias voltage the only electrons which contribute to the image are those with energy close to the Fermi level. Because the STM is sensitive to the square of the wave function, the Fourier transform displays the Fermi contour scaled by a factor of two, as it has been previously pointed out (section 2.3.2).

A direct visualization of both Fourier transform patterns, corresponding to clean gold and PTCDA monolayer suggests no significant differences as can be seen by the comparison of figure 2.27(c) and (d). Except of PTCDA reciprocal lattice periodicity observed in figure 2.27(d), a circular shape of the Fermi contour can be observed in both *k*-space images. However, a superposition of both FT patterns gives a direct evidence for the existence of two different Fermi wavelengths which contribute to the *k*-space image. In figure 2.27(e), which represents the contribution of both clean and PTCDA covered substrate, we unambiguously observe the existence of two concentric rings with a slightly different radius.

From the average radius of the outer ring (blue colored in figure 2.28(a)), the Fermi wave vector for the surface states on Au(111) is estimated to be k_F(Au)=0.17±0.05 Å^{-1}, which is in good agreement with photoemission results where k_F=0.173 Å^{-1}.

By measuring the average radius of the inner ring (red colored in figure 2.28(a)) which corresponds to contribution from surfaces states at the PTCDA/Au(111) interface we determine a Fermi wave vector value of k_F(PTCDA)=0.15±0.05 Å^{-1}.

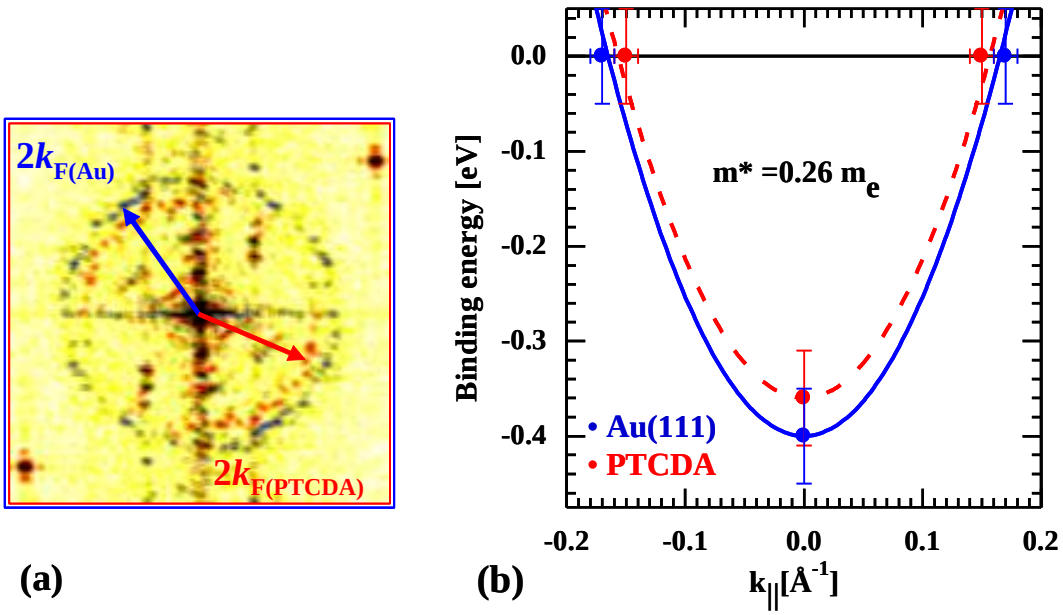

Figure 2.28 *(a) Surface Fermi contour as obtained from the FT pattern of an STM image consisting of both clean and PTCDA covered areas. (b) Surface state band dispersion for clean Au(111) surface (solid line)and for 1ML PTCDA/Au(111) interface (dashed line). The shift of the surface states band bottom and the k_F value are consistent with STS and FT results obtained for 1ML PTCDA on the gold surface.*

Thus by performing Fourier transform of images consisting of both clean and PTCDA covered gold areas we are able to determine simultaneously the contribution of the Fermi wave vector of different areas. The simultaneous measurement of the k_F(Au) and k_F(PTCDA) eliminates the systematic errors due to the thermal drift or piezo creep which can occur by determining these values from different acquired STM images. From these results we determined that PTCDA overlayer exhibits electron standing waves pattern with a longer Fermi wavelength as compared to those of the bare Au(111) substrate.

The surface state band dispersion of the clean Au(111) surface is plotted in figure 2.28(b). We have used an effective mass of 0.26m_e from UPS standard measurements [Forster 2004] and we have fixed the band bottom to the experimentally determined value by STS (section 2.6.1). We have also plotted the k_F value for Au(111) as determined from figure 2.28(a). A similar plot was performed for the interface state band found at the PTCDA/Au interface. The dashed line in figure 2.28(b) represents a parabolic

dispersion for the surface states existing at the interface, assuming the same effective as for the clean surface ($m^*=0.26m_e$) and using the bottom of the band value measured with STS is section 2.6.1. The k_F value for the PTCDA layer as determined from (a) is also plotted. Earlier reports concerning the adsorption of noble gases (Ar, Kr, Xe) on Au(111) have shown that the effective mass does not change significantly from the values obtained for a clean Au surface. Thus, by assuming the same effective mass, we obtained a surface state band dispersion which is consistent with an upward shift of the surface states band bottom and a smaller Fermi wavevector value, as compared to the bare gold surface.

Changes in the binding energy of the surface states band bottom upon adsorption have been previously observed for various systems where a physisorption process was reported at the interface [Park 2000, Hovel 2001, Andreev 2004]. In particular the noble gases adsorption on several (111) noble metal surfaces preserves the surface states, leading to a slight modification of the band energy, in particular an upward shift (toward lower binding energies) of the surface states band minimum. It has been found out that the degree of the shift increases with decreasing nobleness of the adsorbate. For example, the adsorption of rare gases monolayers on Au(111) surface produces a surface state band shift of ~60meV, ~80meV and ~140meV for the adsorption of Ar, Kr and Xe, respectively [Forster 2004, Forster 2006]. The observed upward shifts in energy have been qualitatively interpreted in terms of Pauli repulsion.

Weakly adsorbed species, as systems with a closed shell electronic structure, on metal surfaces can be described by a physisorption process. In this process two interaction mechanisms can contribute. On the one hand, the long range attractive van der Waals interaction, which arises from interaction of fluctuating dipoles of the adsorbate with the image dipole in the solid. On the other hand, at very close distances, short-range Pauli repulsion interaction becomes important. This Pauli repulsion is a consequence of the overlapping of the electronic wave functions of the metal surface, decaying exponentially outside the crystal, with the wave functions of systems with closed shell electronic structure. In order to reduce this overlap, part of the electron density tailing from the free surface is pushed back into the solid upon adsorption. This electronic density change at the metal surface is energetically unfavorable, and consequently results in a reduction of surface states electrons binding energy.

2.11 Conclusions

By the combination of various techniques, as STM/STS, UPS and XPS we have obtained a detailed characterization of the PTCDA adsorption on Au(111) substrate.

- STM results obtained for 1ML PTCDA adsorbed on Au(111) substrates suggest a weak molecule-substrate interaction at the PTCDA/Au(111) interface. This weak interaction is supported by several aspects found in STM experiments as: the spontaneously assembling of molecules and high diffusion on the metallic surface, the unmodified substrate reconstruction upon adsorption and a molecular structure at the interface similar to that of PTCDA bulk crystal.
- The weak interaction at the interface is supported also by the observation of almost unperturbed molecular orbitals, closely resembling the native LUMO and HOMO of free PTCDA
- STS and UPS results show that the Shockley type surface state of Au(111) substrate is not suppressed upon PTCDA adsorption, being still visible through PTCDA monolayer. ARUPS measurements clearly demonstrate the existence of the gold surface states at the interface, though slightly modified. These results are confirmed by LT-STM experiments which unambiguously show a modification of the surface state, in particular an upward shift in surface states energy band minimum.
- XPS results support the formation of an unreacted PTCDA/Au(111) interface, in good agreement with STS and UPS. These XPS results are an additional proof that the interface states in the PTCDA band gap that appear for 1ML PTCDA coverage are due to the metallic gold substrate rather than being the result of a chemical reaction at the interface.

References

[Andreev 2004] T. Andreev, I. Barke and H. Hovel, *Adsorbed Rare-Gas Layers on Au(111): Shift of the Shockley Surface State Studied with Ultraviolet Photoelectron Spectroscopy and Scanning Tunneling Spectroscopy*, Physical Review B **70,** 205426 (2004).

[Azuma 2000] Y. Azuma, S. Akatsuka, K. K. Okudaira, Y. Harada and N. Ueno, *Angle-Resolved Ultraviolet Photoelectron Spectroscopy of In-[Perylene-3,4,9,10-Tetracarboxylic Dianhydride] System*, Journal of Applied Physics **87**, 766 (2000).

[Bannani 2007] A. Bannani, C. Bobisch and R. Moller, *Ballistic Electron Microscopy of Individual Molecules*, Science **315**, 1824 (2007).

[Barth 1990] J. V. Barth, H. Brune, G. Ertl and R. J. Behm, *Scanning Tunneling Microscopy Observations on the Reconstructed Au(111) Surface: Atomic Structure, Long-Range Superstructure, Rotational Domains, and Surface Defects*, Physical Review B **42**, 9307 (1990).

[Braun 2005] D. Braun, A. Schirmeisen and H. Fuchs, *Molecular Growth and Sub-Molecular Resolution of a Thin Multilayer of PTCDA on Ag(110) Observed by Scanning Tunneling Microscopy*, Surface Science **575**, 3 (2005).

[Chizhov 2000] I. Chizhov, A. Kahn and G. Scoles, *Initial Growth of 3,4,9,10-Perylenetetracarboxylic-Dianhydride (PTCDA) on Au(111): A Scanning Tunneling Microscopy Study*, Journal of Crystal Growth **208**, 449 (2000).

[Chkoda 2003] L. Chkoda, M. Schneider, V. Shklover, L. Kilian, M. Sokolowski, C. Heske and E. Umbach, *Temperature-Dependent Morphology and Structure of Ordered 3,4,9,10-Perylene-Tetracarboxylicacid-Dianhydride (PTCDA) Thin Films on Ag(111), Chemical Physics Letters* **371**, 548 (2003).

[Crommie 1993] M. F. Crommie, C. P. Lutz and D. M. Eigler, *Imaging Standing Waves in a 2-Dimensional Electron-Gas*, Nature **363**, 524 (1993).

[Custance 2002] O. Custance, *PhD Thesis*, Universidad Autonóma Madrid (2002).

[Custance 2003] O. Custance, S. Brochard, I. Brihuega, E. Artacho, J. M. Soler, A. M. Baro and J. M. Gomez-Rodriguez, *Single Adatom Adsorption and Diffusion on Si(111)-(7×7) Surfaces: Scanning Tunneling Microscopy and First-Principles Calculations*, Physical Review B **67,** 235410 (2003).

[Dori 2006] N. Dori, M. Menon, L. Kilian, M. Sokolowski, L. Kronik and E. Umbach, *Valence Electronic Structure of Gas-Phase 3,4,9,10-Perylene Tetracarboxylic Acid Dianhydride: Experiment and Theory*, Physical Review B **73**, 195208 (2006).

[Eremtchenko 2003] M. Eremtchenko, J. A. Schaefer and F. S. Tautz, *Understanding and Tuning the Epitaxy of Large Aromatic Adsorbates by Molecular Design*, Nature **425**, 602 (2003).

[Eremtchenko 2004] M. Eremtchenko, D. Bauer, J. A. Schaefer and F. S. Tautz, *Polycyclic Aromates on Close-Packed Metal Surfaces: Functionalization, Molecular Chemisorption and Organic Epitaxy*, New Journal of Physics **6**, 4 (2004).

[Fenter 1995] P. Fenter, P. E. Burrows, P. Eisenberger and S. R. Forrest, *Layer-by-Layer Quasi-Epitaxial Growth of a Crystalline Organic Thin-Film*, Journal of Crystal Growth **152**, 65 (1995).

[Fenter 1996] P. Fenter, P. Eisenberger, P. Burrows, S. R. Forrest and K. S. Liang, *Epitaxy at the Organic-Inorganic Interface*, Physica B **221**, 145 (1996).

[Fenter 1997] P. Fenter, F. Schreiber, L. Zhou, P. Eisenberger and S. R. Forrest, *In Situ Studies of Morphology, Strain, and Growth Modes of a Molecular Organic Thin Film*, Physical Review B **56**, 3046 (1997).

[Forrest 1997] S. R. Forrest, *Ultrathin Organic Films Grown by Organic Molecular Beam Deposition and Related Techniques*, Chemical Reviews **97**, 1793 (1997).

[Forster 2003] F. Forster, G. Nicolay, F. Reinert, D. Ehm, S. Schmidt and S. Hufner, *Surface and Interface States on Adsorbate Covered Noble Metal Surfaces*, Surface Science **532**, 160 (2003).

[Forster 2004] F. Forster, S. Hufner and F. Reinert, *Rare Gases on Noble-Metal Surfaces: An Angle-Resolved Photoemission Study with High Energy Resolution*, Journal of Physical Chemistry B **108**, 14692 (2004).

[Forster 2006] F. Forster, A. Bendounan, J. Ziroff and F. Reinert, *Systematic Studies on Surface Modifications by ARUPS on Shockley-Type Surface States*, Surface Science **600**, 3870 (2006).

[Gartland 1975] P. O. Gartland and B. J. Slagsvold, *Transitions Conserving Parallel Momentum in Photoemission from the (111) Face of Copper*, Physical Review B **12**, 4047 (1975).

[Gerlach 2007] A. Gerlach, S. Sellner, F. Schreiber, N. Koch and J. Zegenhagen, *Substrate-Dependent Bonding Distances of PTCDA: A Comparative X-Ray Standing-Wave Study on Cu(111) and Ag(111)*, Physical Review B **75**, 045401 (2007).

[Glockler 1998] K. Glockler, C. Seidel, A. Soukopp, M. Sokolowski, E. Umbach, M. Bohringer, R. Berndt and W. D. Schneider, *Highly Ordered Structures and Submolecular Scanning Tunnelling Microscopy Contrast of PTCDA and DM-PBDCI Monolayers on Ag(111) and Ag(110)*, Surface Science **405**, 1 (1998).

[Harten 1985] U. Harten, A. M. Lahee, J. P. Toennies and C. Wöll, *Observation of a Soliton Reconstruction of Au(111) by High-Resolution Helium-Atom Diffraction*, Physical Review Letters **54**, 2619 (1985).

[Hasegawa 1993] Y. Hasegawa and P. Avouris, *Direct Observation of Standing Wave Formation at Surface Steps Using Scanning Tunneling Spectroscopy*, Physical Review Letters **71**, 1071 (1993).

[Hauschild 2005] A. Hauschild, K. Karki, B. C. C. Cowie, M. Rohlfing, F. S. Tautz and M. Sokolowski, *Molecular Distortions and Chemical Bonding of a Large Pi-Conjugated Molecule on a Metal Surface*, Physical Review Letters **94**, 036106 (2005).

[Henze 2007] S. K. M. Henze, O. Bauer, T.-L. Lee, M. Sokolowski and F. S. Tautz, *Vertical Bonding Distances of PTCDA on Au(111) and Ag(111): Relation to the Bonding Type*, Surface Science **601**, 1566 (2007).

[Heyraud 1980] J. C. Heyraud and J. J. Metois, *Anomalous 422 Diffraction Spots from {111} Flat Gold Crystallites: (111) Surface Reconstruction and Moire Fringes between the Surface and the Bulk*, Surface Science **100**, 519 (1980).

[Hill 1998] I. G. Hill, A. Rajagopal, A. Kahn and Y. Hu, *Molecular Level Alignment at Organic Semiconductor-Metal Interfaces*, Applied Physics Letters **73**, 662 (1998).

[Hill 2000] I. G. Hill, A. Kahn, Z. G. Soos and R. A. Pascal, *Charge-Separation Energy in Films of Pi-Conjugated Organic Molecules*, Chemical Physics Letters **327**, 181 (2000).

[Hirose 1996] Y. Hirose, A. Kahn, V. Aristov, P. Soukiassian, V. Bulovic and S. R. Forrest, *Chemistry and Electronic Properties of Metal-Organic Semiconductor Interfaces: Al, Ti, in, Sn, Ag, and Au on PTCDA*, Physical Review B **54**, 13748 (1996).

[Hirose 1997] Y. Hirose, C. I. Wu, V. Aristov, P. Soukiassian and A. Kahn, *Chemistry and Electronic Properties of Metal Contacts on an Organic Molecular Semiconductor*, *Applied Surface Science* **114**, 291 (1997).

[Hooks 2001] T. F. D. E. Hooks, M. D. Ward, *Epitaxy and Molecular Organization on Solid Substrates*, Advanced Materials **13**, 227 (2001).

[Hoshino 1994] A. Hoshino, S. Isoda, H. Kurata and T. Kobayashi, *Scanning Tunneling Microscope Contrast of Perylene-3,4,9,10-Tetracarboxylic-Dianhydride on Graphite and Its Application to the Study of Epitaxy*, Journal of Applied Physics **76**, 4113 (1994).

[Hovel 2001] H. Hovel, B. Grimm and B. Reihl, *Modification of the Shockley-Type Surface State on Ag(111) by an Adsorbed Xenon Layer*, Surface Science **477**, 43 (2001).

[Ishii 1997] H. Ishii and K. Seki, *Energy Level Alignment at Organic/Metal Interfaces Studied by UV Photoemission: Breakdown of Traditional Assumption of a Common Vacuum Level at the Interface*, IEEE Transactions on Electron Devices **44**, 1295 (1997).

[Ishii 1999] K. Ishii, E. Ito, K. Seki, *Energy Level Alignment and Interfacial Electronic Structures at Organic/Metal and Organic/Organic Interfaces*, Advanced Materials **11**, 605 (1999).

[Kevan 1987] S. D. Kevan and R. H. Gaylord, *High-Resolution Photoemission-Study of the Electronic-Structure of the Noble-Metal (111) Surfaces*, Physical Review B **36**, 5809 (1987).

[Kilian 2004] L. Kilian, E. Umbach and M. Sokolowski, *Molecular Beam Epitaxy of Organic Films Investigated by High Resolution Low Energy Electron Diffraction (SPA-LEED): 3,4,9,10-Perylenetetracarboxylicacid-Dianhydride (PTCDA) on Ag(111)*, Surface Science **573**, 359 (2004).

[Kilian 2006] L. Kilian, E. Umbach and M. Sokolowski, *A Refined Structural Analysis of the PTCDA Monolayer on the Reconstructed Au(111) Surface "Rigid or Distorted Carpet?"* Surface Science **600**, 2633 (2006).

[Knoth 2002] L. Knoth, *PhD Thesis*, University of Würzburg (2002).

[Krause 2002] B. Krause, A. C. Durr, K. Ritley, F. Schreiber, H. Dosch and D. Smilgies, *Structure and Growth Morphology of an Archetypal System for Organic Epitaxy: PTCDA on Ag(111)*, Physical Review B **66,** 235404 (2002).

[LaShell 1996] S. LaShell, B. A. McDougall and E. Jensen, *Spin Splitting of an Au(111) Surface State Band Observed with Angle Resolved Photoelectron Spectroscopy*, Physical Review Letters **77**, 3419 (1996).

[Lindgren 1978] S. A. Lindgren and L. Wallden, *Cu Surface-State and Cs Valence-Electrons in Photoelectron-Spectra from Cu(111)-Cs Adsorption System*, Solid State Communications **28**, 283 (1978).

[Mannsfeld 2001] S. Mannsfeld, M. Toerker, T. Schmitz-Hubsch, F. Sellam, T. Fritz and K. Leo, *Combined LEED and STM Study of PTCDA Growth on Reconstructed Au(111) and Au(100) Single Crystals*, Organic Electronics **2**, 121 (2001).

[Méndez 2006] J. Méndez, R. Caillard, G. Otero, N. Nicoara, J.A. Martin-Gago, *Nanostructured Organic Material: From Molecular Chains to Organic Nanodots*, Advanced Materials **18**, 2048 (2006).

[Mobus 1992] M. Mobus, N. Karl and T. Kobayashi, *Structure of Perylene-Tetracarboxylic-Dianhydride Thin-Films on Alkali-Halide Crystal Substrates*, Journal of Crystal Growth **116**, 495 (1992).

[Nicoara 2006] N. Nicoara, E. Roman, J. M. Gomez-Rodriguez, J. A. Martin-Gago and J Mendez, *Scanning Tunneling and Photoemission Spectroscopies at the PTCDA/Au(111) interface*, Organic Electronics **7**, 287 (2006).

[Ordejon 1996] P. Ordejon, E. Artacho and J. M. Soler, *Self-Consistent Order-N Density-Functional Calculations for Very Large Systems*, Physical Review B **53**, 10441 (1996).

[Oszwaldowski 2003] R. Oszwaldowski, H. Vazquez, P. Pou, J. Ortega, R. Perez and F. Flores, *Exchange-Correlation Energy in the Orbital Occupancy Method: Electronic Structure of Organic Molecules*, Journal of Physics-Condensed Matter **15**, S2665 (2003).

[Paniago 1995] R. Paniago, R. Matzdorf, G. Meister and A. Goldmann, *Temperature Dependence of Shockley-Type Surface Energy Bands on Cu(111), Ag(111) and Au(111)*, Surface Science **336**, 113 (1995).

[Park 2000] J. Y. Park, U. D. Ham, S. J. Kahng, Y. Kuk, K. Miyake, K. Hata and H. Shigekawa, *Modification of Surface-State Dispersion Upon Xe Adsorption: A Scanning Tunneling Microscope Study*, Physical Review B **62**, 16341 (2000).

[Pascual 1998] J. I. Pascual, *PhD Thesis*, Universidad Autónoma Madrid (1998).

[Perdereau 1974] J. Perdereau, J. P. Biberian and G. E. Rhead, *Adsorption and Surface Alloying of Lead Monolayers on (111) and (110) Faces of Gold*, Journal of Physics F: Metal Physics **4**, 798 (1974).

[Perdew 1981] J. P. Perdew and A. Zunger, *Self-Interaction Correction to Density-Functional Approximations for Many-Electron Systems*, Physical Review B **23**, 5048 (1981).

[Reinert 2001] F. Reinert, G. Nicolay, S. Schmidt, D. Ehm and S. Hüfner, *Direct Measurements of the L-Gap Surface States on the (111) Face of Noble Metals by Photoelectron Spectroscopy*, Physical Review B **63**, 115415 (2001).

[Reinert 2003] F. Reinert, *Spin-Orbit Interaction in the Photoemission Spectra of Noble Metal Surface States*, Journal of Physics-Condensed Matter **15**, S693 (2003).

[Reinert 2004] F. Reinert and G. Nicolay, *Influence of the Herringbone Reconstruction on the Surface Electronic Structure of Au(111)*, Applied Physics A: Materials Science & Processing **78**, 817 (2004).

[Repp 2005] J. Repp, G. Meyer, S. M. Stojkovic, A. Gourdon and C. Joachim, *Molecules on Insulating Films: Scanning-Tunneling Microscopy Imaging of Individual Molecular Orbitals*, Physical Review Letters **94,** 026803 (2005).

[Schmitz-Hübsch 1997] T. Schmitz-Hübsch, T. Fritz, F. Sellam, R. Staub and K. Leo, Epitaxial *Growth of 3,4,9,10-Perylene-Tetracarboxylic-Dianhydride on Au(111): A STM and RHEED Study*, Physical Review B **55**, 7972 (1997).

[Seidel 1997] C. Seidel, C. Awater, X. D. Liu, R. Ellerbrake and H. Fuchs, *A Combined STM, Leed and Molecular Modelling Study of PTCDA Grown on Ag(110)*, Surface Science **371**, 123 (1997).

[Shklover 2000] V. Shklover, F. S. Tautz, R. Scholz, S. Sloboshanin, M. Sokolowski, J. A. Schaefer and E. Umbach, *Differences in Vibronic and Electronic Excitations of PTCDA on Ag(111) and Ag(110)*, Surface Science **454**, 60 (2000).

[Shockley 1939] W. Shockley, *On the Surface States Associated with a Periodic Potential*, Physical Review **56**, 317 (1939).

[Soler 2002] J. M. Soler, E. Artacho, J. D. Gale, A. Garcia, J. Junquera, P. Ordejon and D. Sanchez-Portal, *The Siesta Method for Ab Initio Order-N Materials Simulation*, Journal of Physics-Condensed Matter **14**, 2745 (2002).

[Stahl 1998] U. Stahl, D. Gador, A. Soukopp, R. Fink and E. Umbach, *Coverage-Dependent Superstructures in Chemisorbed NTCDA Monolayers: A Combined LEED and STM Study*, Surface Science **414**, 423 (1998).

[Stohr 2002] M. Stohr, M. Gabriel and R. Moller, *Investigation of the Growth of PTCDA on Cu(110): An STM Study*, Surface Science **507**, 330 (2002).

[Taborski 1995] J. Taborski, *NEXAFS Investigations on Ordered Adsorbate Layers of Large Aromatic Molecules*, J. Electr. Spec. Rel. Phenom. **75**, 129 (1995).

[Tanishiro 1981] Y. Tanishiro, H. Kanamori, K. Takayanagi, K. Yagi and G. Honjo, *UHV Transmission Electron Microscopy on the Reconstructed Surface of (111) Gold : I. General Features*, Surface Science **111**, 395 (1981).

[Tautz 2002] F. S. Tautz, *Strong Electron-Phonon-Coupling at a Metal/Organic Interface: PTCDA/Ag(111)*, Phys. Rev. B **65**, 125405 (2002).

[Temirov 2006] R. Temirov, S. Soubatch, A. Luican and F. S. Tautz, *Free-Electron-Like Dispersion in an Organic Monolayer Film on a Metal Substrate*, Nature **444**, 350 (2006).

[Troullier 1991] N. Troullier and J. L. Martins, *Efficient Pseudopotentials for Plane-Wave Calculations*, Physical Review B **43**, 1993 (1991).

[Tsiper 2002] E. V. Tsiper, Z. G. Soos, W. Gao and A. Kahn, *Electronic Polarization at Surfaces and Thin Films of Organic Molecular Crystals: PTCDA*, Chemical Physics Letters **360**, 47 (2002).

[Ugeda M. M.] M. M. Ugeda *et al.*, in preparation.

[Umbach 1990] E. Umbach, *Characterization of Organic Overlayers on Well-Defined Substrates*, Progress in Surface Science **35**, 113 (1990).

[Umbach 1998] E. Umbach, *Surface Architecture with Large Organic Molecules: Interface Order and Epitaxy*, Surface Science **402**, 20 (1998).

[Van Hove 1981] M. A. Van Hove, R. J. Koestner, P. C. Stair, J. P. Biberian, L. L. Kesmodel, I. Bartos and G. A. Somorjai, *The Surface Reconstructions of the (100) Crystal Faces of Iridium, Platinum and Gold: I. Experimental Observations and Possible Structural Models*, Surface Science **103**, 189 (1981).

[Vazquez 2004] H. Vazquez, R. Oszwaldowski, P. Pou, J. Ortega, R. Perez, F. Flores and A. Kahn, *Dipole Formation at Metal/PTCDA Interfaces: Role of the Charge Neutrality Level*, Europhysics Letters **65**, 802 (2004).

[Vazquez 2007] H. Vazquez, F. Flores and A. Kahn, *Induced Density of States Model for Weakly-Interacting Organic Semiconductor Interfaces*, Organic Electronics **8**, 241 (2007).

[Wagner 2004] T. Wagner, A. Bannani, C. Bobisch, H. Karacuban, M. Stohr, M. Gabriel and R. Moller, *Growth of 3,4,9,10-Perylenetetracarboxylic-Dianhydride Crystallites on Noble Metal Surfaces*, Organic Electronics **5**, 35 (2004).

[Wöll 1989] C. Wöll, S. Chiang, R. J. Wilson and P. H. Lippel, *Determination of Atom Positions at Stacking-Fault Dislocations on Au(111) by Scanning Tunneling Microscopy*, Physical Review B **39**, 7988 (1989).

[Yamane 2003] H. Yamane and S. Kera, *Intermolecular Energy-Band Dispersion in PTCDA Multilayers*, Physical Review B **68**, 033102 (2003).

[Zou 2006] Y. Zou, L. Kilian, A. Scholl, T. Schmidt, R. Fink and E. Umbach, *Chemical Bonding of PTCDA on Ag Surfaces and the Formation of Interface States*, Surface Science **600**, 1240 (2006).

CHAPTER 3

The Highly Interacting System PTCDA/Si(111)-7×7

3 The Highly Interacting System PTCDA/Si(111)-7×7

3.1 Introduction

The modification of semiconductor surfaces by incorporation of organic molecules has attracted recently considerable interest, opening a new route in the field of molecular electronics. The wide range of organic molecules and the possibility to tailor their properties by the use of appropriate functional groups, combined with conventionally used silicon surfaces offer the opportunity to create novel hybrid devices, which may compete with the already used inorganic semiconductor devices.

Since the invention of STM and its development it has become possible to achieve unprecedented insight into a number of fundamental processes related to the interaction of organic molecules with surfaces such as molecular diffusion, bonding of adsorbate on surfaces and molecular self-assembly. STM studies have led to detailed understanding of many adsorbate/semiconductor systems. In the beginning, most of the studies have involved atomic or very small molecular species where the adsorbate structure could be determined directly from STM images. Later, relatively complex covalently bound organic molecules on silicon were investigated. In this cases the molecules and often the surface were significantly modified both geometrically and electronically resulting in a complex structure and non-trivial appearance in STM images. While STM can provide an atomically resolved view of clean semiconductor surfaces, it can not in general provide the sub molecular scale information necessary to fully elucidate the structure of a molecule-surface complex. Whereas in the simple cases the position and the spatial symmetry of an adsorbate allowed to get some hints concerning the structure, for more complex adsorbates detailed structural assignments based only on STM features was not possible. It is essential then to use theoretical modeling for better understanding STM features.

While various molecules including alkenes, polyenes, benzene or phthalocyanines were investigated on Si(100)-2×1 surfaces [Wolkow 1999], so far only few studies were reported on the deposition of organic molecules on the Si(111)-(7×7) reconstructed surface. Among these studies, we can mention some relevant examples as subphthalocyanines (SubPc) or C60 molecules adsorption on Si(111)-(7×7). In these studies the specific adsorption site and chemical reactions with the substrate were

elucidated. STM allowed the direct imaging not only of the adsorbed molecules but also of their surface chemistry at atomic resolution.

Specific molecular features depending on the adsorption site were determined to correspond to single molecules. For SubPc adsorption on silicon substrates [Yanagi 2000], the STM features of single molecules and the molecule-substrate interaction were found to depend on the adsorption site, and was described as a physisorption or chemisorption. The differences in the interaction strength were interpreted based on a site-dependent reactivity study, previously reported for the Si(111)-(7×7) silicon substrate [Hamers 1986].

In some cases, e.g. the adsorption of single C60 molecules onto the Si(111)-(7×7) substrate, the interpretation of molecular features observed in STM images have required a complex theoretical calculation, where symmetry breaking effects were included to explain the observed shapes of individual molecules [Hou 1999, Pascual 2000] .

It is worth mentioning that valuable information about molecule-surface interaction has been gained also from a variety of other surface sensitive techniques such as UPS, AES, or XPS. However, the information obtained from these techniques is averaged over large areas of the sample. This clearly limits the ability to yield information on local properties, which is essential in the study of single molecule adsorption.

In this chapter, we present a study of the adsorption of PTCDA on Si(111)-(7×7) substrates. The combination of scanning tunneling microscopy experiments and density functional (DFT) first-principles calculations have allowed us to elucidate the complex shifts and splitting of the original molecular orbitals (MO) of the PTCDA molecule upon adsorption. The intramolecular resolution observed in the experimental STM images can not be understood as the result of a simple rigid shift of the MO of the free molecule. On the contrary, our DFT calculations of the molecule-surface system and the corresponding simulations of STM images with realistic tips show large splittings of the original MO when PTCDA is adsorbed on the silicon surface, that contribute in a complex way to the tunnel current. These splittings can be understood under symmetry and charge transfer arguments that characterize a strong partially-ionic covalent bonding involving the carbonyl groups of the molecule and the silicon dangling bonds of the surface.

3.2 Experimental details

The experiments were carried out in an ultra-high vacuum system equipped with a home-built STM. The Si(111) samples [Siltronix], previously degreased with acetone and ethanol were loaded into the UHV chamber and degassed for several hours at 600ºC. Clean reconstructed Si(111)-(7×7) surfaces were prepared by flashing the samples at approximately 1150ºC, followed by a fast quenching at 850ºC and then a slow cooling down to room temperature (RT) at a rate of 10ºC/minute. During the whole process the heating of the sample should be homogeneous and the pressure should not exceed 3×10^{-10} Torr in order to obtain large and well reconstructed surfaces. PTCDA molecules were deposited by thermal evaporation from a Ta home-made cell, kept at 200ºC. Low coverages of PTCDA (≈ 0.1-0.3ML) were deposited on substrates kept at room temperature, at very low evaporation rate (≈0.02ML/second). Here 1 ML PTCDA is defined as 1 molecule/Si(111)-(7×7) unit cell.

3.3 The Si(111)-7×7 reconstructed surface

Silicon is a group IV semiconductor with a bulk crystal structure that is a face centered cubic with a two atom basis, known as the diamond structure. When the (111) surface is exposed by truncation of the bulk crystal, each surface atom contains one dangling bond. Under suitable preparation conditions which usually include annealing, the surface reconstructs reducing the number of the dangling bond and thus minimizes the energy of the system. The most stable reconstruction of the Si(111) surface is the (7×7) structure. Although it was discovered decades ago [Schlier 1959] the complexity of the Si(111)-(7×7) reconstruction have unable for a long time the precise determination of the geometric structure.

The first real-space results were obtained by STM [Binnig 1983] and several years later Takayanagi *et al*. [Takayanagi 1985] proposed the dimer-adatom-stacking-fault (DAS) model which explained the complex surface reconstruction involving the topmost four Si atomic layers. According to the DAS model the Si(111)-(7×7) surface has a rhombic unit cell with a lattice constant of 2.68 nm. The unit cell can be regarded as containing two subunits (triangles) separated by the short diagonal.

Figure 3.1 displays the DAS model of the (7×7) reconstruction in which five silicon atomic layers are schematically drawn. The topmost layer consists of 12 adatoms (red

circles) which have dangling bonds. Below the adatoms layer, there is a bilayer containing restatoms and dimer atoms. Notice that part of the rest atoms (gray circles) have saturated bonds due to the adatoms sited on T_4 position. Nevertheless, there are still six restatoms (blue circles) which do not saturate their bonds. The same bilayer contains the dimer chains (yellow circles) which represent the boundaries of the unit cell.

The subsequent Si(111) bilayer, with the atomic positions almost unmodified by the reconstruction, contains in the upper layer the corner holes. The corner hole, which presents a dangling bond, is found on the vertex of the unit cell.

Although half-cells contain six adatoms and three restatoms locally arranged in a (2×2) periodicity, they are not equivalent. They differ in the stacking structure of the first bilayer. While one of the half unit cell, the unfaulted (U), has the same stacking sequence as the ideal Si(111) crystal, the other half-cell, the faulted (F), has the first bilayer rotated 180º, resulting vertically aligned with the unreconstructed Si(111) bilayer underneath.

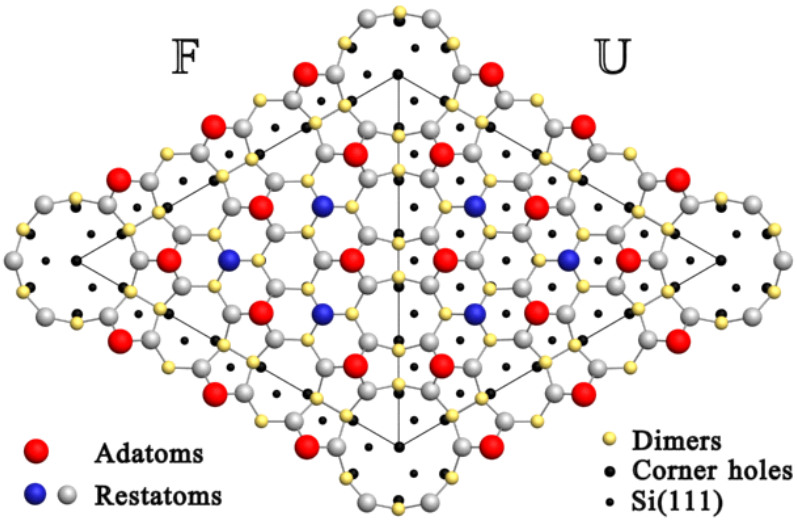

Figure 3.1 *Schematic illustration (top view) of the dimer-adatom-stacking-fault (DAS) model of the Si(111)-7×7 reconstruction. Red circles designate the adatoms in the topmost layer. Blue and gray circles designate restatoms and yellow circles, dimer atoms, all in the first bilayer. Black circles correspond to corner holes and Si atoms in the subsequent bilayer. Faulted (F) and unfaulted (U) half-cells differ in the stacking sequence of the first bilayer.*

As a consequence of the different stacking sequence, the electronic properties of the faulted and unfaulted half-cells are different. A charge transfer from the unfaulted to the faulted half-cell results in a different contrast in STM images. According to first-

principles calculations, there is also a topographic contribution to the different contrast of F and U half-cells [Pérez 1997, Ke 2000].

Figure 3.2(a) and (b) show STM images acquired simultaneously at V=+1.5V and V=-1.5V, respectively for the clean Si(111)-7×7 surface. It can be observed that while in the empty states image the atoms in both half-cells have the same contribution to the tunneling current, the filled states images reflects the difference between the faulted and unfaulted half-cell. The atoms in the faulted half-cell appear brighter than those in the unfaulted half-cell.

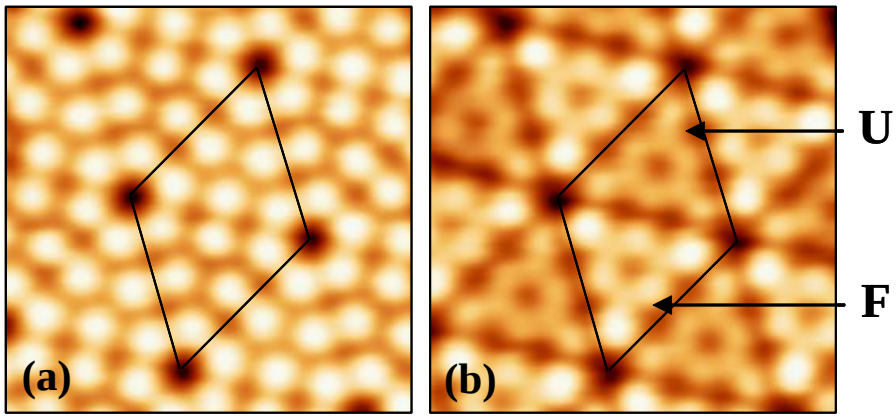

Figure 3.2 *RT-STM images simultaneously acquired at opposite polarity on a Si(111)-(7×7) reconstructed surface. Image size 6.0nm×6.0nm, I=0.3nA. (a) Empty states V=+1.5V, (b) Filled states V=-1.5V.*

The main contribution to the tunneling current in the STM images is given by the dangling bonds associated to different atoms. For each unit cell there are 19 dangling bonds (DB): 12 partially filled bonds located at the 12 adatoms in the surface layer, six filled bonds at the six restatoms in the second layer and one filled bond at the corner hole atom in the fourth layer. Thus, in the empty states image (figure 3.2(a)), the observed protuberances correspond to the 12 DB of the adatoms, whereas the depressions located at the vertex of the unit cell correspond to the DB of the corner hole atom.

The filled states image (figure 3.2 (b)) has also contribution associated to the adatoms dangling bonds. For images recorded at voltages lower than -0.8V a contribution from the dangling bonds of the six restatoms can be observed also. Furthermore, in filled states STM image it is possible to distinguish between adatoms inside the unit cell. For example, the adatoms located at the corners of the half-cells (*corner adatoms*) appear brighter than the adatoms located in the center (*center adatoms*). An explanation for this different adatom intensity is based on charge transfer. The center adatoms transfer part

of their electronic charge to the restatoms. The charge transfer is more efficient for the center adatoms because they have two neighboring rest atoms, while the corner adatoms have only one neighboring rest atom.

Although the 7×7 reconstruction reduces significantly the number of the dangling bonds (from 49 for an ideal unreconstructed Si(111) surface to 19), the surface is highly reactive.

The electronic structure of the Si(111)-(7×7) surface was first studied by photoemission spectroscopy [Fauster 1983, Himpsel 1984]. Later STM experiments were able to provide energy resolved real-space images, by means of CITS experiments [Hamers 1986, Hamers 1987], in which it was possible to relate electronic states previously identified in UPS and IPES experiments, with specific sites in the reconstructed surface.

From the spatially resolved I-V curves, several surface states were found at different energies and were associated with different atoms in the reconstructed surface. Electronic states with energies close to the Fermi level (-0.2eV and +0.5eV) were found to be associated to a dangling bond state originated from the adatoms. An occupied band observed at -0.8eV was attributed to rest atom dangling bonds. Besides, surface states associated to Si-Si backbonds surrounding the adatoms and corner hole were found at -1.7 eV, respectively.

Since both the rest atom and corner hole dangling bond derived states were found well below the Fermi level they must be fully occupied. This was explained by a charge transfer of dangling bond electrons from the adatom states into the rest atom and corner hole states. The complete filling of the rest atom and corner hole states implies a reduction of the 12 electrons of adatom DB to five electrons. In a band picture, as reported by Uhrberg *et al.*, these five DB electrons can give rise to two fully occupied and one half-full surface band. Photoemission experiments [Uhrberg 1998] performed at 55K have identified a new band at -0.5eV associated to corner adatoms, besides the other two at -0.2eV and +0.5 previously reported and associated to adatom states.

Even if silicon is a semiconductor with a 1.1eV bulk gap between the maximum of the valence band and the minimum of conduction band, STM and UPS have shown significant emission at the Fermi level from the Si(111)-(7×7) surface. This indicates a metallic character of the reconstructed surface which is consistent with the odd number of adatom dangling bond electrons.

3.4 PTCDA deposition at low coverage

A low coverage of PTCDA molecules was deposited on the Si(111)-(7×7) surface kept at room temperature. Figures 3.3(a) and (b) show typical STM topographic images obtained for the evaporation of approximately ~0.3ML PTCDA. In these images, the adsorbates are imaged as bright spots, randomly located on the reconstructed surface. The relative small size of these spots suggests the adsorption of individual molecules, rather than molecular aggregates. Small variations in the size and shape of the spots are probably due to different bonding configuration and/or adsorption sites.

Among all these adsorbates, only few of them can be discriminated as having similar shapes and sizes, namely those adsorbed in the corner hole site of the reconstructed substrate (marked by green circles in the images).

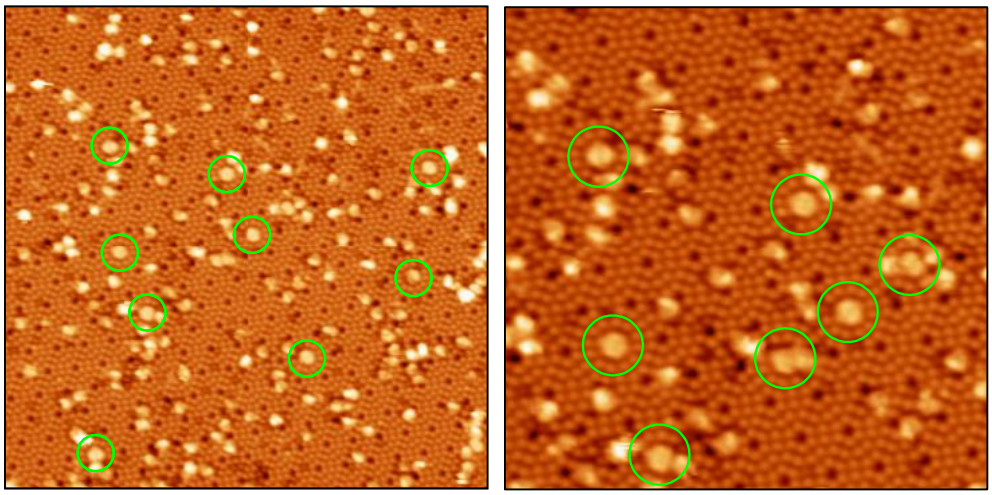

(a) (b)

Figure 3.3 *STM images of the Si(111)-(7×7) reconstructed surface after exposure to low coverage PTCDA molecules at room temperature. Randomly adsorbed molecules can be distinguished as bright spots on top of the Si surface. (a) 50nm×50nm, (b) 30nm×30nm, I=0.3nA, V=+1.5V.*

The diversity of the other observed adsorbates and the lack of any correspondence between a particular shape and a specific adsorption site, together with the fact that they were not fully reproduced through various experiments, have determined us to restrict our study only to the molecules adsorbed in the corner hole site.

A detailed view of a surface area where a single PTCDA molecule is adsorbed on the corner hole site is shown in figure 3.4(a). It can be observed that the molecule is located in the space left by the adatoms surrounding a corner hole.

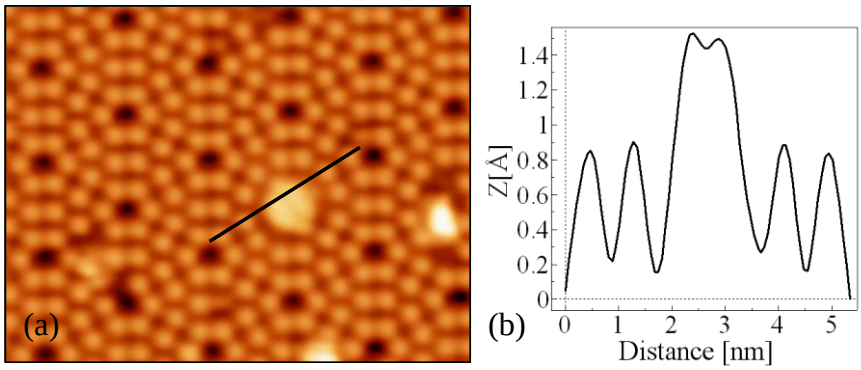

Figure 3.4 *(a) STM image of an individual PTCDA molecule adsorbed on the corner hole of the Si(111)-(7×7) reconstructed surface. (b) Profile line across the molecule showing the apparent height of the PTCDA molecule with respect to the neighboring adatoms. Image size: 13nm×10nm, I=0.2nA, V=+1.5V.*

The individual PTCDA molecule is imaged as a rounded shape with an internal structure characterized by two lateral lobes. These two lobes, separated by a hollow are clearly visible in the profile line across the molecules, as displayed in figure 3.4(b).

The apparent height of the molecule is ~0.6Å with respect to adatoms surrounding the corner hole. The distance between the two lobes (~10Å) and the relatively low height suggests a planar adsorption of the molecule, i.e. the perylene core is aligned parallel to the substrate.

Under negative bias condition the molecular shape appears to be different. In this case, the individual molecule is imaged as five parallel stripes of different lengths. These features can be observed in the STM image and in the corresponding profile line across the molecule in figures 3.5(a) and (b), respectively.

The distance between the outer stripes is ~11Å, whereas the length of the stripes is ~5Å, ~7Å for the shorter and the larger stripe, respectively. According to these distances and taking into account the dimensions of the PTCDA molecule (11.28Å×4.48Å), we consider that the larger measured distance corresponds to the long axis of the molecule, while the shorter distance corresponds to the short axis of the molecule.

As in STM images representing the occupied states of the sample it is possible to distinguish between the faulted and unfaulted subunits, it can be noticed that the long axis of the molecule is aligned parallel to the dimer line which separates the faulted and unfaulted subunits, i.e. the $[01\bar{1}]$ direction of the substrate.

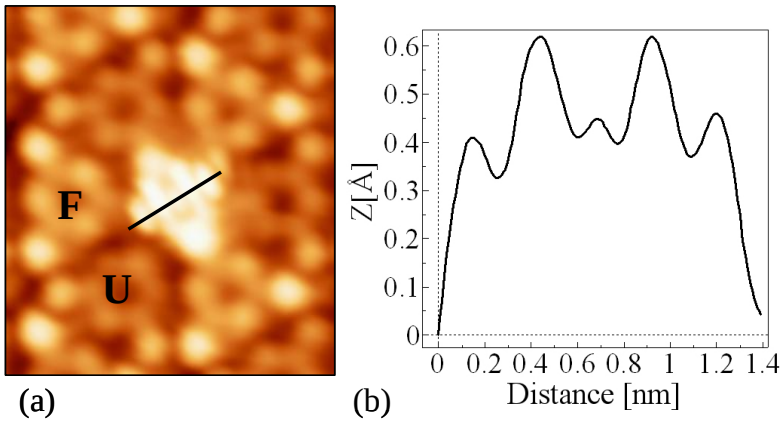

Figure 3.5 *(a) STM image of an individual PTCDA molecule adsorbed on the corner hole of the Si(111)-7×7 reconstructed surface. (b) Profile line across the molecule where the five parallel stripes of the molecular shape are noticeable. Image size: 4.6nm×5.3nm, I=0.25nA, V=-1.5V.*

Besides, from the twofold symmetry of the molecular shape it can be clearly seen that the center of the molecule is located just on top of the corner hole site. The almost perfect fit of the molecule, in the space left by the corner hole can be explained if relevant distances in the (7×7) unit cell are compared to PTCDA dimensions. To this end, the DAS model and the PTCDA molecule are displayed in figure 3.6(a) at the same scale.

By measuring the projection along the $[01\bar{1}]$ direction of the distance between the corner hole and the nearest corner adatom in the subunit, as outlined in the schematic DAS model, we obtain a value of 5.76Å. It can be noticed that this distance approximately equals half of the length of the PTCDA long axis, which is 11.28Å. Moreover, STM images show that the long axis of PTCDA is aligned parallel to the dimer line separating the faulted and unfaulted subunits. This indicates that PTCDA short side should be located in the space between the closest two corner adatoms (marked with green crosses in the model).

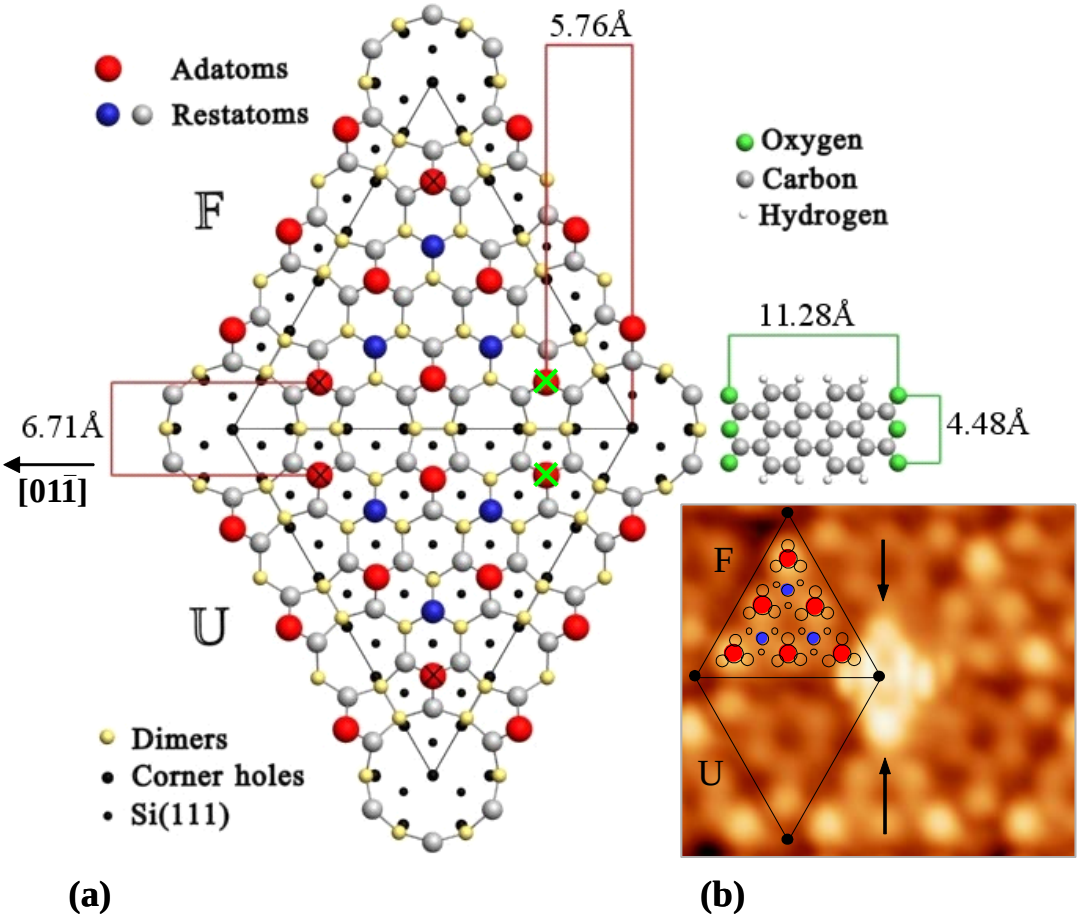

Figure 3.6 *(a) Schematic drawing (left side) of the DAS model of the Si(111)-7×7 and PTCDA structural model (right side). (b) STM image obtained at negative sample bias for a single PTCDA molecule adsorbed on a corner hole. For occupied states of the sample the faulted half of the unit cell appears brighter than the unfaulted half. Image size: 5.5nm×4.5nm, I=0.25nA, V=-1.5V.*

Although, the distance between these two corner adatoms is relatively larger (6.71Å) than the length of the PTCDA short axis (4.48Å), a bond formation between the outer oxygen atoms and the Si corner adatom dangling bond could explain this difference. Moreover there is no other possible combination which would explain a perfect fit of the molecule in the corner hole.

According to the obtained high resolution STM images, which clearly resolve the internal features of single molecules adsorbed on the corner hole site, and taking into account the dimensions of the PTCDA molecule and relevant distances in the (7×7) unit cell, a geometric model is proposed for the adsorption of PTCDA on the corner hole site.

The STM image displayed in figure 3.6(b) shows that, apparently, several adatoms from three unit cells are involved in the adsorption of PTCDA in the corner hole. Therefore a

complete model with 3 unit cells is schematically drawn in figure 3.7, for a better visualization and comparison to experimental images.

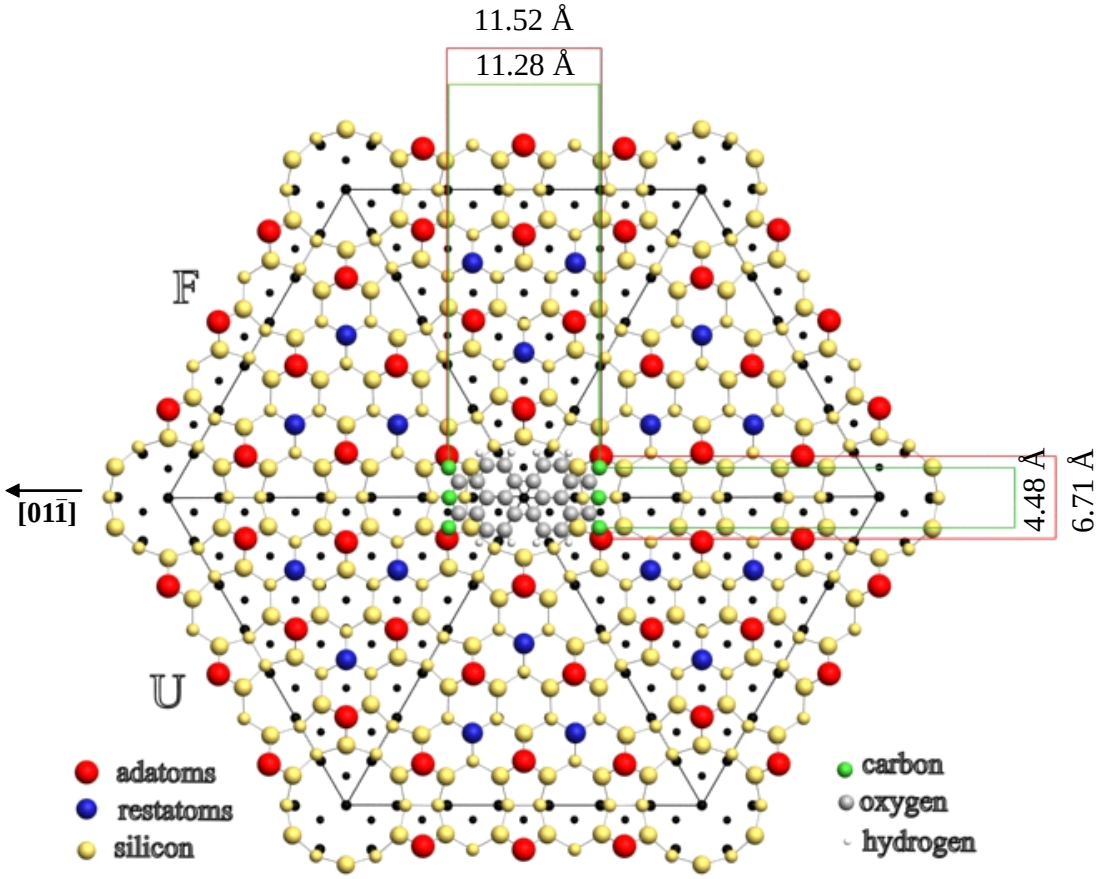

Figure 3.7 *Proposed geometric model for the adsorption of PTCDA molecule in the corner hole site of the Si(111)-(7×7) surface.*

In this model, the PTCDA central benzene-type ring is placed exactly on top of the corner hole. It can be observed that while the short PTCDA axis fits the distance between the two closest corner adatoms in the same unit cell, the oxygen atoms positioned on the long PTCDA axis fits the distance between the corner adatoms of two adjacent unit cells.

According to this model, the remaining two corner adatoms, surrounding the molecule seems not to be involved in PTCDA adsorption, since they are located relatively far from the molecule. This is confirmed by the STM image shown in figure 3.6(b). The two corner adatoms (marked by arrows) are still visible in the image; they are very close to the inner stripes of the molecule. On the other hand, the four Si corner adatoms, which are more likely involved in the PTCDA/substrate interaction, are not visible anymore. The suppression of the Si corner adatom dangling bonds upon interaction suggests the possibility of a new Si-O bond formation.

Once the orientation and adsorption configuration of PTCDA molecule in the corner hole was established from STM results, theoretical calculations were performed in order to gain new information concerning the bonding and electronic structure of the adsorbed molecule.

3.5 First-principles calculations

Theoretical calculations of PTCDA/Si(111)-(7×7) system were further performed in order to get a better understanding of the experimentally studied system. This work was done by O. Paz and J. M. Soler. The calculations were performed within density functional theory (DFT) [Kohn 1965] in the local density approximation (LDA) [Perdew 1981] using the SIESTA method [Ordejón 1996, Soler 2002]. Core electrons were replaced by norm-conserving pseudo-potentials, whereas valence electrons were described using a double-ζ plus polarization (DZP) basis set. A real-space grid with a plane wave cutoff of 50Ry was set in all systems. Only the Γ-point was used in the reciprocal space, due to the large unit cell of the surface. The geometries of both systems: molecule-substrate and tip were relaxed independently until the maximum residual force was below 0.04 eV/Å.

The tunneling current (I) between the tip and the sample was computed, for a large variety of sample voltages (V) and tip-surface distances (R), with a new very efficient method [Paz 2005]. The values of the tunneling current I(R, V) resulting from the calculation were dumped on files which were then read by the experimental data-acquisition program WSxM [Horcas 2007] and processed in exactly the same way as the experimental data. A detailed description of the computational details can be found in a recent report [Paz 2006].

First-principles calculations of the clean Si(111)-(7×7) reconstructed surface have been carried out previously by O. Paz *et al*. [Paz 2005] and successfully reproduced a rich variety of topographic and spectroscopic characteristics, despite the large size of the unit cell.

For the present work the Si(111)-(7×7) substrate was modeled using a repeated slab geometry with four layers of silicon, of these the lowest layer was saturated with hydrogen atoms. Additionally the PTCDA molecule was placed on top of the corner hole site of the reconstructed surface, according to the model previously described. The

whole molecule-substrate system was relaxed until it reached the minimum residual force. The geometry optimization of the molecule-substrate system lasted several months due to the large number of atoms involved: a total of 287 atoms (249+38) atoms corresponding to the substrate and PTCDA molecule, respectively.

Independently the geometry optimization was performed for the tip. Several tips were proposed, of them we mention two. The first one was made of ten silicon atoms in the configuration of (111) planes, as proposed by R. Pérez [Pérez 1998], in which all dangling bonds, except that of the apex, were saturated with hydrogen atoms, as shown in figure 3.8. The second tip was a tungsten bcc pyramid pointing in the (111) direction with 20 atoms.

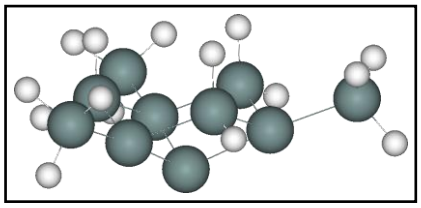

Figure 3.8 *Configuration of the tip used for STM images simulation: Si(111) pyramid saturated with hydrogen atoms.*

The results obtained after the geometry optimization of the PTCDA/Si system indicate that upon adsorption, both the substrate and the molecule geometric structures are modified.

Table 3.1 displays a summary of modified bond lengths in the PTCDA molecule. Significant differences (~7% increment) appear in the C=O bonds contained in the outer carboxyl group, which are mostly modified upon PTCDA adsorption. Minor changes are also determined for the surrounding C-C (~-4%) and C-O (~-1.7%) bonds due to the molecular relaxation. Overall, these modifications lead to a small increase in the PTCDA long and short axes (11.29Å×4.51Å), in comparison to the free molecule dimensions (11.28Å×4.48Å).

Structural relaxations occur not only for the molecule, but also for the substrate. The most significant changes are observed for the adatoms in the topmost silicon layer, in particular for the corner adatoms involved in the interaction. The distances between corner adatoms connecting oxygen atoms on the short and on the long PTCDA axis are slightly modified (11.53Å×6.16Å), in comparison to distances of the unrelaxed silicon substrate (11.52Å×6.71Å).

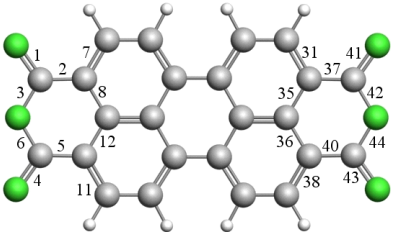

Figure 3.9 *PTCDA geometric structure.*

Bond label	PTCDA Bond length [Å]	Adsorbed PTCDA (strain %)
1, 41	1.216	+7.32
4, 43		+7.57
2, 37	1.445	-4.1
5		-4.0
40		-4.22
7, 11, 31, 38	1.395	+2.84
8, 12, 35, 36	1.394	+0.86
3, 42	1.402	-1.64
6		-1.78
44		-1.71

Table 3.1 *Structural parameters of the free and adsorbed PTCDA molecule according to theoretical results.*

Besides the modification of bond lengths, the PTCDA molecule in its adsorbed configuration presents a bended shape. In figure 3.10, it can be observed that the outer oxygen atoms of PTCDA (colored in green) are positioned slightly higher in comparison with the central benzene ring of the perylene core, relative to the [111] substrate direction or the normal to the molecular plane. In other terms, the angle formed between two vectors connecting the central benzene ring and opposite oxygen atoms on the PTCDA long axis is 177.5°.

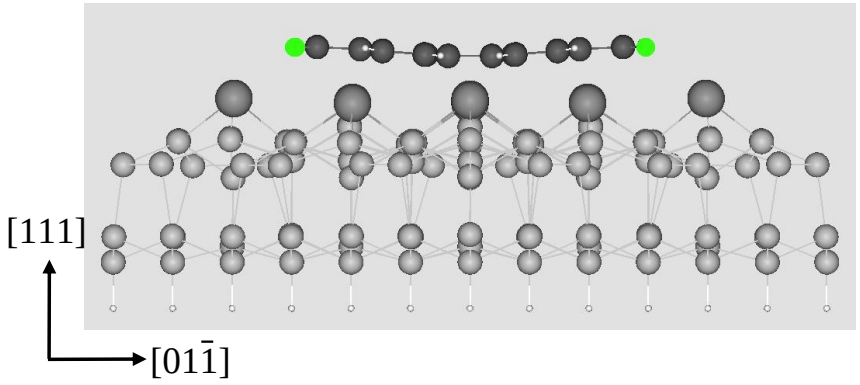

Figure 3.10 *Side view along the short diagonal of the unit cell. An upward shift of the PTCDA outer oxygen atoms is observed in comparison to the central part of the molecule after geometry optimization for PTCDA adsorbed in the corner hole.*

3.6 Electronic structure

Present STM results have shown that the intramolecular features of individual PTCDA molecules adsorbed on the corner hole site of the reconstruction are dependent on the bias voltage. It has been observed that under negative bias voltage (figure 3.11(a)) the single molecule appears as five parallel stripes of different lengths. These stripes were found perpendicularly aligned relative to the long axis of the PTCDA molecule.

For large positive bias (higher than +1.4V) the molecule is imaged as two lobes separated by a hollow (figure 3.11(b)). When decreasing the bias voltage (at positive polarity) the appearance of the internal structure changes. For sample bias of +0.4V the molecule appears as five parallel stripes as can be seen in figure 3.11(c). These stripes are very similar to those resolved in the filled state image of figure 3.11(a).

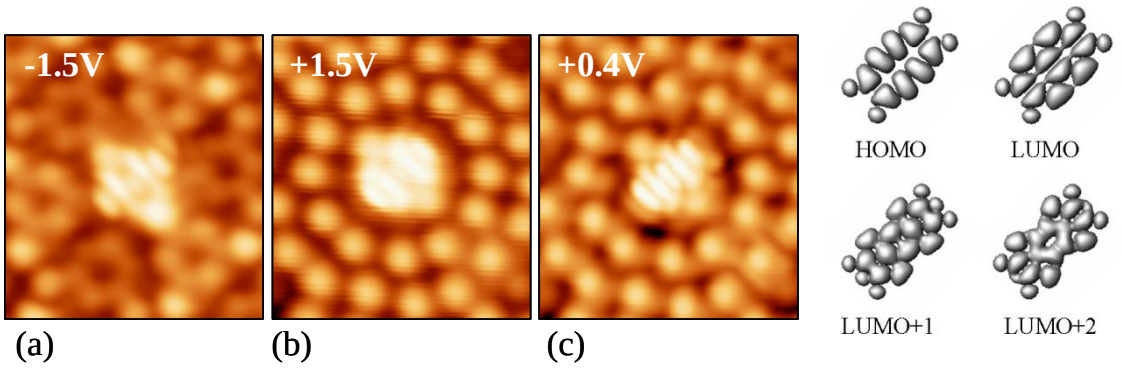

Figure 3.11 *Constant current STM images showing the bias dependence of internal structure of a PTCDA molecule adsorbed on the corner hole site of Si(111)-(7×7) surface. (a) Filled states image recorded at V=-1.5V, I=0.26nA. (b) Empty states image recorded at V=+1.5V, I=0.13nA. (c) Empty states image recorded at V=+0.4V, I=0.13nA. Images size: 4.2nm×4.6nm. The molecular orbitals calculated for the free PTCDA molecule are shown on the right side of the figure.*

From a direct comparison of the molecular orbitals, calculated for the free PTCDA molecule (shown on the right side of figure 3.11), it can observed that the LUMO+1 spatial distribution is the only one which resembles the resolved molecular shape in figure 3.11(a) and (c).

The observation of the LUMO+1 for energies close to the Fermi level could be explained by a considerable charge transfer from the substrate into the unoccupied molecular orbitals.

In order to explain the internal structure of the PTCDA molecule observed in STM images, theoretical calculations in the Tersoff-Hamann (T-H) approximation [Tersoff 1985] were performed. These calculations render images representing the local density of state (LDOS) of the whole PTCDA/Si(111)-(7×7) system. Each of the images shown in figure 3.12 represents the LDOS integrated over a given energy range.

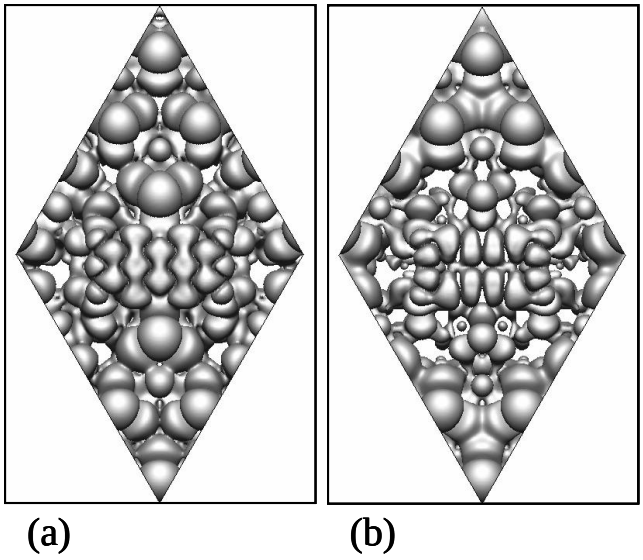

Figure 3.12 *Images representing the local density of states of the PTCDA/Si(111)-(7×7) system. Each of the images is integrated over an energy range defined with respect to the Fermi level (E_F=0). (a) Integrated from -0.1eV to +0.1eV. (b) Integrated from +0.2eV to 0.4eV.*

In the LDOS image, integrated from -0.1eV to +0.1eV (figure 3.12(a)), the symmetry and the shape of the adsorbed PTCDA molecule is very similar to the LUMO+1 calculated for the free molecule. A direct comparison of this spatial distribution obtained in the LDOS image, integrated for energies very close to the Fermi level, with the intramolecular features resolved in experimental STM images shows a close similarity, at least for the STM images acquires at voltages between -1.5V (figure 3.11(a)) and +0.4V (figure 3.11(c)).

In the LDOS image integrated from +0.2eV to +0.4eV (figure 3.12(b)) the molecular shape is more likely related to the HOMO of the free molecule. In contrast to the previous situation, this LDOS image can not explain the experimentally resolved intramolecular features, obtained for the empty states images. Moreover this HOMO-related spatial distribution is somehow unexpected in this energy range, since HOMO related features are expected to be found in occupied sample states.

Despite the fact that some of the experimental STM images were well reproduced with this approach, the inconsistency found for other images suggests that the Tersoff-Hamann approximation is not the most adequate to fully describe the STM results. This inconsistency must probably arise from the fact that tip DOS contribution, which may influence significantly the simulated STM images [Paz 2005, Paz 2006], is not taken into account in the T-H approximation.

Since the HOMO-related shape observed in the LDOS image of figure 3.12(b) and the changes which undergo the intramolecular features with increasing voltage (positive polarity) in the experimental STM images can not be intuitively understood, further calculations have been done using realistic STM tips.

For an accurate comparison, STM topographic images were simulated using a silicon tip as described in section 3.5. A silicon tip was considered due to the fact that the atomic resolution in STM images was usually obtained after intentional slight tip-sample contacts, which may lead to Si termination of the original W tips.

Several experimental STM topographic images were measured at different bias voltages in order to compare them to the simulated ones. Figure 3.13 displays experimental (top) and simulated (bottom) STM topographic images.

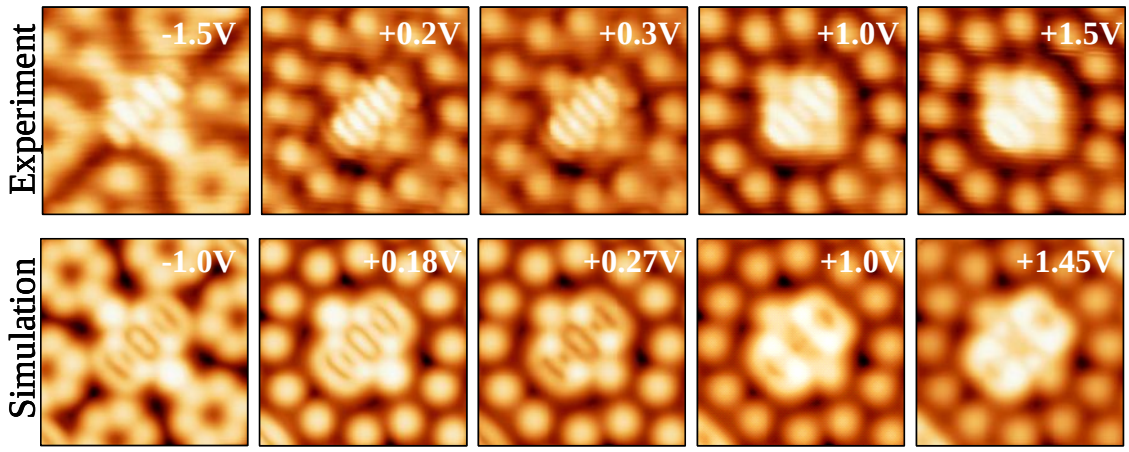

Figure 3.13 *Comparison of experimental and simulated STM topographic images of a PTCDA molecule adsorbed on the corner hole site of Si(111)-(7×7) surface. The top shows experimental constant current STM images recorded at different bias voltages, with a set point current of 0.13nA. The bottom shows simulated STM images, with the same tunnel current (0.13nA) as the experimental images and voltages as shown in the figure. Images size: 3.2nm×3.2nm.*

A very good agreement is found between the experimentally and simulated STM images, over a wide range of energies and tip-sample distances. It can be observed that

simulated STM images covering appropriate energy intervals reproduce the shape, the symmetry and the relative size of single molecule features.

The simulated image for large positive bias (+1.45V), reproduce well the intramolecular features resolved in the STM image, characterized by the two lateral lobes separated by a depression. A close similarity is observed, also, by comparing simulated and experimental images at +1.0V. In both cases, each of the lateral lobes observed before, undergoes a splitting giving rise to two clear stripes on each lateral side of the molecule.

For voltages close to the Fermi energy, the simulated images show an additional stripe in the centre of the molecule reproducing well the five parallel stripes which characterize the molecule at low positive bias (~0.3V).

In the simulated STM image at -1.0V, the intramolecular features can be described by several parallel stripes (perpendicularly aligned relative to the long axis of the molecule), reproducing the molecular shape resolved in the experimental STM image acquired at -1.5V. The small difference between both images consists in two additional stripes which appear in the case of the simulated images. We mention that during the STM experiments this "seven-stripes" shape was observed, but was not always reproducible, being dependent on the tip condition. Profile lines measured perpendicular to these stripes, however, yield a similar separation of ~10Å in both cases, if only the five stripes are considered in the simulated STM images.

The molecular shapes in experimental and simulated STM images closely resemble the molecular orbitals of the free PTCDA molecules. However, the energetic positions of these orbitals seem to be modified as compared to the ground state of molecular levels in the free PTCDA molecule.

By means of further theoretical calculations, it has been possible to relate the original molecular orbitals of the free PTCDA with the energy dependent features observed in STM images. As it is shown below, important shifts and splitting of these orbitals can be deduced from the calculations.

Figure 3.14 shows the projected density of states (PDOS) of the PTCDA/Si(111)-(7×7) system onto the molecular orbitals of the isolated molecule (i.e. HOMO, LUMO, LUMO+1, LUMO+2). From the spectra it can be observed that the energy positions of molecular orbitals are significantly shifted with respect to their original positions found for the free PTCDA molecule (see Table 1.4 in section 1.2.2).

The LUMO (gray filled peak) is found in occupied states in an energy range between -1.4eV and -1.1eV, whereas the LUMO+1 (light gray), is found to cross the Fermi level being therefore, partially filled. Notice the correspondence between the color of the peak area in the spectra and the background of the PTCDA molecular orbitals images (shown above the spectra). Close to the Fermi level there is also some contribution from the LUMO+2, in an energy range between +0.1eV to +0.5eV. HOMO states (dark gray peak) are found in an energy interval, between -3.0eV and -2.0eV.

Besides these shifts, we have also observed large splittings of molecular orbitals. HOMO related states can be observed, also, close to the Fermi energy, represented by the low intensity peak found between +0.1eV and +0.4eV. Other molecular orbital which undergoes splitting is LUMO+2, since LUMO+2 contribution is found also at ~+1.0eV.

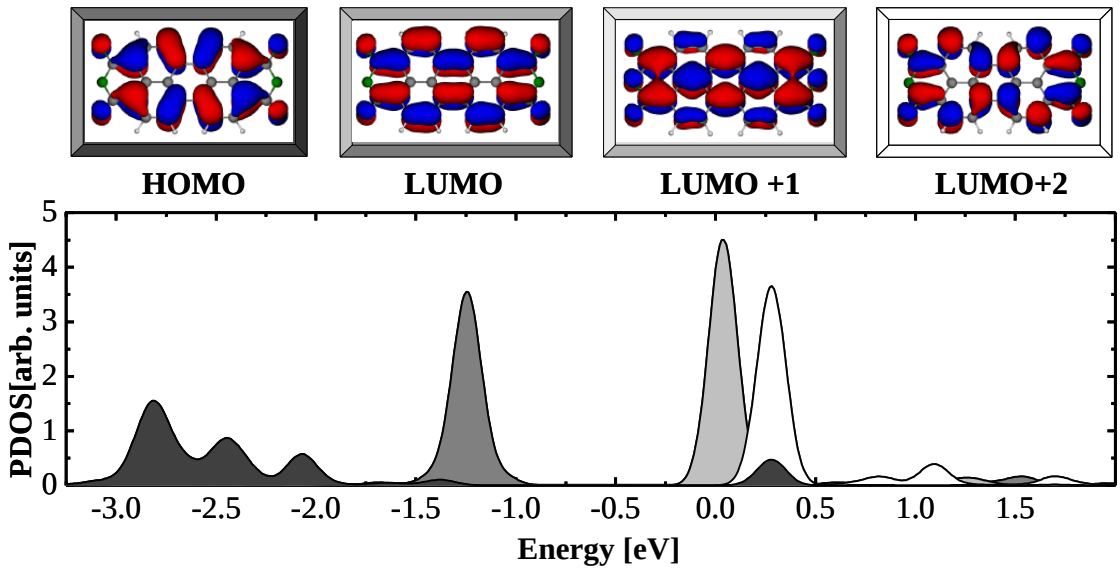

Figure 3.14 *Projected density of states (PDOS) of the PTCDA/Si(111)-(7×7) system onto the molecular orbitals calculated for the isolated molecule, in the bent (adsorbed) configuration, using a broadening of 0.1eV. The top pictures display the local density of states (LDOS) for the unperturbed HOMO (dark gray), LUMO (gray), LUMO+1 (light gray), and LUMO+2 (white) states of a flat PTCDA molecule (notice that the viewpoint is slightly rolled). Blue/red colors stand for the sign of the wave function.*

These shifts in energy of the molecular orbitals can be understood in terms of a charge transfer process, resulting from the chemical reaction which take places at the PTCDA/Si(111) interface.

Symmetry considerations, on the other hand, should be taken into account in order to interpret the large molecular orbital splittings observed in the calculated PDOS *vs.* energy spectra shown in figure 3.14. In general, orbital splitting may occur when: *i)* the

interacting orbitals are of the same symmetry (in this case the interacting orbitals are those of the adsorbate and those of the substrate), and *ii)* there exists an efficient overlap between the interacting orbitals.

Since orbital splittings were observed in particular for the HOMO and the LUMO+2, this implies that these molecular orbitals should interact with substrate orbitals: *i)* of matching symmetry and *ii)* localized in the same region as HOMO and LUMO+2 (close to E_F), in order to provide an efficient overlap.

It is mentioned that due to the distorted adsorption geometry, the symmetry of PTCDA changes from that corresponding to the D_{2h} point group to that corresponding to the C_{2v} point group. In this case HOMO and LUMO+2 are described by the same a_2 representation, whereas LUMO and LUMO+1 are described by the b_2 and the a_1 representation as shown in the character table in figure 3.15(d).

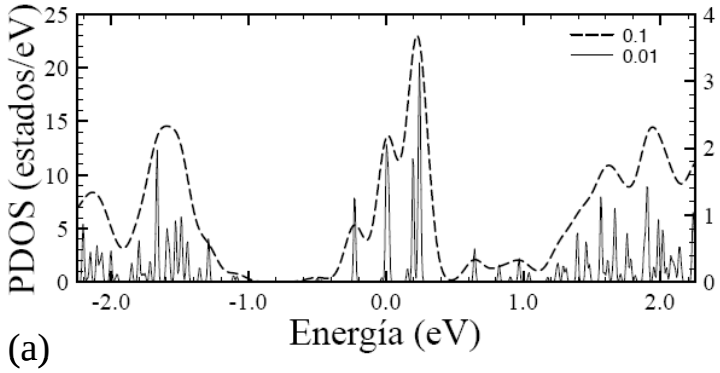

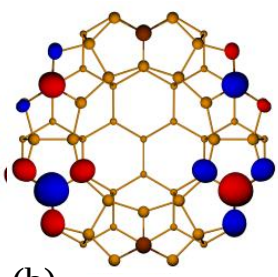
(b)

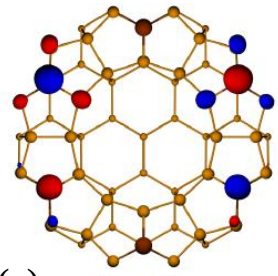
(c)

C_{2v}	E	C_2	$\sigma_{(xz)}$	$\sigma_{(yz)}$
a_1	1	1	1	1
a_2	1	1	-1	-1
b_1	1	-1	1	-1
b_2	1	-1	-1	1

(d)

Figure 3.15 *(a) Represents the density of states of the clean Si(111)-7×7 surface projected onto the atomic orbitals of the four Si corner adatoms involved in the bonding, using a broadening of 0.1eV (dashed line) and 10meV (solid line), respectively. (b) and (c) An a_2 symmetry is inferred for two of the substrate surface states localized at the Fermi level (at 0.0eV in (b) and at +0.02eV in (c)), by representing the spatial charge distribution on the four silicon adatoms involved in the bonding. Blue/red colors stand for the sign of the wave function. (d) Character table corresponding to the C_{2v} point group.*

In order to verify which of the substrate states are mainly involved in the interaction, a similar approach has been used, as before. This approach consists in the representation

of the density of the states projected this time onto the silicon substrate atomic orbitals. In particular only the atomic orbitals of the silicon corner adatoms which are involved in the bonding were considered.

An increased density of states arising from the silicon corner adatom dangling bonds is found localized in the region close to the Fermi level, as can be observed in figure 3.15(a).

The symmetry of these states can be inferred by representing the spatial charge distribution of the corner adatoms involved in the bonding.

With this approach it has been found that only two of the states localized close to the Fermi level have identical symmetry (i.e. a_2) with the HOMO and the LUMO+2. These states are localized at ~0.0eV and ~+0.02eV and their spatial charge distribution is represented in figure 3.15(b) and (c).

The existence of these silicon surface states localized in the same energy region and with identical symmetry as the PTCDA molecular orbitals may support an efficient overlap which explain therefore the splitting of the HOMO and the LUMO+2 of PTCDA.

3.7 Si-O bond formation

The PTCDA/Si(111)-(7×7) bonding and the charge transfer is further investigated by theoretical calculations. The bonding configuration is described by a structural model of the PTCDA molecule adsorbed on the corner hole site of the (7×7) reconstructed Si(111) surface, as displayed in figure 3.16.

It was found that the four silicon corner adatoms react with the oxygen atoms in the C=O group and formed partially-ionic covalent Si-O bonds. The strong molecule-substrate coupling is accompanied by an electronic charge transfer. This charge transfer process is reflected by the modified electron density, both of the substrate and PTCDA atoms.

The most significant change in the electron density is seen to occur at the surface-adsorbate interface where electrons transfer from partially occupied silicon adatom dangling bonds to the outermost oxygen atoms in PTCDA molecule.

The contour color map of the plane crossing the Si-O-C bond, displayed in figure 3.16(b), shows an increase in the electrons density in the oxygen atoms, while a decrease in electron density is observed for the corresponding bonded silicon adatoms.

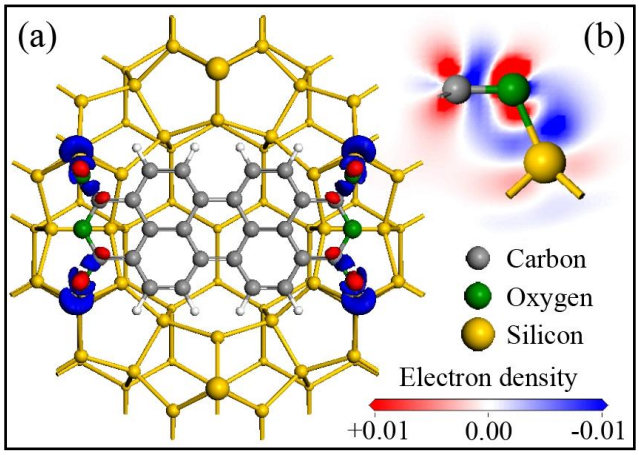

Figure 3.16 *Electron density $\delta\rho$ in units of electrons/Bohr^3. Top view of a PTCDA molecule adsorbed on the corner hole site of the Si(111)-(7×7) surface. The outermost oxygen atoms of the molecule are bonded to four adatoms in the substrate. Isosurfaces at ±0.01 are rendered in red/blue. Red color represents an increase in electron density while blue color represents a decrease in electron density. (b) Contour color map of a plane crossing the Si-O-C bonds.*

The significant shift of molecular levels is due to a charge transfer process which arises as a consequence of a strong molecule-substrate coupling.

Upon PTCDA adsorption on the Si(111)-(7×7) surface, the adsorbate molecular states are highly perturbed. As a consequence of the chemical reaction at the interface, the MO energy positions are modified with respect to the ground state of the molecular levels. This provides a consistent interpretation of the observed shifts in the PDOS vs. energy spectra shown in figure 3.14. The charge transfer into LUMO and LUMO+1 molecular states leads to a filled LUMO and partially filed LUMO+1 states.

3.8 Conclusions

In this work we have studied the adsorption of single PTCDA organic molecules on the Si(111)-(7×7) surface.

- The combination of scanning tunneling microscopy experiments and density functional (DFT) first-principles calculations have allowed us to demonstrate that upon adsorption on Si(111)-(7×7) surfaces the electronic structure of PTCDA molecule is strongly modified. In particular, this combined study shows the complex shifts and splitting of the original molecular orbitals (MO) of the PTCDA molecule upon adsorption.
- The intramolecular resolution observed in the experimental STM images can not be understood as the result of a simple rigid shift of the MO of the free molecule. On the contrary, the DFT calculations of the molecule-surface system and the corresponding simulation of STM images with realistic tips show large splittings of the original MO when PTCDA is adsorbed on the silicon surface, that contribute in a complex way to the tunnel current.
- These splittings can be understood under symmetry and charge transfer arguments that characterize a strong partially-ionic covalent bonding involving the carbonyl groups of the molecule and the silicon dangling bonds of the surface.

References

[Binnig 1983] G. Binnig, H. Rohrer, C. Gerber and E. Weibel, *7×7 Reconstruction on Si(111) Resolved in Real Space*, Physical Review Letters **50**, 120 (1983).

[Fauster 1983] T. Fauster and F. J. Himpsel, *Momentum-Resolved Bremsstrahlung Spectroscopy with a Tunable Photon Detector*, Journal of Vacuum Science & Technology A: Vacuum, Surfaces, and Films **1**, 1111 (1983).

[Hamers 1986] R. J. Hamers, R. M. Tromp and J. E. Demuth, *Surface Electronic Structure of Si (111)-(7×7) Resolved in Real Space*, Physical Review Letters **56**, 1972 (1986).

[Hamers 1987] R. J. Hamers, R. M. Tromp and J. E. Demuth, *Electronic and Geometric Structure of Si(111)-(7×7) and Si(001) Surfaces*, Surface Science **181**, 346 (1987).

[Himpsel 1984] F. J. Himpsel and T. Fauster, *Probing Valence States with Photoemission and Inverse Photoemission*, Journal of Vacuum Science & Technology A*:* Vacuum, Surfaces, and Films **2**, 815 (1984).

[Horcas 2007] I. Horcas, R. Fernandez, J. M. Gomez-Rodriguez, J. Colchero, J. Gomez-Herrero and A. M. Baro, *WSxM: A Software for Scanning Probe Microscopy and a Tool for Nanotechnology*, Review of Scientific Instruments **78**, 013705 (2007).

[Hou 1999] J. G. Hou, J. Yang, H. Wang, Q. Li, C. Zeng, H. Lin, W. Bing, D. M. Chen and Q. Zhu, *Identifying Molecular Orientation of Individual C60 on a Si(111)-(7×7) Surface*, Physical Review Letters **83**, 3001 (1999).

[Ke 2000] S. H. Ke, T. Uda and K. Terakura, *Surface Topography of the Si(111)-7×7 Reconstruction*, Physical Review B **62**, 15319 (2000).

[Kohn 1965] W. Kohn and L. J. Sham, *Self-Consistent Equations Including Exchange and Correlation Effects*, Physical Review **140**, A1133 (1965).

[Ordejón 1996] P. Ordejón, E. Artacho and J. M. Soler, *Self-Consistent Order-N Density-Functional Calculations for Very Large Systems*, Physical Review B **53**, R10441 (1996).

[Pascual 2000] J. I. Pascual, J. Gómez-Herrero, A. M. Baró, D. Sánchez-Portal, E. Artacho, P. Ordejón and J. M. Soler, *Comment on "Identifying Molecular Orientation of Individual C60 on a Si(111)-(7×7) Surface"*, Physical Review Letters **85**, 2653 (2000).

[Paz 2005] O. Paz, I. Brihuega, J. M. Gomez-Rodriguez and J. M. Soler, *Tip and Surface Determination from Experiments and Simulations of Scanning Tunneling Microscopy and Spectroscopy*, Physical Review Letters **94**, 056103 (2005).

[Paz 2006] Ó. Paz, J. M. Soler *Efficient and Reliable Method for the Simulation of Scanning Tunneling Images and Spectra with Local Basis Sets*, Physica Status Solidi b **243**, 1080 (2006).

[Perdew 1981] J. P. Perdew and A. Zunger, *Self-Interaction Correction to Density-Functional Approximations for Many-Electron Systems*, Physical Review B **23**, 5048 (1981).

[Pérez 1997] R. Pérez, M. C. Payne, I. Stich and K. Terakura, *Role of Covalent Tip-Surface Interactions in Noncontact Atomic Force Microscopy on Reactive Surfaces*, Physical Review Letters **78**, 678 (1997).

[Pérez 1998] R. Pérez, I. Stich, M. C. Payne and K. Terakura, *Surface-Tip Interactions in Noncontact Atomic-Force Microscopy on Reactive Surfaces: Si(111)*, Physical Review B **58**, 10835 (1998).

[Schlier 1959] R. E. Schlier and H. E. Farnsworth, *Structure and Adsorption Characteristics of Clean Surfaces of Germanium and Silicon*, The Journal of Chemical Physics **30**, 917 (1959).

[Siltronix] The main characteristics of the Si(111) surfaces are: p-type (B-doped), resistivity: 0.07-0.013Ωcm, thickness: 250-300μm, orietation (111)±0.5°, one side polished; purchased from Siltronix (*www.siltronix.com*).

[Soler 2002] J. M. Soler, E. Artacho, J. D. Gale, A. Garcia, J. Junquera, P. Ordejon and D. Sanchez-Portal, *The Siesta Method for Ab Initio Order-N Materials Simulation*, Journal of Physics-Condensed Matter **14**, 2745 (2002).

[Takayanagi 1985] K. Takayanagi, Y. Tanishiro, M. Takahashi and S. Takahashi, *Structural Analysis of Si(111)-7×7 by UHV-Transmission Electron Diffraction and Microscopy*, Journal of Vacuum Science & Technology A: Vacuum, Surfaces, and Films **3**, 1502 (1985).

[Tersoff 1985] J. Tersoff and D. R. Hamann, *Theory of the scanning tunneling microscope*, Physical Review B **31**,805 (1985).

[Uhrberg 1998] R. I. G. Uhrberg, T. Kaurila and Y.-C. Chao, *Low-Temperature Photoemission Study of the Surface Electronic Structure of Si(111)-7×7*, Physical Review B **58**, R1730 (1998).

[Wolkow 1999] R. A. Wolkow, *Controlled Molecular Adsorption on Silicon: Laying a Foundation for Molecular Devices*, Annual Review of Physical Chemistry **50**, 413 (1999).

[Yanagi 2000] H. Yanagi, D. Schlettwein, H. Nakayama and T. Nishino, *Site-Specific Physisorption and Chemical Reaction of Subphthalocyanine Molecules on Silicon(111)-(7×7)*, Physical Review B **61**, 1959 (2000).

CHAPTER 4

PTCDA on passivated semiconductor surfaces

4 PTCDA on passivated semiconductor surfaces

Organic molecular semiconductors exhibit interesting electronic and optical properties and their potential applications are broad, as seen in numerous contributions. The possibility of including organic semiconductors as active components in the inorganic semiconductor-based devices has increased the interest in these materials in the last years. By exploiting this organic-inorganic approach the advantages are two-fold. On the one hand, one can benefit from well-defined surface structure properties and overall quality of the currently used semiconductors such as Si or GaAs. On the other hand, a wide range of organic molecules along with their tailorable optical and electronic properties may provide new hybrid-devices with enhanced capabilities. Nevertheless, the controlled deposition of these organic materials to produce epitaxial thin films, required for optimum functional properties of devices, still represents a considerable challenge. It is known that an ordered molecular growth on these inorganic semiconductor surfaces is difficult to achieve as their surfaces are significantly reactive due to the presence of chemically active dangling bonds. Since device performance (power consumption, life time, conductivity or the mobility of charge carriers) is directly influenced by the quality of the organic thin films, much effort has been focused on finding ways to obtain a high degree of structural order.

As shown in chapter 3, the deposition of PTCDA at low coverage on clean Si(111)-(7×7) surfaces results in chemisorbed molecules, randomly distributed over the surface. Comparable results were obtained for PTCDA deposition on clean GaAs(100) [Hirose 1994] or Si(100) [Gustafsson 2004, Soubiron 2005] surfaces. The initial stage of deposition usually resulted in a random adsorption of molecules either by reaction with surface dangling bonds or by molecules pinned at defect sites. This led to an initial disordered layer, which to some extent saturates the surface dangling bonds and prevents incoming molecules from interacting with the substrate. Subsequent deposition has resulted in spontaneous formation of PTCDA islands on top of this disordered layer. Although the formed PTCDA islands have the correct bulk molecular stacking, considerable disorder was found in the plane parallel to the substrate. A strategy to overcome this difficulty, the surface reactivity, is the use of surface-passivated Si or GaAs semiconductors.

Improved structural order was observed when reactive semiconductors surfaces were passivated, e.g. by reaction with chalcogen or hydrogen atoms in the case of GaAs and Si substrates respectively, prior to organic film growth. The passivation induces a reduction of the chemically active sites, mainly by saturating the surface dangling bonds. Different surface treatments have been probed in order to achieve an optimum passivation of the semiconductor surface. For silicon, hydrogen-passivated surfaces were obtained either by wet chemical etching methods or by *in situ*-UHV passivation using atomic hydrogen. Both methods usually result in atomically flat surfaces. For PTCDA deposited on H-terminated Si(111) surfaces [Chen 2003, Sazaki 2004] crystalline structure was reported, with a Volmer-Weber growth mode consistent with previous LEED, Raman spectroscopy and AFM studies [Kampen 2000, Morozov 2000, Tengelin-Nilsson 2000]. The importance of surface passivation in promoting well-ordered film growth of PTCDA has been also shown for GaAs surfaces passivated either by selenium [Hirose 1995a, 1995b] or sulphur [Nicoara 2002, Nicoara 2003] by wet chemical etching methods. For these passivated surfaces, clusters formation was observed for the initial stages of deposition. A low coverage of PTCDA was found also to exist between formed clusters due to the pinning of molecules at defects sites. However a higher degree of structural order and superior quality of organic films was obtained, in contrast to unpassivated semiconductor surfaces.

Another approach to passivate semiconductor surfaces, can be exploited by adsorbing metal atoms, such as Ag, Pb, Sn, on Si(111) substrates. The resulting substrates will have metallic or semiconductor surfaces, depending on the metal coverage and surface reconstruction. In this way, substrates whose surface reactivity is systematically varied can be used to probe the molecular growth. For these surfaces, adsorbate-substrate interaction is expected to be intermediate in strength, between the clean Si(111)-(7×7) surface on which PTCDA is chemisorbed and the H-passivated Si(111) surface on which the molecules have a relatively high diffusivity. Ordered molecular layers with various structures have been obtained for organic molecules such as C60 [Upward 1997], phthalocyanines [Upward 1999], pentacene [Guaino 2003], or perylene derivatives [Swarbrick 2005] deposited on Ag/Si(111) surfaces. On the same surface, interesting ordered structures have been obtained by a sequential deposition of two different molecular species, perylene derivatives and additional molecules, which promoted directional

intermolecular interactions such as hydrogen bonds, stabilizing intermixed molecular species [Theobald 2003, Ma 2006].

In the following sections of this chapter alternative methods to passivate Si(111) or GaAs(100) semiconductor surfaces have been probed in order to investigate the adsorption and growth of PTCDA, with the aim to find whether an improvement in the PTCDA molecular growth may be achieved.

4.1 PTCDA on the Pb/Si(111) system

In the present section the interface and the growth of PTCDA thin films on passivated Pb/Si(111) surfaces are studied at room temperature by means of scanning tunneling microscopy. By exploiting an alternative passivation method for the silicon surface the evolution of PTCDA film formation is investigated, for substrates whose reactivity is systematically varied. By gradually varying the substrate reactivity it is aimed to find which of the substrate properties are suitable to obtain an ordered PTCDA molecular growth. Experimental details for sample preparation and a brief review of the literature on the Pb/Si(111) phases are presented before describing the current results. The structural characterization of the interface and multilayer growth of PTCDA on distinct Pb/Si(111) phases and the substrate influence on the sample morphology are described subsequently.

4.1.1 Experimental

The experiments were performed in a home-built ultra-high vacuum system with a base pressure of 1×10^{-10} Torr. Si(111)-(7×7) surfaces were prepared by the standard procedure described in the previous chapter. Pure Pb (99.99999%, from Goodfellow) was evaporated from a home-made Ta crucible, heated by electron bombardment, at an evaporation rate of 0.1ML per minute. Pb coverage close to 1ML (1ML corresponds to 7.84×10^{14} Pb atoms/cm^2) was deposited on the Si(111)-(7×7) reconstructed surface at room temperature, followed by 4-5 minutes annealing at 450°C. After cooling down the sample at RT different phases were obtained, depending on the Pb coverage. The structural changes of the Pb/Si(111) surfaces as a function of Pb coverage were initially monitored by LEED which provided a fast method to check the prepared sample. PTCDA molecules were evaporated from a home-made sublimation cell onto the Pb/Si(111) surfaces, at an evaporation rate of ~0.03ML/minute. In this study 1ML PTCDA corresponds to a close-packed herringbone structure with two molecules per unit cell area of ~290Å^2.

4.1.2 Review of the Pb/Si(111) phases

Earlier studies of thin metal films growth on semiconductor substrates included Pb/Si(111) system. Due to the negligible mutual solubility of Pb and Si this system has been considered as a model for which the interface, growth mode, phase diagram and phase transitions have been extensively studied. Studies related to the growth of Pb on Si(111)-(7×7) surfaces reported a Stranski-Krastanov (layer plus island) growth mode at room temperature deposition [Ganz 1991a, Petkova 1999], whereas a Frank-van der Merwe (layer-by-layer) growth mode was observed for Pb deposition on sample at lower temperature. The layer-by-layer growth was only observed starting with three-four MLs, with the first layers initially highly disordered [Petkova 2001a].

Different Pb/Si(111) phases can be obtained by the room temperature deposition of Pb on Si(111)-(7×7) substrates and subsequent annealing of the samples. For coverage between 1ML and 1.5ML, Pb form a wetting layer on top of the Si(111) substrate whose (7×7) reconstructed surface is preserved unaltered. In the annealing process, at temperature slightly above 330ºC, the Pb layer melts and the substrate periodicity is destroyed. Upon cooling down to room temperature a Pb layer is formed together with large Pb islands. Further annealing of the sample at higher temperature, i.e. 450ºC, results in desorption of Pb atoms, leading to a decreasing of Pb coverage on the surface. Hence, depending on the Pb amount remaining on the substrate and the Pb binding site, different phases can be obtained when cooling down to RT. The surface layer of Si(111) has several positions of high symmetry which are potential binding sites for the adsorbate atoms. These sites named T_1, T_4 and H_3, are shown in figure 4.1.

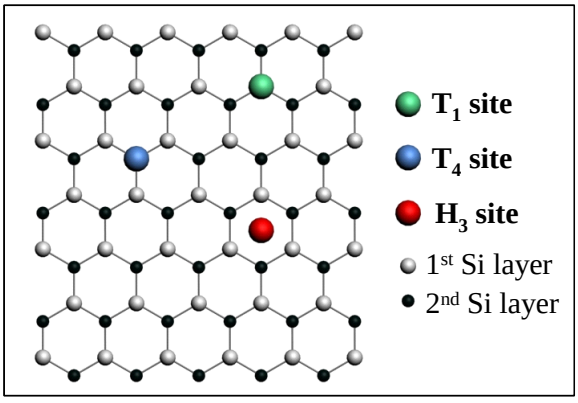

Figure 4.1 *Typical sites for the adsorption of adatoms on Si(111) surfaces.*

Questions concerning the number of distinct Pb/Si(111) phases, their exact coverage, atomic structure and commensurability have been intensively debated in the literature. Controversy originated mainly from the complex phase diagram in which coverage,

temperature and annealing history are all important. The different Pb/Si(111) phases obtained from experiments, for 1/6ML<θ<4/3ML Pb coverage, are summarized in figure 4.2 [Chan 2003].

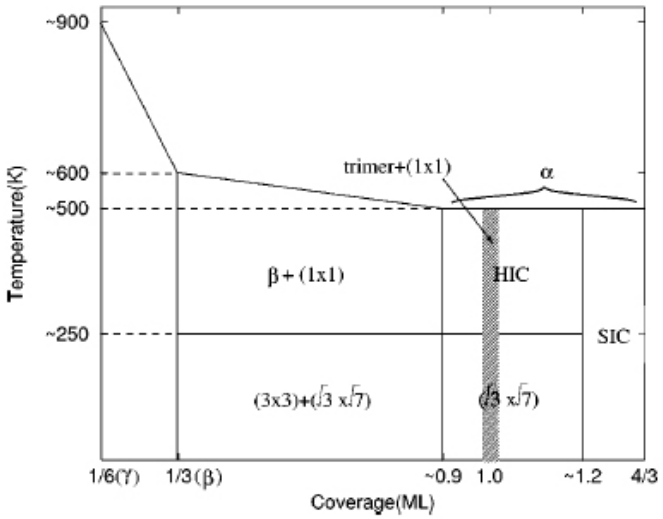

Figure 4.2 *Different Pb/Si(111) phases proposed from experiments for Pb coverage between 1/6 and 4/3 ML. After reference [Chan 2003].*

At 1/6ML Pb coverage, Ganz *et al.* employing STM, LEED and Rutherford backscattering spectroscopy (RBS) [Ganz 1991a], reported the so-called mosaic or γ-phase. For a higher coverage, 1/3ML Pb, a different phase, known as β-phase, was first reported by Estrup *et al*. using (LEED) [Estrup 1964] and confirmed later by different authors [Saitoh 1985, Le Lay 1988]. First-principles calculations, in agreement with the previous experimental results, determined that γ- and β-phases are $(\sqrt{3}\times\sqrt{3})R30°$ reconstructions with Pb atoms adsorbed on T_4 sites [Chan 2003]. Moreover, STM results have shown very recently a phase transition $(\sqrt{3}\times\sqrt{3})R30°\leftrightarrow(3\times3)$ for T_c=86K [Custance 2001a, Brihuega 2005]. At 2/3ML Pb a stable phase was observed by Le Lay *et al*. [Le Lay 1988] who proposed a $(\sqrt{3}\times\sqrt{3})$ structure with 2 Pb atoms per unit cell. Studies of the Pb/Si(111) phases with Pb coverage close to 1ML, (α-phases), were reported by several authors. Experiments performed with different techniques, deficiency in estimation of the exact phase coverage and discrepancies in the interpretation of results originated considerable controversy for these high coverage phases. For ~0.9ML Pb, Ganz *et al*. [Ganz 1991a, Ganz 1991b] reported a (1×1) phase, while for coverage close to 1.3ML, they reported a 30º-rotated incommensurate close-packed phase. Later, from STM experiments it was shown that the incommensurate (IC) phase observed previously, is composed of alternating domains with $\sqrt{3}\times\sqrt{3}$ reconstruction. Based on high resolution images, Hwang *et al*. [Hwang 1995] proposed that the domains, separated by quasi (1×1) regions, consist of two types of Pb trimers, displaced from T_1 sites either

to H_3 or T_4 sites. Information obtained with diffraction has been difficult to interpret since the superstructure spots related to the $\sqrt{3}\times\sqrt{3}$ reconstruction do not appear at the expected commensurate wave vectors. This has led to the assignment of the phases as "incommensurate" [Seehofer 1995, Horikoshi 1999]. At lower temperature, a different phase with a $\sqrt{7}\times\sqrt{3}$ reconstruction was observed with incompatible coverage assignment for this phase: 1ML [Slezák 1999, Hwang 2004] versus 1.2 ML [Kumpf 2000, Custance 2001, Brochard 2002].

Two different phases were mostly discussed: the hexagonal incommensurate (HIC) and the striped incommensurate (SIC) phases. Petovka *et al*. using high resolution SPA-LEED [Petkova 2001a] investigated the HIC and SIC phases and concluded that they were commensurate phases. They explained the obtained diffraction patterns by models corresponding to two superstructures, $\sqrt{31}\times\sqrt{3}$-Pb and $13\times\sqrt{3}$-Pb which are commensurate with the $\sqrt{3}\times\sqrt{3}$ unit cell. More recently, Tringides's group using STM [Hupalo 2002], SPA-LEED [Stepanovsky 2006] and first-principles calculations [Chan 2003] reported extensive studies of the Pb/Si(111) system, elucidating in particular the structure and stoichiometry of the high coverage phases. The authors, based on STM results, determined that the HIC and SIC phases are commensurate structures, composed of triangular $\sqrt{3}\times\sqrt{3}$ domains, separated by light domain walls with an almost $\sqrt{7}\times\sqrt{3}$ reconstruction. Even if these phases were found to be commensurate, the nomenclature HIC and SIC (although it is not correct) is maintained in the literature for an easier reading of the earlier reports. A detailed phase diagram, in the coverage range 6/5ML<Θ<4/3ML Pb shows the experimentally determined phases, as displayed in figure 4.3.

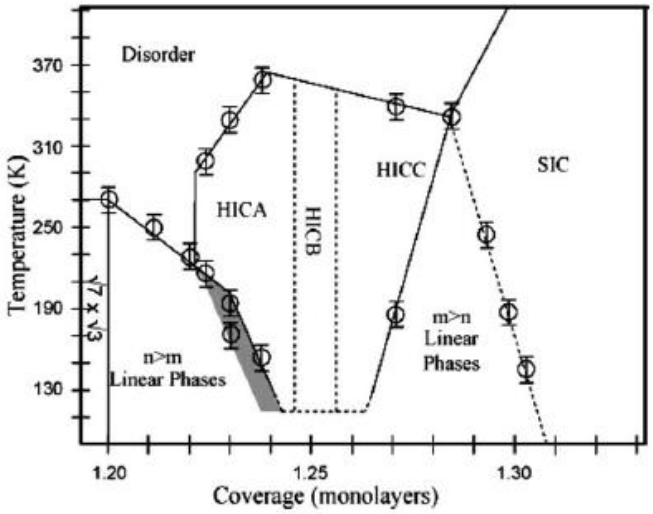

Figure 4.3 *T-θ phase diagram of the Pb/Si(111) system for Pb coverage between 6/5 and 4/3ML. Linear phases, three types of HIC phases and the SIC phase are observed. After reference [Stepanovsky 2006].*

Besides the SIC phase found for Pb coverage close to 1.3ML, three types of HIC phases at 1.25, 1.26 and 1.28ML were identified, from high resolution STM images. Moreover the authors determined that, prior to the formation of these phases, other intermediate phases form, bellow room temperature, by combining integer numbers (m, n) of $\sqrt{7}\times\sqrt{3}$ and $\sqrt{3}\times\sqrt{3}$ unit cells. With the proposed structure for the commensurate phases and the discovery of the intermediate phases, the authors have explained some of the conflicting results in the literature. For example the $\sqrt{31}\times\sqrt{3}$ phase identified to be a HIC phase corresponds, instead, to an intermediate phase with n=1 and m=2, while the $13\times\sqrt{3}$ phase identified as the SIC phase corresponds to the n=1 and m=7 phase.

4.1.3 Pb/Si(111) phases at room temperature by STM

The Pb/Si(111) samples studied in the present work were obtained by the exposure of the clean reconstructed Si(111)-(7×7) surfaces to Pb coverages >1ML, and subsequent annealing. Depending on the temperature and the annealing time, different phases corresponding to different Pb coverages were obtained.

4.1.3.1 α-Si(111)-(√3×√3)R30°-Pb phase

α-Si(111)-Pb phases were prepared by room temperature deposition of approximately 1.5ML Pb onto the clean reconstructed Si(111)-(7×7) surface. Subsequently, the samples were annealed at approximately 450ºC, for 4-5 minutes. Upon cooling down to RT, two phases can be found in the coverage range $6/5ML<\Theta<4/3ML$ Pb. The hexagonal incommensurate (HIC) phase is obtained for Pb coverages between 1.2 and 1.3ML, whereas the striped incommensurate (SIC) phase is obtained for a slightly higher coverage. In the following the HIC phase is described in detail, as this phase was further used in the present work for PTCDA deposition.

An STM image of the HIC phase is displayed in figure 4.4. The bright protrusions observed in the image are arranged in a $(\sqrt{3}\times\sqrt{3})$ reconstruction and form triangular domains. These triangular domains, as it will be shown later, are separated by domain walls with a different structure.

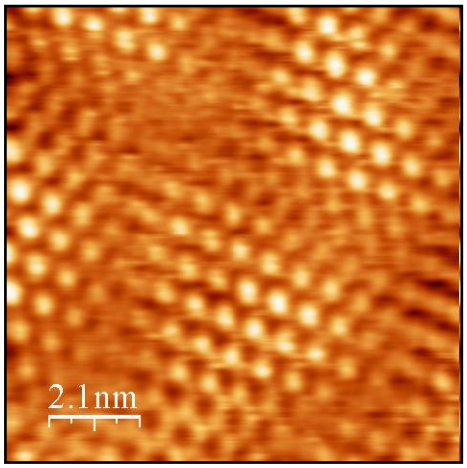

Figure 4.4 *STM image of the hexagonal incommensurate phase. The HIC phase consists of alternating triangular domains characterized by bright protrusions arranged in a √3×√3 reconstruction.*

The √3×√3 unit cell, within the triangular domains, consists of four Pb atoms. Among these, three Pb atoms are located close to T_1 sites, while the other Pb atom is located either on the T_4 or H_3 site. As a consequence of the two different binding sites (H_3 *vs.* T_4) occupied by Pb atoms, two types of domains are formed, explaining the alternating triangular domains observed in STM images. High resolution, bias dependent images displayed in figure 4.5(a) and (b) show the two types of Pb atoms in the √3×√3 unit cell.

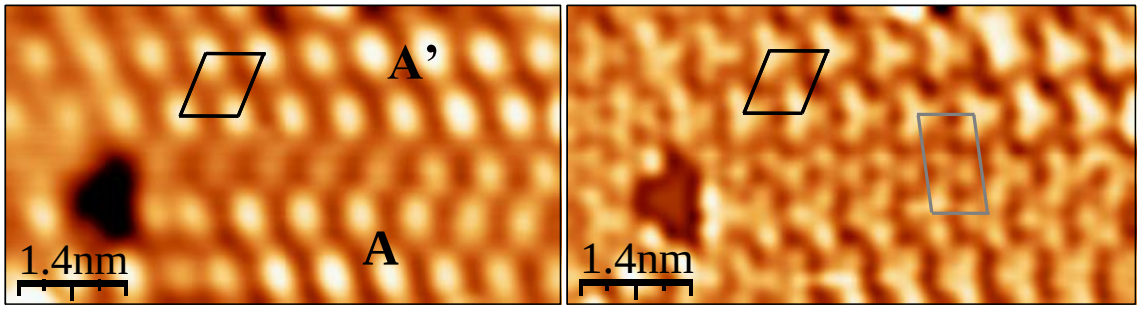

Figure 4.5 *Bias dependent STM images acquired in a region of the HIC phase, close to the domain wall, separating two types of domains (A and A'). (a) For large bias voltage (+1.6V), Pb atoms in the unit cell occupying either H_3 or T_4 sites in adjacent domains are visible as bright protrusions arranged in a (√3×√3) reconstruction. (b) For lower bias voltage (+0.5V) the other three Pb atoms in the unit cell, are also visible. The domain wall has an almost (√7×√3) reconstruction, as seen from the unit cell marked in gray in (b). Images size: 7.0nm×3.5nm, I=0.1nA.*

For large bias voltage (V=+1.6V) the Pb atoms on T_4 or H_3 sites are visible as bright protrusion in a √3 reconstruction (see the marked unit cell in figure 4.5(a)), whereas for low bias voltage the four Pb atoms in the unit cell are observed forming a kind of "Y" shaped protrusion (figure 4.5(b)). Additionally it can be observed, that the domain wall

between A and A' domains, has an almost ($\sqrt{7}\times\sqrt{3}$) reconstruction. In the regular ($\sqrt{7}\times\sqrt{3}$) reconstruction Pb atoms in adjacent rows occupy H_3-H_3 sites [Brochard 2002], whereas in this case Pb atoms occupy H_3-T_4 sites. Thus, the unit cell of the commensurate HIC phase corresponds to a superstructure, built of ($\sqrt{3}\times\sqrt{3}$) alternating triangular domains, separated by domain walls with almost ($\sqrt{7}\times\sqrt{3}$) reconstruction.

4.1.3.2 Si(111)-(1×1)-Pb and β-Si(111)-($\sqrt{3}\times\sqrt{3}$)R30º-Pb phases

If the Pb/Si(111) sample with an initial coverage of ~1.5 ML is annealed at ~450ºC for longer times as those used for the α-phase, in order to reduce the Pb coverage between 0.8 and 0.33ML, two coexisting phases can be obtained at room temperature [Custance 2001a]. One is the Si(111)-(1×1)-Pb phase, corresponding to 1ML, and the other one, is the β-Si(111)-($\sqrt{3}\times\sqrt{3}$)R30º-Pb phase, corresponding to 1/3ML Pb coverage.

The STM image in figure 4.6(a), acquired at RT shows the coexistence of the two phases. On the left side, the (1×1)-Pb phase appears as a flat surface with almost no corrugation, whereas on the right side the β-phase with the ($\sqrt{3}\times\sqrt{3}$) reconstruction, 30º rotated relative to (1×1), is clearly resolved. High resolution images (figure 4.6(b)) show that the periodicity of the 1ML phase is better resolved for low bias voltages, if compared to large bias voltage images, suggesting a metallic character of this phase.

For the 1/3ML phase, STM images (figure 4.6(c)) show Pb atoms in a ($\sqrt{3}\times\sqrt{3}$)R30º reconstruction. For either bias polarity the same protrusions are observed and they correspond to Pb adatoms on T_4 sites as it is discussed later. It is also interesting to remark that this phase possesses a high density of defects (black spots in figure 4.6(a)) which correspond to substitutional Si adatoms [Brihuega 2007].

Although there is not yet a well established structural model for the (1×1)-Pb phase, this reconstruction is thought to consist of 1ML of Pb adatoms adsorbed on top sites (T_1), saturating all the dangling bonds of the Si atoms on the top layer (see the (1×1) unit cell marked by a green line in figure 4.7(a)).

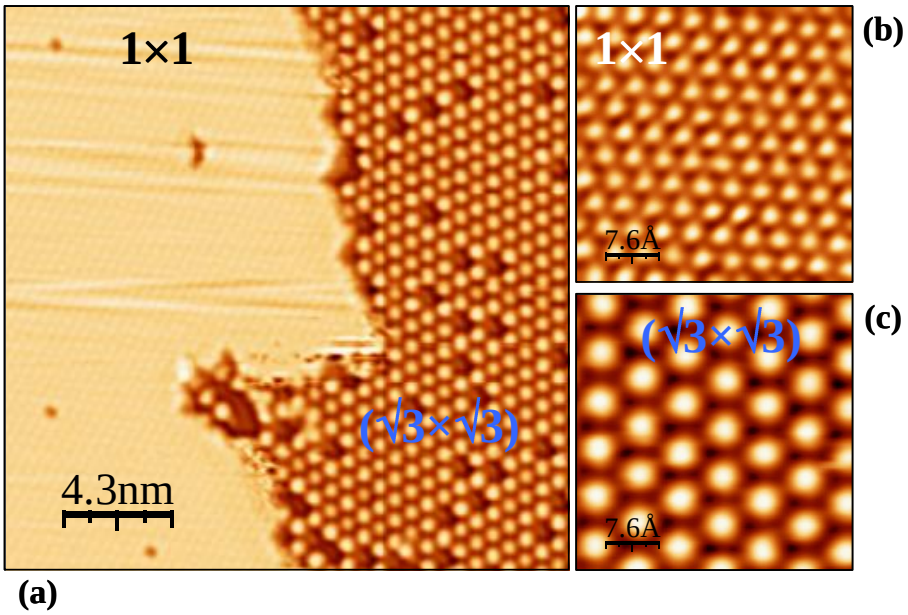

Figure 4.6 *(a) RT-STM image of Pb/Si(111) sample (0.33ML<Θ<0.8ML) showing the coexistence of the two phases: Si(111)-(1×1)-Pb and β-Si(111)-(√3×√3)R30º-Pb. Size: 21nm×21nm, V=-1.5V, I=0.1nA. Both periodicities (1×1) and (√3×√3)R30º are clearly resolved in high resolution images (b) and (c). (b) 3.8nm×3.8nm, V=+0.1V, I=0.3nA. (c) 3.8nm×3.8nm, V=+1.0V, I=0.4nA.*

For 1/3ML, the β-Si(111)-(√3×√3)R30º-Pb phase consists of a √3×√3 structure with 1 Pb atom per unit cell on T_4 site, as it is shown in figure 4.7(b).

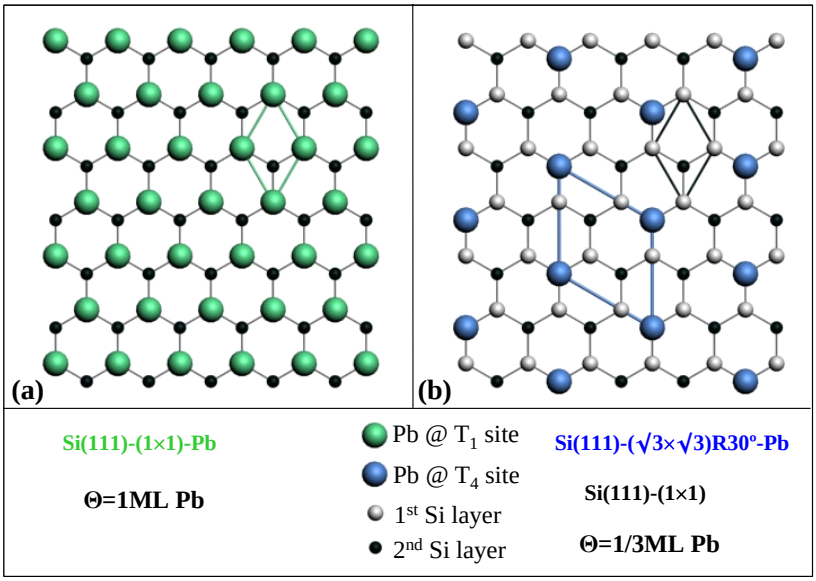

Figure 4.7 *Structural models for Si(111)-(1×1)-Pb (a) and β-Si(111)-(√3×√3)R30º-Pb (b).*

4.1.3.3 γ-Si(111)-(√3×√3)R30º-Pb phase

If the annealing process is continued until a coverage of 1/6ML is reached, a new phase is formed: the γ-Si(111)-(√3×√3)R30º-Pb or the so-called mosaic phase. During the annealing, Si adatoms fill the holes created by desorbed Pb adatoms, and mutual interaction leads to the formation of alternating and disordered chains of the same type of adatoms. This phase ideally consists, then, in a surface alloy with two types of adatoms (Si and Pb) in equal proportions.

The two types of adatoms in the top layer can be identified in STM images acquired at both polarities, as displayed in figure 4.8(a) and (b). While in the empty state image (a) both Si and Pb adatoms have the same contrast, in the filled state image only bright spots are visible and these were found to correspond to the Pb adatoms.

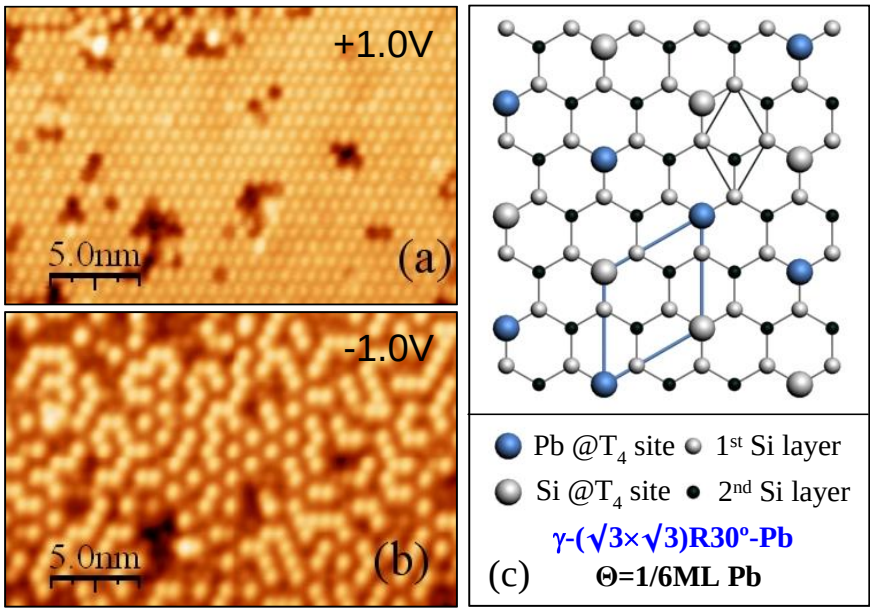

Figure 4.8 *(a) and (b) RT-STM images acquired at both polarities for the mosaic or γ-Pb/Si(111) phase corresponding to 1/6ML Pb (25nm×16nm, I=0.2nA). (c) Structural model of the γ-phase. The √3×√3 unit cell consists of an equal number of Pb and Si adatoms on T_4 sites.*

This contrast difference between Pb and Si adatoms was interpreted as a charge transfer from the Si adatom dangling bond orbital to the Pb adatom dangling bond orbital, based on STS results which showed an empty and an occupied state corresponding to Si and Pb adatoms dangling bond, respectively [Gomez-Rodriguez 1997]. These results were consistent with photoemission studies [Karlsson 1992] which reported a semiconducting character of the γ-phase attributed to such a charge transfer.

4.1.4 PTCDA on Pb/Si(111) surfaces

4.1.4.1 PTCDA on the dense α-Pb/Si(111) phase

The exposure of the hexagonal incommensurate (HIC) surface to PTCDA generates an initial two dimensional molecular layer. Figure 4.9(a) shows a STM image of the HIC phase after the deposition of approximately 0.5ML PTCDA. At this coverage the PTCDA layer with a close-packed molecular structure covers partially the substrate. Clean HIC areas are still visible on the left side in figure 4.9(a). The brightest features observed on the sample are also associated to PTCDA molecules adsorbed at surface defect sites.

With further increasing coverage, PTCDA domains extend covering the whole substrate as shown in figure 4.9(b) which corresponds to ~1ML. The molecular packing within the overlayer corresponds to a herringbone structure.

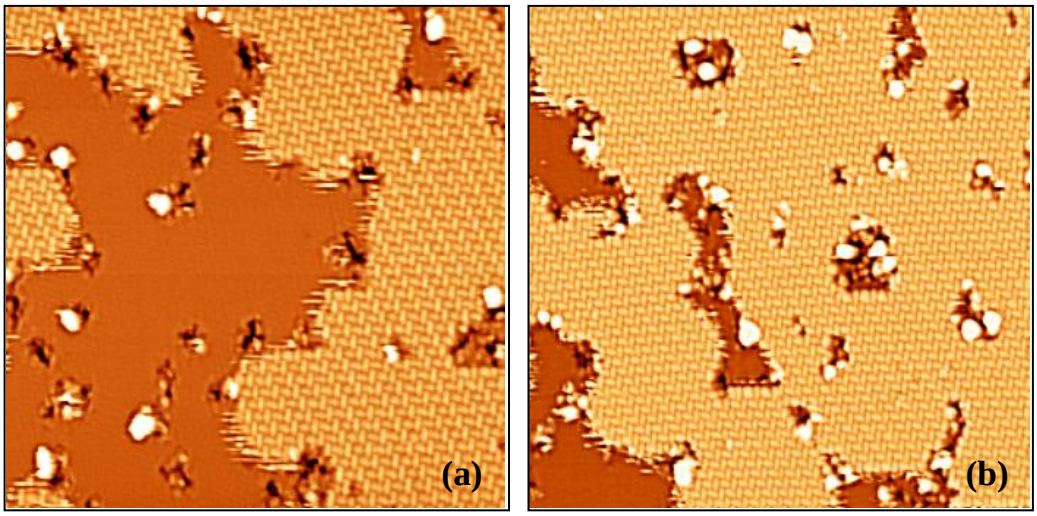

Figure 4.9 *STM images of PTCDA molecules deposited on the hexagonal incommensurate phase of Pb/Si(111). (a) ~ 0.5ML, image size: 60nm×60nm, V=-1.3V, I=0.1nA. (b)~ 1ML, image size: 70nm×70nm, V=-1.7V, I=0.1nA.*

From high resolution images, as shown in figure 4.10, it can be observed that the PTCDA structure consists of two molecules in a nearly rectangular unit cell. The unit cell vectors determined from STM results are $\boldsymbol{b_1}$=21.5±0.5Å and $\boldsymbol{b_2}$=13.5±0.5Å. The angle formed by the $\boldsymbol{b_1}$ and $\boldsymbol{b_2}$ unit cell vectors is δ=(87±2)º and the herringbone angle (i.e. the angle between both molecules in the unit cell) is γ=(85±2)º.

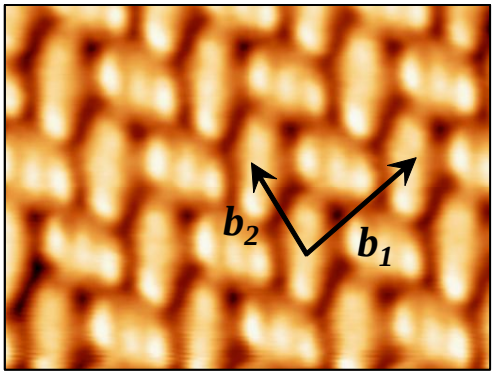

Figure 4.10 *STM image of PTCDA on the HIC phase showing the herringbone reconstruction with two molecules per unit cell (7.6nm×5.6nm).*

The registry of the PTCDA lattice with respect to the substrate lattice can be inferred from high resolution STM images where the (√3×√3) substrate reconstruction and the PTCDA structure are resolved simultaneously. Figure 4.11(a) displays such a STM image which shows the substrate periodicity at the bottom side and the PTCDA herringbone reconstruction at the top side of the image.

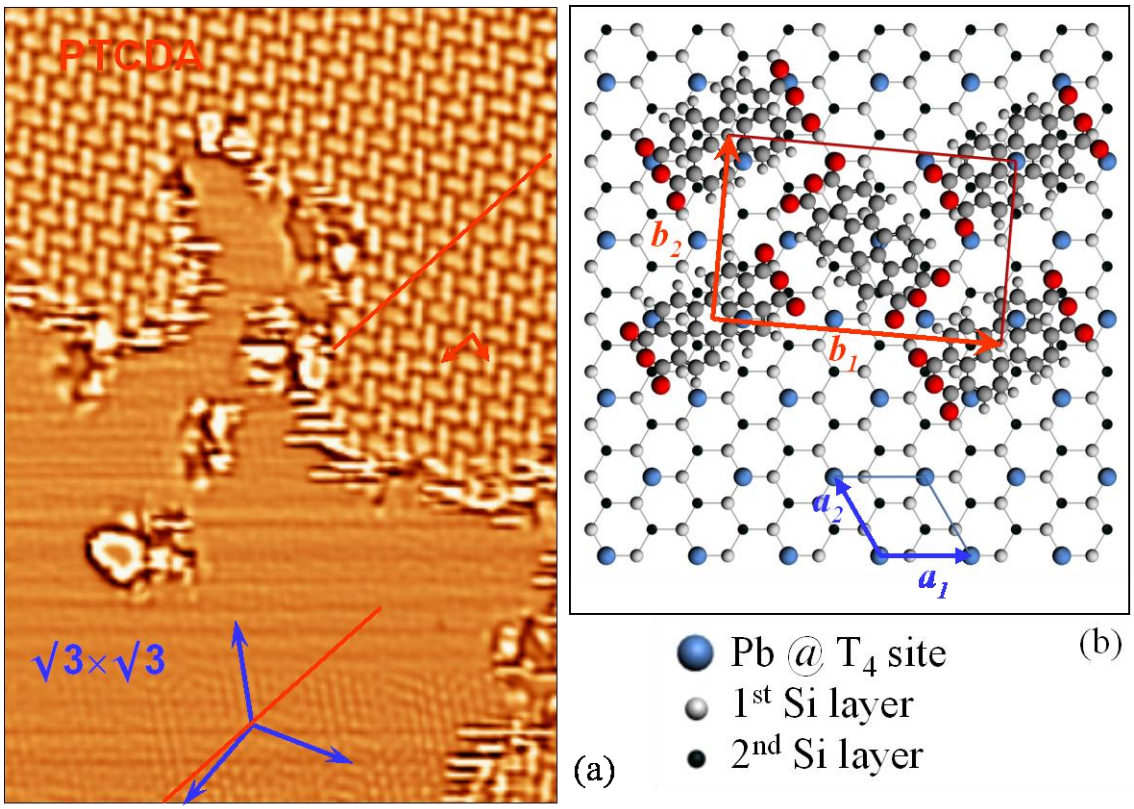

Figure 4.11 *(a) High resolution STM image of ~0.5ML PTCDA on the HIC phase. The PTCDA unit cell vectors (red) and the high symmetry directions of the (√3×√3) substrate (blue) are indicated in the image (31nm×44nm). (b) Proposed structural model for the PTCDA on the HIC phase.*

Taking into account the high symmetry directions of the (√3×√3) reconstructed substrate, indicated in the image as a reference (blue), it can be observed that the long axis ($\boldsymbol{b_1}$) of the PTCDA unit cell (marked by a red line) is oriented ~5° relative to one of the three equivalent symmetry directions of the substrate.

Considering the unit cell parameters and the orientation of the unit cell vectors relative to the substrate directions measured from STM data, a model is proposed for the PTCDA on the HIC substrate, as shown in figure 4.11(b), with the corresponding parameters displayed in table 4.1. According to this model, PTCDA do not form a commensurate structure; however a coincident structure (H-1) can be found by considering a (3×3) PTCDA supercell as shown in figure 4.12.

PTCDA/HIC	$\boldsymbol{b_1}$ [Å]	$\boldsymbol{b_2}$ [Å]	$<(\boldsymbol{b_1}, \boldsymbol{b_2})=\delta°$	$<(\boldsymbol{b_1}, \sqrt{3}$ symmetry direction$)=\theta°$
STM data	21.5±0.5	13.5±0.5	87±2°	5°
Model **H-1**	21.13	13.46	90°	5°

Table 4.1 *Unit cell parameters derived from STM data and from the proposed model for PTCDA on HIC phase.*

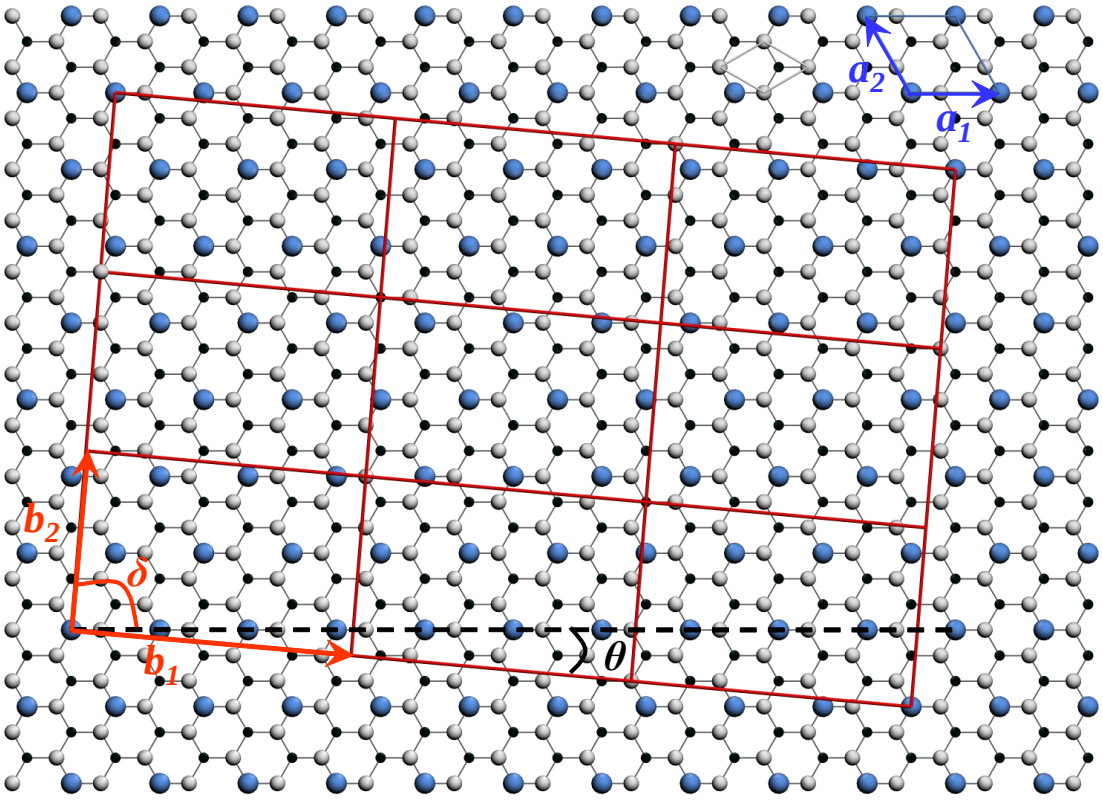

Figure 4.12 *Proposed coincident (3×3) PTCDA superstructure on the HIC phase.*

In this model it can be observed that the PTCDA overlayer forms a (3×3) supercell, whose corner points are in registry with the substrate lattice points (i.e. Pb atoms on T_4 sites). The overlayer and the substrate lattice vectors (for the measured azimuthal orientation θ=5°), are related through the transformation matrix (C) in the expression: $\begin{pmatrix} \boldsymbol{b_1} \\ \boldsymbol{b_2} \end{pmatrix} = (C) \begin{pmatrix} \boldsymbol{a_1} \\ \boldsymbol{a_2} \end{pmatrix}$, where the matrix coefficients are: $(C) = \begin{pmatrix} \frac{10}{3} & \frac{1}{3} \\ 1 & \frac{7}{3} \end{pmatrix}$, as determined from the proposed model (the substrate lattice vectors are $\boldsymbol{a_1}$=$\boldsymbol{a_2}$=6.65Å, and the angle between $\boldsymbol{a_1}$ and $\boldsymbol{a_2}$ substrate vectors is 120°).

The proposed coincident PTCDA superstructure, derived from the measured lattice parameters of the PTCDA primitive unit cell, should be reflected in STM images as a Moiré pattern with a periodicity consistent with the (3×3) supercell. Nevertheless, this coincident epitaxy has not been identified in the current STM results. Since the Moiré pattern reflects a spatial modulation of the tunneling current due to the superposition of the density of states of the overlayer and substrate, it is possible that the bias voltages used in the current experiments were not the most appropriated to allow the visualization of this coincident superstructure.

Previous STM studies of PTCDA on HOPG and MoS_2 [Ludwig 1994] or Cu(111) [Wagner 2007] surfaces have shown the formation of such coincident superstructures. In the case of PTCDA on HOPG, both the measured overlayer lattice parameters and the visualization of a Moiré pattern indicated clearly a coincident epitaxy. On the contrary, in the case of the PTCDA on MoS_2, it has been shown that despite the absence of a Moiré pattern in STM images, the reported matrices were consistent with a coincident structure, demonstrating that the absence of Moiré pattern does not rule out a coincident epitaxy. In a recent report [Wagner 2007], it has been shown that the Moiré pattern associated to a coincident superstructure was only identified for specific tunneling conditions, indicating its dependence with the bias voltage.

Even though the absence of the Moiré pattern in the present STM study, may be attributed to incommensurism, the proposed model, derived from the measured lattice parameters of the PTCDA primitive unit cell, supports the formation of a coincident (3×3) PTCDA superstructure on the HIC phase, suggesting a substrate-mediated interaction which results in a coincident epitaxy.

4.1.4.2 PTCDA on β-Pb/Si(111) and (1×1)-Pb phases

As it was shown previously, for Pb coverages between 1/3 and 1ML, two distinct Pb/Si(111) phases coexist at room temperature: the (1×1)-Pb and the (√3×√3)R30°-Pb.

A large scale (130nm×130nm) STM image obtained for the deposition of ~0.7ML PTCDA on substrates where both phases coexist is shown in figure 4.13(a). A well-ordered PTCDA layer is observed on the (1×1)-Pb phase. PTCDA islands, covering partially the substrate are observed on the upper and the lower terraces (there is a step crossing from top to bottom the right side of the image), as seen in figure 4.13(a). Due to the large scale of the image, the molecular structure within the islands can not be appreciated properly; however from the orientation of the molecular rows (indicated by black lines), three different PTCDA domains can be identified. A closer view of the surface displayed in figure 4.13(b) shows that the molecular packing within PTCDA domains on (1×1)-Pb areas corresponds also to a herringbone structure.

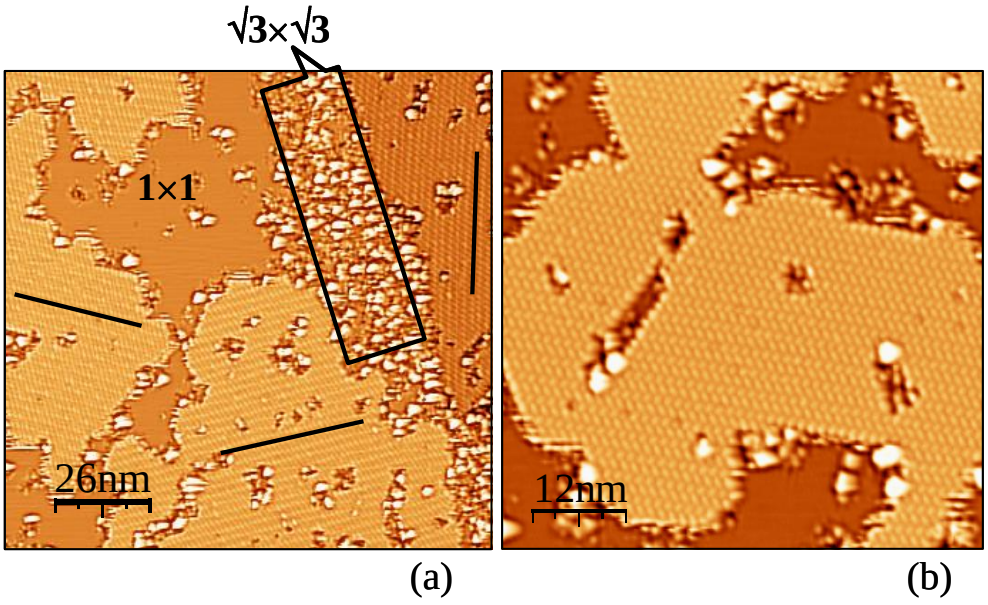

Figure 4.13 *(a) STM image obtained for ~0.7 ML PTCDA deposited on the Pb/Si(111) substrate. PTCDA islands are mainly formed on (1×1)-Pb areas, whereas randomly adsorbed molecules are observed on (√3×√3) areas close to the step edge. (b) Higher resolution image of PTCDA on (1×1)-Pb areas shows a molecular packing within the overlayer corresponding to a herringbone structure. (a) 130nm×130nm, V=-1.8V, I=0.1nA, (b) 60nm×60nm, V=-1.8V, I=0.1nA.*

By contrast, in the region close to the step edge (indicated by a rectangle in the image) which corresponds to a (√3×√3) area, several bright spots with different size and shape are observed. These bright spots are associated to isolated molecules and PTCDA

clusters probably adsorbed at surface defect sites. Apparently no ordered molecular layers are formed for this phase. Nevertheless, a detailed analysis of STM results for the PTCDA covered (√3×√3) areas shows that a short-range order can be obtained on this phase. For larger regions of the (√3×√3)-Pb phase, on which small defect-free areas can be observed (figure 4.14(a)), it is found that PTCDA form small domains with relatively ordered molecules, as indicated by white circles marked on figure 4.14(b). It is believed that these ordered domains are formed on top of the defect-free (√3×√3) areas. This is suggested by the fact that the defect free areas on the clean surface and the obtained PTCDA domains are of similar sizes.

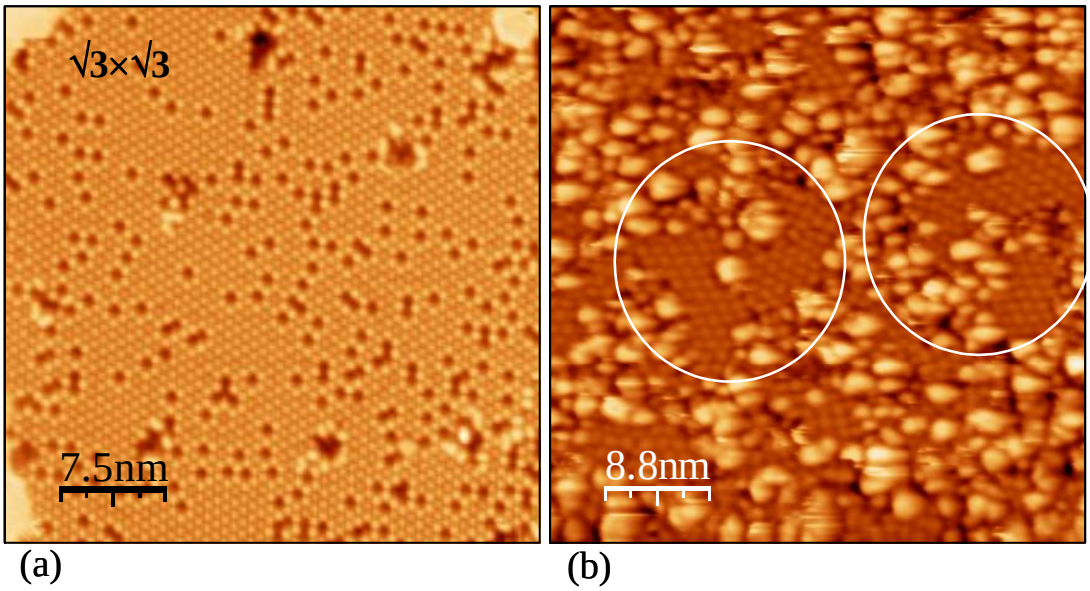

Figure 4.14 *(a) Higher resolution image shows high density of defects on clean √3×√3. (b) Short-range ordered PTCDA domains form on top of defect-free √3×√3 areas. (a) 37nm×37nm, V=-1.5V, I=0.1nA, (b) 44nm×44nm, V=-1.8V, I=0.1nA.*

A detailed analysis of the PTCDA domains obtained on the (1×1)-Pb phase has shown that the PTCDA molecules assembled in a herringbone structure, similar to that found on the HIC substrates. In the present case, however, two different herringbone structures have been observed. In large scale STM images (as displayed in figure 4.15(a)) several domains with different orientations can be identified. From the image contrast it can be observed that the PTCDA domains on the right side of the image have a different appearance as compared to the single PTCDA domain on the left side of the image.

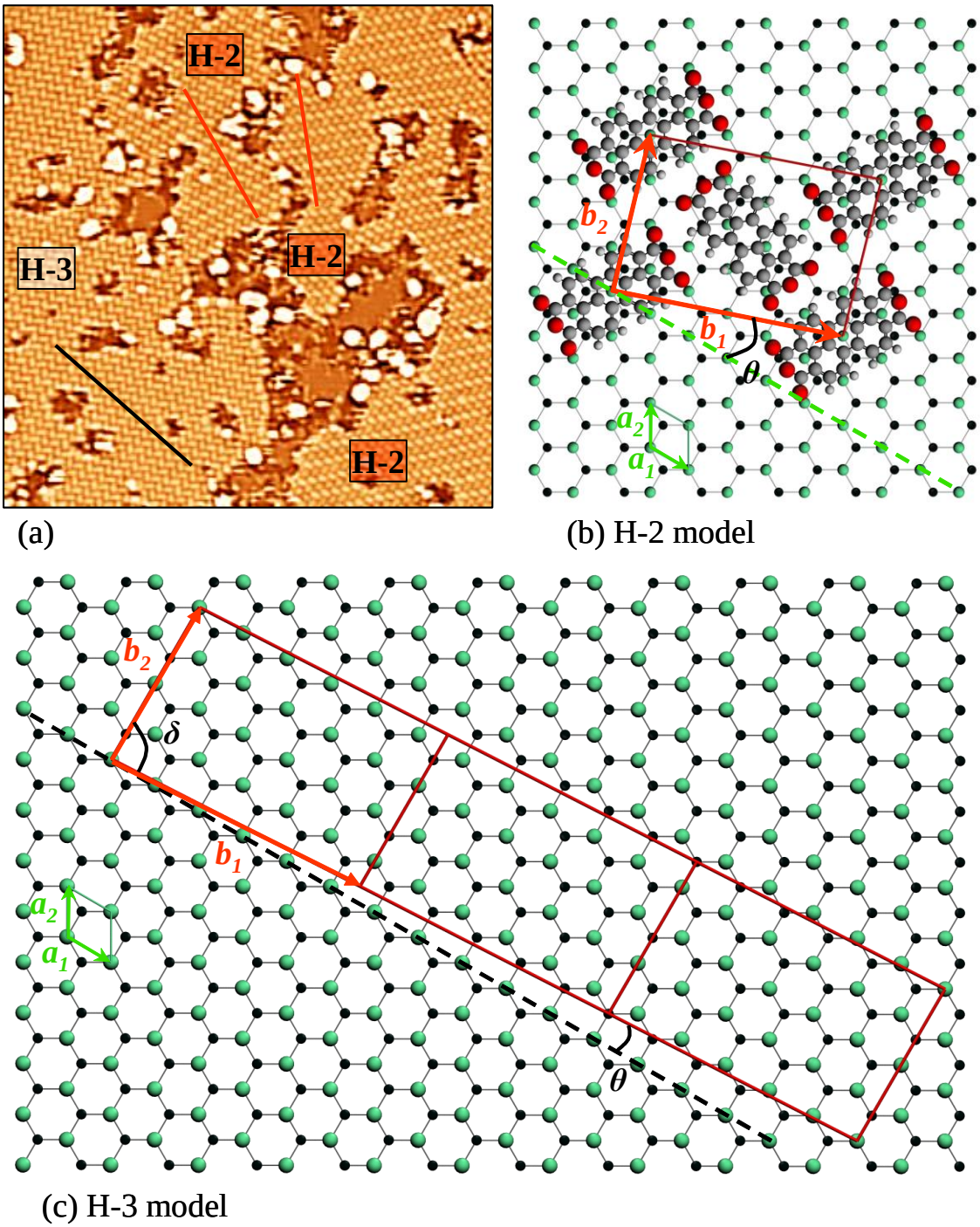

Figure 4.15 *(a) STM image of ~0.8ML PTCDA on (1×1)-Pb phase (61nm×61nm, V=-1.8V, I=0.3nA). Two different PTCDA herringbone structures are formed: H-2 and H-3. Proposed structural models for the commensurate H-2 structure (a) and for the (3×1) coincident superstructure (c).*

In particular, the PTCDA domains with the herringbone structure labeled H-2, have two nonequivalent molecules per unit cell (i.e. one molecule appears brighter than the other one). A different herringbone structure (H-3), with two molecules per unit cell, with the

same apparent brightness, is observed for the single PTCDA domain on the left side of the image. The unit cell parameters measured from STM results and summarized in table 4.2, are similar to those obtained for PTCDA on the HIC substrate, for both H-2 and H-3 phases.

PTCDA/ (1×1)	$\boldsymbol{b_1}$ [Å]	$\boldsymbol{b_2}$ [Å]	<($\boldsymbol{b_1}$, $\boldsymbol{b_2}$)=δ	<($\boldsymbol{b_1}$, (1×1) symmetry direction)=θ
STM data	21.5±0.5	13.5±0.5	87±2	20°(H-2) and ~3°(H-3)
Model **H-2**	20.31	13.84	87	19°
Model **H-3**	21.14	13.3	87	3°

Table 4.2 *Unit cell parameters derived from STM data and from the proposed model for PTCDA on (1×1)-Pb phase.*

The H-2 and H-3 phases mainly differ in the orientation of their unit cell vector $\boldsymbol{b_1}$ with respect to the substrate direction (e.g. substrate unit cell vector $\boldsymbol{a_1}$). For the H-2 phase the angle formed between the substrate and the PTCDA unit cell vector ($\boldsymbol{a_1}$, $\boldsymbol{b_1}$) is θ~20°, while for the H-3 phase is θ~3°. According to the PTCDA lattice parameters measured from STM results, two models are proposed for the H-2 and H-3 phases, as shown in figure 4.15(b) and (c). The model in figure 4.15(b) shows a commensurate structure relative to the Si(111)-(1×1) substrate. The overlayer structure can be described by the matrix coefficients: $(C) = \begin{pmatrix} 6 & 2 \\ 1 & 4 \end{pmatrix}$. This commensurate structure would explain the different appearance of the two molecules per unit cell, observed in STM images. For the H-3 structure (figure 4.15(c)), a coincident (3×1) supercell can be modeled. The resulting lattice parameters of the primitive unit cell are close to those found for the coincident PTCDA structure on the HIC phase. The overlayer structure can be described with the matrix coefficients: $(C) = \begin{pmatrix} \frac{17}{3} & \frac{1}{3} \\ 2 & 4 \end{pmatrix}$. As in the case of the coincident PTCDA superstructure on the HIC phase, there is no direct evidence (i.e. Moiré pattern) in STM images of the (3×1) supercell, however the lattice parameters of the proposed model are very close to those found experimentally, therefore it is believed that the formation of a coincident structure it is also not excluded for PTCDA on the (1×1)-Pb phase.

The evolution of sample morphology with subsequent PTCDA deposition is shown in figure 4.16. With increasing coverage, large PTCDA islands extend over the terraces until the first molecular layer is completed. For a PTCDA coverage of ~1.9ML, a second layer forms on top of the first one as can be observed in figure 4.16(a). The image contrast shows two small areas with ordered molecules corresponding to the first layer.

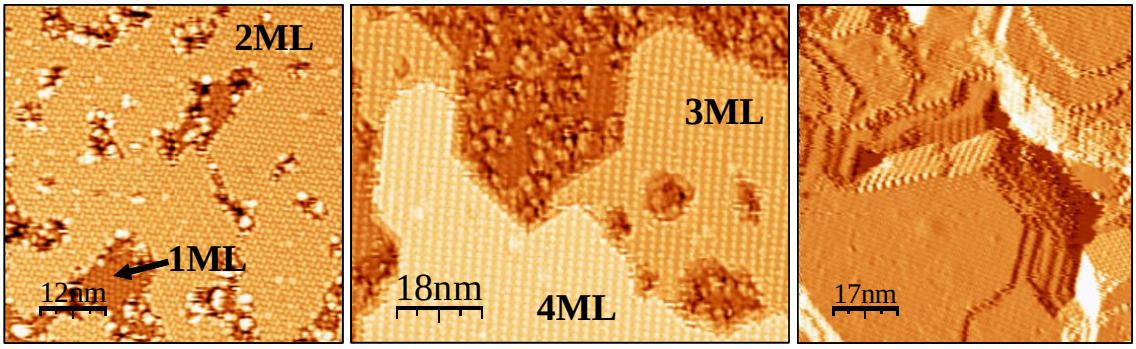

Figure 4.16 *Representative STM images showing the evolution of sample morphology for PTCDA deposition on substrates with coexisting 1×1-Pb and √3×√3-Pb phases. (a) A layer-by-layer growth is observed for the first two layers. (b) At 3ML coverage, √3×√3-Pb areas are covered by a disordered layer, while island formation is observed on 1×1-Pb areas. (c) A Stranski-Krastanov growth mode is observed for multilayer coverage. (a) 60nm×60nm, V=-1.8V, (b) 87nm×68nm, V=+1.7V, (c) 86nm×860nm, V=+1.8V; I=0.1nA.The coverages are: 1.9ML (a), 3ML (b) and 7ML (c).*

Layer-by-layer growth is observed only for molecules adsorbed on 1×1-Pb phase. This is indicated in another image (figure 4.16(b)) which corresponds to PTCDA coverage of ~3ML. The image shows an ordered PTCDA film with heights corresponding to 3 and 4MLs, which partially covers the surface, whereas a disordered layer is visible in the upper part of the image. The disordered layer is assumed to result from the randomly adsorbed PTCDA molecules on √3×√3 areas.

A further increase in the PTCDA coverage gives rise to the spontaneous formation of PTCDA crystalline islands on the whole substrate. Figure 4.16(c) shows a representative STM image of the substrate for the deposition of approximately 7ML, in which large island of different height are seen to form.

The presence of islands onto the whole substrate indicates that √3×√3 areas are also covered by crystalline islands. This suggests that the disordered layer found for this

phase finally acts as passive layer preventing incoming molecules from the interaction with the substrate and favoring thus the formation of crystalline islands.

The molecular structure and PTCDA lattice parameters for higher coverage PTCDA structure can be determined from high resolution images as displayed in figure 4.17. The PTCDA herringbone arrangement is maintained for multilayer growth and the lattice parameters are found to be similar to those observed for the first layer. By comparing the PTCDA lattice in successive molecular stacks, it can be found which of the PTCDA bulk crystal polymorphs (α- or β-polymorph) is preferred when PTCDA grow on these surfaces.

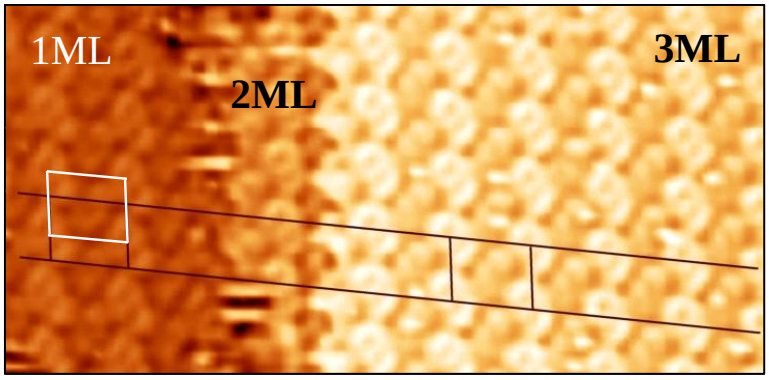

Figure 4.17 *High resolution STM image indicates that PTCDA molecular structure for multilayer growth is very similar to that of the β-polymorph of the PTCDA bulk crystal. Image size: 20nm×10nm, V=+1.7V, I=0.6nA.*

STM results in figure 4.17 shows a lateral shift of ~3Å, parallel to the short unit cell vector, when PTCDA unit cells are compared in consecutive layers. This displacement parallel to the short unit cell vector suggests a molecular structure similar to that of the β-polymorph.

4.1.4.3 PTCDA on the γ-Pb/Si(111) phase

The deposition of PTCDA on the mosaic phase (1/6ML) does not lead to the formation of an ordered layer. Figure 4.18(a) shows a STM image of a clean mosaic phase on which PTCDA adsorb randomly on the surface giving rise to disordered features as seen in figure 4.18(b).

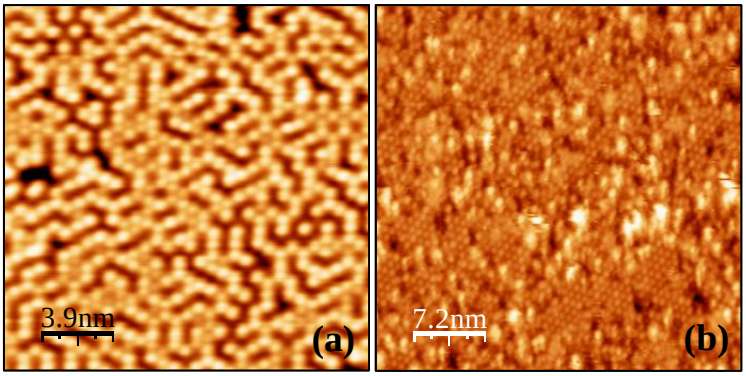

Figure 4.18 *(a) STM image of the clean mosaic phase corresponding to 1/6ML Pb on Si(111), image size: 20nm×20nm, V=-1.5V, I=0.2nA. (b) For low PTCDA coverage, the molecule adsorb randomly on the mosaic phase (36nm×36nm, V=+1.8V, I=0.1nA).*

The absence of ordered PTCDA structures on this mosaic phase must be related to the high reactivity of the substrate due to the presence of the Si adatoms dangling bonds. These results show that the Pb coverage, corresponding to this phase, is not sufficient to "passivate" the silicon substrate. As a result of a strong molecule-substrate interaction, the molecules are not free to diffuse on the surface and this, consequently, leads to the formation of disordered PTCDA structures.

4.1.5 Summary and conclusions

The adsorption and growth of PTCDA molecules deposited on Pb/Si(111) surfaces have been investigated by RT-STM. The evolution of the sample morphology with increasing PTCDA coverage has been studied for samples whose reactivity was gradually varied by changing the amount of Pb. On these passivated surfaces it was expected that the adsorbate-substrate interaction would be significantly lower than in the case of unpassivated silicon surfaces.

- Nevertheless, it has been found that low Pb coverage surfaces as the mosaic phase are still highly reactive and PTCDA adsorption results in a disordered overlayer. The absence of long-range ordered domains on the 1/3ML β-($\sqrt{3}\times\sqrt{3}$)-Pb phase is mainly related to the increased number of defects usually found on these substrates. Most probably, larger PTCDA domains could form if sample preparation methods could improve the substrate surface, with respect to its density of defects.
- In contrast, highly ordered PTCDA layers are obtained for high Pb coverage phases i.e. the hexagonal incommensurate (HIC) and the (1×1)-Pb. For these substrates the STM results indicate that the diffusion of the PTCDA molecules at room temperature is relatively high, allowing the formation of close-packed structures even at low coverage. Two possible coincident structures of the PTCDA overlayer, formed on the HIC and (1×1)-Pb phase, may be inferred from the measured lattice parameters and the STM image contrast. Additionally a commensurate structure has been identified on the (1×1)-Pb phase.
- For multilayer coverage a Stanski-Krastanov growth mode is found for substrates with coexisting phases: (1×1)-Pb and β-($\sqrt{3}\times\sqrt{3}$)-Pb. The PTCDA molecular structure with 3D islands is very similar to that of the β-polymorph of the PTCDA bulk crystal.
- The improved molecular order on the higher Pb coverage phases compared to the mosaic phase is due to the particular arrangement of Pb atoms on the Si(111) substrate which actuate as a passive layer for the silicon dangling bonds, leading to a decreased molecule-substrate interaction.

4.2 PTCDA on the Sn/Si(111) system

In this section the adsorption of PTCDA on Sn/Si(111) surfaces has been studied using RT-STM. A sequential deposition of PTCDA has been performed for substrates kept at room temperature in order to investigate the adsorption and growth mode of the organic molecules as a function of coverage. The Sn/Si(111) surface has been selected as substrate due to its similarity to the Pb/Si(111) system, for which ordered PTCDA molecular layers have been obtained as shown in the preceding section. Since the Sn/Si(111) system forms different phases depending on the Sn coverage, PTCDA growth can be investigated for surfaces with different reconstruction and reactivity. Thus, depending on the surface morphology and its evolution with increasing PTCDA coverage, it may be possible to establish the influence of the substrate surface on the PTCDA growth and to find whether there exists a limitation for an ordered molecular growth.

As in the previous case of Pb/Si(111) system, it can be expected that Sn topmost surface layer could act as a passive layer, which is required for the improvement of molecular growth on silicon-based surfaces. However, different surface periodicities, corrugations and reactivities are expected to influence the PTCDA adsorption site and molecular growth on the Sn/Si(111) surfaces. The aim is to find how the variations in the substrate reactivity affect the molecular adsorption geometry, the lateral ordering and eventually substrate induced modification of the electronic states of the organic molecules at the interface.

In the following, details of the experimental procedure and a brief overview of the Sn/Si(111) system are presented. STM results showing the morphology of the clean and PTCDA covered surfaces are described next. Finally, the adsorption geometry and the obtained PTCDA molecular structure are discussed.

4.2.1 Experimental

The experiment was performed in a home built ultra-high vacuum system with a base pressure of 1×10^{-10} Torr. Si(111)-(7×7) surfaces were prepared by the standard procedure described in the previous sections. Pure Sn (99.99999%, from Goodfellow) was evaporated from a home-made Ta crucible, heated by electron bombardment. Sn coverage close to 1ML (1ML corresponds to 7.84×10^{14} Sn atoms/cm^2) was deposited on the Si(111)-(7×7) reconstructed surface at room temperature, followed by 2 minutes annealing at 650°C. After cooling down the sample at RT, two coexisting phases are obtained: Si(111)-($\sqrt{3}\times\sqrt{3}$)R30°-Sn and Si(111)-($2\sqrt{3}\times2\sqrt{3}$)R30°-Sn. PTCDA molecules were evaporated from a home-made sublimation cell onto the Sn/Si(111) surfaces, at an evaporation rate of ~0.03ML/minute. In this study 1ML PTCDA corresponds to one molecule per ($2\sqrt{3}\times2\sqrt{3}$)-Sn unit cell.

4.2.2 Sn/Si(111) system overview

Similar to the case of Pb/Si(111) system, the room temperature deposition of Sn on Si(111) reconstructed surface induces different Sn/Si(111) phases, depending on the annealing temperature and Sn coverage on the sample. In a first study of Sn/Si(111) system, Estrup *et al.*, using LEED, reported various phases for Sn coverage up to 1ML. The observed phases were: two different Si(111)-($\sqrt{3}\times\sqrt{3}$)R30°-Sn structures and a Si(111)-($2\sqrt{3}\times2\sqrt{3}$)R30°-Sn structure [Estrup 1964]. Similar results were reported from reflection high energy electron diffraction (RHEED) experiments [Ichikawa 1984]. The authors confirmed the existence of two ($\sqrt{3}\times\sqrt{3}$) structures at room temperature for Sn coverage below 1ML. Subsequent studies established that the ($\sqrt{3}\times\sqrt{3}$) structure is induced by the adsorption of 1/3ML Sn atoms on T_4 sites and that the surface is metallic [Kinoshita 1987, Nogami 1989, Conway 1989, Tornevik 1994].

A second ($\sqrt{3}\times\sqrt{3}$) phase, observed for high annealing temperature, and corresponding to 1/6ML was confirmed later [Tornevik 1994]. It was determined that this ($\sqrt{3}\times\sqrt{3}$) surface has equal amounts of Sn and Si adatoms, on T_4 sites similar to the mosaic phase obtained for 1/6ML Pb on Si(111). Experimental KRIPES and STM/STS results as well as DFT-LDA calculations indicated a semiconducting behavior for this surface [Charrier 2001].

Based on STM, XPS and RBS (Rutherford backscattering spectroscopy) experiments, a first structural model of the ($2\sqrt{3}\times2\sqrt{3}$) phase was proposed [Törnevik 1991]. While STM images have shown only four Sn atoms per unit cell, RBS results indicated a much larger coverage (between 1.0 and 1.2ML) corresponding to this phase. Therefore, it was suggested that the ($2\sqrt{3}\times2\sqrt{3}$) phase is a two-layer structure, and according to STM results, the authors proposed a bonding configuration of Sn atoms similar to that of α-Sn(111). The resulting model consists of 14 Sn atoms per unit cell, which corresponds to a Sn coverage of 1.17ML.

While several reports supported the above described model [Worthington 1992, Griffiths 1993], other authors proposed alternative models. In particular, Levermann *et al.*, based on surface X-ray diffraction (SXRD) results, suggested that a structural model in which an atomic geometry of Sn atoms more similar to that of a bulk Sn, would be more appropriate for the ($2\sqrt{3}\times2\sqrt{3}$) reconstruction [Levermann 1996].

A new model of the ($2\sqrt{3}\times2\sqrt{3}$) phase, based on STM results and *ab initio* calculations has been recently proposed by Ichikawa and Cho [Ichikawa 2003]. The authors considered a unit cell composed of 13 Sn atoms, which correspond to a Sn coverage of 13/12 ML. The double layer structure proposed previously [Törnevik 1991] was found stable, however Sn atom positions were found to change significantly in comparison to the previous model. The most important changes were observed for Sn adatoms pairs localized on the topmost layer. The model was in agreement with the SXRD results previously mentioned, and was confirmed recently by other authors in a non-contact AFM study [Sugimoto 2006].

Related to the electronic structure of the ($2\sqrt{3}\times2\sqrt{3}$)-Sn phase, Kinoshita *et al.* [Kinoshita 1987] suggested a semiconducting surface from ARUPS experiments. This was later confirmed by STM experiments where a strong bias dependence was observed in STM images, indicating a semiconducting nature for this surface [Törnevik 1991]. Other authors reported also an opening of a surface band gap in a photoemission study [Griffiths 1993]. However, the band gap value is still controversial. While STS experiments reported a band gap value of 1.6eV [Lin 1996], other authors in a combined LT-STM/STS, XPS and UPS study [Ottaviano 2004] reported a band gap value of 0.8±0.2eV. Currently, the ($2\sqrt{3}\times2\sqrt{3}$) phase is considered as a semiconductor surface with a structural model as proposed by Ichikawa and Cho [Ichikawa 2003].

4.2.3 The substrate: Sn/Si(111) phases by STM

At room temperature, areas of (2√3×2√3)R30°-Sn structure (2√3-Sn in the following) are obtained in coexistence with (√3×√3)R30°-Sn areas (√3-Sn in the following), for Sn coverages close to 1ML. Figure 4.19 displays a typical STM image obtained at RT, where two different phases are observed: 2√3-Sn phase on the left and √3-Sn phase on the right side, respectively.

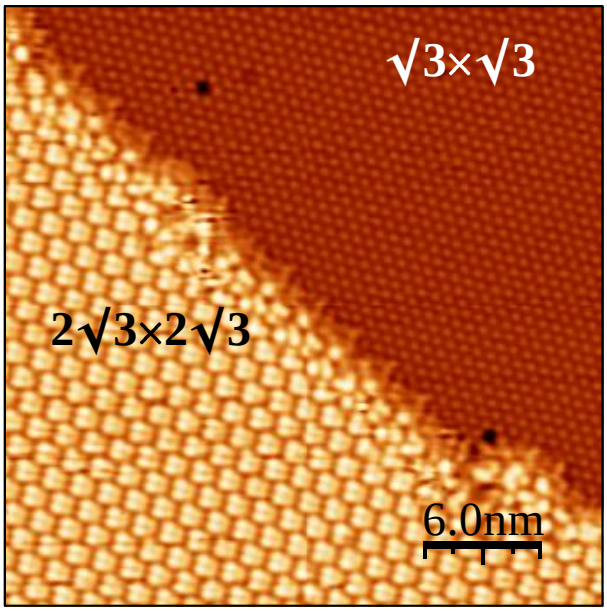

Figure 4.19 *Typical STM images obtained by the deposition of ~1ML Sn on the Si(111)-(7×7) substrate, followed by subsequent annealing. At RT two phases coexist: Si(111)-(2√3×2√3)-Sn and Si(111)-(√3×√3)-Sn. (30nm×30nm, I=0.1nA, V=+1.8V)*

Surfaces with exclusively 2√3-Sn or √3-Sn reconstructions could be obtained by depositing precise amounts of Sn, i.e. 1/3ML for √3-Sn and 13/12ML for 2√3-Sn, however the coexistence of phases was not critical in the present work. Although in this STM image only a single substrate domain is observed, three equivalent domains, 120° rotated one to each other were identified during experiments, for the 2√3-Sn phase. The number of defects in the √3-Sn phase (mainly substitutional Si adatoms as in the case of the β-Si(111)-Pb phase) is slightly larger in comparison to the 2√3-Sn phase which presents almost defect-free areas.

The √3-Sn structure forms at a coverage of 1/3ML Sn and has a similar structure to the 1/3 ML Pb/Si(111) phase, with one Sn atom per unit cell, occupying the T_4 site. The structural model is similar to that shown in figure 4.7(b).

Currently, the accepted structural model for the 2√3-Sn phase is that proposed by Ichikawa *et al*. A schematic model, consistent with the reported relaxed atoms positions is shown in figure 4.20(b). According to this model, the 13 Sn atoms within the unit cell, are distributed in a two layer-structure on top of the Si(111) surface. The topmost layer consists of two Sn adatom pairs, labeled Sn-I and Sn-II, which differ in both vertical and lateral positions. The Sn-II pair appears slightly lower in comparison to Sn-I pair, and has the adatoms closer one to each other with respect to the lateral positions. This can be seen both in the top view and in the cross section along the $[\bar{1}\bar{1}2]$ direction, displayed on the left side of figure 4.20(b).

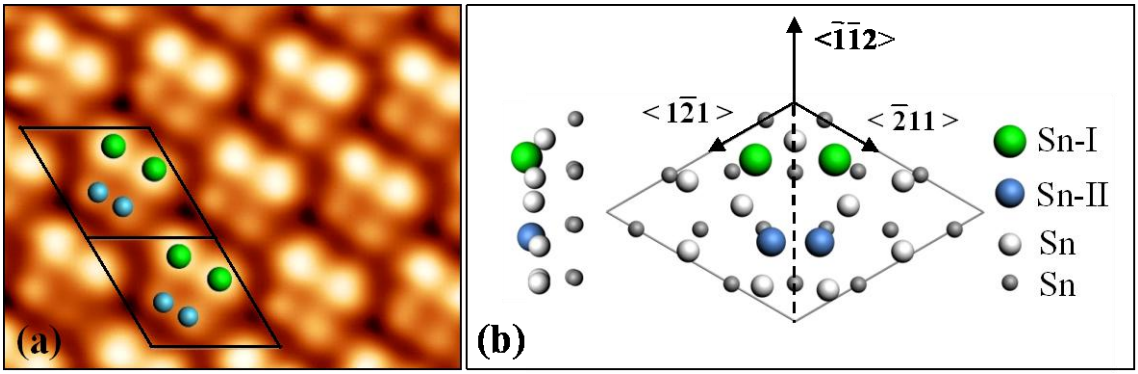

Figure 4.20 *(a) High resolution STM image of the Si(111)-(2√3×2√3)R30°-Sn reconstruction. A simplified structural model superimposed to the image allows to attribute the brighter protrusions to the Sn-I pair and the less bright protrusions to the Sn-II adatom pair (5.0nm×4.0nm, I=0.1nA, V=+2.2V). (b) Structural model of the 2√3-Sn phase, adapted from reference [Ichikawa 2003]. The dashed line represents a symmetry axis of the2√3-Sn unit cell.*

In the STM image of figure 4.20(a), the 2√3-Sn unit cell is indicated. A simplified model showing only the topmost layer, superimposed to the image, allows to attribute the brighter protrusion to the Sn-I pair (in green), and the less bright protrusions to the Sn-II pair (in blue). The difference in the apparent height between the lower and the higher Sn pairs measured from STM is ~0.6Å in agreement with the Sn adatoms heights extracted from first-principles calculations and previous experimental results.

4.2.4 PTCDA on Sn/Si(111) phases. Structural characterization

4.2.4.1 Submonolayer PTCDA coverage on 2√3-Sn phase

Figures 4.21(a)-(d) show large scale topographic STM images after submonolayer deposition of PTCDA at room temperature. In figure 4.21(a), at coverage close to 0.18 ML, the surface is partially covered by individual molecules, which appear as bright protrusions, randomly distributed on the sample. These bright protrusions have similar size and shape but differ in their orientation. A closer inspection of the molecular shapes indicates two distinct orientations of the molecules relative to the substrate.

With increasing PTCDA coverage, a short range molecular order is observed, as can be seen in figure 4.21(b), corresponding to 0.2ML. PTCDA self-assemble in molecular rows, whose lengths vary depending on the number of molecules within the row. For this coverage, rows consisting of a maximum of six molecules are observed. The rows are composed of molecules with the same orientation. The two different orientations of the molecules, observed as before, explain the two different alignments of the rows with respect to the substrate (marked by two white ovals in the figure).

With further PTCDA deposition, the length and the density of the molecular rows increase. Longer molecular chains are observed for a coverage of 0.35ML, in figure 4.21(c). Once more, the two different alignments of the molecular rows with respect to the substrate, is related to the two different orientations of the molecules.

We mention that each of the images (a), (b), and (c) shown in figure 4.21 represents one of the three 2√3-Sn substrate domains as inferred from the $[11\bar{2}]$ substrate direction, which is determined from the atomically resolved Sn adatoms pairs within each unit cell.

For PTCDA coverage close to 0.5ML, the molecular rows extend homogeneously over the entire surface creating a highly ordered structure with regularly spaced molecular rows. Although the molecular row structure would provide sufficient space for the adsorption of additional PTCDA, in between the rows, such a molecular arrangement was not observed for this coverage.

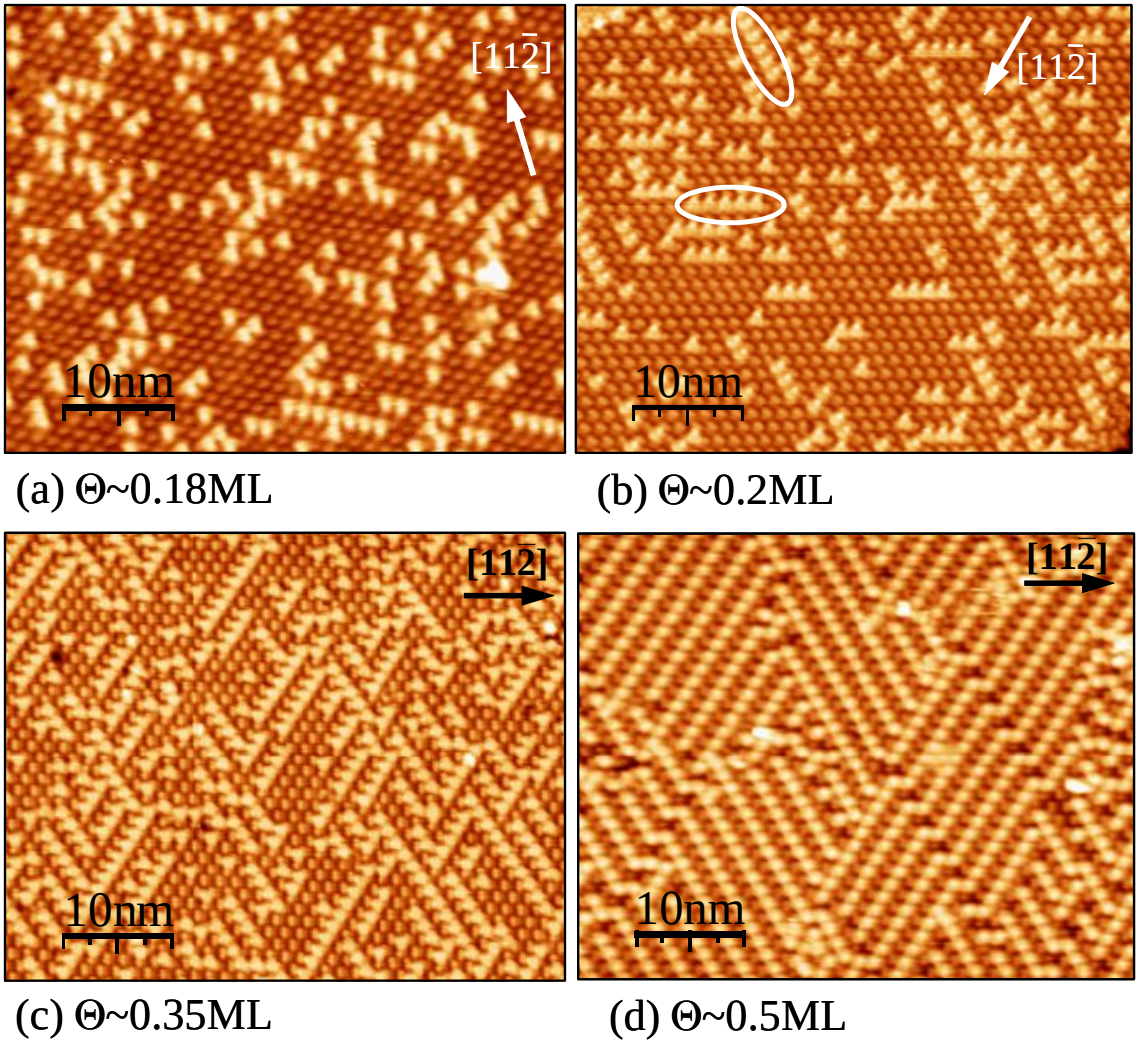

Figure 4.21 *Representative STM images of the 2√3-Sn surface after the deposition of PTCDA 0.18<Θ<0.5ML. (a) At 0.18ML individual molecules are observed randomly distributed on the surface. (b) A subsequent deposition results in the formation of molecular rows. (c) With increasing coverage the length and the density of molecular rows increase. (d) At 0.5ML, highly ordered molecular rows extend over the entire surface. In all cases, two orientations of PTCDA rows can be observed for a single substrate domain. Images size: 50nm×40nm, (a) V=+2.0V, I=1.0nA. (b),(c) V=+2.2V, I=0.1nA. (d) V=-2.0V, I=0.1nA.*

4.2.4.2 Submonolayer PTCDA coverage on √3-Sn phase

For the √3-Sn phase no molecular order is observed either for low or higher PTCDA coverages. Figure 4.22(a) shows a large scale STM image corresponding to ~0.15ML PTCDA on a surface with coexisting 2√3-Sn and √3-Sn phases. While the bottom part of the image shows the early stage of row formation on the 2√3-Sn phase, only bright areas of irregular sizes are observed on the √3-Sn phase, in the upper part of the image.

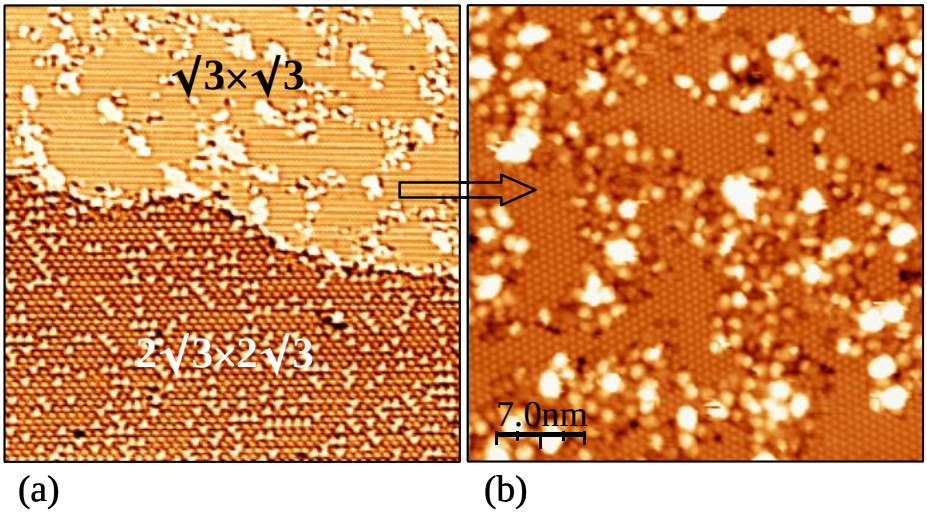

Figure 4.22 *(a) Large scale STM image of PTCDA (0.15ML) on a surface with coexisting √3-Sn and 2√3-Sn areas. (b) Only isolated molecules and PTCDA clusters are observed on the √3-Sn phase. (a) 65nm×65nm, V=+1.8V, I=0.1nA. (b) 35nm×35nm, V=+2.2V, I=0.1nA.*

These bright areas correspond to PTCDA clusters which formed upon adsorption. Apparently, at RT PTCDA diffuse on the √3-Sn phase, but individual molecules are pinned at surface defect sites and with increasing coverage only the cluster formation is observed. A detailed view of PTCDA covered √3-Sn area is displayed in figure 4.22(b) where isolated molecules and clusters give rise to a disordered PTCDA structure.

4.2.5 PTCDA adsorption geometry

For PTCDA deposited on the 2√3-Sn phase, the adsorption geometry can be determined from high resolution images, where intramolecular features of individual molecules are resolved. Figure 4.23 shows bias dependent high resolution images for surfaces with 0.5ML PTCDA. For this coverage, as previously shown, the molecular rows cover the entire substrate. Within the molecular rows, single molecules are clearly resolved.

From a detailed observation of figures 4.23(a) and (b), it can be seen that individual molecules are characterized by several distinct features. The STM image in figure 4.23(a), representing occupied states of the sample, shows that molecules are characterized by two prominent maxima observed on one side of the molecules and five lobes on the other side, as indicated by blue circles marked on the image.

Despite the fact that the overall appearance of individual molecules could be modified by the adsorption, similarities between the resolved intramolecular features and shapes of specific molecular orbitals of the free molecule can be found. For example, the distribution of the five lobes resolved on one side of the molecules clearly resembles the LUMO of the free PTCDA molecule. As shown in the inset of figure 4.23(a), the LUMO can be described by two groups of five maxima separated by a nodal plane perpendicular to the molecular plane and along the long axis of the PTCDA molecule. Thus the five maxima observed in the STM images, can be associated with the five maxima of the LUMO, distributed on one side of the long axis.

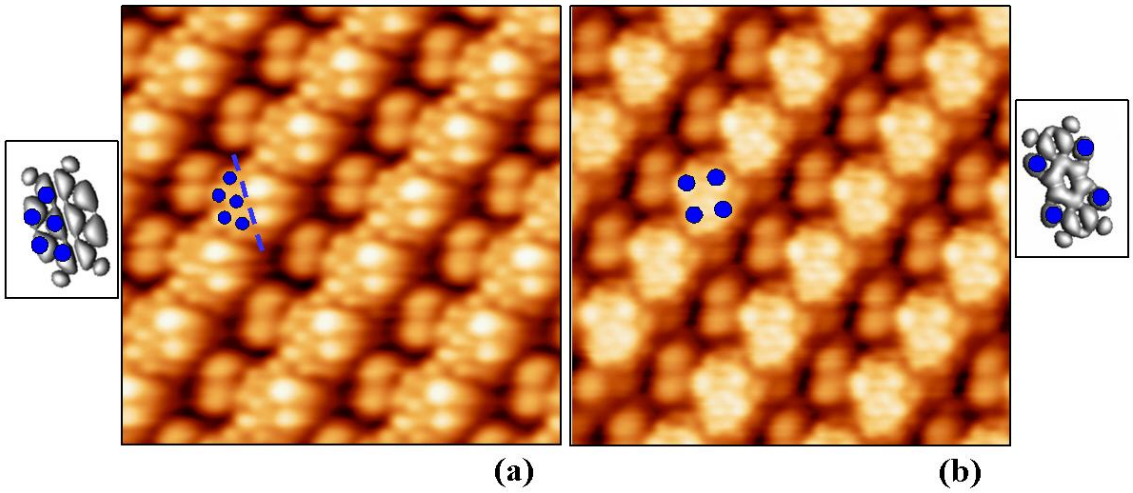

Figure 4.23 *Bias-dependent STM images clearly resolve intramolecular features of individual PTCDA molecules within rows. The observed intramolecular features resemble the free PTCDA LUMO and LUMO+2 in (a) and (b) respectively. Images sizes: 8.0nm×8nm. (a) V=-2.0V, I=1.0nA. (b) V=+1.5V, I=1.0nA.*

In the STM image of figure 4.23(b) recorded at +1.5V, in spite of a poorer resolution, the LUMO+2 orbital can be inferred from the intramolecular features resolved for individual molecules.

Thus, the resolved intramolecular features and their similarities to the molecular orbitals of the free molecule allow the identification of PTCDA long axis, as indicated in the figure 4.23(a) by the dashed blue line. The observed molecular shape also suggests a planar adsorption of the molecule, i.e. the molecular plane is parallel to the substrate surface. However, a slightly tilted adsorption configuration is not excluded as STM data can not provide accurate information related to this aspect.

Compatible imaging parameters allow resolving simultaneously individual molecules and the substrate lattice. In figure 4.24(a), besides the observed molecular shape, Sn adatom pairs are resolved next to each molecule. Each of the Sn adatom pairs corresponds to the highest Sn adatoms pair, labeled Sn-I in figure 4.20(b).

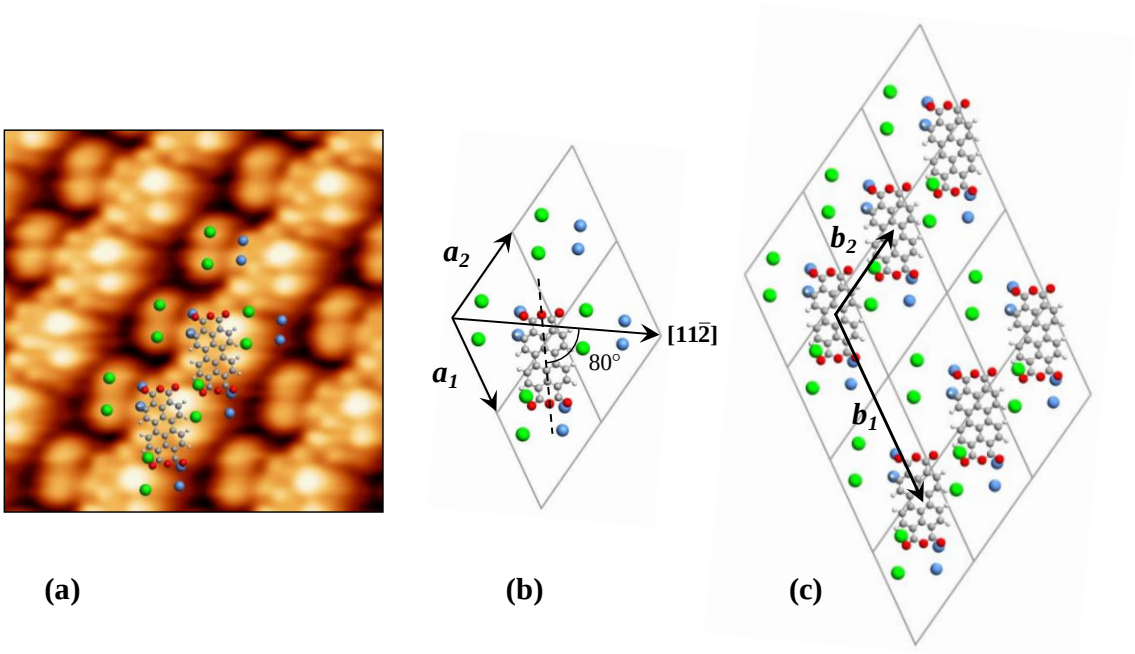

Figure 4.24 *(a) Simultaneously resolved PTCDA intramolecular features and substrate atomic resolution (5.0nm×5.0nm, V=-2.0V, I=0.1nA). (b) Proposed structural model for the PTCDA adsorption geometry, according to STM data. (c) At 0.5ML PTCDA form a commensurate (4√3×2√3) structure with the unit cell defined by the* $\boldsymbol{b_1}$ *and* $\boldsymbol{b_2}$ *vectors.*

The other Sn-II pair is not visible, but it is assumed to be hidden by the molecule positioned on top. This can be shown by superimposing the substrate lattice according to the structural model in figure 4.20. For simplicity, we consider only the substrate topmost layer consisting of Sn-I and Sn-II adatom pairs (marked by green and blue spheres, respectively). Hence, the symmetry axis of the 2√3-Sn unit cell, running along the $[11\bar{2}]$substrate direction can be determined from the atomically resolved Sn adatoms pairs, within each 2√3 unit cell. Once a reference substrate direction and PTCDA long axis are defined, the orientation of PTCDA relative to the substrate can be determined.

As shown in figure 4.24(b), the long axis of the molecule is found to be oriented 80° with respect to the $[11\bar{2}]$ direction of the substrate, or 20° relative to 2√3-Sn unit cell $\boldsymbol{a_1}$ vector. Since STM results, in general, can not provide accurate determination of

molecular adsorption sites, from the present results it can be suggested that the corner oxygen atoms in the dianhydride group are located very close to Sn-II pair, as shown in figure 4.24(b).

Within the rows, the molecules adopt a close-packed side-by-side orientation, with a separation of 13.3±0.5Å along the $[\bar{2}11]$ substrate direction, in close agreement with the lattice spacing of the $2\sqrt{3}$-Sn substrate of 13.28Å. For the spacing between the rows, the measured distance is 26.5±0.5Å, which corresponds to twice the substrate lattice spacing. According to data obtained from STM images a structural model is proposed for the adsorption of 0.5ML PTCDA on the $2\sqrt{3}$ structure, as shown in figure 4.24(c). As derived from experimental results, the corner oxygen atoms in the dianhydride group are located close to the Sn-II adatoms pair, and the long PTCDA axis is oriented 80º relative to the $[11\bar{2}]$ substrate direction. With this adsorption geometry and the measured lattice parameters the STM images are well reproduced, as can be observed by superimposing the model on the image. Thus, it is determined that PTCDA at 0.5ML coverage form a commensurate ($4\sqrt{3}\times2\sqrt{3}$) reconstruction with the unit cell defined by $\boldsymbol{b_1}$ and $\boldsymbol{b_2}$ vectors and one molecule per unit cell, as shown in figure 4.24(c).

As it was previously mentioned, two different orientations of PTCDA molecules were observed on a single substrate domain as displayed in figure 4.25(a).

The two differently oriented molecules observed in the images have an equivalent adsorption site, with the oxygen atoms close to the Sn-II adatom pair. The angle formed between the PTCDA long axis and the $[11\bar{2}]$ substrate direction, the symmetry axis of the substrate unit cell, is +80° and -80° respectively.

Thus, mirror plane symmetry with respect to the $[11\bar{2}]$ direction explains the two differently oriented molecules. This is schematically shown in figure 4.25(b) where a structural model is proposed in agreement with STM data.

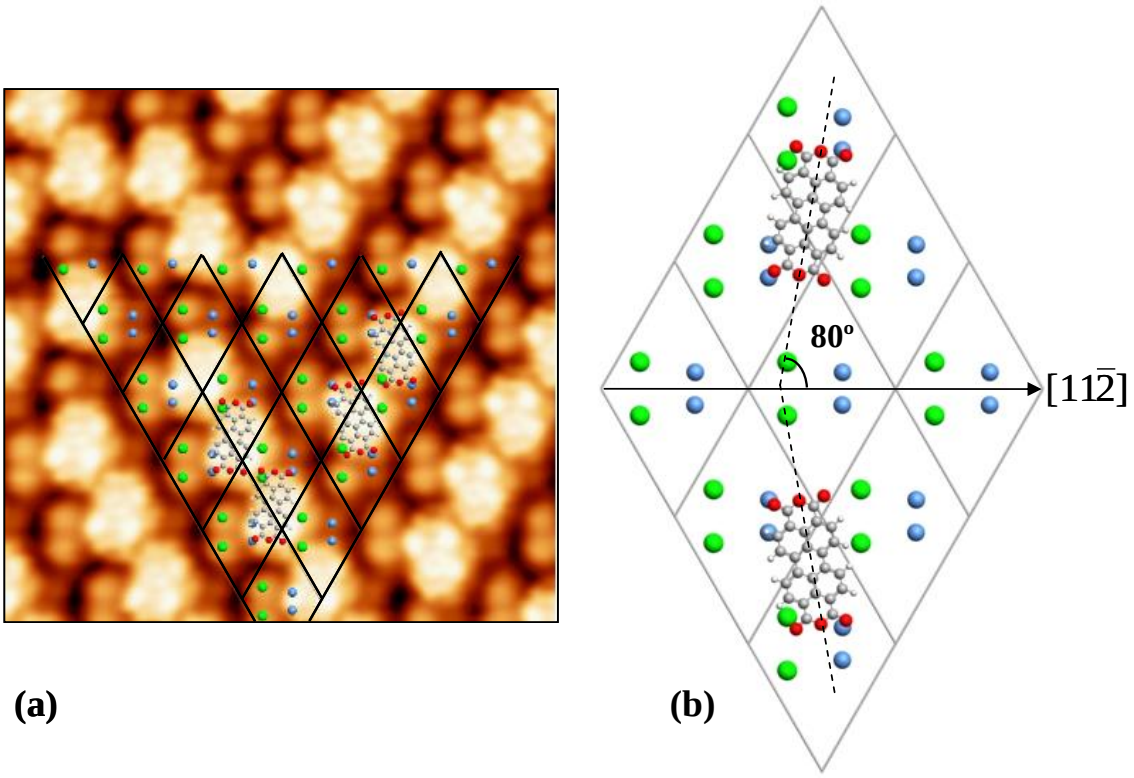

Figure 4.25 *(a) STM image shows two preferential orientations of PTCDA relative to substrate domain (10nm×10nm, V=+2.0V, I=0.1nA). (b) Structural model according to the STM image where mirror symmetry relative to the* $[11\bar{2}]$ *substrate direction is observed.*

Figure 4.26 shows three large scale STM images, obtained for 0.5ML PTCDA coverage on the 2√3-Sn surface. The $[11\bar{2}]$ substrate direction is indicated on all images as a reference direction. Each of the images represents one of the three 2√3-Sn domains of the substrate, 120º rotated one respect to each other as evidenced by the marked arrows. Within each substrate domain there are two preferential orientations of the molecule, resulting from the mirror symmetry relative to the $[11\bar{2}]$ substrate direction. Since the molecular rows consist of molecules of the same orientation there are two types of molecular rows which differ in their alignment with respect to the substrate. Considering the three domains of the 2√3-Sn substrate and two equivalent molecular adsorption geometries within one substrate domain, a total of six orientations of PTCDA rows results for a coverage of 0.5ML PTCDA on the 2√3-Sn substrate, as it is schematically shown in figure 4.26(d). The molecular rows run parallel to the three equivalent symmetry directions of the 2√3-Sn substrate.

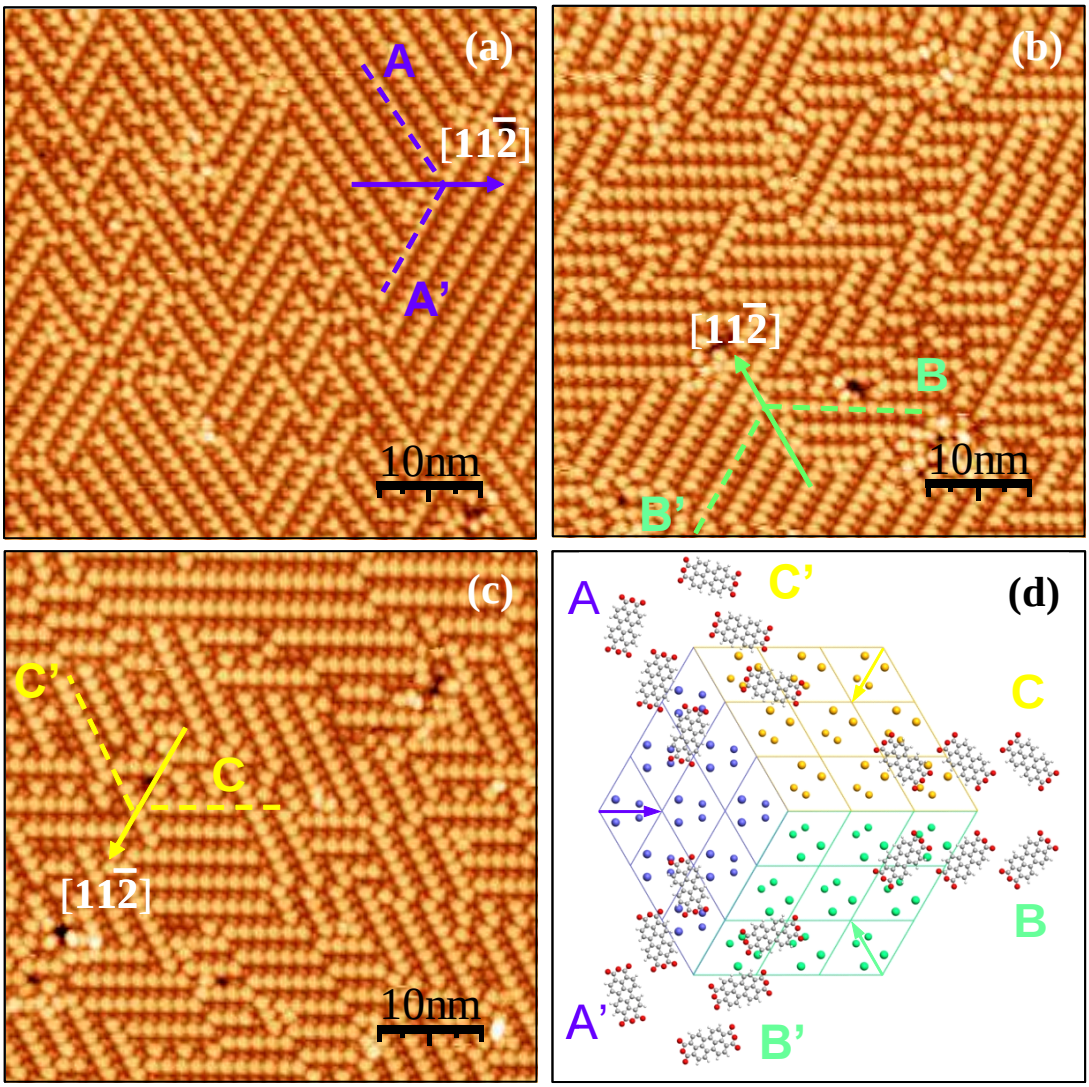

Figure 4.26 *(a, b, c) STM images of 0.5ML PTCDA on 2√3-Sn substrate. Each of the images corresponds to one of the three substrate domains. Within each substrate domain, there are two preferential orientations of the molecule related by mirror symmetry relative to the [11$\bar{2}$] substrate direction. (50nm×50nm, V=+2.2V, I=0.1nA). (b) Structural model according to the STM data which shows PTCDA molecular rows running parallel to the three symmetry direction of the 2√3-Sn substrate.*

The finding that PTCDA molecules did not self-assembled into highly ordered compact islands with the herringbone reconstruction, as in the case of PTCDA deposition on inert surfaces, and form instead molecular rows indicates a significant interaction of PTCDA with the underlying 2√3-Sn substrate. At the same time, at RT the molecules have sufficient thermal energy to diffuse on the surface in order to reach specific adsorption sites. Thus, a fine balance between the substrate mediated interactions and

enough mobility of molecules on the surface allow the formation of one dimensional PTCDA rows.

Based on the intramolecular contrast, resolved for individual molecules within rows, it has been deduced that PTCDA occupy equivalent adsorption sites on the $2\sqrt{3}$-Sn structure, with the oxygen atoms in the dianhydride group preferentially adsorbed in the proximity of the Sn-II adatom pairs.

In previous studies which investigated the In/PTCDA interface using photoemission spectroscopies (ARUPS [Azuma 2000], XPS and UPS [Hirose 1996]), it has been found that In atoms highly react with oxygen atoms in the carbonyl group (C=O) inducing a high density of interface states in the PTCDA band gap. These results were later confirmed using MAES and UPS [Kera 2001]. In the same study the authors extended the results with DFT calculations, and reported significant charge transfer from In to oxygens atoms, as a result of a new In-O bond formation.

Studies of Sn/PTCDA interface using XPS and UPS [Hirose 1996] reported similar results. The authors reported a chemical reaction between Sn atoms and oxygens atoms in the C=O groups, process which is accompanied by a substantial Sn to PTCDA charge transfer.

According to these reports we may suggest a possible Sn-O bond formation, since the oxygen atoms of the C=O group are located close to the Sn-II adatoms pair as inferred from the STM results. The chemisorption process, which implies a charge transfer from Sn atoms into the PTCDA molecular states C=O group would explain, also, the modified molecular orbitals resulted upon molecular adsorption, as observed in STM images. Molecular states associated to lowest unoccupied MO are found in occupied states images which indicate large shifts of MO in comparison to ground states of MO of the free molecule, which can be explained by a charge transfer process.

4.2.6 Conclusions

The adsorption and growth of PTCDA molecules on the Si(111)-($\sqrt{3}\times\sqrt{3}$)R30°-Sn and Si(111)-($2\sqrt{3}\times2\sqrt{3}$)R30°-Sn surfaces has been investigated by RT-STM, at submonolayer coverage.

- For the $\sqrt{3}$-Sn phase no molecular order has been obtained, despite the metallic nature of the surface. PTCDA deposition at RT results in a disordered structure consisting in isolated molecules and PTCDA clusters pinned at surface defect sites.
- For the deposition of PTCDA on the $2\sqrt{3}$-Sn phase, individual molecules, randomly adsorbed on the surface are observed at Θ<0.2ML. With increasing coverage, PTCDA form a novel structure, consisting in quasi one-dimensional molecular rows. At 0.5ML, the molecular rows extend homogeneously over the entire surface, creating a highly ordered structure with regularly-spaced rows.
- The registry of the PTCDA molecule was determined from high resolution STM images where intramolecular PTCDA features and $2\sqrt{3}$-Sn lattice substrate are resolved simultaneously. Within the rows, the molecules adopt a close-packed side-by-side orientation with the PTCDA long axis rotated 80° with respect to the $[11\bar{2}]$ substrate direction. Individual molecules have the oxygen atoms of the C=O group located on top of the lowest Sn adatom pair. A commensurate ($4\sqrt{3}\times2\sqrt{3}$)R30° PTCDA structure is found at 0.5ML coverage. Three symmetry-equivalent PTCDA domains are found. In addition, splitting in two domains by a mirror plane exists with the rotation angle R=+/−20° with respect to the three equivalent surface crystal axis of the Sn/Si(111) substrate.
- In the absence of first-principles calculations of the PTCDA/Si(111)-($2\sqrt{3}\times2\sqrt{3}$)-Sn system, we propose that the molecular anchoring process may be the result of a Sn-O bond formation which stabilizes the molecular rows and promotes the commensurate ($4\sqrt{3}\times2\sqrt{3}$) PTCDA structure at 0.5ML PTCDA coverage. The symmetry and orientation of molecular domains suggest that the molecular arrangement is mainly governed by a molecule-substrate interaction.
- The studied system, for which unprecedented 1D PTCDA structure has been obtained, may be used as an organic template to further functionalize silicon-based semiconductor surfaces.

4.3 PTCDA on the S/GaAs(100) system

In this section the growth of the organic films of PTCDA on sulphur passivated gallium arsenide S-GaAs(100) surfaces is investigated by scanning tunneling microscopy and scanning tunneling spectroscopy. Two different approaches were employed for the substrate passivation. The first one is based on an *ex situ* wet chemical etching method and the second one consists in an *in situ* passivation of MBE prepared GaAs(100) surfaces. The molecular growth and sample morphology are compared for the PTCDA deposition on the two different passivated S-GaAs(100) surfaces. The electronic properties of the organic thin films on MBE prepared sample, which present an improved ordering, are probed.

4.3.1 Experimental

Experiments were performed in the same ultra-high vacuum system described in the previous sections. The samples used were n-type GaAs(100), silicon doped ($1\text{-}4\times10^{18}$ cm^{-3}), provided by Freiberger Compounds. Two different methods were performed in order to obtain passivated GaAs(100) substrates.

A. The first method involves an *ex situ* chemical treatment [Li 1994]. Samples were chemically cleaned in an ultrasonic bath with acetone, ethanol and de-ionized water for 5min each and dried by flowing nitrogen. After degreasing, the samples were dipped in S_2Cl_2:CCl_4 =1:3 solution for 15s. The effect of the etching is to remove the native oxide and to form S-terminated surfaces. To remove the residual S_2Cl_2 on the surface, the sample was rinsed in CCl_4 (5 sec), acetone, ethanol and de-ionized water. The CCl_4 rinse, which follows the etching, plays an important role avoiding the reaction of S_2Cl_2 with water molecules, which will result in failure of passivation. The sample was then loaded into the UHV system. Prior to the growth of the PTCDA organic film, the sample was annealed for 20 min at 450ºC in order to remove the residual sulphur and other contaminants.

B. A second preparation method has been used. As received GaAs(100) wafers were re-grown (by Dr. Jorge Garcia-Martinez at the Instituto de Microelectronica de Madrid-CSIC) in a separate molecular beam epitaxy (MBE) system [Martinez Boubeta 2001].

After desorption of the native oxide, re-growth of 0.5μm GaAs (Si doped 2×10^{18} cm^{-3}) with controlled Ga and As fluxes was performed. MBE grown GaAs(100) samples capped with a thick As layer were then transferred through ambient conditions to our UHV-STM system. After thermal desorption of the As cap at about 300ºC and annealing to 450ºC, for 10 minutes, an As-terminated (2×4) surface was observed by LEED. To obtain sulphur-passivated surfaces, the samples were exposed to a sulphur flux from a SnS_2 evaporator. Final annealing at 500ºC removed sulphur excess from the sample [Zahn 2000], and sulphur-terminated GaAs were obtained.

Onto these surfaces, PTCDA films were grown. The molecules were deposited at various substrate temperatures at a rate of approximately 0.04 ML/s as determined by a quartz crystal microbalance.

STM and STS analysis were performed in order to obtain information about substrate and the growth of the organic material on these samples. Before the STM-STS experiments were performed, tips were prepared by thermal annealing and field emission, until stable field emission currents were obtained. Reproducible STS results were obtained after *in situ* tip treatment and using tips that provide low-resolution images.

Spectroscopic results were obtained measuring I-V curves at selected points. Two types of measurements were performed. The first one was made by increasing the set-point current to reduce the tip-sample distance. The second one was made by direct distance variation. This second type was performed starting with fixed feedback settings (I, V). Then, with open feedback, the tip was approached to the sample a certain distance Z (between 0-7Å) while acquiring the I-Z curve. At the end of the approach an I-V curve was recorded. Then the tip was withdrawn to recover the initial parameters. In order to extract the information from the data, I-V characteristics are presented in three different ways: (a) the I-V characteristic (b) the logarithmic representation and (c) the normalized derivative i.e. (dI/dV)/(I/V) *vs.* V, which is approximately proportional to the local density of states (LDOS) [Feenstra 1987].

From the comparison between I-V curves obtained over the same points, a maximum limit for the gap is obtained from the logarithmic representation of the I-V characteristics. Similar values for the gap can be obtained in the normalized derivative from the FWHH (full width at half-height) between maxima of the edge peaks.

4.3.2 STM results: PTCDA on the S/GaAs(100) system

The surface structure and the roughness of GaAs(100) surfaces prepared by two different methods and the growth of PTCDA on these substrates were investigated by LEED and STM.

4.3.2.1 PTCDA on chemically treated S/GaAs(100) sample

After the chemical treatment of the GaAs(100) sample, LEED patterns corresponding to a (2×1) periodicity are observed for the sulphur-passivated GaAs(100) sample, as displayed in figure 4.27(a). Although, investigation of the samples using STM did not resolve the surface reconstruction, roughness analysis measuring the root mean square (RMS) from STM images gave values close to 0.66nm (for 250nm×250nm images), which indicated very rough surfaces.

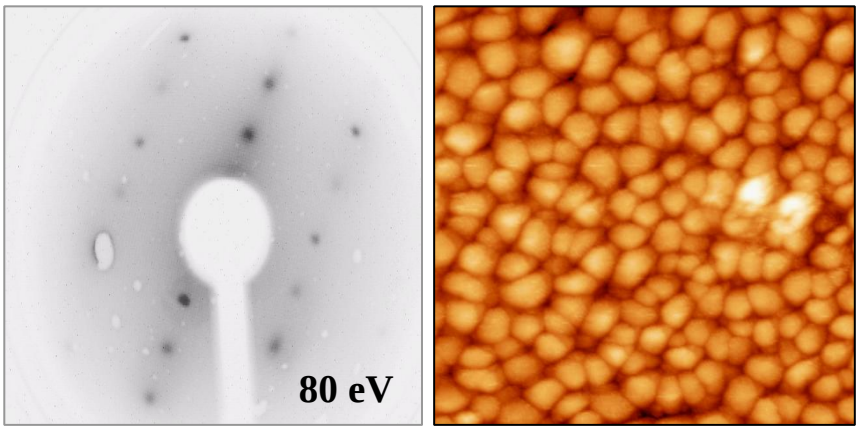

Figure 4.27 *(a) LEED pattern (80eV) that shows a (2×1) periodicity corresponding to the sulphur-passivated GaAs(100) substrate prepared by chemical treatment. (b) STM image (500nm×500nm) obtained after PTCDA deposition on chemically treated S-GaAs(100) substrates. The RT deposition of PTCDA results in formation of clusters with different shape and size.*

After PTCDA deposition on the chemically treated samples, no ordered molecular layers are observed in STM images. Figure 4.27(b) shows a large scale STM image where only cluster formation is observed. From the present STM results it is not possible to conclude whether the randomly oriented clusters have a crystalline structure or not, however the aspect observed in STM indicates a rather disordered growth. We

can only point that the organic layers formed on the chemically prepared samples present no facets, which would clearly indicate a crystalline nature.

4.3.2.2 PTCDA on MBE prepared S/GaAs(100) samples

The GaAs(100) substrates, prepared as described in section 4.3.1B have As-terminated surfaces, with a structure corresponding to a (2×4) periodicity. Atomic resolution STM images of this surface are obtained only for negative sample bias. Figure 4.28(a) shows a typical STM image of the (2×4) reconstruction, where As dimer rows along the $[\bar{1}10]$ direction are observed on two different atomic layers. The brighter features observed in the image possibly correspond to an excess of As. Higher resolution images, as the one displayed in figure 4.28(b), show the dimer rows with 16.9Å periodicity along [110] direction and 8.4Å periodicity along $[\bar{1}10]$ direction, in agreement with the reported values of 16.0Å and 8.0Å. Models for this reconstruction have been previously reported [Hashizume 1994, Hashizume 1995].

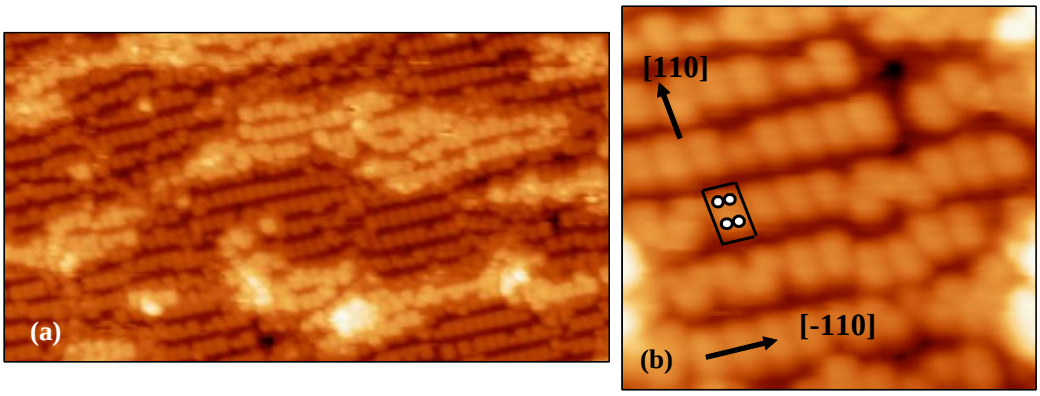

Figure 4.28 *(a) STM image of clean GaAs(100)-(2×4) reconstructed substrate. The surface is characterized by As dimer rows along the* $[\bar{1}10]$ *substrate direction (45nm×24nm, I=2.0nA, V=−3.0V). (b) Higher resolution image shows a detail view of the reconstructed substrate. The As dimers in the topmost layer and the (2×4) unit cell are marked on the image (10nm×10nm, I=1.0nA, V=−3.0V).*

Prior to PTCDA deposition, the MBE GaAs(100)-(2×4) reconstructed substrates were passivated by exposure to S from a SnS_2 evaporator. Subsequently the substrates were annealed in order to remove the sulphur excess. The room temperature deposition of ~7 ML of PTCDA on sulphur passivated GaAs(100) leads to the formation of molecular crystals. At this coverage, the surface is characterized by areas covered by ordered PTCDA films as observed on the lower right corner and also by PTCDA islands of

hexagonal shape as seen on the left side of the image, in figure 4.29(a). For the rest of the surface, in the areas surrounding the ordered PTCDA structures, stripe-like features can be observed; they are assumed to correspond to the interface PTCDA layer.

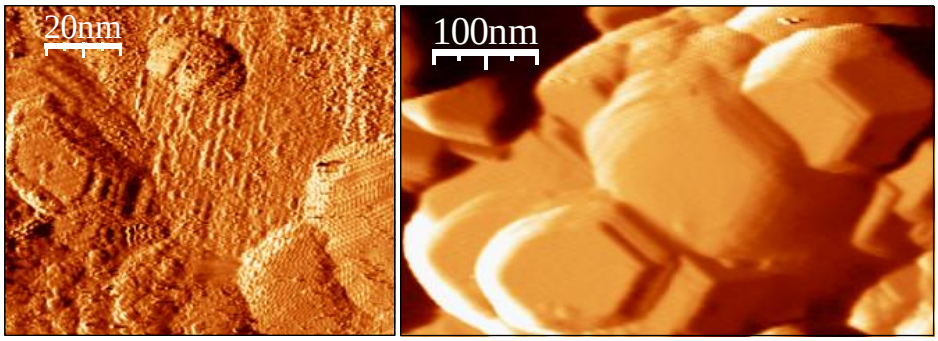

Figure 4.29 *(a) Derivative STM image obtained after deposition of ~7ML PTCDA. PTCDA crystals and relatively ordered films cover partially the surface (100nm×100nm, I=0.1nA, V=-3.0V). (b) Derivative AFM image (570nm×340nm) shows larger size PTCDA crystals for an increased coverage (~20ML).*

Further deposition increases the size and the density of the crystals. Figure 4.29(b) displays a large scale AFM image showing several PTCDA crystals covering the whole surface. Higher resolution STM images (figure 4.30) show the crystal surface structure with PTCDA molecules arranged in a herringbone structure.

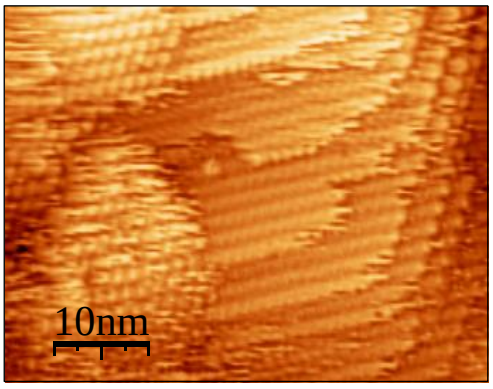

Figure 4.30 *High resolution STM image resolving the PTCDA crystal structure. The molecules are arranged in a herringbone structure similar to that of bulk PTCDA (50nm×40nm, I=0.1nA, V=-3.3 V).*

The unit cell parameters obtained from STM results are $\boldsymbol{b_1}$=18.0±0.5Å and $\boldsymbol{b_2}$=12±0.5 Å. These values are close to those of the (102) plane of α-PTCDA phase (19.91Å and 11.96Å) or the β-PTCDA in the (102) plane (19.30Å and 12.45Å) [Forrest 1997].

4.3.3 Comparison of sample preparation methods

The STM results obtained for the GaAs(100) substrates indicates considerable differences in the surface morphology between the different preparation methods. In order to avoid local effects, RMS roughness analysis has been performed on different areas and using different image sizes. Table 4.3 shows the results obtained from the RMS analysis for samples prepared under different conditions.

S-passivated GaAs(100) Chemical preparation RMS(nm)		GaAs(100) MBE preparation RMS(nm)		Annealing temperature (°C)
50nm×50nm	250nm×250nm	50nm×50nm	250nm×250nm	
0.38	0.66	0.21	0.39	T=450
		0.22	0.27	T=500
		0.11	0.19	T=550
PTCDA on S-passivated GaAs(100) Chemical preparation RMS(nm)		PTCDA on S-passivated GaAs(100) MBE preparation RMS(nm)		
50nm×50nm	250nm×250nm	50nm×50nm	500nm×500nm	
0.56	1.0	0.53	1.49	

Table 4.3 *RMS roughness analysis from STM results.*

Much rougher surfaces are obtained for the chemically prepared samples in comparison to MBE prepared sample, as shown in table 4.3. The absence of smooth surfaces may be related to the fact that during the etching process the chemical attack is not very uniform and affects thus the quality of the surface, in terms of its flatness. Despite the fact that the passivation process itself seems to be effective for both preparation methods, ordered PTCDA structures have been obtained mainly for MBE prepared samples. This suggests that the improvement in the molecular growth is closely related also to the surface morphology properties.

4.3.4 Scanning tunneling spectroscopy results

Scanning tunneling spectroscopy measurements performed on clean GaAs(100) and PTCDA/S-GaAs(100) surfaces are shown in figure 4.31, on the left and right side, respectively. Figure 4.31A (a) shows typical semiconductor behavior for the clean GaAs substrate for three different set-point currents. The GaAs band gap value can be estimated from the logarithmic representation shown in figure 4.31A (b). Close to zero voltage, the noise level of our experimental setup is of the order of 1pA.

The expected gap value of 1.4eV as reported in the literature [Levinshtein 1999] is obtained for the smallest tip-sample distance (at a set-point current of 3nA). Figure 4.31A(c) represents the normalized derivative where similar values for the gap are obtained from the FWHH (full width at half height) between maxima of the peaks.

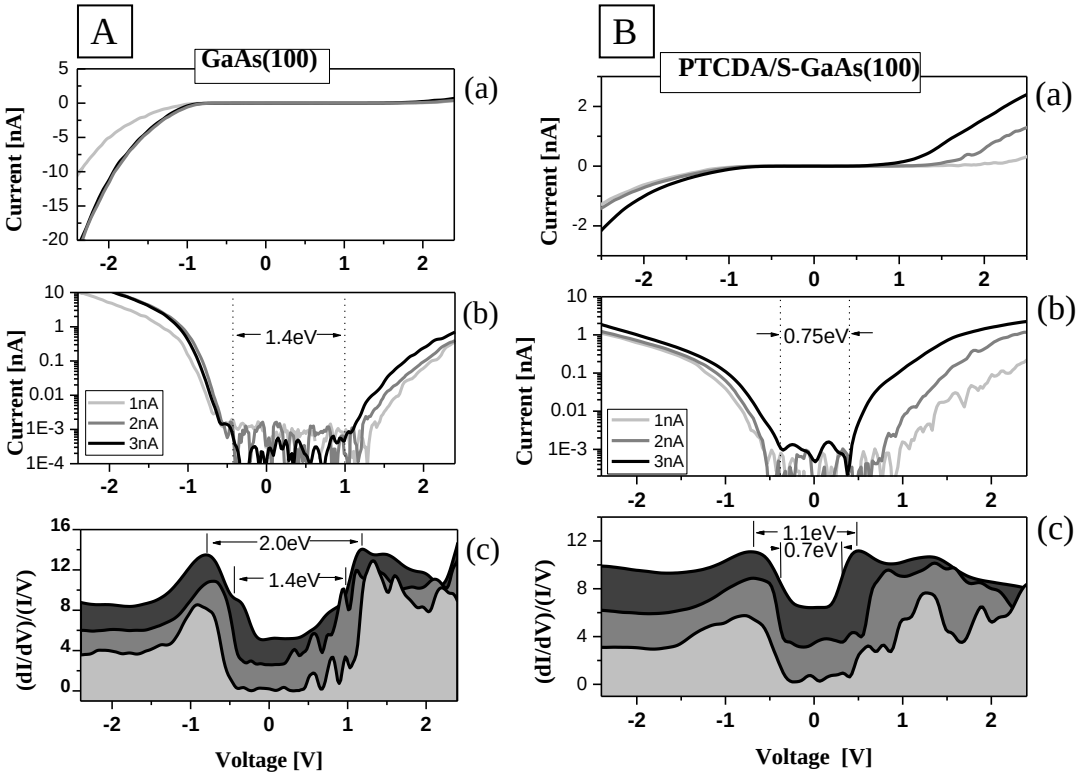

Figure 4.31 *Tunneling spectroscopy results obtained for clean and PTCDA/sulphur-passivated GaAs surfaces are shown on the left and right spectra, respectively. The spectra were acquired for different set-point currents (1.0, 2.0 and 3.0 nA) at V=+3.0V. (a) I-V characteristic, (b) I-V logarithmic representation, (c) Normalized derivative vs. voltage.*

STS measurements performed for the PTCDA/S-GaAs(100) system, on top of the PTCDA crystals, are shown in figure 4.31B. Following a similar procedure as for the clean surface, the I-V plots acquired on PTCDA ordered areas show semiconducting

behavior as seen in figure 4.31B(a). These spectroscopic results show more symmetrical curves for the PTCDA in comparison to the substrate. This has been previously observed for other organics systems [Tian 1998]. The gap value of 0.75eV obtained in the logarithmic representation at 3nA (figure 4.31B (b)), is significantly lower in comparison to reported band gap values for PTCDA. In the normalized derivative plot (figure 4.31B (c)), a peak at positive voltages appears to shift towards the Fermi level as the set-point current increases (the tip-sample distance decreases).

The small value of the gap is quite unexpected. In order to ensure that this corresponds to a real reduction of the gap when the PTCDA forms ordered crystals on the S-GaAs(100) surface, we performed direct measurements of the dependence of the tunnel current on tip-sample distance at fixed tunnel voltage (I-Z plots). These measurements show a non-exponential behavior and/or too low values of the apparent tunnel barrier height. Such effects can occur in STM when very strong interactions (or even contact) between tip and sample exist. This led us to reconsider the way to acquire the I-V plots.

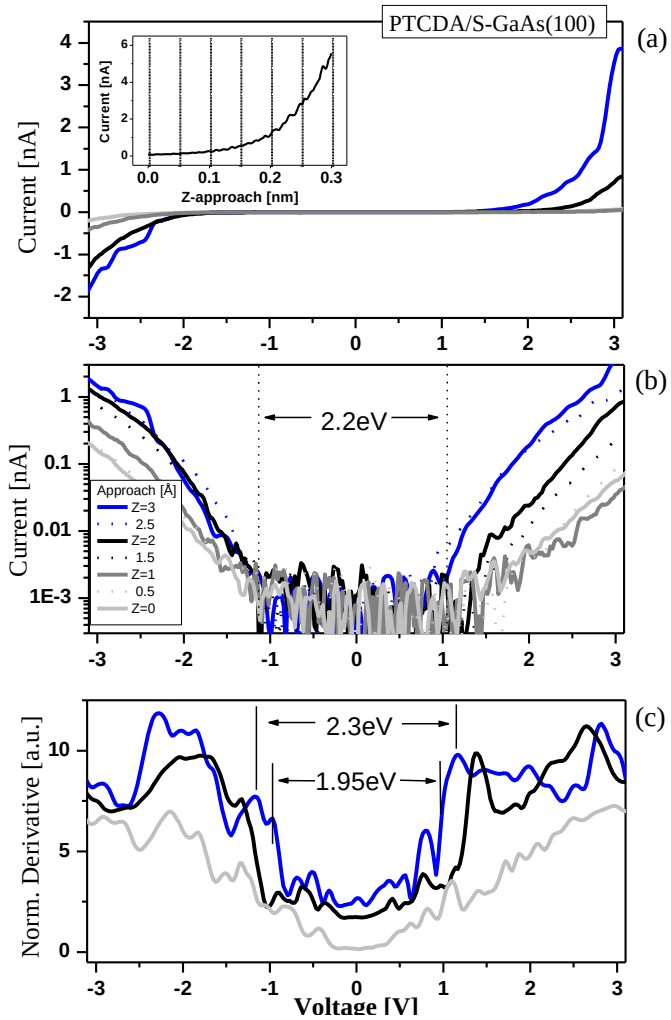

Figure 4.32 *STS measurements acquired on PTCDA/S-GaAs surfaces, after a previous checking of the exponential behavior of I-Z plot (shown in the inset of (a)). (a) I-V plots measured at different approaching Z distances. (b) I-V logarithmic representation. (c) Normalized derivative vs. voltage. Initial feedback parameters: I=0.1nA, V=-3.2V.*

Therefore, first we stabilize the feedback at lower tunnel current set-points in order to increase the starting tip-sample distance. Second, we record the I-Z plot when reducing the tip-sample distance. After checking that the current increases exponentially with the distance (see inset in figure 4.32(a)), we measure I-V curves at different distances in a range 0-7Å. When the current-distance plot becomes non-exponential, we consider that there is an interaction with the organic layer and we stop the procedure. In figure 4.32 we present a set of results for different distances (0-3Å), where the limit value of the PTCDA gap of 2.2 eV is obtained for the smallest tip-sample distance (before leaving the exponential variation). As in the other case, the curves present a more symmetrical behavior in comparison with the substrate.

4.3.5 Discussion

From the STM results, we conclude that PTCDA grows on the sulphur passivated gallium arsenide forming ordered crystals with similar structure as the PTCDA-bulk, for the case of MBE-prepared substrates. On the contrary, the relatively high roughness of the chemically prepared samples does affect the growth of the organic molecules, therefore no order of the organic layers is observed for the chemically prepared substrates.

On PTCDA covered substrates, spectroscopic measurements exhibit diverse results. For the first acquisition procedure of the current-voltage curves (successive I-V plots as the set-point current is increased) we observe a reduction of the band-gap with the distance. At the highest set-point current (the smallest tip-sample distance) the gap is 0.75eV. In the normalized derivative a peak localized at positive values (empty states) shifts towards the Fermi level producing more symmetrical I-V curves. As the current-distance dependence showed a non-exponential behavior, we deduce that the tip is contaminated or that the tip-sample system is not in tunnel regime. Since we have observed these results for all tip conditions and special care was taken for the tip preparation previous and during the experiments, we conclude that there is a strong interaction between the tip and the organic layer.

The second acquisition procedure (I-V plots as the tip approaches the sample), allows us direct identification of the tunnel conditions state from the I-Z variation. From the I-Z curve it is possible to realize whether the tip is in contact with the organic layer, or

contaminated. For common tunnel conditions, with a clean tip and no contact with the surface, the current-distance exhibits an exponentially behavior. For these situations we obtain gap values of ~2.2eV. The small variation of the gap values with the distance (observed in figure 4.32) can be explained as an STS-measurement effect, similar to the one observed for the GaAs substrate.

By monitoring the current behavior, we ensure that there is no contact between the tip and the organic layer and that we keep in tunnel regime. Furthermore, when the tip approaches the sample so much that the current-distance variation (I-Z) leaves the exponential behavior, the measured gaps are small, similar to the ones obtained with the first procedure.

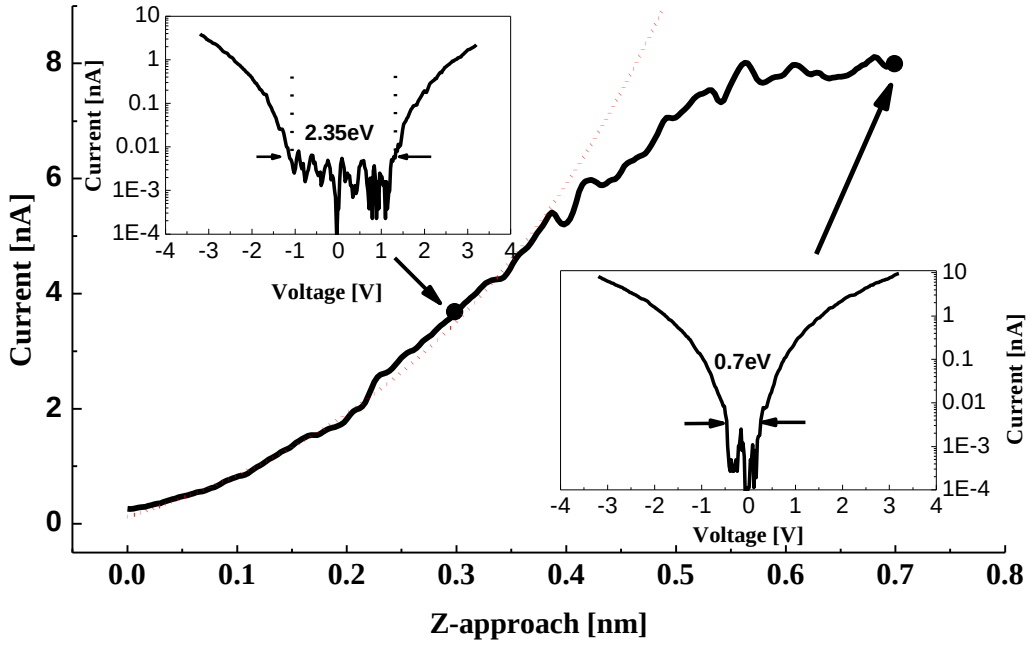

Figure 4.33 *Current vs tip-sample distance curve (I-Z) showing the deviation from the exponential behavior at an approach distance of 4Å. Initial feedback parameters I=0.26nA, V=-3.2V. Insets: two I-V plots in logarithmic representation acquired at 3Å and 7Å, corresponding to exponential and non-exponential behavior respectively. The measured gap values are 2.35eV and 0.7eV respectively.*

Figure 4.33 presents the current variation when the tip is approached 7Å to the sample. The plot deviates from the exponential behavior around 4Å. Two I-V plots acquired at 3Å and 7Å approaching distances are shown in the logarithmic representation. The measured gap values are 2.35eV and 0.7eV respectively. The first one corresponds to

the expected value of the PTCDA gap, while the second one is indicative of a strong interaction between the tip and the organic layer, or a possible contact between them.

4.3.6 Conclusions

The organic/inorganic semiconductor system consisting on PTCDA deposited on sulphur passivated S-GaAs(100), has been studied by scanning tunneling microscopy and spectroscopy (STM/STS). We have compared two different preparation methods for sulphur passivation of GaAs(100) surfaces.

- Ordering of the organic PTCDA layer was only obtained for the MBE-prepared samples where the crystalline growth with bulk-like structure was observed. In order to obtain information about the electronic properties of the organic/inorganic system, we propose measuring I-V plots at different distances, while observing that the current increases exponentially when approaching the tip to the sample.
- With this method, avoiding a strong interaction between the tip and the organic layer, we have obtained a value of 2.2eV from spectroscopic results for the PTCDA gap. We suggest that such strong interactions (or even deformations of the organic layer) could lead to the measurement of anomalously low apparent gap values.

References

[Azuma 2000] Y. Azuma, S. Akatsuka, K. K. Okudaira, Y. Harada and N. Ueno, *Angle-Resolved Ultraviolet Photoelectron Spectroscopy of In-[Perylene-3,4,9,10-Tetracarboxylic Dianhydride] System*, Journal of Applied Physics **87**, 766 (2000).

[Brihuega 2005] I. Brihuega, O. Custance, R. Perez and J. M. Gomez-Rodriguez, *Intrinsic Character of the (3×3) to (√3×√3) Phase Transition in Pb/Si(111)*, Physical Review Letters **94**, 046101 (2005).

[Brihuega 2007] I. Brihuega, O. Custance, M. M. Ugeda and J. M. Gomez-Rodriguez, *Defects in the (√3×√3)↔(3×3) Phase Transition in the Pb/Si(111) System*, Physical Review B **75**, 155411 (2007).

[Brochard 2002] S. Brochard, E. Artacho, O. Custance, I. Brihuega, A. M. Baro, J. M. Soler and J. M. Gomez-Rodriguez, *Ab Initio Calculations and Scanning Tunneling Microscopy Experiments of the Si(111)-(√7×√3)-Pb Surface*, Physical Review B **66**, 205403 (2002).

[Chan 2003] T.-L. Chan, C. Z. Wang, M. Hupalo, M. C. Tringides, Z.-Y. Lu and K. M. Ho, *First-Principles Studies of Structures and Stabilities of Pb/Si(111)*, Physical Review B **68**, 045410 (2003).

[Charrier 2001] A. Charrier, R. Pérez, F. Thibaudau, J.-M. Debever, J. Ortega, F. Flores and J.-M. Themlin, *Contrasted Electronic Properties of Sn-Adatom-Based (√3×√3)R30°; Reconstructions on Si(111)*, Physical Review B **64**, 115407 (2001).

[Chen 2003] Q. Chen, T. Rada, T. Bitzer and N. V. Richardson, *Growth of PTCDA Crystals on H : Si(111) Surfaces*, Surface Science **547**, 385 (2003).

[Conway 1989] K. M. Conway, J. E. Macdonald, C. Norris, E. Vlieg and J. F. van der Veen, *The Structure of the Surface Determined Using X-Ray Diffraction*, Surface Science **215**, 555 (1989).

[Custance 2001] O. Custance, J. M. Gomez-Rodriguez, A. M. Baro, L. Jure, P. Mallet and J.-Y. Veuillen, *Low Temperature Phases of Pb/Si(111)*, Surface Science **482-485**, 1399 (2001).

[Custance 2001a] O. Custance, I. Brihuega, J.-Y. Veuillen, J. M. Gomez-Rodriguez and A. M. Baro, *STM Study of Dynamical Effects on Submonolayer Phases of Pb/Si(111)*, Surface Science **482-485**, 878 (2001).

[Estrup 1964] P. J. Estrup and J. Morrison, *Studies of Monolayers of Lead and Tin on Si(111) Surfaces*, Surface Science **2**, 465 (1964).

[Feenstra 1987] R. M. Feenstra, J. A. Stroscio and A. P. Fein, *Tunneling Spectroscopy of the Si(111)-2×1 Surface*, Surface Science **181**, 295 (1987).

[Forrest 1997] S. R. Forrest, *Ultrathin Organic Films Grown by Molecular Beam Deposition and Related Techniques*, Chem. Rev. **97**, 1793 (1997).

[Ganz 1991a] E. Ganz, H. Ing-Shouh, X. Fulin, S. K. Theiss and J. Golovchenko, *Growth and Morphology of Pb on Si(111)*, Surface Science **257**, 259 (1991).

[Ganz 1991b] E. Ganz, F. Xiong, I.-S. Hwang and J. Golovchenko, *Submonolayer Phases of Pb on Si(111)*, Physical Review B **43**, 7316 (1991).

[Gómez-Rodríguez 1997] J. M. Gómez-Rodríguez, J. -Y. Veuillen, R. C. Cinti, *Scanning Tunneling Microscopy Study of the Si(111)-(√3×√3)-Pb mosaic phase*, Surface Science **377-379**, 45 (1997).

[Griffiths 1993] C. L. Griffiths, H. T. Anyele, C. C. Matthai, A. A. Cafolla and R. H. Williams, in Proceedings of the 20th annual conference on the physics and chemistry of semiconductors interfaces (AVS, Williamburg, Virginia, USA), **11**, 1559 (1993).

[Guaino 2003] P. Guaino, D. Carty, G. Hughes, P. Moriarty and A. A. Cafolla, *Scanning Tunneling Microscopy Study of Pentacene Adsorption on Ag/Si(111)-(√3×√3)R30°*, Applied Surface Science **212-213**, 537 (2003).

[Gustafsson 2004] J. B. Gustafsson, E. Moons, S. M. Widstrand and L. S. O. Johansson, *Thin PTCDA Films on Si(001): 1. Growth Mode*, Surface Science **572**, 23 (2004).

[Hashizume 1994] T. Hashizume, Q. K. Xue, J. Zhou, A. Ichimiya and T. Sakurai, *Structures of As-Rich GaAs(001)-(2×4) Reconstructions*, Physical Review Letters **73**, 2208 (1994).

[Hashizume 1995] T. Hashizume, Q.-K. Xue, A. Ichimiya and T. Sakurai, *Determination of the Surface Structures of the GaAs(001)-(2×4) As-Rich Phase*, Physical Review B **51**, 4200 (1995).

[Hirose 1994] Y. Hirose, W. Chen, E. I. Haskal, S. R. Forrest and A. Kahn, *Structural and Electronic-Properties of an Organic-Inorganic Semiconductor Interface-PTCDA GaAs(100)*, Journal of Vacuum Science & Technology B **12**, 2616 (1994).

[Hirose 1995a] Y. Hirose, *Ordered, Quasi-Epitaxial Growth of Organic Thin Film on Se-Passivated GaAs(100)*, Appl. Phys. Lett. **66**, 944 (1995).

[Hirose 1995b] Y. Hirose, *Quasiepitaxial Growth of the Organic Molecular Semiconductor 3,4,9,10-Perylenetetracarboxylic Dianhydride*, Phys. Rev. B **52**, 14040 (1995).

[Hirose 1996] Y. Hirose, A. Kahn, V. Aristov, P. Soukiassian, V. Bulovic and S. R. Forrest, *Chemistry and Electronic Properties of Metal-Organic Semiconductor Interfaces: Al, Ti, In, Sn, Ag, and Au on PTCDA*, Physical Review B **54**, 13748 (1996).

[Horikoshi 1999] K. Horikoshi, X. Tong, T. Nagao and S. Hasegawa, *Structural Phase Transitions of Pb-Adsorbed Si(111) Surfaces at Low Temperatures*, Physical Review B **60**, 13287 (1999).

[Hupalo 2002] M. Hupalo, T. L. Chan, C. Z. Wang, K. M. Ho and M. C. Tringides, *Atomic Models, Domain-Wall Arrangement, and Electronic Structure of the Dense Pb/Si(111)-(√3×√3) Phase*, Physical Review B **66**, 161410 (2002).

[Hwang 1995] I.-S. Hwang, R. E. Martinez, C. Liu and J. A. Golovchenko, *Soft Incommensurate Reconstruction on Pb/Si(111): Structure, Stress Modulation, and Phase Transition*, Physical Review B **51**, 10193 (1995).

[Hwang 2004] I.-S. Hwang, S.-H. Chang, C.-K. Fang, L.-J. Chen and T. T. Tsong, *Observation of Finite-Size Effects on a Structural Phase Transition of 2D Nanoislands*, Physical Review Letters **93**, 106101 (2004).

[Ichikawa 1984] T. Ichikawa, *Structural Study of Ultrathin Sn Layers Deposited onto Ge(111) and Si(111) Surfaces by RHEED*, Surface Science **140**, 37 (1984).

[Ichikawa 2003] T. Ichikawa, K. Cho, *Structural Study of Si(111)-(2√3×2√3)R30°-Sn Surfaces*, Japanese Journal of Applied Physics **42**, 5239 (2003).

[Kampen 2000] T. U. Kampen, G. Salvan, M. Friedrich, D. A. Tenne, S. Park and D. R. T. Zahn, *Optical Characterization of PTCDA Films Grown on Passivated Semiconductor Substrates*, Applied Surface Science **166**, 387 (2000).

[Karlsson 1992] C. J. Karlsson, E. Landemark, Y.-C. Chao and R. I. G. Uhrberg, *Photoemission Study of the Si(111)-(√3×√3)-Pb Mosaic Phase: Observation of a Large Charge Transfer*, Physical Review B **45**, 6321 (1992).

[Kera 2001] S. Kera, H. Setoyama, M. Onoue, K. K. Okudaira, Y. Harada and N. Ueno, *Origin of Indium-[Perylene-3,4,9,10-Tetracarboxilic Dianhydride] Interface States Studied by Outermost Surface Spectroscopy Using Metastable Atoms*, Physical Review B **63**, 115204 (2001).

[Kinoshita 1987] T. Kinoshita, H. Ohta, Y. Enta, Y. Yaegashi, S. Suzuki, S. Kono, *Empty- and Filled Electronic States of the Si(111)√3×√3-Sn, √3×√3-In and 2√3×2√3-Sn Surfaces*, Journal of Physical Society of Japan, **11**, 4015 (1987).

[Kumpf 2000] C. Kumpf, O. Bunk, J. H. Zeysing, M. M. Nielsen, M. Nielsen, R. L. Johnson and R. Feidenhansl, *Structural Study of the Commensurate-Incommensurate Low-Temperature Phase Transition of Pb on Si(111)*, Surface Science **448**, L213 (2000).

[Le Lay 1988] G. Le Lay, J. Peretti, M. Hanbucken and W. S. Yang, *Surface Spectroscopy Studies of Pb Monolayers on Si(111)*, Surface Science **204**, 57 (1988).

[Levermann 1996] A. H. Levermann, P. B. Howes, K. A. Edwards, H. T. Anyele, C. C. Matthai, J. E. Macdonald, R. Feidenhans'l, L. Lottermoser, L. Seehofer, G. Falkenberg and R. L. Johnson, *The Atomic Structure of the Si(111) Reconstruction*, Applied Surface Science **104-105**, 124 (1996).

[Levinshtein 1999] M.E Levinshtein, M. Rumyantsev and M. S. Shur, *Handbook Series on Semiconductors Parameters*, Vol. 2, Singapore: World Scientific (1999).

[Li 1994] Z. S. Li, W. Z. Cai, R. Z. Su, G. S. Dong, D. M. Huang, X. M. Ding, X. Y. Hou and X. Wang, *S_2Cl_2 Treatment: A New Sulfur Passivation Method of GaAs Surface*, Applied Physics Letters **64**, 3425 (1994).

[Lin 1996] X. F. Lin, I. Chizhov, H. A. Mai and R. F. Willis, *Scanning Tunneling Spectroscopy Examination of Surface Electronic Structures of Surface*, Applied Surface Science **104-105**, 223 (1996).

[Ludwig 1994] C. Ludwig, B. Gompf, J. Petersen, R. Strohmaier and W. Eisenmenger, *STM investigations of PTCDA and PTCDI on graphite and MoS_2. A systematic study of epitaxy and STM image contrast*, Zeitschrift für Physik B Condensed Matter **93**, 365 (1994).

[Ma 2006] J. Ma, B. L. Rogers, M. J. Humphry, D. J. Ring, G. Goretzki, N. R. Champness and P. H. Beton, *Dianhydride-Amine Hydrogen Bonded Perylene Tetracarboxylic Dianhydride and Tetraaminobenzene Rows*, J. Phys. Chem. B **110**, 12207 (2006).

[Martinez Boubeta 2001] C. Martinez Boubeta, J. L. Menendez, J. L. Costa-Kramer, J. M. Garcia, J. V. Anguita, B. Bescos, A. Cebollada, F. Briones, A. V. Chernykh, I. V. Malikov and G. M. Mikhailov, *Epitaxial Metallic Nanostructures on GaAs*, Surface Science **482-485**, 910 (2001).

[Morozov 2000] A. O. Morozov, T. U. Kampen and D. R. T. Zahn, *PTCDA Film Formation on Si(111): H-1×1 Surface: Total Current Spectroscopy Monitoring*, Surface Science **446**, 193 (2000).

[Nicoara 2002] N. Nicoara, I. Cerrillo, D. Xueming, J. M. Garcia, B. Garcia, C. Gomez-Navarro, J. Mendez and A. M. Baro, *Preparation and Passivation of GaAs(001) Surfaces for Growing Organic Molecules*, Nanotechnology **13**, 352 (2002).

[Nicoara 2003] N. Nicoara, O. Custance, D. Granados, J. M. Garcia, J. M. Gomez-Rodriguez, A. M. Baro and J. Mendez, *Scanning Tunneling Microscopy and Spectroscopy on Organic PTCDA Films Deposited on Sulfur Passivated GaAs(001)*, Journal of Physics-Condensed Matter **15**, S2619 (2003).

[Nogami 1989] J. Nogami, S.-I. Park and C. F. Quate, *Structure of Submonolayers of Tin on Si(111) Studied by Scanning Tunneling Microscopy*, Journal of Vacuum Science & Technology A: Vacuum, Surfaces, and Films **7**, 1919 (1989).

[Ottaviano 2004] L. Ottaviano, G. Profeta, L. Petaccia, C. B. Nacci and S. Santucci, *Structural and Electronic Properties of the Sn/Si(111)-(2√3×2√3)R30° Surface Revised*, Surface Science **554**, 109 (2004).

[Petkova 1999] A. Petkova, J. Wollschläger, H. L. Günter and M. Henzler, *Formation of an Intermediate 3×3 Phase from Pb on Si(111) at High Temperature*, Journal of Physics: Condensed Matter **11**, 9925 (1999).

[Petkova 2001a] A. Petkova, J. Wollschlager, H.-L. Gunter and M. Henzler, *Formation and Commensurate Analysis of "Incommensurate" Superstructures of Pb on Si(111)*, Surface Science **471**, 11 (2001).

[Petkova 2001b] A. Petkova, J. Wollschlager, H.-L. Gunter and M. Henzler, *Order and Disorder in Ultrathin Pb Films Grown on Si(111)-7×7 Substrates at Low Temperatures*, Surface Science **482-485**, 922 (2001).

[Saitoh 1985] M. Saitoh, K. Oura, K. Asano, F. Shoji and T. Hanawa, *Low Energy Ion Scattering Study of Adsorption and Desorption Processes of Pb on Si(111) Surfaces*, Surface Science **154**, 394 (1985).

[Sazaki 2004] G. Sazaki, T. Fujino, J. T. Sadowski, N. Usami, T. Ujihara, K. Fujiwara, Y. Takahashi, E. Matsubara, T. Sakurai and K. Nakajima, *Epitaxial Relation and Island Growth of Perylene-3,4,9,10-Tetracarboxylic Dianhydride (PTCDA) Thin Film Crystals on a Hydrogen-Terminated Si(111) Substrate*, Journal of Crystal Growth **262**, 196 (2004).

[Seehofer 1995] L. Seehofer, G. Falkenberg, D. Daboul and R. L. Johnson, *Structural Study of the Close-Packed Two-Dimensional Phases of Pb on Ge(111) and Si(111)*, Physical Review B **51**, 13503 (1995).

[Slezák 1999] J. Slezák, P. Mutombo and V. Cháb, *STM Study of a Pb/Si(111) Interface at Room and Low Temperatures*, Physical Review B **60**, 13328 (1999).

[Soubiron 2005] T. Soubiron, F. Vaurette, J. P. Nys, B. Grandidier, X. Wallart and D. Stievenard, *Molecular Interactions of PTCDA on Si(100)*, Surface Science **581**, 178 (2005).

[Stepanovsky 2006] S. Stepanovsky, M. Yakes, V. Yeh, M. Hupalo and M. C. Tringides, *The Dense Alpha-(√3×√3)R30°-Pb/Si(111) Phase: A Comprehensive STM and SPA-LEED Study of Ordering, Phase Transitions and Interactions*, Surface Science **600**, 1417 (2006).

[Sugimoto 2006] Y. Sugimoto, P. Pou, O. Custance, P. Jelinek, S. Morita, R. Perez and M. Abe, *Real Topography, Atomic Relaxations, and Short-Range Chemical Interactions in Atomic Force Microscopy: The Case of the Alpha-Sn/Si(111)-(√3×√3)R30° Surface*, Physical Review B **73**, 205329 (2006).

[Swarbrick 2005] J. C. Swarbrick, J. Ma, J. A. Theobald, N. S. Oxtoby, J. N. O'Shea, N. R. Champness and P. H. Beton, *Square, Hexagonal, and Row Phases of PTCDA and PTCDI on Ag-Si(111)-(√3×√3)30°*, Journal of Physical Chemistry B **109**, 12167 (2005).

[Tengelin-Nilsson 2000] M. Tengelin-Nilsson, L. Ilver and J. Kanski, *Photoemission and Low-Energy Electron Diffraction Studies of 3,4,9,10-Perylene Tetracarboxylic Dianhydride Layers on Si(111): H*, Surface Science **464**, 265 (2000).

[Theobald 2003] J. A. Theobald, N. S. Oxtoby, M. A. Phillips, N. R. Champness and P. H. Beton, *Controlling Molecular Deposition and Layer Structure with Supramolecular Surface Assemblies*, Nature **424**, 1029 (2003).

[Tian 1998] W. Tian, S. Datta, S. Hong, R. Reifenberger, J. I. Henderson and C. P. Kubiak, *Conductance Spectra of Molecular Wires*, The Journal of Chemical Physics **109**, 2874 (1998).

[Törnevik 1991] C. Törnevik, M. Hammar, N. G. Nilsson and S. A. Flodström, *Epitaxial Growth of Sn on Si(111): A Direct Atomic-Structure Determination of the (2√3×2√3)R30°; Reconstructed Surface*, Physical Review B **44**, 13144 (1991).

[Törnevik 1994] C. Törnevik, M. Gothelid, M. Hammar, U. O. Karlsson, N. G. Nilsson, S. A. Flodstrom, C. Wigren and M. Ostling, *Adsorption of Sn On Si(111)-7×7: Reconstructions in the Monolayer Regime*, Surface Science **314**, 179 (1994).

[Upward 1997] M. D. Upward, P. Moriarty and P. H. Beton, *Double Domain Ordering and Selective Removal of C60 on Ag/Si(111)-(√3×√3)R30°*, Physical Review B **56**, R1704 (1997).

[Upward 1999] M. D. Upward, P. H. Beton and P. Moriarty, *Adsorption of Cobalt Phthalocyanine on Ag Terminated Si(111)*, Surface Science **441**, 21 (1999).

[Wagner 2007] Th. Wagner, A. Bannani, C. Bobisch, K. Karacuban, R. Möller, *The initial growth of PTCDA on Cu(111) studied by STM*, Journal of Physics-Condensed Matter **19**, 056009 (2007).

[Worthington 1992] M. S. Worthington, J. L. Stevens, C. S. Chang and I. S. T. Tsong, in 38th National Symposium of the American Vacuum Society (AVS, Seattle, Washington (USA)), 10, 657 (1992)

[Zahn 2000] D. R. T. Zahn, T. U. Kampen, S. Hohenecker and W. Braun, *GaAs Surface Passivation by Ultra-High Vacuum Deposition of Chalcogen Atoms*, Vacuum **57**, 139 (2000).

General conclusions

The experimental investigation of the organic PTCDA molecules on metal, semiconductor and passivated semiconductor surfaces by means of STM/STS and complementary photoemission spectroscopy (UPS/XPS) for the organic/metal system, performed within the framework of the present thesis, yield a great diversity of results showing a complex behavior of the PTCDA molecules, originating primary from the impact of the substrate reactivity on the molecular properties. Molecule-substrate mediated interactions result in the formation of molecular structures, ranging from randomly chemisorbed molecules on highly reactive substrates to one-dimensional row formation on moderately reactive surfaces and well-ordered overlayers in the case of physisorbed PTCDA molecules on weakly reactive surfaces.

The main conclusions drawn from this study are summarized in the following.

❖ By the combination of various surface sensitive techniques (STM, STS, UPS and XPS) we have obtained a detailed characterization of the **PTCDA adsorption on the Au(111) surface.**

- The high molecular diffusivity on the metallic surface, the unmodified Au(111) substrate reconstruction and the observation of a PTCDA herringbone reconstruction, similar to that of the PTCDA bulk, allow to describe the PTCDA/Au(111) interface as a weakly interacting system.
- The weak molecule-substrate interaction is supported, also, by the possibility of detecting derived molecular states (HOMO and LUMO) very similar to those of the free PTCDA molecule, with a band gap relatively close to values of the bulk PTCDA band gap.
- STS and UPS results show that the Shockley type surface state of Au(111) substrate is not suppressed upon PTCDA adsorption, being still visible through PTCDA monolayer. ARUPS measurements clearly demonstrate the existence of the gold surface states at the interface, though slightly modified. These results are confirmed by LT-STM experiments which unambiguously show a modification of the surface state, in particular an upward shift of surface states energy band minimum.

- UPS/XPS results determined a weak interfacial molecule-substrate coupling, reflected in a small interface dipole formation and negligible charge transfer, supporting also the physisorption process at the interface.

❖ In contrast to the inert metallic surfaces, the **PTCDA** adsorption on highly reactive semiconductor surfaces, as **Si(111)-(7×7)** results in a random adsorption of the molecule, pinned at defect site or surface specific sites.

- The combination of scanning tunneling microscopy experiments and density functional (DFT) first-principles calculations have allowed us to demonstrate that upon adsorption on Si(111)-(7×7) surfaces the electronic structure of PTCDA molecule is strongly modified. In particular, this combined study shows the complex shifts and splitting of the original molecular orbitals (MO) of the PTCDA molecule upon adsorption.

- The intramolecular resolution observed in the experimental STM images can not be understood as the result of a simple rigid shift of the MO of the free molecule. DFT calculations of the molecule-surface system and the corresponding simulation of STM images with realistic tips show large splittings of the original MO when PTCDA is adsorbed on the silicon surface, that contribute in a complex way to the tunnel current.

- These splittings can be understood under symmetry and charge transfer arguments that characterize a strong partially-ionic covalent bonding involving the carbonyl groups of the molecule and the silicon dangling bonds of the surface.

A systematic STM study of the interface formation and thin film growth of PTCDA has been performed for various semiconductor surfaces which were "passivated" by different methods.

❖ The investigation of **PTCDA** growth on **Pb/Si(111) surfaces** yields the following conclusions:

- For Pb/Si(111) system it has been found that low Pb coverage surfaces as the mosaic phase are still highly reactive and PTCDA adsorption results in a disordered overlayer.

- In contrast, highly ordered PTCDA layers are obtained for high Pb coverage phases i.e. the hexagonal incommensurate and the (1×1)-Pb. For these substrates the STM results indicate that the diffusion of the PTCDA molecules on these surfaces at room temperature is relatively high allowing the formation of close packed structures even at low coverage. For these last two situations the PTCDA overlayer structure is based on a nearly rectangular unit cell with the dimensions close to those found for the (102) of the bulk crystal.

- The improved molecular order on the higher Pb coverage phases compared to the mosaic phase is due to the particular arrangement of Pb atoms on the Si(111) substrate which actuate as a passive layer for the silicon dangling bonds, leading to a decreased molecule-substrate interaction.

❖ The adsorption and growth of PTCDA molecules has been investigated on Sn/Si(111) surfaces.

- For the Si(111)-($\sqrt{3}\times\sqrt{3}$)R30°-Sn phase no molecular order has been obtained, despite the metallic nature of the surface. PTCDA deposition at RT results in a disordered structure consisting in isolated molecules and PTCDA clusters pinned at surface defect sites.

- For the deposition of PTCDA on the Si(111)-($2\sqrt{3}\times2\sqrt{3}$)R30°-Sn phase, a novel PTCDA structure has been identified consisting in one-dimensional molecular rows.

- The registry of the PTCDA molecule was determined from high resolution STM images where intramolecular PTCDA features and $2\sqrt{3}$-Sn lattice substrate are resolved simultaneously. A commensurate ($4\sqrt{3}\times2\sqrt{3}$)R30° PTCDA structure is found at 0.5ML coverage.

- In the absence of first-principles calculations of the PTCDA/Si(111)-($2\sqrt{3}\times2\sqrt{3}$)-Sn system, we propose that the molecular anchoring process may be the result of a Sn-O bond formation which stabilizes the molecular rows and promotes the commensurate ($4\sqrt{3}\times2\sqrt{3}$) PTCDA structure at 0.5ML PTCDA coverage. The symmetry and orientation of molecular domains suggest that the molecular arrangement is mainly governed by a molecule-substrate interaction.

❖ The organic/inorganic semiconductor system consisting on PTCDA deposited on sulphur passivated S-GaAs(100), has been studied by scanning tunneling microscopy and spectroscopy (STM/STS).

- We have compared two different preparation methods for the sulphur passivation of GaAs(100) surfaces. Ordering of the organic PTCDA layer was only obtained for the MBE-prepared samples for which a crystalline growth has been observed.
- In order to obtain information about the electronic properties of the organic/inorganic system, we propose measuring I-V plots at different distances, while observing that the current increases exponentially when approaching the tip to the sample. With this method, avoiding a strong interaction between the tip and the organic layer, we have obtained a value of 2.2eV from spectroscopic results for the PTCDA gap.
- We suggest that such strong interactions (or even deformations of the organic layer) could lead to the measurement of anomalously low apparent gap values.

Conclusiones generales

La presente tesis doctoral constituye una aportación original al estudio de la adsorción, crecimiento y propiedades de capas moleculares de PTCDA sobre diversas superficies metálicas y semiconductoras. La investigación experimental que aquí se presenta, llevada a cabo esencialmente mediante STM/STS, muestra una gran diversidad de resultados en función de las superficies utilizadas cuyo origen está relacionado directamente con la reactividad de los substratos. La distinta relación entre las interacciones molécula-substrato y molécula-molécula en cada una de las superficies estudiadas da lugar a la formación de muy distintas estructuras moleculares que abarcan tanto la quimisorción de moléculas aisladas de forma aleatoria en superficies altamente reactivas, como la formación de hileras unidimensionales ordenadas de moléculas en superficies moderadamente reactivas y el crecimiento de capas moleculares bidimensionales bien ordenadas en superficies muy poco reactivas.

Las principales conclusiones obtenidas del presente estudio se resumen en los siguientes puntos.

❖ Mediante la combinación de varias técnicas experimentales con sensibilidad superficial (STM, STS, UPS y XPS) se ha obtenido una caracterización detallada de la adsorción de **PTCDA en superficies de Au(111)**.

- La alta difusión superficial de las moléculas en el substrato metálico, la no modificación de la reconstrucción del mismo y la existencia de una reconstrucción de tipo *herringbone* de las capas moleculares, muy parecida a la del volumen del cristal molecular, permiten describir la intercara PTCDA/Au(111) como un sistema débilmente interactuante.
- La débil interacción molécula-substrato se ve apoyada, asimismo, por la detección de estados moleculares (HOMO y LUMO) con distribuciones espaciales muy parecidas a las de la molécula libre de PTCDA y con valores del *gap* muy próximos a los del volumen.

- Los resultados obtenidos mediante STS y UPS muestran que el estado Shockley del Au(111) no desaparece con la adsorción de PTCDA, siendo visible a través de una monocapa de PTCDA. Medidas de ARUPS demuestran claramente la existencia del estado de superficie en la intercara si bien, ligeramente modificado. Estos resultados se confirman en los experimentos de LT-STM (microscopia de efecto túnel a baja temperatura), que muestran inequívocamente una modificación del estado de superficie, en concreto un desplazamiento del mínimo de energía hacia valores mas altos.
- De acuerdo con los resultados de UPS y XPS obtenidos, existe un acoplamiento muy débil en la intercara molécula-substrato, con formación de un dipolo de intercara muy bajo y una despreciable transferencia de carga. Todo ello apoya la existencia de un proceso de fisisorción en la intercara.

❖ Al contrario de lo que ocurre en superficies más inertes, la adsorción a bajo recubrimiento de **PTCDA** en las superficies de semiconductores altamente reactivas de **Si(111)-(7×7)** resulta en moléculas individuales ancladas en defectos de la superficie o en sitios específicos de la misma.

- La combinación de experimentos de STM con cálculos DFT de primeros principios han permitido demonstrar que la adsorción en la superficie de Si(111)-(7×7) modifica fuertemente la estructura electrónica de la molécula de PTCDA. En concreto, este estudio combinado muestra complejos desdoblamientos y desplazamientos en energía de los orbítales moleculares (OM) originales de la molécula de PTCDA.
- La resolución intramolecular observada en las imágenes experimentales de STM realizadas en el sistema PTCDA/Si(111)-(7x7) no puede entenderse de forma sencilla a partir de un desplazamiento “rígido” de los OM de la molécula libre. Por el contrario, los cálculos DFT del sistema molécula-superficie así como la correspondiente simulación de imágenes de STM con puntas realistas muestran la existencia de grandes desdoblamientos de los OM originales, los cuales contribuyen de forma compleja a la corriente de túnel.
- Estos desdoblamientos se pueden entender utilizando argumentos de simetría y de transferencia de carga y caracterizan un fuerte enlace covalente parcialmente

iónico que involucra los grupos carbonilo de la molécula y los enlaces colgantes de los átomos de silicio de la superficie.

Se ha estudiado de forma sistemática mediante STM la formación de intercaras y crecimiento de láminas delgadas de PTCDA sobre superficies de semiconductores "pasivadas" con distintos métodos.

❖ Así, se ha investigado el crecimiento de **PTCDA en superficies de Pb/Si(111)**. De este trabajo, las principales conclusiones son las siguientes:

- Se han obtenido capas altamente ordenadas de moléculas de PTCDA para las fases del Pb/Si(111) de alto recubrimiento, esto es, la llamada fase inconmensurada y la fase (1×1)-Pb. Los resultados de STM indican que la difusión superficial de las moléculas de PTCDA es alta a temperatura ambiente, permitiendo la formación de capas bien ordenadas. Varias reconstrucciones de tipo *herringbone* se han identificado en este sistema.
- Para la fase de menor recubrimiento de Pb/Si(111), la fase mosaico, no han podido obtenerse capas moleculares ordenadas. La mejora del orden molecular de las fases de alto recubrimiento en Pb frente a la fase mosaico está directamente relacionada con la alta reactividad de esta última superficie, caracterizada por la presencia de enlaces colgantes de silicio en la capa más externa.

❖ Se ha investigado la adsorción y crecimiento de moléculas de **PTCDA sobre superficies de Sn/Si(111**).

- La sublimación a temperatura ambiente de moléculas de PTCDA sobre superficies de Si(111)-($2\sqrt{3}\times 2\sqrt{3}$)R30º-Sn, produce la formación de hileras unidimensionales de moléculas para recubrimientos inferiores a 0.5ML. En el límite de 0.5ML, una estructura conmensurada ($4\sqrt{3}\times 2\sqrt{3}$)R30°-PTCDA ha sido detectada por primera vez.
- De acuerdo con las imágenes de alta resolución de STM donde se pueden detectar de forma simultánea los átomos del substrato y características electrónicas intra-moleculares en el PTCDA, se ha propuesto un modelo de adsorción como

resultado de la formación de enlaces Sn-O. La simetría y orientación de los dominios moleculares sugieren que la disposición molecular viene determinada en buena medida por la interacción molécula-substrato.

❖ En último lugar, se ha estudiado, asimismo, mediante microscopía y espectroscopía de efecto túnel el crecimiento y propiedades de capas moleculares de **PTCDA en superficies de GaAs(100) terminadas en azufre.**

- Se han comparado dos métodos de pasivación de superficies de GaAs(100) con azufre. De ellos, solamente en las muestras preparadas por MBE se ha conseguido observar orden molecular de PTCDA.
- En la obtención de las características electrónicas de este sistema mediante espectroscopía de efecto túnel se ha propuesto un nuevo método en el cual se verifica de forma simultánea a la medida de curvas I-V la posible interacción entre la punta del STM y la capa molecular. Así, se ha mostrado cómo una fuerte interacción de la punta y la capa molecular puede llevar a la determinación de valores de *gap* anómalamente bajos.